Design and Implementation of an Ultrabroadband Millimeter-Wavelength Vector Sliding Correlator Channel Sounder and In-Building Multipath Measurements at 2.5 & 60 GHz

by

Christopher R. Anderson

Thesis Submitted to the Faculty of the
Virginia Polytechnic Institue and State University
in partial fulfillment of the requirements for the degree of

MASTER OF SCIENCE
in
Electrical Engineering

Dr. Theodore S. Rappaport (Chair)
Dr. Dennis G. Sweeney
Dr. Sanjay Raman

May 6, 2002
Blacksburg, VA

Keywords: channel sounder, aggregate partition loss, broadband, multipath, millimeter-wavelength, wireless propagation

© 2002 Christopher R. Anderson

Design and Implementation of an Ultrabroadband Millimeter-Wavelength Vector Sliding Correlator Channel Sounder and In-Building Multipath Measurements at 2.5 & 60 GHz

Christopher R. Anderson

Abstract

Over the past decade, the market for wireless service has grown at an unprecedented rate. The industry has grown from cellular phones and pagers to broadband and ultra-broadband wireless services that can provide voice, data, and full-motion video in real time. This growing hunger for faster data rates and larger bandwidths has prompted a need for a deeper understanding of the wireless channels upon which these devices communicate. In order for the visions of real time full-motion video, multimedia, and high speed data delivery inherent in the 3rd and 4th generations of wireless communication standards to be fully realized, system design engineers must have a thorough understanding of the wireless channels upon which these devices operate. Additionally, for these networks to deliver their promised data rates, they must operate at very high microwave and millimeter-wave frequencies, where large segments of spectrum are readily obtained.

Unfortunately, little is known about the propagation characteristics at these frequencies and bandwidths. As a consequence, there has been a significant demand for wireless test equipment that is capable of characterizing these new wireless channels. The objective of this research was to design and develop a wireless test instrument that can not only characterize these new wireless channels, but has the portability to be quickly and easily re-located to various measurement sites, as well as the flexibility to characterize a wide variety of frequencies and bandwidths in addition to the ultra-broadband channels investigated in this work. This measurement system is also designed to be capable of characterizing both the magnitude and phase response of these wireless channels, which not only provides a more complete channel characteristic, but the potential capability to measure the Doppler spectrum introduced by a dynamic channel.

This work was supported through a Bradley Fellowship and a National Science Foundation Grant, Number EIA-9974960.

This Thesis is dedicated to those who have always
inspired and believed in me:

My Parents, Bennie and Betsy Anderson
Mrs. Scotty Ellerbe
And the late Col. Roy W. Forehand

Acknowledgements

I wish I could say “I did this all myself.” As with any significant undertaking, however, the assistance of numerous individuals was required in order to make this project a success.

I am greatly indebted to Aaron Orndorff for tirelessly proofreading the entire thesis—one chapter at a time. His feedback was an enormous aid in helping this thesis progress beyond the draft stages. I would also like to thank James Hicks, Max Robert, John Kim, and Amanda Martin Staley for proofreading various chapters. Additionally, Alex Verstak ran several ray tracer simulations at 2.5 GHz and 60 GHz; so that I had simulated power delay profiles to compare with my measured power delay profiles.

My Thesis committee of Dr. Raman and Dr. Sweeney, as well as my Advisor Dr. Rappaport, has been very helpful in sharing their time and expertise, for which I am extremely grateful. Additionally, Dr. Greg Durgin provided a sounding board and a “low pass filter” for a lot of my initial channel sounder designs—in addition to sharing his wealth of knowledge on wireless propagation and measurement campaigns.

My parents have always been supportive of my educational endeavors; without them, pursing a Masters degree would have been a more arduous journey.

It is my pleasure to acknowledge the generous donations of time, equipment, and expertise from numerous individuals and corporations. Without their support, this research project would never have progressed beyond the design stages.

Neil Hobbs and John Hodorowski of Mikom shared their wealth of knowledge on RF Design and Board layout, as well as a substantial donation of miscellaneous parts.

Dave Rainey of Grayson Wireless arranged for the donation of GPS oscillators during a critical time in the fabrication of the Channel Sounder, so that I could avoid deviating from the project timeline and budget.

Greg Bull of Rogers Corporation generously provided a seemingly endless supply of circuit board materials.

Stan Slingerland and Carl Gerst from Anaren Micowave donated the I/Q Mixers used in the receiver.

Fred Ott of Agilent Technologies loaned out V- and R-band waveguide power sensors so that the gain and output power levels of the 38 and 60 GHz upconverters could be measured.

Ed Valentine of EMS Consulting provided advice on PCB layout, fabrication, and assembly, so that I could squeeze the maximum performance out of the PN Generator boards.

Randall Nealy was kind enough to measure the antenna patterns for the biconical antennas used on the 2.5 GHz Channel Sounder configuration.

Motorola and ON Semiconductor generously supplied a large quantity of various ECL logic chips for use in the PN Generator and PN Clock Signal Generator.

I would also like to thank the DSP lab at MPRG for loaning me one of their signal generators when the one I was using developed a bad power supply during the measurements campaign.

The staff at MPRG are truly exceptional people; they help create a enjoyable work environment and make MPRG run like a well-oiled machine.

As always, all glory belongs to God the Father and His Son Jesus Christ, for endowing me with the abilities and perseverance to undertake a project of this magnitude.

Contents

Abstract **ii**

Acknowledgements **iv**

1 Introduction **1**

1.1 Motivation……..... 1

1.2 Project Background…… 2

1.3 Purpose……... 3

1.4 Project Overview…… 5

1.5 Thesis Overview……. 7

2 Channel Measurement Theory and Application **9**

2.1 The Effects of Multipath on Communication Systems…….. 9

2.1.1 Doppler Spreading……... 13

2.1.2 Time Dispersion…….. 13

2.1.3 Small Scale Fading…….. 15

2.2 Transfer Function Representation…….. 16

2.3 Transfer Function Measurement…… 18

2.3.1 Periodic Pulse…….. 19

2.3.2 Frequency Domain…….. 20

2.3.3 Pulse Compression Technique…… 21

2.3.4 Swept Time Delay Crosscorrelation…… 26

2.3.5 Magnitude and Phase Impulse Response Measurement using the Sliding Correlator Principle……... 30

2.4 Information available from Impulse Response Measurements…….. 33

2.4.1 Multipath Amplitude and Delay…….. 34

2.4.2 Channel RMS Delay Spread…..…….. 34

2.4.3 Coherence Bandwidth…… 35
2.4.4 Average Path Loss……... 36
2.4.5 Total Multipath Power Gain……..……. 36
2.4.6 Doppler Spectrum and Spread……. 37
2.5 Conclusion…….. 38

3 Measurement System Design Issues 39
3.1 Overall System Constraints…… 39
3.1.1 Miniaturized Measurement System……. 40
3.1.2 Frequency Flexability…….. 41
3.1.3 High Resolution of Multipath…….. 42
3.1.4 Magnitude and Phase Measurement Capability…….. 43
3.2 PN Generator…….. 44
3.2.1 PCB Layout and Fabrication Constraints…… 46
3.3 Approaches to Measuring Magnitude and Phase……... 52
3.3.1 Discussion…… 52
3.3.2 Achieving Stability of Local Oscillators……. 59
3.3.2.1 Cable Connected Method…….…….. 60
3.3.2.2 Broadcast and Recover Carrier Method……. 61
3.3.2.3 Atomic Master Oscillator Method…….. 62
3.3.2.4 Digital Downconversion……. 65
3.3.2.5 GPS Disciplined Oscillators……... 68
3.3.2.6 Implementation……... 69
3.4 I/Q Correlator Unit……. 70
3.5 Conclusion……..…… 72

4 Sliding Corelator Transmitter 74
4.1 Overview……..... 74
4.2 Implementation……... 76
4.2.1 GPS Disciplined Oscillator…….. 76
4.2.2 LO, Power Splitter, and Mixer…… 76
4.2.3 PN Clock Signal Generator……. 77
4.2.4 PN Generator……..…….. 79

4.2.5 Upconverters…… 82
4.3 Conclusion……...……... 83

5 Sliding Correlator Receiver 84
5.1 Overview…… 84
5.2 Receiver LO and Power Splitter……. 87
5.3 Downconverters…….. 87
5.4 Receiver PN Generator and Trigger Pulse Generator…… 89
5.5 I/Q Demodulation……... 92
5.5.1 Quadrature Mixer…… 92
5.5.2 I/Q Correlator Design…….. 93
5.5.3 I/Q Correlator PCB Layout……. 96
5.5.4 Data Acquisition and Post Processing……. 97
5.6 Conclusion…….. 102

6 Measurement System Verification and Calibration 103
6.1 Overview…… 103
6.2 Equipment Verification…….. 104
6.2.1 PN Clock Signal Generator……. 104
6.2.2 PN Generator……... 105
6.2.3 GPS Disciplined Oscillators…… 107
6.2.4 Transmitter Modulation……... 108
6.2.5 Receiver Demodulation……... 108
6.2.6 I/Q Correlator Unit…….. 109
6.3 System Calibration and Repeatability Evaluation…….. 111
6.3.1 Calibration……... 111
6.3.1.1 Equipment Setup…… 112
6.3.1.2 Calibration Measurements……. 114
6.3.1.3 Processing Calibration Measurements……... 115
6.3.2 Repeatability Testing……... 118

6.4 System Calibration and Repeatability Evaluation for 60 GHz Channel Sounder Configuration…….. 119
6.4.1 Channel Sounder Calibration…….. 119
6.4.2 Channel Sounder Repeatability Evaluation……. 121
6.5 Conclusion…….. 122

7 Indoor Measurements at 2.5 and 60 GHz 123
7.1 Measurement Scope…… 123
7.2 Measurement Plan…….. 123
7.2.1 Channel Sounder Setup……... 123
7.2.2 Measurement Procedure…….. 126
7.2.3 Site Descriptions and Maps……. 128
7.3 Measurement Results…….. 132
7.3.1 Summary Results Table……... 132
7.3.2 Partition Based Path Loss Analysis……. 138
7.3.3 Discussion of Results…….. 143
7.4 Conclusion…….. 144

8 Conclusions 145
8.1 Summary of Findings…….…… 145
8.1.1 Miniaturized Channel Sounder…… 145
8.1.2 Data Post Processing Software…… 146
8.1.3 Indoor Measurements at 2.5 GHz and 60 GHz……... 146
8.2 Further Research…….…… 146
8.3 Conclusion…….……. 148

A Schematics 149

B Power Delay Profiles and Site Photos for 2.5 & 60 GHz Measurements 156
B.1 2.5 GHz Power Delay Profiles…….. 158
B.1.1 2.5 GHz Location 1 PDPs, 4th Floor Durham Hall, Virginia Tech……. 158
B.1.2 2.5 GHz Location 2 PDPs, 4th Floor Durham Hall, Virginia Tech……. 160
B.1.3 2.5 GHz Location 3 PDPs, 4th Floor Durham Hall, Virginia Tech……. 162

B.1.4 2.5 GHz Location 4 PDPs, 4th Floor Durham Hall, Virginia Tech……. 163
B.1.5 2.5 GHz Location 5 PDPs, 4th Floor Durham Hall, Virginia Tech……. 165
B.1.6 2.5 GHz Location 6 PDPs, 4th Floor Durham Hall, Virginia Tech……. 167
B.1.7 2.5 GHz Location 7 PDPs, 4th Floor Durham Hall, Virginia Tech……. 168
B.1.8 2.5 GHz Location 8 PDPs, 4th Floor Durham Hall, Virginia Tech……. 169
B.2 60 GHz Power Delay Profiles…… 170
B.2.1 60 GHz Location 1 PDPs, 4th Floor Durham Hall, Virginia Tech…….. 170
B.2.2 60 GHz Location 1 PDPs, 4th Floor Durham Hall, Virginia Tech…….. 174
B.2.3 60 GHz Location 1 PDPs, 4th Floor Durham Hall, Virginia Tech…….. 177
B.2.4 60 GHz Location 1 PDPs, 4th Floor Durham Hall, Virginia Tech…….. 179
B.2.5 60 GHz Location 1 PDPs, 4th Floor Durham Hall, Virginia Tech…….. 183
B.2.6 60 GHz Location 1 PDPs, 4th Floor Durham Hall, Virginia Tech…….. 187
B.2.7 60 GHz Location 1 PDPs, 4th Floor Durham Hall, Virginia Tech…….. 189
B.2.8 60 GHz Location 1 PDPs, 4th Floor Durham Hall, Virginia Tech…….. 191
B.3 2.5 GHz Transmitter and Receiver Site Photos……. 192
B.3.1 2.5 GHz Location 1 Series, 4th Floor Durham Hall, Virginia Tech…… 192
B.3.2 2.5 GHz Location 2 Series, 4th Floor Durham Hall, Virginia Tech…… 193
B.3.3 2.5 GHz Location 3 Series, 4th Floor Durham Hall, Virginia Tech…… 194
B.3.4 2.5 GHz Location 4 Series, 4th Floor Durham Hall, Virginia Tech…… 195
B.3.5 2.5 GHz Location 5 Series, 4th Floor Durham Hall, Virginia Tech…… 196
B.3.6 2.5 GHz Location 6 & 7 Series, 4th Floor Durham Hall, Virginia Tech……. 197
B.3.7 2.5 GHz Location 8 Series, 4th Floor Durham Hall, Virginia Tech…… 198
B.4 60 GHz Transmitter and Receiver Site Photos…….. 199
B.4.1 60 GHz Location 1 Series, 4th Floor Durham Hall, Virginia Tech…….…… 199
B.4.2 60 GHz Location 2 Series, 4th Floor Durham Hall, Virginia Tech…….…… 200
B.4.3 60 GHz Location 3 Series, 4th Floor Durham Hall, Virginia Tech…….…… 201
B.4.4 60 GHz Location 4 Series, 4th Floor Durham Hall, Virginia Tech…….…… 202
B.4.5 60 GHz Location 5 Series, 4th Floor Durham Hall, Virginia Tech…….…… 203
B.4.6 60 GHz Location 6 & 7 Series, 4th Floor Durham Hall, Virginia Tech……..… 204
B.4.7 60 GHz Location 8 Series, 4th Floor Durham Hall, Virginia Tech…….…… 205

C Channel Sounder Users Guide 206
C.1 Introduction…… 206

C.2 Channel Sounder Operation……... 206
C.2.1 Setup……... 206
C.2.1.1 Transmitter Setup……..…… 210
C.2.1.2 Receiver Setup……... 211
C.2.1.3 Operating Instructions for the PN Clock Signal Generator……... 214
C.2.2 Recording Calibration Measurements…..……... 215
C.2.3 Recording Propagation Measurements……... 218
C.2.4 Reconfiguring the Channel Sounder for a Different Frequency or PN Code Length……. 221
C.2.4.1 Reconfiguring for a Different Frequency…….. 221
C.2.4.2 Reconfiguring for a Different PN Code Length…… 223
C.3 LabVIEW Data Analysis Software…… 227
C.3.1 Calibration…….. 229
C.3.2 Power Delay Profiles…….. 231
C.3.3 Doppler and Multipath Phase……. 233
C.3.4 Delay Profile Phase Plots…… 236

D Measurement Data and Source Code File Listing 238
D.1 Data Files Related to Measurements……. 238
D.1.1 2.5 GHz Measurement Data Files……... 238
D.1.2 60 GHz Measurement Data Files…… 239
D.2 LabVIEW Analysis Software Source Code Files……..... 241

References 243
Vita 251

List of Tables

3.1 Current Channel Sounder Subsystems and Suggested Replacements…..……. 41
3.2 Measurement System Dependence on Various PN Generator Properties…….. 44
3.3 PN Generator Timing Budget Analysis……. 49
3.4 Comparison of Commercially Available Frequency Standards…… 57
3.5 Comparison of Rubidium and Cesium Oscillators at 5.4 GHz……. 63
3.6 Comparison of Rubidium and Cesium Oscillators at 900 MHz…… 64
3.7 Comparison of Commercially Available AMOs……... 64
3.8 Comparison of Commercially High Speed ADC's……... 68
3.9 Comparison of Commercially Available GPS Disciplined Oscillators…… 69
3.10 Performance of GPS Disciplined Oscillators at 5.4 GHz with 450 MHz PN Code…….. 70

4.1 Performance of 38 & 60 GHz Channel Sounder with 400 MHz PN Code……... 76
4.2 38 and 60 GHz Upconverter Specifications…….. 83

5.1 38 and 60 GHz Downconverter Specifications……. 89
5.2 Correlator Low Pass Filter Bandwidth Required for Maximum and Minimum PN Clock Rate……... 94

6.1 Example of Calibration Data Points…….. 116
6.2 Example of Calibration Voltage-Power Data…… 117
6.3 Example Repeatability Analysis…… 119
6.4 Link Budget for 60 GHz Calibration……. 119
6.5 Repeatability Analysis for 60 GHz Channel Sounder Configuration……... 122

7.1 2.5 GHz & 60 GHz Single Floor Office Building Path Loss…… 134
7.2 Summary of 2.5 GHz Measurement Results **on a Single Floor of a Modern Office Building……..**……... 135

7.3 Summary of 60GHz Measurement Results **on a Single Floor of a Modern Office Building**……. 136

7.4 **Measured Partition Losses at 2.5 GHz and 60 GHz on a Single Floor of a Modern Office Building……...** 139

7.5 Reported Partition Losses for Drywall Type Material…….. 140

7.6 Reported Partition Losses for Plywood Type Material……. 140

7.7 Reported Partition Losses for Miscellaneous Building Materials……. 141

List of Figures

1.1 MPRG PCB Rapid Prototyping Facility…….…….. 6

2.1 Illustration of Line of Sight and Multipath Signals…..……...….. 10

2.2 Mobile Receiver in a 2-Ray Multipath Environment…… 12

2.3 Channel Frequency Response for Various Multipath Time Delay and Number of Multipath…..……. 15

2.4 Large and Small Scale Fading Response of a Channel……..…...…… 16

2.5 Example of Received Multipath Signals……..……. 17

2.6 Graphical Representation of Channel Transfer Function……..…… 18

2.7 Block Diagram of a Periodic Pulse RF Channel Sounder……..……... 19

2.8 Block Diagram of a Swept Frequency Channel Sounder……..…… 20

2.9 Plot of $R_{xx}(\tau)$, for N_0=1…….....……... 22

2.10 Basic Measurement System to Measure the Impulse Response Using the Correlation Properties of White Noise…..……..……...……. 22

2.11 Block Diagram of a PN Generator……... 25

2.12 Autocorrelation of PN waveform……. 25

2.13 Block Diagram of a Sliding Correlator Channel Sounder…….…… 27

2.14 Basic Coherent Receiver Design…….……...……... 30

2.15 Example Power Delay Profile, measured at 2.5 GHz on the 2nd Floor of Torgerson Hall at Virginia Tech…….…… 33

2.16 Doppler Spectrum Plot for a 60 GHz Receiver Moving at a Constant Velocity of 0.01 m/s……...…..……. 33

3.1 Repetition Rate of Inphase and Quadrature Delay Profiles……... 45

3.2 Board Layout for 11-bit and 18-bit PN Generators……..…….….... 47

3.3 Cross-section of Microstrip Circuit Trace……..…….. 50

3.4 Comparison of Components Relative to the Head of a Match…..……... 51

3.5 Component Tombstoning and Misalignment……...……..…… 51
3.6 Illustration of Jitter in a Digital Signal……...……..,…… 53
3.7 Graphical Representation of Determining Normalized Frequency Difference and Frequency Instability……. 55
3.8 Block Diagram of a Fixed Length Cable Connected Channel Sounder……..…….…… 60
3.9 Block Diagram of a Broadcast and Recover Carrier Channel Sounder……...…. 61
3.10 Block Diagram of an Atomic Master Oscillator Based Channel Sounder……..... 62
3.11 Illustration of Direct I/Q Sampling……..…….. 65
3.12 Bandpass Sampling Example…… 66

4.1 Transmitter Block Diagram……... 75
4.2 Channel Sounder Transmitter Images……... 75
4.3 PN Clock Signal Generator PCB Layout…….. 78
4.4 PN Clock Signal Generator Implementation……. 78
4.5 Comparison of Old 11-bit PN Generator Top and Bottom Layers and New 11-bit PN Generator Top and Bottom Layers…….. 81
4.6 PN Generator PCB…… 81
4.7 Block Diagram of Upconverter……. 82
4.8 38 GHz and 60 GHz Upconverters…… 83

5.1 Receiver Block Diagram……... 86
5.2 Channel Sounder Receiver Images…… 86
5.3 Block Diagram of Downconverter…… 88
5.4 38 and 60 GHz Downconverters……... 88
5.5 11-bit Receiver PN Generator Board Top and Bottom Layers……. 91
5.6 18-bit Receiver PN Generator Board Top and Bottom Layers……. 91
5.7 Receiver PN Trigger Pulse Generator Board…… 91
5.8 Receiver PN Generator and Trigger Pulse Generator……... 92
5.9 I/Q Correlator Unit Block Diagram……... 93
5.10 I/Q Correlator Low-Pass Filter Frequency Response..…….. 95
5.11 I/Q Correlator Board Layout Top and Bottom Layers…….. 97
5.12 I/Q Correlator Implementation…….. 97
5.13 LabVIEW Channel Sounder Data Acquisition System……. 98
5.14 LabVIEW Data Postprocessing System…… 99

5.15 LabVIEW Data Postprocessing Power Delay Profile……... 99
5.16 Comparison of Measured PDPs with Ray Tracer Simulated PDPs…….. 100
5.17 Doppler Spectrum Example for a 60 GHz Receiver Moving at a Constant Velocity of 0.01 m/s.……...…..……. 100
5.18 Multipath Phase Plot Example…….. 101
5.19 PDP Snapshots Along a Linear Track and Azimuthal Sweep…….. 102

6.1 PN Clock Signal Generator Output……... 105
6.2 450 MHz PN Generator Output Waveform……..……. 106
6.3 400 MHz PN Generator Output Spectrum……...……. 106
6.4 Overclocked PN Generator Output……... 107
6.5 Transmitter IF Spectrum with 400 MHz PN Code…… 108
6.6 Effect of Offset of Local Oscillators on Received Signal……. 109
6.7 Crosscorrelation of Two PN Sequences…… 110
6.8 Crosscorrelation of Two Overclocked PN Sequences……... 110
6.9 Inphase and Quadrature Voltage Delay Profiles……..……. 111
6.10 Fresnel Zone Boundaries…….…….. 113
6.11 Plot of Example Calibration Data…….. 116
6.12 Plot of Received Voltage vs. Power Using Example Calibration Data……. 117
6.13 60 GHz Voltage vs. Receiver Attenuation Calibration Plot…….. 120
6.14 Comparison of Actual Received Power Levels with Linear Regression from Calibration…… 121

7.1 Azimuth and Elevation Antenna Patterns for the 60 GHz Configuration.……. 124
7.2 2.5 GHz Channel Sounder Block Diagram.……... 125
7.3 Azimuth (left) and Elevation Antenna Patterns for the 2.5 GHz Configuration. Antenna Pattern has been Normalized to the Maximum Gain…….. 126
7.4 Map of the 4th Floor of Durham Hall at Virginia Tech……. 126
7.5 Automated Track Measurement System……... 127
7.6 Measurement Locations 1.1 – 1.4, 4th Floor, Durham Hall, Virginia Tech. The transmitter is located in Room 475, Receivers 1.1 and 1.2 are located in Room 471; Receiver 1.3 is in the conference room in the 476 computer lab, and Receiver 1.4 is located in the hallway adjacent to 475……. 128
7.7 Measurement Locations 2.1—2.3 and 3.1 – 3.2, 4th Floor, Durham Hall, Virginia Tech. Transmitter 2 is located outside of Room 450, Transmitter 3 is located adjacent to Room 412. Receivers are at various positions in the hallway…….. 129

7.8 Measurement Locations 4.1 – 4.4, 4th Floor, Durham Hall, Virginia Tech. The Transmitter is located just inside the entrance to Room 476. Receiver locations are at various positions in 476, as well as the adjacent hallway…… 130

7.9 Measurement Locations 5.1 – 5.4, 4th Floor, Durham Hall, Virginia Tech. The Transmitter is located next to the receptionist's desk in Room 432. Receiver location 5.1 is in room 433, Receiver locations 5.2 and 5.3 are in the atrium next to the elevators, and Receiver location 5.4 is in the hallway next to 432……. 131

7.10 Measurement Locations 6.1 – 6.2, 7.1—7.2, and 8.1, 4th Floor, Durham Hall, Virginia Tech. Transmitters 6 and 7 are located in the atrium next to the elevators, while Transmitter 8 is located in a side hallway adjacent to the Women's Restroom. Receiver locations 6.1, 6.2, 7.1, and 7.2 are at various positions in the main hallway. Receiver location 8.1 is in the hallway next to Room 475…… 132

7.11 Scatterplot of all Measured Path Loss Values (Excluding Antenna Gains) at 2.5 GHz on a Single Floor of a Modern Office Building. Transmitter and Receiver use Omnidirectional Biconical Antennas with 6dBi Gain…… 137

7.12 Scatterplot of all Measured Path Loss Values (Excluding Antenna Gains) at 60 GHz. Transmitter and Receiver use Pyramidal Horn Antennas with 25dBi Gain and 50° First-Null Beamwidth…… 137

7.13 Normalized Attenuation of Drywall vs. Frequency, from Measured and Reported Data. 142

7.14 Normalized Attenuation of Plywood vs. Frequency, from Measured (Values for Whiteboard Used) and Reported Data…….. 142

A.1 11-Bit Transmitter PN Generator Schematic…… 150

A.2 18-Bit Transmitter PN Generator Schematic…… 151

A.3 11-Bit Receiver PN Generator Schematic…… 152

A.4 18-Bit Receiver PN Generator Schematic…… 153

A.5 Trigger Pulse Generator Schematic…….. 154

A.6 I/Q Correlator Board Schematic…….. 155

B.1 2.5 GHz Location 1.1 Power Delay Profiles…… 158

B.2 2.5 GHz Location 1.2 Power Delay Profiles…… 158

B.3 2.5 GHz Location 1.3 Power Delay Profiles…… 159

B.4 2.5 GHz Location 1.4 Power Delay Profiles…… 159

B.5 2.5 GHz Location 2.1 Power Delay Profiles…… 160

B.6 2.5 GHz Location 2.2 Power Delay Profiles…… 160

B.7 2.5 GHz Location 2.3 Power Delay Profiles…… 161

B.8 2.5 GHz Location 3.1 Power Delay Profiles…… 162

B.9 2.5 GHz Location 3.2 Power Delay Profiles…… 162
B.10 2.5 GHz Location 4.1 Power Delay Profiles…… 163
B.11 2.5 GHz Location 4.2 Power Delay Profiles…… 163
B.12 2.5 GHz Location 4.3 Power Delay Profiles…… 164
B.13 2.5 GHz Location 4.4 Power Delay Profiles…… 164
B.14 2.5 GHz Location 5.1 Power Delay Profiles…… 165
B.15 2.5 GHz Location 5.2 Power Delay Profiles…… 165
B.16 2.5 GHz Location 5.3 Power Delay Profiles…… 166
B.17 2.5 GHz Location 5.4 Power Delay Profiles…… 166
B.18 2.5 GHz Location 6.1 Power Delay Profiles…… 167
B.19 2.5 GHz Location 6.2 Power Delay Profiles…… 167
B.20 2.5 GHz Location 7.1 Power Delay Profiles…… 168
B.21 2.5 GHz Location 7.2 Power Delay Profiles…… 168
B.22 2.5 GHz Location 8.1 Power Delay Profiles…… 169
B.23 60 GHz Location 1.1 Power Delay Profiles…… 170
B.24 60 GHz Location 1.2 Power Delay Profiles…… 171
B.25 60 GHz Location 1.3 Power Delay Profiles…… 172
B.26 60 GHz Location 1.4 Power Delay Profiles…… 173
B.27 60 GHz Location 2.1 Power Delay Profiles…… 174
B.28 60 GHz Location 2.2 Power Delay Profiles…… 175
B.29 60 GHz Location 2.3 Power Delay Profiles…… 176
B.30 60 GHz Location 3.1 Power Delay Profiles…… 177
B.31 60 GHz Location 3.2 Power Delay Profiles…… 178
B.32 60 GHz Location 4.1 Power Delay Profiles…… 179
B.33 60 GHz Location 4.2 Power Delay Profiles…… 180
B.34 60 GHz Location 4.3 Power Delay Profiles…… 181
B.35 60 GHz Location 4.4 Power Delay Profiles…… 182
B.36 60 GHz Location 5.1 Power Delay Profiles…… 183
B.37 60 GHz Location 5.2 Power Delay Profiles…… 184
B.38 60 GHz Location 5.3 Power Delay Profiles…… 185
B.39 60 GHz Location 5.4 Power Delay Profiles…… 186
B.40 60 GHz Location 6.1 Power Delay Profiles…… 187

B.41 60 GHz Location 6.2 Power Delay Profiles…… 188
B.42 60 GHz Location 7.1 Power Delay Profiles…… 189
B.43 60 GHz Location 7.2 Power Delay Profiles…… 190
B.44 60 GHz Location 8.1 Power Delay Profiles…… 191
B.45 2.5 GHz Location 1 Series Site Photos…… 192
B.46 2.5 GHz Location 2 Series Site Photos…… 193
B.47 2.5 GHz Location 3 Series Site Photos…… 194
B.48 2.5 GHz Location 4 Series Site Photos…… 195
B.49 2.5 GHz Location 5 Series Site Photos…… 196
B.50 2.5 GHz Location 6 & 7 Series Site Photos…… 197
B.51 2.5 GHz Location 8 Series Site Photos…… 198
B.52 60 GHz Location 1 Series Site Photos…… 199
B.53 60 GHz Location 2 Series Site Photos…… 200
B.54 60 GHz Location 3 Series Site Photos…… 201
B.55 60 GHz Location 4 Series Site Photos…… 202
B.56 60 GHz Location 5 Series Site Photos…… 203
B.57 60 GHz Location 6 & 7 Series Site Photos…… 204
B.58 60 GHz Location 8 Series Site Photos…… 205

C.1 Channel Sounder Transmitter Block Diagram…… 207
C.2 Channel Sounder Receiver Block Diagram…… 207
C.3 Channel Sounder Transmitter Baseband and IF Section…… 208
C.4 Channel Sounder Receiver Baseband and IF Section…… 209
C.5 Channel Sounder DAQ Program…… 213
C.6 PN Clock Signal Generator…… 214
C.7 Calibration Configuration Screen…… 216
C.8 Calibration Routine Screen…… 217
C.9 Track Configuration Screen…… 220
C.10 Transmitter Close Up Image…… 222
C.11 Receiver Close Up Image…… 223
C.12 PN Signal Generator Front Panel Detail…… 224
C.13 PN Signal Generator Circuit Board and Connections…… 225
C.14 Receiver PN Generator and Trigger Pulse Generator Boards…… 226

C.15 Desoldering the 5V Power Jumper……... 226
C.16 Desoldering RX PN and Run/Stop Wires……. 227
C.17 LabVIEW Analysis Software Main Screen…….. 228
C.18 Select Directory Containing Calibration Files…….. 229
C.19 Calibration Screen……. 230
C.20 Select Directory Containing Track Measurements……... 231
C.21 Plot PDPs Screen…….. 232
C.22 Doppler Array Screen……... 233
C.23 Doppler Array File Dialog…… 234
C.24 Doppler and Phase Over Time Screen…….. 235
C.25 Phase Screen……. 236
C.26 Phase Screen Dialog Box…….. 236

Chapter 1

Introduction

1.1 Motivation

Over the past decade, the market for wireless service has grown at an unprecedented rate. The industry has grown from cellular phones and pagers to Personal Communication Systems (PCS) delivering voice and data, wireless local area networks (WLANs), and ultra-broadband (also called ultra-wideband) wireless services that will eventually provide voice, data, and full-motion video in real time. This growing hunger for faster data rates and larger bandwidths has prompted a need for a deeper understanding of the wireless channels upon which these devices communicate [1]. In order for the visions of real time full-motion video, multimedia, and high speed data delivery inherent in the 3rd and 4th generations of wireless communication standards to be fully realized, system design engineers must have a thorough understanding of the wireless channels upon which these devices operate. Without this understanding, networks will be subject to dropped or lost packets, interference, and coverage problems [12].

In addition, for these networks to deliver their promised bandwidth, they must operate at very high microwave and millimeter-wave frequencies, where large segments of spectrum are readily obtained. Unfortunately, little is known about the propagation characteristics of these frequencies and bandwidths, so detailed statistical channel models that can predict the behavior of these channels are unavailable. Also, as frequencies increase into the millimeter-wavelength bands, site-specific measurement data must be used to supplement statistical channel models. This is a necessity because minor variables that were unimportant at lower frequencies—surface roughness of buildings, window treatments, specular reflections due to surface moisture—

become critical at these higher frequencies. Since no channel model, no matter how detailed, can accurately process all variables for all propagation environments, the solution is to use a more general channel model and optimize it with measurement data for a given propagation environment. The only difficulty in implementing such a system is in the measurement device. Currently no commercially off the shelf equipment exists that has both the versatility to measure a wide variety of channels and bandwidths, as well as the portability to be easily transported from one site to another. The objective of this research was to design and develop a wireless test instrument that can not only characterize these new wireless channels, but has the portability to be quickly and easily re-located to various measurement sites, as well as the flexibility to characterize a wide variety of frequencies and bandwidths in addition to the ultrabroadband channels investigated in this work.

1.2 Project Background

Ultrabroadband communications is an emerging technology that holds the promise of solving key propagation problems inherent in conventional communication systems: huge wireless channels with bandwidths of a Gigahertz or more, higher Bits/Hertz/m^2 capacities, and the ability to share spectrum without causing harmful interference [1]. As mentioned in the previous section, these systems must by necessity operate at very high frequencies, which were—until recently—relatively poorly understood and unused. With the creation of the Local Multipoint Distribution System and the 60 GHz ISM band, containing 1100 MHz and 5 GHz of spectrum, respectively, the interest in developing communication systems that operate at these frequencies has increased significantly. Additionally, the FCC is currently reviewing a proposal to open spectrum at 94 GHz, to provide point-to-point communication data rates of up to 100 Gigabits/second [4].

In order to better understand the behavior of these ultrabroadband channels, measurement equipment is being developed that can characterize the channel at these frequencies and bandwidths [16, 33, 43, 64, 65]. These devices are designed to measure the transfer function of a wireless channel. Knowledge of the transfer function for a wireless channel means that for any input signal transmitted through the channel, the received can be determined by convolving the input signal with the channel transfer function (further discussed in Chapter 2). Knowing the

transfer function of a wireless channel provides engineers with a plethora of knowledge that allows them to employ the optimum transceiver architecture and modulation scheme to maximize throughput across the channel.

Measuring the impulse response of a wireless channel is not a trivial task, and multiple techniques, such as Periodic Pulse, Frequency Domain, or Sliding Correlator may be used [2, 12, 17], and are discussed further in Chapter 2. All of these techniques have their advantages; however, the focus of this research was to develop a spread spectrum sliding correlator channel sounder, due to the noise and interference rejection properties of spread spectrum transmissions [3].

1.3 Purpose

The purpose of this research was to design and develop a highly versatile, portable spread spectrum channel sounder, capable of wideband magnitude and phase impulse response characterization of wireless channels. This system will have four major distinguishing characteristics:

- Compact, portable, and easily deployable
- Easily reconfigurable to measure a variety of frequencies and bandwidths
- High time and spatial resolution of the channel impulse response
- Magnitude and phase measurement capability

These characteristics were chosen to overcome design limitations in the broadband channel sounder currently in use at the Mobile and Portable Radio Research Group at Virginia Tech, as well as provide future researchers with a tool capable of studying the wireless channel under a diverse range of experimental setups.

A compact and highly portable channel sounder is a major advantage to researchers that wish to study the channel across a variety of links. The mobility of such a system eliminates the need to disassemble, stow the equipment for transport, and then re-assemble at the new site. This is a lengthy process that requires time consuming and painstaking adjustments when setting up the equipment at the new location, and results in a significant amount of downtime during a measurements campaign. Also, a miniaturized channel sounder eliminates the need for large measurement carts to haul the equipment, making it easier to maneuver into and out of buildings, as well as reducing the physical space required to set up and operate the system.

In addition to being compact and portable, the measurement system will be easily reconfigurable for use across a wide variety of frequencies and bandwidths. This feature allows several design engineers working in different frequency bands (5.8 GHz U-NII, 38 GHz LMDS, or 60 GHz unlicensed bands) to share the same measurement system, reducing cost and overhead. Furthermore, researchers conducting experiments on the effects of channel phenomenon such as rain, snow, or fog, can quickly shift from one band to another, in order to investigate whether different bands or antenna polarizations will exhibit different effects.

Beyond operating across a broad spectrum of frequencies, the upgraded channel sounder will have the capability to measure the channel impulse response with a very high resolution. This is accomplished by probing the channel with a spread spectrum signal generated by a pseudo-random noise (PN) sequence, a technique that will be further discussed in Chapter 2. This provides a time-domain resolution equal to the chip rate of the PN sequence, and spatial resolution of 1 foot per 1 nanosecond of time resolution, as explained in [2, 3]. For example, if the PN sequence in the channel sounder is set to a chip rate of 400 MHz, the time domain resolution of channel phenomenon will be 2.5 nanoseconds, corresponding to a spatial resolution of 2.5 feet (0.75 meters).

The high resolution of this measurement system is a necessity for studying indoor and short building-to-building links. In both of these situations, obstructions such as doorways, windows, and office furniture can cause significant degradation of the channel [5]. Since the link distance in these cases is extremely short (on the order of a hundred meters or less), and the obstructions would typically be densely packed, signal perturbations will be very closely spaced in time, requiring a high-resolution measurement system to distinguish them.

Finally, communication with a mobile user creates a time-varying link, manifested in a Doppler shift of the signal spectrum. Many digital communication standards currently use some form of phase shift keying as their modulation. One of the limitations of such a modulation scheme is an offset or drift between the frequency standards at the base station and the mobile unit. Most digital receivers can tolerate some degree of offset; however, if the offset becomes significant enough, it can cause high bit error rates at the receiver, even though the channel may be otherwise clear. In the case where one of these units is moving relative to the other, a Doppler frequency shift is observed that is proportional to both the velocity of the unit and the frequency they are transmitting on, inducing a frequency offset between the two units in addition

to any offset that may be present in the frequency standards. This becomes a more serious problem at very high frequencies, such as 60 GHz, because a lower velocity is required to achieve a given Doppler frequency shift than at a lower frequency. With the proliferation of personal mobile communication systems at a variety of frequencies, the measurement systems must have the capability to characterize the Doppler spectrum introduced by a dynamic channel, so that engineers may design modulation and coding schemes that are more robust to these effects. Characterizing the Doppler spectrum is accomplished by measuring both the magnitude and phase of the channel transfer function, known as the complex channel transfer function.

1.4 Project Overview

The first phase of this project was to develop a printed circuit board (PCB) rapid prototyping facility at the Mobile and Portable Radio Research Group at Virginia Tech, which was completed as an undergraduate honors thesis project [6], and is shown in Figure 1.1. The facility is comprised of a LPKF Protomat® 91s/VS milling/drilling machine, PCAD 2000 PCB layout software, and a Hakko 851 hot air surface mount device rework station. The facility allows in-house design, layout, fabrication, assembly, and testing of printed circuit boards, speeding the design process by removing the need to use an external board manufacturer for simple board designs and layouts. The primary limitation of the facility is that the Protomat® can only produce two-layer circuit boards, which creates layout constraints on high speed digital and RF circuit boards [6, 53]. The PCB rapid prototyping facility would be used to implement much of the new channel sounder on printed circuit boards, so that a significant size reduction can be realized, facilitating the goal of creating a more compact measurement system.

Figure 1.1: MPRG PCB Rapid Prototyping Facility

The second phase of this project was to upgrade the existing system to have ultrabroadband measurement capabilities. This task involved designing a pseudo-random noise generator capable of achieving a chip rate of 450 MHz, and fabricating it with the in-house rapid prototyping facility described above. This PN generator would replace the then current 100 MHz PN generator, and give the channel sounder the capability to distinguish channel phenomenon with a resolution of 2.25 nanoseconds. This phase was started as part of an undergraduate honors research [6], and was completed as the first part of this thesis work. Beyond being merely a high-resolution measurement system, the channel sounder can be thought of as a simplified communication system, and thus the inclusion of the 450 MHz PN generator would demonstrate the viability of broadband communication links.

The third phase was to design and develop an inphase and quadrature receiver for the channel sounder, implementing as much as practical on printed circuit boards, while being attentive to the overall goal of reducing the system size. This new receiver would replace two of the bulkiest components then in use on the channel sounder—the spectrum analyzer and digital oscilloscope—with a unit that was not only more compact, but added increased functionality to the channel sounder as well. The inphase and quadrature output of the receiver could then be digitized, and the magnitude and phase response of the complex channel transfer function as well as the Doppler spectrum can be calculated (see Chapter 2).

Finally, a brief measurements campaign was conducted to verify the operation of the upgraded channel sounder as well as investigate wideband in-building propagation at 2.5 & 60 GHz. This campaign investigated in-building links such as hallways, cluttered office areas, and non-line of sight propagation through walls and doors. These communication links are an active area of research, and this data will be very beneficial to engineers that are developing future broadband wireless systems.

1.5 Thesis Overview

The design and implementation of an ultrabroadband, high-resolution channel sounder capable of characterizing the complex transfer function of a wireless channel is presented in this thesis. The design of this measurement system requires basic background knowledge of wireless propagation, and channel measurement techniques, and will be discussed in Chapter 2.

Next is a discussion regarding the central issue in this research work: the design of a receiver capable of recording magnitude and phase measurements of the channel impulse response. In many cases recovery of the phase of a received signal is simple; however, in the case of this measurement system the goal was to determine the phase of the received signal relative to the phase of the signal at the transmitter, so that the only variable capable of affecting the phase of the transmitted signal is the channel. Measuring phase perturbations imparted by only the channel is a task that is difficult at lower frequencies and bandwidths, and is non-trivial at the range of frequencies this system is designed to operate in. Therefore, a detailed discussion of system design options, their limitations, and tradeoffs is contained in Chapter 3, along with the design specifications for the completed system.

In Chapters 4 and 5, a detailed discussion of the transmitter and receiver implementation is presented. These chapters will present an overview of the design, and will analyze both transmitter and receiver operation in terms of their various subsystems and extensive details about the system design are presented. Chapter 5 also contains a discussion of the data acquisition and analysis software used to record and display channel measurements.

Once constructed, the system is thoroughly analyzed, tested, and evaluated to determine whether the completed system met its design objectives. The results of this extensive analysis are presented in Chapter 6, along with a summary of the operating requirements and limitations of the system, in addition to a system setup and calibration procedure.

Chapter 7 then presents the results of a brief measurement campaign at 2.5 & 60 GHz using in-building radio links at Virginia Tech. The measurement results not only verify the proper operation of the channel sounder, but also include statistical data about the links which will assist future network engineers design, analyze, and deploy 60 GHz wireless networks.

Chapter 8 summarizes the contributions of this work, as well as suggests several future modifications that could make the system more compact and robust.

Finally, several appendices are attached to this thesis. Appendix A contains schematics for the subsystems that were designed and fabricated as a part of this research. Appendix B contains measurement results and site photographs for each of the 2.5 & 60 GHz measurements discussed in Chapter 7. Appendix C is a user's guide that covers how to set up, calibrate, and operate the channel sounder as well as the post-processing software. This guide is written so that a user can quickly make the system fully operational, in accordance with the objective of creating a rapidly deployable measurement system with minimal overhead involved in setup and calibration. Appendix D contains a description of the file and directory format for raw and post-processed measurement data, as well as a listing of the source code files necessary to run the *LabVIEW Analysis Software* for post-processing channel measurement data.

Chapter 2

Channel Measurement Theory and Application

2.1 The Effects of Multipath on Communication Systems

The reliable operation of a wireless communication system is dependent upon the propagation channel over which it operates, as the channel is the primary contributor to many of the problems and limitations that plague wireless communication systems [30]. Interfering signals, electromagnetic noise, and signal multipath all combine to cause signal distortion, severely limiting the performance of both analog and digital communication systems.

Multipath—a major characteristic of most communication channels—is a propagation phenomenon which results in signals reaching the receiving antenna by two or more paths, creating constructive and destructive interference as well as signal echoes [3, 15]. Multipath is caused by reflection, diffraction, and scattering of electromagnetic waves from various objects in the propagation environment, and a simple example is illustrated in Figure 2.1.

The effects of multipath can manifest themselves in a variety of ways. For example, in a commercial FM radio transmission, multipath causes echoes to be heard in the audio signal; in a Television transmission multipath causes “ghost” images to appear on the screen. For a digital communication system, multipath can be a limiting factor on the maximum data rate that can be transmitted through the channel, and a brief example of the effect of multipath is described below.

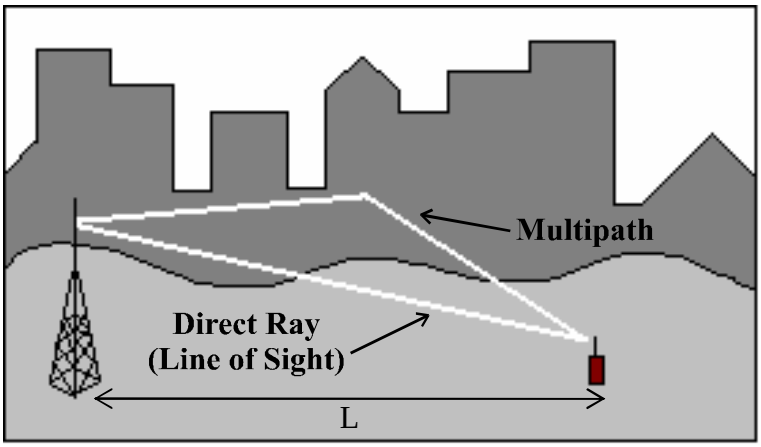

Figure 2.1: Illustration of Line of Sight and Multipath Signal

Consider the simplified case of a continuous wave transmission in a static (non time-varying) channel, consisting of a line of sight signal and a single multipath arriving at a receiver, with transmitter-receiver separation distance L (Figure 2.1). The line of sight signal $s_{LOS}(t)$ and the multipath signal $s_{MP}(t)$ are represented by the following equations.

$$s_{LOS}(t) = A_{LOS}\cos(2p\, f_c t + f_{LOS}) \tag{2.1}$$

$$s_{MP}(t) = A_{MP}\cos(2p\, f_c t + f_{MP}) \tag{2.2}$$

Where: A_{LOS} is the received amplitude of the line of sight signal
A_{LOS} is the received amplitude of the multipath signal
f_c is the carrier frequency of the signal
f_{LOS} is the received phase of the line of sight signal
f_{MP} is the received phase of the multipath signal

Here, the time delay of the multipath signal is manifested as a phase offset from the line of sight signal, comprised of the phase offset due to the difference in path lengths as well as the phase shift due to the reflection . It can be shown that the power received due to the interference of both of these signals is:

$$P_{REC} = \frac{|A_{LOS}|^2}{R} + \frac{|A_{MP}|^2}{R} + \frac{2|A_{LOS}||A_{MP}|}{R}\cos(f_{MP} - f_{LOS}) \tag{2.3}$$

Where: R is the impedance of the antenna

As equation 2.3 shows, when the line of sight signal and the multipath signal interfere destructively, there is a significant decrease in the received power. In the worst case—where the

amplitude of the multipath signal is equal to that of the line of sight signal and there is a 180° phase difference between the two signals—the received power level goes to zero, and the receiver experiences a "fade". It is also interesting to note that in the case of constructive interference, the received signal power experiences a net increase equal to quadruple that of a line of sight component.

The above example can be expanded slightly to the case of a mobile receiver, where the channel is no longer static. As the mobile moves about the environment, it will see variations in the phase of the received signals caused by varying transmitter-receiver separation distance. The time-varying behavior of the wireless channel can be mathematically described by utilizing to the following two-step process developed by Bello [29]. First, the motion of the mobile is discretized into time steps of length Δt which are short enough that the received signal level is approximately constant and the channel may be considered approximately static. In the time Δt the mobile will move a distance $\Delta \ell$, from its original location (Figure 2.1) to a second location, such that the resulting transmitter-receiver separation distance is $L + \Delta \ell$ (Figure 2.2). The received power at the second location is then:

$$P_{REC}(t_0 + \Delta t) = \frac{\left|A_{2,LOS}\right|^2}{R} + \frac{\left|A_{2,MP}\right|^2}{R} + \frac{2\left|A_{2,LOS}\right|\left|A_{2,MP}\right|}{R}\cos(f_{2,MP} - f_{2,LOS}) \qquad (2.4)$$

Where:

$A_{2,LOS}$ is the received amplitude of the line of sight signal at the second location ($L + \Delta \ell$)

$A_{2,MP}$ is the received amplitude of the multipath signal at the second location

$f_{2,LOS}$ is the received phase of the line of sight signal at the second location

$f_{2,MP}$ is the received phase of the multipath signal at the second location

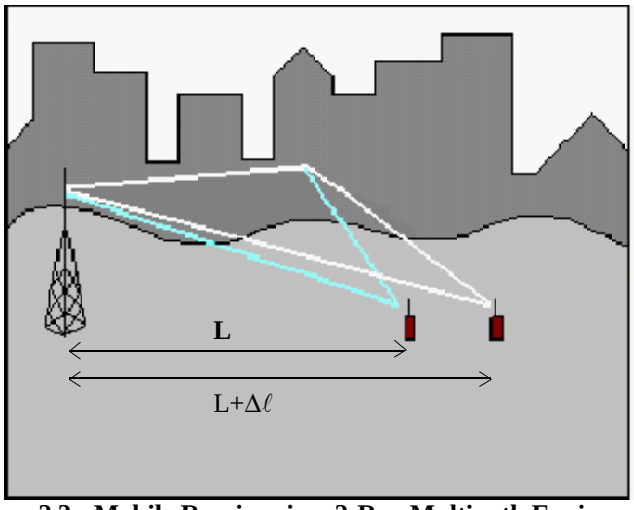

Figure 2.2: Mobile Receiver in a 2-Ray Multipath Environment

Repeating the process again, the receiver moves another $\Delta\ell$ to a third location (such that the resulting transmitter-receiver separation distance is $L+2\Delta\ell$), in one time step of length Δt, whereupon another snapshot in time is observed. At this new instant in time, $t_0+2\Delta t$ the received power will be:

$$P_{REC}(t_0+2\Delta t) = \frac{|A_{3,LOS}|^2}{R} + \frac{|A_{3,MP}|^2}{R} + \frac{2|A_{3,LOS}||A_{3,MP}|}{R}\cos(f_{3,MP}-f_{3,LOS}) \quad (2.5)$$

Therefore, the time-varying received power as the receiver moves around a local area can be approximated by the following equation:

$$P_{REC}(t_0+n\Delta t) = \frac{|A_{n,LOS}|^2}{R} + \frac{|A_{n,MP}|^2}{R} + \frac{2|A_{n,LOS}||A_{n,MP}|}{R}\cos(f_{n,MP}-f_{n,LOS}) \quad (2.6)$$

Where: $P_{REC}(t_0+n\Delta t)$ is the received power at time step $n\Delta t$, for a transmitter-receiver separation distance $L+n\Delta\ell$

$A_{n,LOS}$ is the received amplitude of the line of sight signal at the n^{th} location ($L+\Delta\ell$)

$A_{n,MP}$ is the received amplitude of the multipath signal at the n^{th} location

$f_{n,LOS}$ is the received phase of the line of sight signal at the n^{th} location

$f_{n,MP}$ is the received phase of the multipath signal at the n^{th} location

The above example can be generalized for the case where a user is moving through a field of N multipath components, whose magnitudes and phases combine as vectors to produce a composite time-varying received power. The motion of the receiver is divided into discrete time steps of Δt during which the receiver will move a distance $\Delta \ell$. The time step is chosen small enough so that the channel can be approximated as either static or Wide Sense Stationary during the interval Δt. To simplify the mathematics, Bello assumes that contributions from multipath signals arriving with different time delays are uncorrelated, so that the overall wireless channel may be approximated as Wide Sense Stationary with Uncorrelated Scatterers (WSSUS) [8, 29].

Unfortunately, time-varying received power is not the only consequence of moving through a field of multipath signals. In addition, the mobile receiver will experience two other important deleterious effects: Doppler Spreading and time dispersion.

2.1.1 Doppler Spreading

Doppler spreading is characteristic of a dynamic channel, where scatteres such as the transmitter, receiver, or objects in the propagation environment are mobile (whereas in the static channel scatterers are stationary), resulting in Doppler frequency shifts on the line-of-sight and multipath signals [12]. The motion of scatterers in the environment leads to time varying phase shifts on the individual reflected signals. When multiple signals arrive at the receiver, all with different Doppler shifts, the resulting composite signal (the vector sum of the line-of-sight signal and all multipath signals) will exhibit a time-varying amplitude [67]. Additionally, the time-varying phase shift imparted on the reflected signals will produce a random phase modulation, usually called random FM (as the derivative of a time-varying phase results in frequency modulation) [12, 30].

2.1.2 Time Dispersion

Time dispersion of the received signals is caused by various multipath signals arriving at different time delays and results in “echoes” of the signal in the time domain. Time dispersion will manifest itself as the aforementioned echoes in FM broadcast, ghost images in TV transmission, or intersymbol interference in digital communication systems [17, 35, 37, 38]. The time dispersive effects of a channel also result in another very important effect: a non-constant frequency response of the channel [26]. To understand why, consider the following simple

example of a 2-ray multipath model consisting of a line of sight signal and a single time-delayed multipath arriving at a receiver, as represented in the following fashion:

$$s_{RX} = s_{LOS}d(t) + s_{MP}d(t-t) \tag{2.7}$$

Where:
- s_{LOS} is a complex coefficient representing magnitude and phase of the line of sight signal
- s_{MP} is a complex coefficient representing magnitude and phase of the multipath signal
- $d(t)$ is the Dirac Delta function
- t is the time delay of the multipath signal in seconds

Equation 2.7 is a simple but powerful manner of showing the amplitude and time delay of the multipath signal (or signals in a more general case) relative to the line of sight signal. Since the time and frequency domains may be related by the Fourier transform, the frequency domain representation of 2.8 is given as [26]:

$$S_{RX}(w) = S_{LOS} + S_{MP}\mathrm{e}^{-j2p\,ft} \tag{2.8}$$

As seen in Figure 2.3, not only is the frequency response non-constant, but changing the delay time t of the multipath signal will result in changing frequency responses of the channel, a phenomenon known as frequency selectivity. As more multipath signals with different time delays are introduced, the frequency response will become increasingly irregular, resulting in increased distortion of the received signal. The distortion of the signal spectrum becomes an important phenomenon when operating wideband communication systems; as different frequencies in the transmitted signal will be affected differently by the channel, the received signal will require equalization to reverse the distortion imparted by the channel [12].

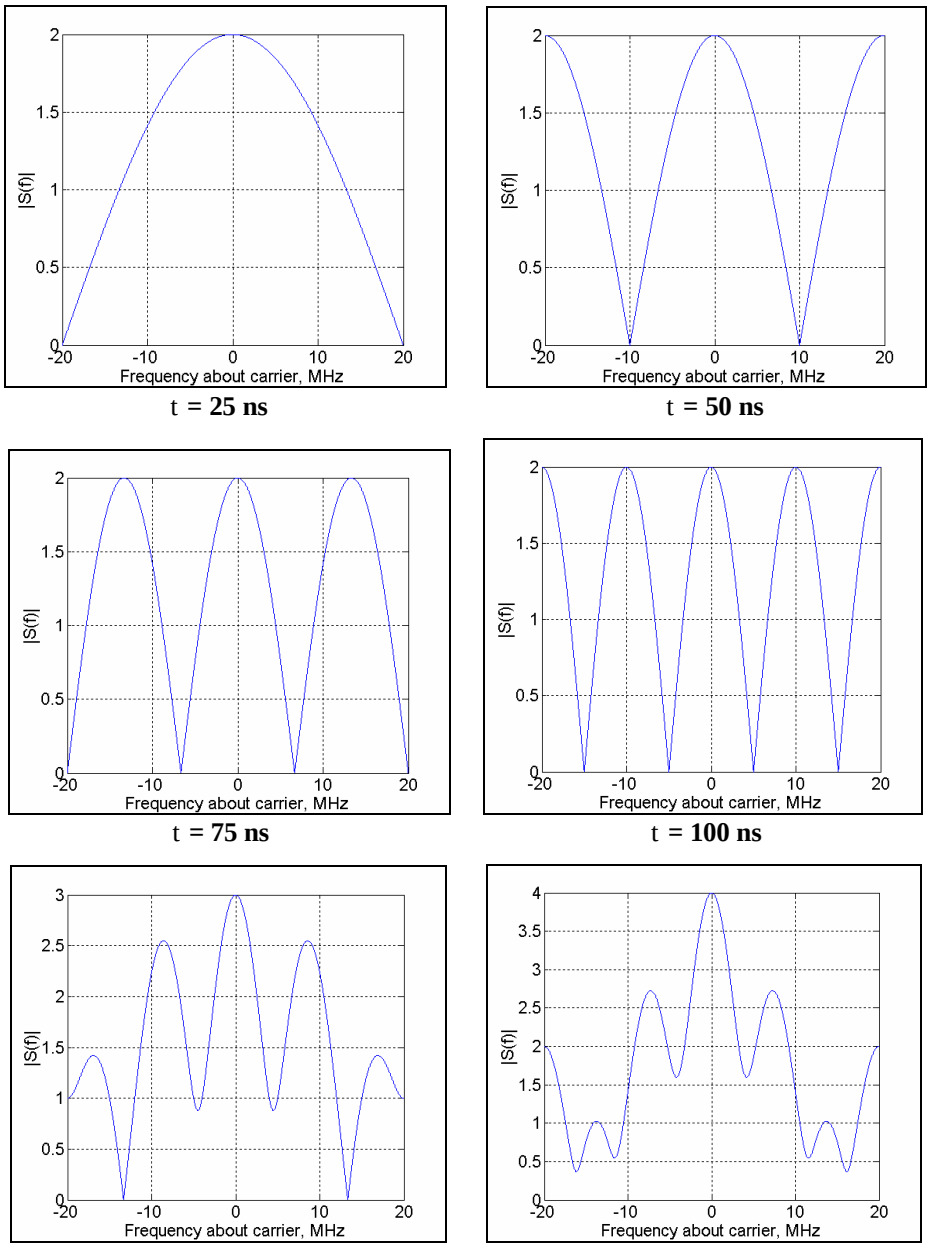

t = **25 ns** t = **50 ns**

t = **75 ns** t = **100 ns**

Two Multipath Signals **Three Multipath Signals**

t_1 = **25 ns,** t_2 = **125 ns** t_1 = **25 ns,** t_2 = **125 ns,** t_3 = **150 ns**

Figure 2.3: Channel Frequency Response for Various Multipath Time Delay and Number of Multipath

2.1.3 Small Scale Fading

Time-varying received power, spreading of the signal spectrum caused by Doppler spreading, and time dispersion are known as small-scale fading effects, caused by two or more interfering multipath signals arriving at the receiver with slightly different amplitudes and propagation times. These signals will then combine as vectors to yield fluctuations in received

amplitude and phase. These effects are considered small-scale because they characterize the channel when the motion of the receiver is on the order of ½ wavelengths during a short period of time [12]. On a macroscopic level, the small-scale effects are averaged out to produce a received power dependent upon the transmitter-receiver separation distance, frequency of operation, and terrain [12, 26]. A general comparison of small-scale vs. large-scale effects can be seen in Figure 2.4.

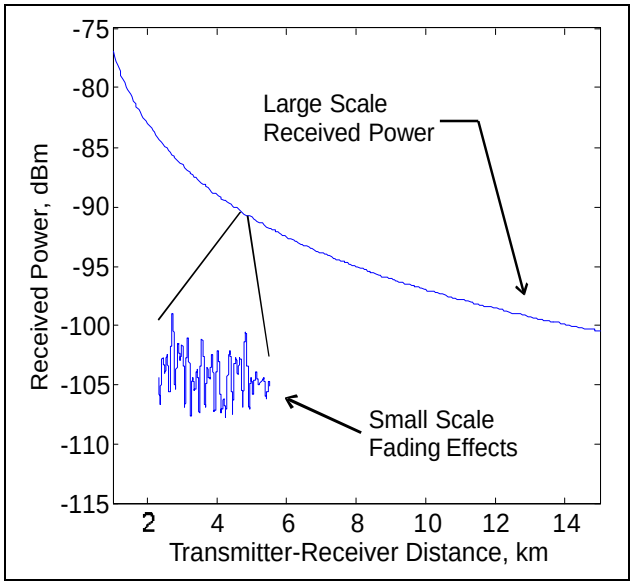

Figure 2.4: Large and Small Scale Response of a Channel

2.2 Transfer Function Representation

The key to designing a communication system that can operate in a multipath environment lies in understanding and predicting the presence of multipath [12, 22]. A wireless propagation medium is, in general, a highly dynamic environment, consisting of mobile users & scatterers, varying terrain, and weather phenomena. Strictly speaking, these channels are non-stationary in nature; however, they may be modeled as randomly time-variant linear filters, so that the mathematical functions describing these channels reduce to random processes [29]. The transfer function representation then allows the channels to be characterized statistically, in addition to allowing them to be described by a time-varying transfer function (impulse response) [12, 17, 29]. In order to characterize such channels, two assumptions are required: that channel fluctuations are slow with respect to the measurement acquisition time, and that the channel is

WSSUS [17, 29]. Under these conditions, the impulse response of such a channel is given below:

$$h(t,t) = \sum_{i=1}^{N} a_i(t) e^{-jq_i(t)} d(t - t_i(t)) \tag{2.9}$$

Where: $h(t,t)$ is the time-varying impulse response of the channel

$a_i(t)$ is the time-varying magnitude of the i[th] signal, representing free-space propagation loss plus any other losses imparted by the channel

$q_i(t)$ is the time-varying phase of the i[th] signal, representing the free-space propagation phase shift plus any phase shift imparted by the channel

$t_i(t)$ is the time-varying *excess delay* of the i[th] signal

Conceptually, Equation 2.9 represents the arrival of a line of sight signal (with some amplitude and phase distortion), and a series of multipath signals (also with associated amplitude and phase distortion), each arriving at some time delay, t_i later (see Figure 2.5 for an example). In other words, it represents the channel response to a unit impulse at time t, evaluated at time delay t from the time of occurrence of the impulse [17, 29, 39]. The exact amplitude, phase, and time delay of each of the multipath components will vary with changes in the channel (e.g. mobile scatterers); hence Figure 2.5 only represents a snapshot of the channel for an impulse occurring at a particular t.

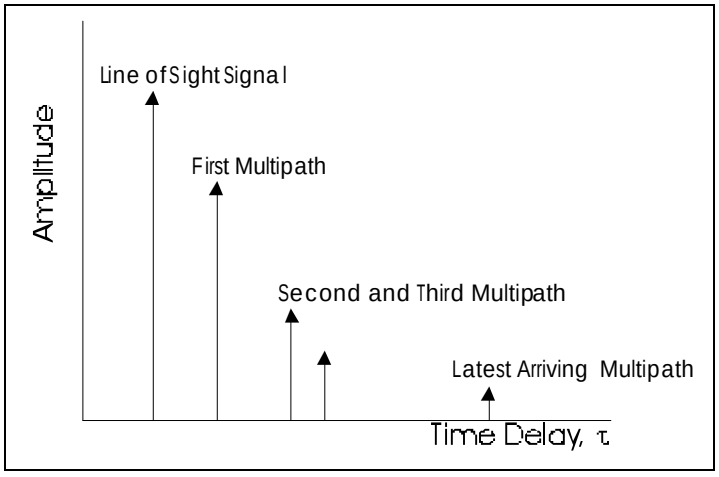

Figure 2.5: Example of Received Multipath Signals

2.3 Transfer Function Measurement

The transfer function representation of a system states that for a given input $x(t)$ to a wireless channel, the output $y(t)$ is the convolution of $x(t)$ with the time-variant channel impulse response $h(t,t)$ (Figure 2.6 and Equation 2.10). Physically, $h(t,t)$ represents the response of the channel t seconds in the future to an excitation at time t [29].

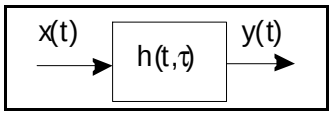

Figure 2.6: Graphical Representation of Channel Transfer Function

$$y(t) = \int_{-\infty}^{\infty} h(t,t)x(t)dt \tag{2.10}$$

Knowing $h(t,t)$ for a particular wireless communication channel allows engineers to predict the small-scale fading distortion the receiver will experience and compensate for it by designing equalizers, matched filters, or RAKE receivers.

Measuring the transfer function of a system is, in general, accomplished by setting $x(t) = d(t)$ (where $d(t)$ is the Dirac delta function) [11]. The sifting property of the delta-functions will cause the output, $y(t)$ to be equal to the transfer function, $h(t,t)$. In practice, a true delta function is impossible to obtain, since it would require generating a signal of infinite amplitude and infinitesimal duration (corresponding to an infinitely large bandwidth). Therefore, several methods have been developed to measure $h(t,t)$ of a wireless channel by approximating an impulse function, and are listed below [2, 12, 17, 30].

- Periodic Pulse (also know as Direct Pulse)
- Frequency Domain
- Pulse Compression
- Swept Time Delay Crosscorrelation

It should be noted that, technically, the output of the measurement system is not technically $h(t,t)$, but rather $h(t,t)$ convolved with the shape of the pulse that is used to sound the channel [30]. However, if the bandwidth of the channel sounder is sufficiently large compared to the channel being evaluated, then the output of the channel sounder may be approximated as $h(t,t)$ for all practical purposes.

2.3.1 Periodic Pulse

The Periodic Pulse method approximates a delta function by using a pseudo-impulse at the transmitter (i.e. a short-duration RF signal) to excite the channel [2, 12, 17], illustrated in Equations 2.11, 2.12, and Figure 2.7.

$$x(t) = \cos(2pf_c t)[u(t) - u(t - t)] \tag{2.11}$$

$$u(t) = \begin{Bmatrix} 0 & t < 0 \\ 1 & t \geq 0 \end{Bmatrix} \tag{2.12}$$

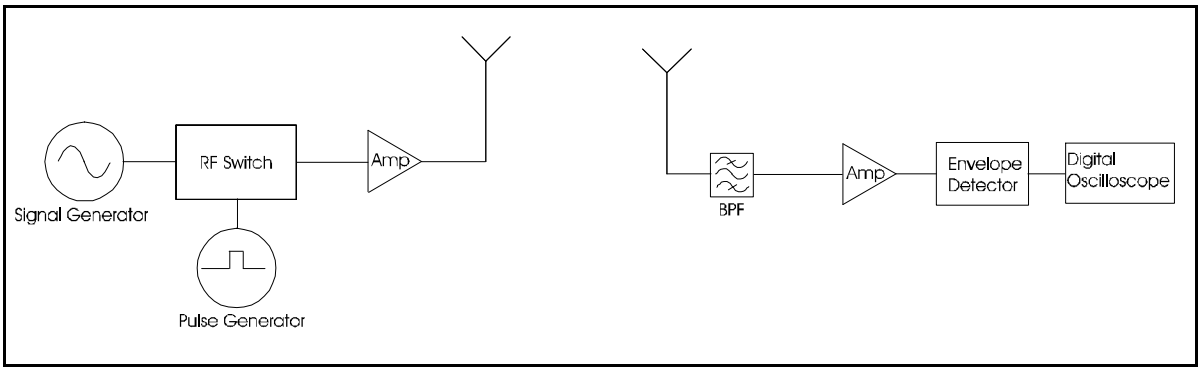

Figure 2.7: Block Diagram of a Periodic Pulse RF Channel Sounder

The operation of the Periodic Pulse system is very basic; the pulse generator will activate the RF switch for a short period of time, causing it to transmit a few cycles of a carrier signal, which corresponds to a narrow pulse in the frequency domain. The received signal is amplified, detected, and displayed on a digital oscilloscope. The first measurements made with a periodic pulse channel sounder were done by Young and Lacy [27] at 450 MHz in New York City. The advantages and limitations of the periodic pulse channel sounder are listed below.

Advantages

- Relatively simple implementation, requiring only an RF switch, signal generator, and pulse generator.
- Provides multipath resolution equal to the equal to the width, τ, of the pulse.
- The received signal can be coherently demodulated to provide Doppler Spectra.

Limitations

- The bandpass filter at the receiver must have a very wide bandwidth ($\frac{1}{2t}$ Hz [2]), making it susceptible to noise and interference.
- High resolution of multipath signals requires a high-speed RF switch and pulse generator.

- The system requires a high peak-to-average power ratio to detect weak multipath, however, most transmitters are peak power limited, thus limiting the dynamic range of the system.

The use of periodic pulse channel sounders was more prevalent in the past, but their use has largely been replaced by Frequency Domain and Swept Time Domain Crosscorrelation systems.

2.3.2 Frequency Domain

The Frequency Domain method of channel sounding, described in [2, 12, 17, 21, 30], takes advantage of the dual relationship between the time domain and frequency domain. As shown in Figure 2.8, a Vector Network Analyzer (VNA) controls a signal generator, which scans through a band of frequencies in discrete steps. The VNA measures $S_{21}(f)$ at each frequency step, and the resulting frequency response is converted into the time domain impulse response by the use of the Inverse Fourier Transform.

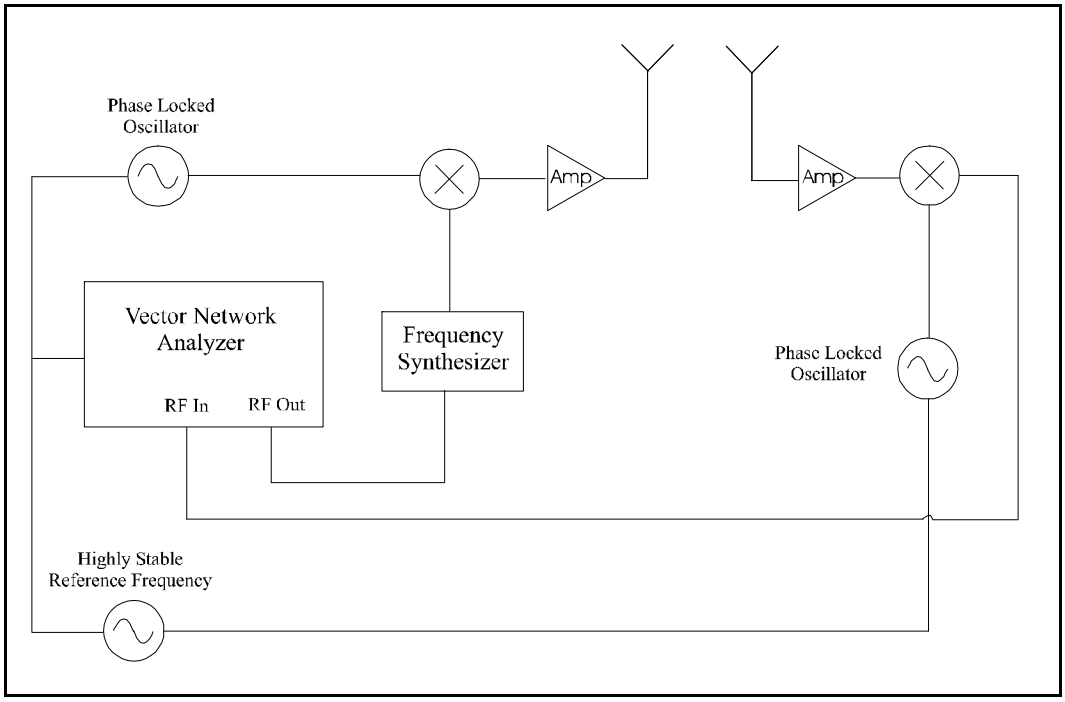

Figure 2.8: Block Diagram of a Swept Frequency Channel Sounder

The Swept Frequency type of channel sounder has many advantages when compared to the Periodic Pulse channel sounder as well as some important limitations, all of which are listed below:

Advantages

- Simplicity of implementation: all that is needed are the VNA, a signal generator capable of operating across the range of frequencies of interest, and antennas.
- High resolution of multipath, proportional to the frequency step size.
- Reduced effects of non-linearites in active devices [21].

Limitations

- The VNA must be physically connected to the transmitter and receiver, making it useful only for channel links where the cable length is practical (e.g. indoor or short outdoor channels).
- The frequency sweep takes a finite amount of time to complete, particularly for large bands or small frequency step sizes, meaning that the system makes non-real time measurements, which has two important implications:
    1. The Inverse Fourier Transform is performed only at the end of the frequency sweep, which makes the Swept Frequency system useful only for either time-invariant channels, or channels which vary slowly with respect to the step time. A dynamic channel would change far too rapidly for the measurement system to characterize it in a meaningful way.
    2. No Doppler shift or spectra can be obtained from the system due to the frequency stepping technique [2, 17, 18].

Despite these limitations, the Frequency Domain technique remains popular due to the simplicity of implementation, and its use is still prevalent [18, 19, 20, 21, 33, 36, 37].

2.3.3 Pulse Compression Technique

The Pulse Compression Technique uses a white noise signal to excite a wireless channel, and the receiver cross-correlates the output of the channel with an identical but time-delayed version of the white noise signal. The result is proportional to $h(t,t)$ evaluated at a particular τ. Understanding the operation of Pulse Compression system involves understanding white noise signals and how their autocorrelation properties may be used to measure the impulse response of a wireless channel.

White Noise

A white noise signal is essentially a random sequence, which Viterbi [9] defines as a sequence of outcomes of independent Bernoulli trials in succession, with two events, “1” and “0”

that each occur with probability ½. These sequences, known in probability theory as Bernoulli sequences, have three fundamental properties [9]:

1. The relative frequencies of "1" and "0" is each ½.
2. Run lengths (a series of all "1's" or "0's" in the sequence) make up $\frac{1}{2^n}$ of the overall sequence, where n is the length of the run. Thus, the series "11" would make up $\frac{1}{4}$ of the sequence, the series "111" would make up $\frac{1}{8}$, and so forth.
3. The autocorrelation of the sequence is an impulse function weighted by the average power in the white noise signal:

$$R_{XX}(t) = N_0 d(t) \tag{2.13}$$

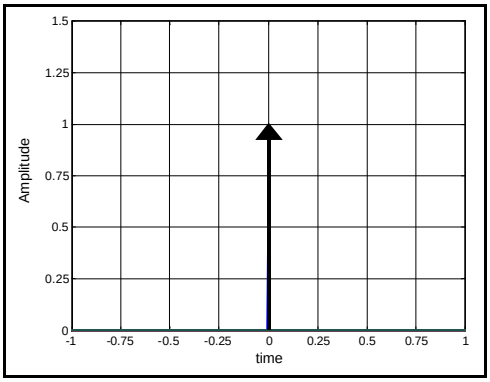

Figure 2.9: Plot of $R_{xx}(t)$, for N_0=1

Impulse Response Measurement using White Noise

Using a white noise signal to measure the impulse response of a wireless channel simply involves transmitting the noise signal and cross-correlating the received signal with a time-delayed version of the white noise signal [8, 17, 21], as illustrated in Figure 2.10.

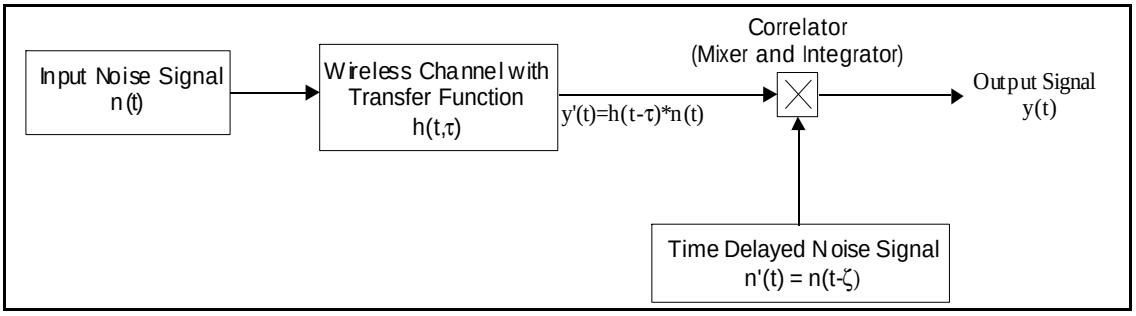

Figure 2.10: Basic Measurement System to Measure the Impulse Response Using the Correlation Properties of White Noise

The signal $y'(t)$ is the convolution of the white noise signal $n(t)$ and the channel transfer function $h(t,t)$, which is shown mathematically below. Note that if the channel impulse

response becomes time-invariant, then $h(t,t)$ becomes $h(t-t)$, and 2.14 converts into a standard convolution integral.

$$y'(t) = \int_0^\infty h(t,t)n(t)dt \tag{2.14}$$

Where: $h(t,t)$ is the channel impulse response
$n(t)$ is the input noise signal

At the correlator, a cross-correlation operation is performed between $y'(t)$ and $n'(t)$, where $n'(t) = n(t-z)$ is a replica of $n(t)$ that has been time-delayed by z. Recall that the definition of the cross- correlation operation is given by [25]:

$$R_{XY}(t_1,t_2) = E[x(t_1)y^*(t_2)] \tag{2.15}$$

Where: $E[...]$ is the Expected Value operator
$x(t_1)$ is the first signal at time t_1
$y^*(t_2)$ is the complex conjugate of the second signal at time t_2

Assuming that the noise signal is purely real, the complex conjugate operation may be ignored. After some algebra, the output of the correlator is:

$$y(t) = \int_0^\infty h(t,t)E\left[n(t)n(t-z)\right]dt \tag{2.16}$$

Recall the definition of the autocorrelation of a signal is given by [25]:

$$R_{XX}(t_1,t_2) = E[x(t_1)x^*(t_2)] \tag{2.17}$$

If the autocorrelation is dependent only upon the time difference $z = t_2 - t_1$, then it may be rewritten as:

$$R_{XX}(z) = E[x(t)x^*(t-z)] \tag{2.18}$$

Therefore, Equation 2.16 becomes:

$$\begin{aligned} y(t) &= \int_0^\infty h(t,t)R_{NN}(z)dt \\ y(t) &= \int_0^\infty h(t,t)N_0 d(z)dt \\ y(t) &= N_0 h(t,z) \end{aligned} \tag{2.19}$$

Thus, the output of the measurement system is a weighted version of the transfer function of the channel which may be evaluated for a particular delay time, ζ, where $\zeta > 0$.

Two major problems with white noise approach are immediately obvious:

(1) The white noise technique requires a priori knowledge of $n(t)$, which is by definition a random signal.

(2) The output $y(t) = N_0 h(t, z)$ is a function of ζ, and to measure $h(t, t)$, the value ζ (which represents the time offset of the two noise sequences) would have to be adjusted to see all of $h(t, t)$. This may require significant processing time and may inhibit real-time measurement of a dynamic channel.

These limitations may be overcome in a practical sense by the use of a deterministically generated high-speed antipodal pseudo-random noise (PN) signal that has autocorrelation properties that approximate those of a white noise signal [9].

Basic Principles of Pseudonoise (PN) Signals and PN Generator Operation

Many authors [7, 8, 9, 10] have treated the subject of PN signals in more rigorous detail than what is presented in this thesis; therefore, the following is a summary of the mathematical theory behind random and pseudo-random noise, how a PN generator operates, and how it may be used to measure the impulse response of a wireless channel.

Intuitively, a pseudo-random sequence behaves statistically like a purely random sequence, with the exception that the PN sequence is finite-length, periodic in time, and the contents are determined a priori. Though many types of pseudo-random sequences exist, the one that is of the most interest in this thesis is the Maximal Length Linear Shift Register sequence, or MLSR sequence.

Figure 2.11 illustrates the basic block diagram of a MLSR pseudo-random noise sequence generator. The PN Generator consists of a series of r shift registers with feedback taps and a modulo-2 adder (add without carry). The shift registers are clocked from a common clock line every T_c seconds. The feedback taps can be arranged in a variety of orders to produce different output codes. The particular taps necessary to generate a variety of MLSR sequences have been tabulated in [7]. The MLSR codes are distinguished from other PN codes in that they have the following properties [7, 9]:

1. The MLSR sequence has a period of N chips, with $N = 2^r - 1$.

2. The statistical distribution of "1's" and "0's" is the same as in the random sequence, with the exception that the total number of "1's" is always one larger than the total number of "0's", independent of the length of the code.
3. The modulo-2 sum of any m-sequence with a shifted version of itself produces another shifted version of the same sequence.
4. All possible r-bit words will appear in the sequence exactly once, except for the all-zeros combination.
5. The autocorrelation of the PN sequence is given by $R_{xx}(\tau)$

$$R_{xx}(t) = -\frac{1}{N}\sum_{\ell=-\infty}^{\ell=\infty}\left(1+\frac{1}{N}\right)\Delta\left(\frac{t-\ell NT_c}{T_c}\right) \tag{2.20}$$

T_c *is the clock rate* (*also known as the chip rate*)

$$\Delta\left(\frac{t}{T}\right) = \begin{cases} 1-\frac{|t|}{T}, & |t| \le T \\ 0, & |t| > T \end{cases}$$

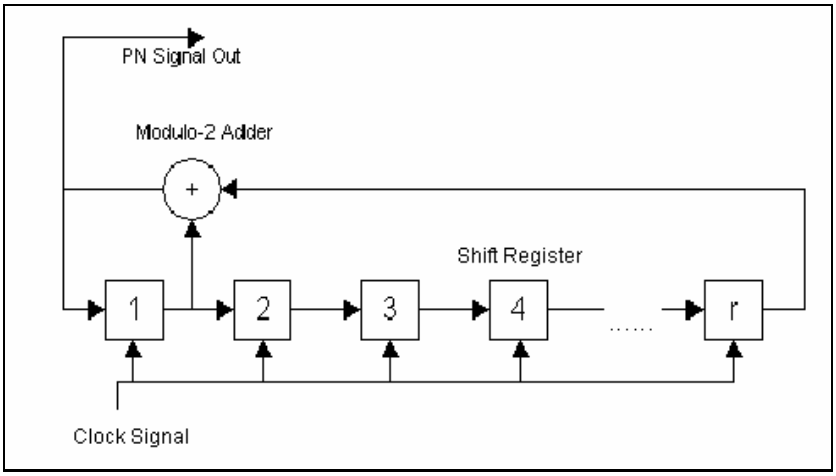

Figure 2.11: Block Diagram of a PN Generator

$R_{xx}(\tau)$ is plotted in Figure 2.12, and shows a periodic waveform with triangular pulses of width $2T_c$ repeated every NT_c seconds with a correlation height of $-\frac{1}{N}$ occurring between pulses.

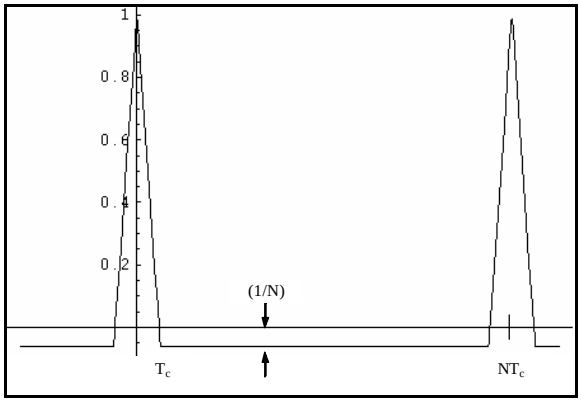

Figure 2.12: Autocorrelation of PN waveform

When evaluated statistically [7, 9], these MLSR sequences can be shown to behave like white noise for practical purposes.

Impulse Response Measurements using Pseudo-Random Sequences

The MLSR PN sequence is useful for a number of applications, one of which is making multipath propagation measurements. Using the pulse compression technique detailed above, the PN signal is transmitted across a wireless channel and the received waveform is recorded and cross-correlated with an identical PN signal that has been time delayed by some amount ζ. The receiver then steps through a series of time delays until it reaches the end of the receiver PN sequence. The resulting output is then proportional to $h(t,t)$. As mentioned above, the correlation operation may require significant processing time and power, making it unsuitable for characterizing a dynamic channel. This limitation may be overcome by use of the Swept Time Delay Crosscorrelation technique.

2.3.4 Swept Time Delay Crosscorrelation

The Swept Time Delay Crosscorrelation technique, also known as the Sliding Correlator technique, operates by taking advantage of the periodic autocorrelation properties of the PN sequence. By clocking the receiver PN generator slightly slower than the transmitter PN generator, the two sequences will "slide" against each other. When the sequences are lined up in time, the received signal will maximally correlate with the receiver's PN generator. At that instant, the transmitted spread-spectrum signal will collapse back into its original bandwidth. When the PN codes are uncorrelated, the received signal will be spread into a bandwidth at least as large as the transmitted signal, allowing a simple low-pass filter to reject the broadband noise [2]. By "sliding" the two signals against each other, the receiver is able to measure the amplitude and delay of any multipath signals in the propagation environment (since signals with different multipath delays will maximally correlate at different times). The first channel measurements using a Swept Time Delay Crosscorrelation channel sounder were obtained by Cox [7] in New York City at 910 MHz.

Recall that using the basic pulse compression technique, the output of the measurement system was $y(t) = N_0 h(t,z)$ which was dependent upon ζ, the time difference between the two

identical noise signals. In the case of a sliding correlator, the sliding operation inherently varies ζ, providing real-time correlation processing, which is shown mathematically below.

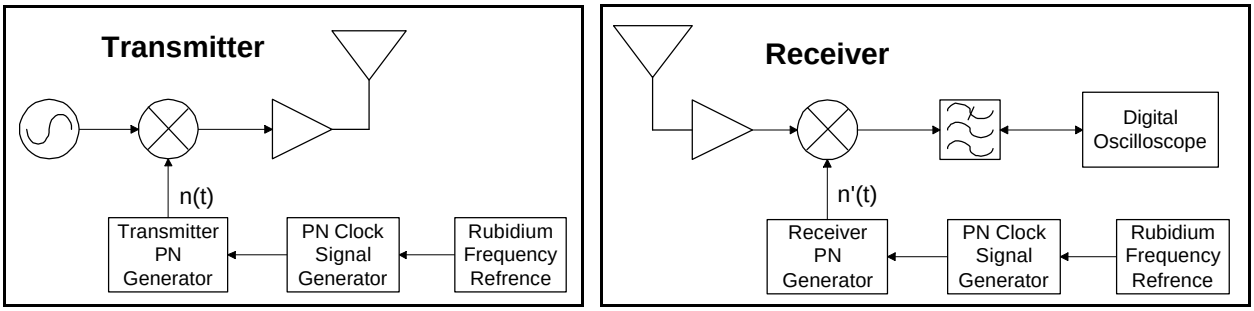

Figure 2.13: Block Diagram of a Sliding Correlator Channel Sounder

Consider the system of Figure 2.13, where the signal $n(t)$ and $n'(t)$ are identical MLSR pseudo-noise signals, except that $n'(t)$ is clocked at a slightly slower frequency, represented by:

$$n'(t) = n\left(t - \frac{f_R}{f_T} t\right) \tag{2.21}$$

Where: f_T is the clock frequency of the transmitter PN signal
f_R is the clock frequency of the receiver PN signal

The signal at the output of the correlator is then:

$$y(t) = \int_0^\infty h(t,t)E\left[n(t)n(t - \frac{f_R}{f_T} t)\right]dt \tag{2.22}$$

Since the pseudo-noise signals are purely real functions, $E\left[n(t)n(t - \frac{f_T}{f_R} t)\right]$ becomes $R_{NN}(\frac{f_R}{f_T} t)$, meaning the output signal $y(t)$ is now:

$$y(t) = \int_0^\infty h(t,t)R_{NN}\left(\frac{f_R}{f_T} t\right)dt \tag{2.23}$$

Equation 2.23 is the transfer function of the wireless channel convolved with the autocorrelation of the transmitter and receiver PN codes. To see how Equation 2.23 may be used in a measurement system, consider the impulse response of a WSSUS wireless channel from Equation 2.9, which is represented by a series of N impulse functions, each with an associated magnitude and phase. Substituting into 2.13 above, and using the sifting properties of the delta function, the result is:

$$y(t) = \sum_{i=1}^{N} a_i e^{-jq} R_{NN}\left(\frac{f_R}{f_T} t - t_i(t)\right) \tag{2.24}$$

One item of note is that the term $\frac{f_R}{f_T}t$ is not constant, and represents a slowing in time of the autocorrelation function, known as *time dilation.* Time dilation has two important effects on the measurement system. The first is that the value of ζ in Equation 2.19 is now automatically varied and the output of the measurement system becomes a function of time. Second, even though multipath may be arriving at very closely spaced time intervals, which would normally require a very broadband receiver, the effect of time dilation effectively "spreads out" the arrival times of the multipath allowing a narrowband receiver to be used [7]. Under these conditions, the actual impulse response, $h(t,t)$, can now be calculated from the time-dilated output of the measurement system [7, 12], by the use of a parameter called the "slide factor", which is mathematically defined as:

$$k = \frac{f_T}{f_T - f_R} \tag{2.25}$$

Where: k is the slide factor

The slide factor represents a multiplier of the time scale at the receiver. For example, if a channel sounder is using a 100 MHz PN code at the transmitter, and a slide factor of k=10,000 (99.99 MHz PN code at the receiver), then the 10 nanosecond wide crosscorrelation pulse will be displayed as a 0.1 millisecond ($10 \cdot 10^{-9} \times 10,000$) wide pulse. Therefore, data post-processing must be performed on all recorded impulse response measurements in order to convert them from time-dilated measurements back into actual-time measurements.

One other advantage to using the sliding correlator is the increase in the Signal to Noise Ratio (SNR) due to the process gain of the PN codes. Dixon [3] defines process gain for a spread spectrum signal as:

$$G_P = 10 \log\left(\frac{0.88 f_{PN}}{R_{\text{info}}}\right) \tag{2.26}$$

Where: G_P is the process gain

f_{PN} is the clock frequency of the PN signal

R_{info} is the data rate in the baseband signal

The Numerator, $0.88 f_{PN}$, represents the 3 dB baseband bandwidth of the PN Sequence

For a sliding correlator channel sounder, it can be shown [12] that the baseband data rate is equal to the frequency difference between the PN clocks at the transmitter and receiver. For

example, if the frequency offset was 10 kHz, and the RF bandwidth of the PN code was 400 MHz, then the system would see 45.5 dB of process gain, corresponding to a 45.5 dB improvement in SNR.

In practice, the process gain calculated from Equation 2.26 will overestimate the actual amount of gain realized in the system. To understand why, a useful PN code must have an extremely low bit error rate. A 100 MHz code, for example, would have to produce 3.6×10^{11} bits to operate error-free for one hour, an aggressive number for high-speed digital logic circuits that are highly susceptible to noise. Therefore, the actual amount of realizable process gain will depend upon quality of the PN code as well as its clock speed; therefore, Equation 2.26 represents an upper bound on the amount of realizable process gain in the system.

Unfortunately, the sliding correlator system has three major limitations:

- The individual multipaths are resolvable only to within $\pm T_c$ seconds, meaning that multipaths arriving within $\pm T_c$ will appear as a single aggregate signal. Separating out very closely spaced multipath consequently requires a faster PN code.
- The PN code will repeat itself every NT_c seconds; therefore the repetition time must be longer than the longest expected time delay for multipath in the propagation environment.
- The ideal dynamic range of a spread-spectrum system is limited by the length of the PN code. Amplifier noise, phase noise, I/Q imbalance, and particularly the isolation of the BPSK modulator, will all combine to degrade the dynamic range, so that the actual value will fall short of the idealized value [3, 34].

$$D_R = 20\log_{10}(N) \tag{2.27}$$

Where: D_R is the dynamic range in dB
N is the PN sequence code length

2.3.5 Magnitude and Phase Impulse Response Measurement using the Sliding Correlator Principle

In the discussion of sliding correlator channel sounders thus far, it has been implicitly assumed that the correlator was capable of measuring both magnitude and phase of a transfer function, so that Doppler spectra may be calculated. In practice, measuring magnitude and phase requires implementing a *coherent* receiver similar to the one shown in Figure 2.14.

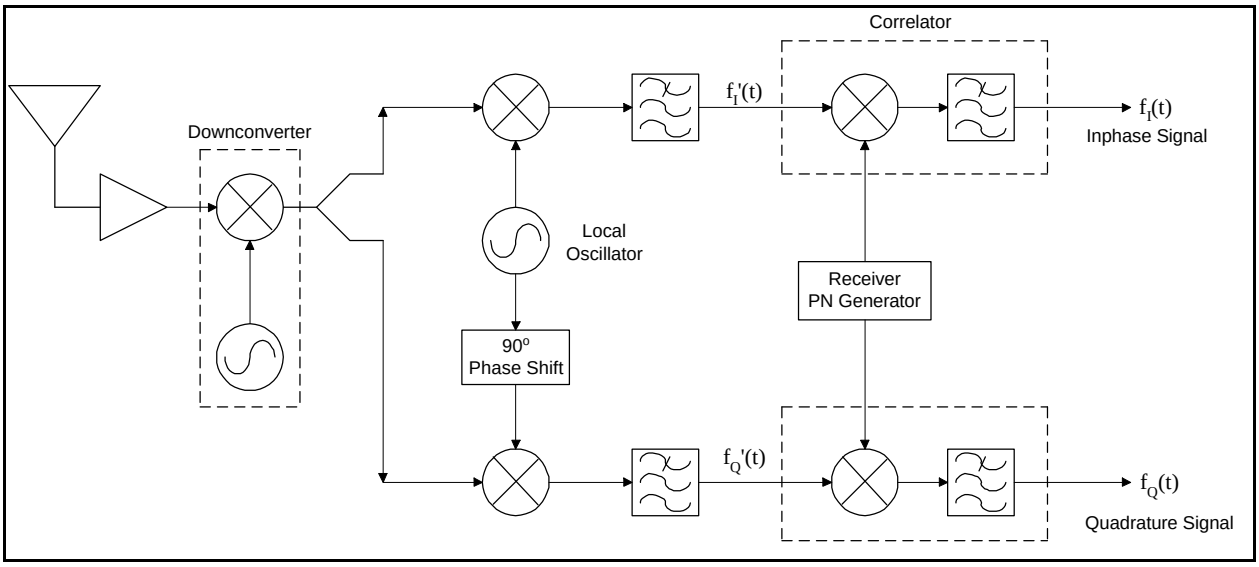

Figure 2.14: Basic Coherent Receiver Design

To understand how the coherent receiver operates, recall that the complex envelope of a wireless transmission can be represented in either the phasor domain or the time domain [31]:

$$v(t) = \mathrm{Re}\left\{R(t)e^{jq(t)}e^{jwt}\right\} \tag{2.28}$$

$$v(t) = x(t)\cos(2p\ f_c t) - y(t)\sin(2p\ f_c t) \tag{2.29}$$

$$R(t) = \sqrt{x^2(t) + y^2(t)} \tag{2.30}$$

$$q(t) = \tan^{-1}\left(\frac{y(t)}{x(t)}\right) \tag{2.31}$$

Where: $v(t)$ is the bandpass complex envelope
$x(t)$ is known as the *inphase modulation* of the complex envelope
$y(t)$ is known as the *quadrature modulation* of the complex envelope
$R(t)$ is the *amplitude modulation* (magnitude) of the complex envelope
$q(t)$ is the *phase modulation* (phase) of the complex envelope

In the case of a sliding correlator channel sounder, recovering the magnitude and phase information of the various multipath means recovering $R(t)$ and $q(t)$ from the received signal using I/Q demodulation.

Figure 2.14 illustrates the basic concept of I/Q demodulation. For the moment, assume that the Local Oscillator at the receiver is exactly synchronized with the Local Oscillator at the transmitter (In practice, local oscillator synchronization is difficult to achieve and will be discussed further in Chapter 3). For the case of a sliding correlator channel sounder, the

transmitted and received waveforms can be represented mathematically in Equations 2.32 and 2.33 [7].

$$V_T(t) = s(t)\cos(2p\ f_c t) \tag{2.32}$$

$$V_R(t) = \sum_i a_i(t)s(t - t_i(t))\cos(2p\ f_c t - 2p\ f_c t_i(t)) \tag{2.33}$$

Where: $V_T(t)$ is the transmitted signal

$s(t)$ is the PN signal

$V_R(t)$ is the received signal, and represents a summation of the line of sight signal plus all received multipath signals.

$a_i(t)$ is the time-varying amplitude of the ith multipath component

$t_i(t)$ is the time-varying delay of the ith multipath component

$s(t - t_i(t))$ is the received PN signal of the ith multipath component. Note that the $t_i(t)$ term represents a shift in the position of the PN code relative to the position of the transmitter PN code

$2p\ f_c t_i(t)$ is the received phase of the ith multipath component. Note that this term represents a phase shift of the multipath signal relative to the line-of-sight transmitted signal.

The received signal is downconverted to an intermediate frequency (IF) signal, which is then split into two separate paths, with the firs`t path being mixed with the Local Oscillator signal and the second path being mixed with a 90° phase shifted version of the Local Oscillator signal. These signals are then correlated with the Receiver PN Generator to yield $f_I(t)$ and $f_Q(t)$. The output of the system is then [7]

$$f_I(t) = \sum_i a_i(t) R_s(\tfrac{t}{k} - t_i(t)) \cos(2p\, f_c t_i(t)) \tag{2.34}$$

$$f_Q(t) = \sum_i a_i(t) R_s(\tfrac{t}{k} - t_i(t)) \sin(2p\, f_c t_i(t)) \tag{2.35}$$

Where: $f_I(t)$ is known as the *inphase correlation function*

$f_Q(t)$ is known as the *quadrature correlation function*

$R_s\left(\tfrac{t}{k} - t_i(t)\right)$ is the autocorrelation function of the PN signal, time dilated by the slide factor *k*, and evaluated at the time delay of the i^{th} multipath component.

These signals can then be combined mathematically into a more useful representation, such as a *Power Delay Profile (PDP)* or *Multipath Phase Response* of the channel, as shown in equations 2.36 & 2.37 below.

$$E(t) = \left|h(t,t)\right|^2 = f_I^2(t) + f_Q^2(t) \qquad scaled\ by\ k \tag{2.36}$$

$$q(t) = \angle h(t,t) = \tan^{-1}\left(\frac{f_Q(t)}{f_I(t)}\right) \qquad scaled\ by\ k \tag{2.37}$$

Where: $E(t)$ is the Power Delay Profile and is mathematically equivalent to the magnitude squared of the channel transfer function.

$q(t)$ is the time varying phase response of the and is mathematically equivalent to the phase of the channel transfer function.

The Power Delay Profile is a plot of the received power and delay times of all multipath components in the channel and is scaled in time by the slide factor k. The Doppler spectrum of the channel is a measure of the spectral broadening of the received signal due to time-varying multipath components. An example Power Delay Profile, measured at 2.5 GHz in the hallway of the 2nd floor of Torgerson Hall at Virginia Tech, as well as Doppler spectrum plot from a 60 GHz receiver moving directly away from the transmitter at a constant velocity of 0.01 m/s are given in Figures 2.15 and 16 below.

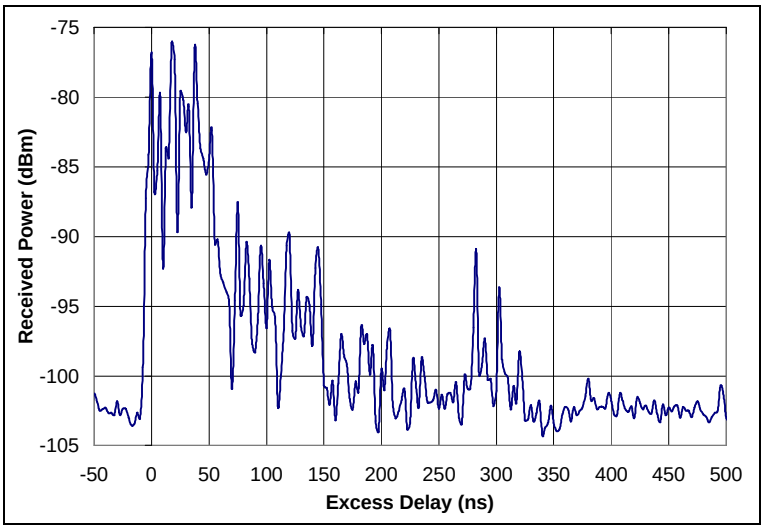

Figure 2.15: Example Power Delay Profile, measured at 2.5 GHz On the 2nd Floor of Torgerson Hall at Virginia Tech

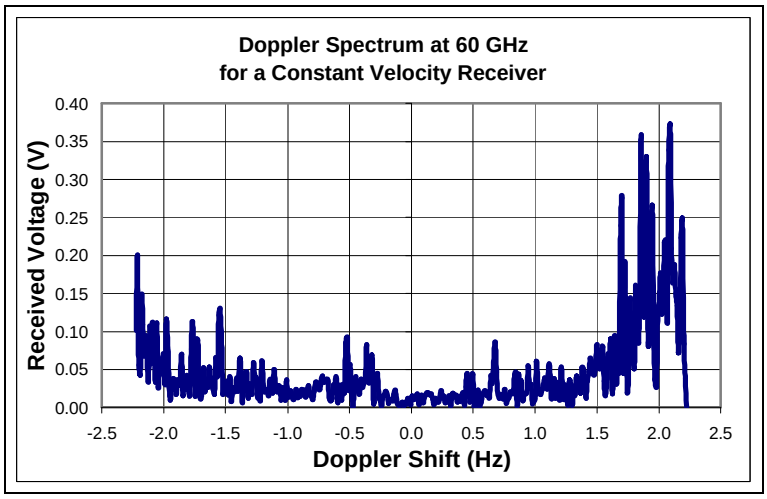

Figure 2.16: Doppler Spectrum Plot for a 60 GHz Receiver Moving at a Constant Velocity of 0.01 m/s

2.4 Information available from Impulse Response Measurements

Software post-processing of the Power Delay Profiles and Envelope Delay Profiles generated by impulse response measurement systems provides a significant amount of information about the channel, including multipath amplitudes and delay times, channel RMS delay spread, Coherence Bandwidth, average path loss, total multipath power gain, and Doppler spectrum (when using a coherent channel sounder). The resulting data can then be used to generate statistical information regarding the channel, allowing engineers to understand and predict how the channel will affect wireless signals.

2.4.1 Multipath Amplitude and Delay

As mentioned in previous sections, the primary output from the channel sounder is a plot of multipath amplitudes and delay times relative to the line of sight signal (see Figures 2.5 & 2.15). Analyzing a number of Power Delay Profiles for a particular propagation environment will allow a communication engineer to statistically predict the relative amplitude and delay times of signal multipath. Based on that analysis, an equalizer or RAKE receiver can be designed to mitigate the effects of destructively interfering multipath.

2.4.2 Channel RMS Delay Spread

Characterizing the channel RMS delay spread helps to determine whether the channel is flat fading (all frequencies within the channel bandwidth experience approximately the same degree of fading) or frequency-selective fading (frequencies within the channel bandwidth will experience various degrees of fading) [13]. A channel can be considered essentially flat fading when the RMS delay spread divided by the symbol period is less than 0.1 [13].

To calculate the RMS delay spread, the mean excess delay and second moment of the excess delay of a Power Delay Profile are calculated using Equations 2.38 and 2.39.

$$\bar{t} = \frac{\sum_i P_i t_i}{\sum_i P_i} \tag{2.38}$$

$$\bar{t}^2 = \frac{\sum_i P_i t_i^2}{\sum_i P_i} \tag{2.39}$$

Where: $\bar{t}$ is the mean excess delay
$\bar{t}^2$ is the second moment of excess delay
P_i is the absolute power of a data point on the PDP
t_i is the excess delay (time delay between the first detectable arriving signal and the data point) of a data point on the PDP

Then, the RMS delay spread is simply:

$$s_t = \sqrt{\bar{t}^2 - (\bar{t})^2} \tag{2.40}$$

2.4.3 Coherence Bandwidth

The coherence bandwidth of a wireless channel is a statistical quantity—derived from the RMS delay spread and frequency correlation function—that measures the range of frequencies over which transmitted signals will exhibit approximately equal amplitude gain (loss). In other words, it represents a range of frequencies where the amplitudes of signals within the band are strongly correlated.

Several different definitions for coherence bandwidth exist, with the only difference being how stringent the requirements are set for the amplitude correlation function. The first [14] defines the coherence bandwidth as the frequency range over which the amplitude correlation is above 0.9, and is given as:

$$B_{c,0.9} = \min[\Delta f] \text{ such that } |R_T(\Delta f)| = 0.9 \tag{2.41}$$

$$B_{c,0.9} \approx \frac{1}{50 s_t} \tag{2.42}$$

Where: $B_{c,0.9}$ is the coherence bandwidth with amplitude correlation greater than 0.9
s_t is the RMS delay spread
Δf is the RMS delay spread
$R_T(\Delta f)$ is the frequency correlation function, and is given below [36]

$$R_T(\Delta f) = \int_{-\infty}^{\infty} E(t) e^{-j2p\Delta f t} dt \tag{2.43}$$

Where: $E(t)$ is the channel Power Delay Profile

Other common definitions [12, 36, 37] relax the degree of amplitude correlation to be greater than 0.5 or 0.7, and are listed below.

$$B_{c,0.7} = \min[\Delta f] \text{ such that } |R_T(\Delta f)| = 0.7 \tag{2.44}$$

$$B_{c,0.5} = \min[\Delta f] \text{ such that } |R_T(\Delta f)| = 0.5 \tag{2.45}$$

$$B_{c,0.5} \approx \frac{1}{5 s_t} \tag{2.46}$$

2.4.4 Average Path Loss

The characterization of average path loss experienced in a wireless channel is useful for a first order approximation of the coverage area [18]. The average path loss parameter simply characterizes the amount of loss experienced in a propagation environment as a function of the transmitter-receiver distance, and is given in Equations 2.47 and 2.48.

$$P_{AV} = A_0 d^n \tag{2.47}$$

$$P_{AV} = A_0 + 10n\log\left(\frac{d}{d_0}\right) \text{ dB} \tag{2.48}$$

Where: P_{AV} is the average path loss
A_0 is the power loss at a free-space reference distance
d is the transmitter-receiver separation distance in meters
d is the free-space reference distance in meters
n is the path loss exponent for the channel

The reference distance should be selected to be beyond the Fraunhofer, or far-field, distance for the antennas so that near field effects of the antennas do not influence the reference measurement. Under far-field conditions, the reference path loss can be defined as a frequency-dependant quantity [18].

$$A_0 = 20\log_{10}(f) + 20\log_{10}(d_{ref}) - 27.65 \text{ dB} \tag{2.49}$$

Where: f is the frequency of operation in MHz
d_{ref} is the reference distance in meters

In order to make use of the average path loss model, path loss exponents must be determined from measured data by measuring a number of average power losses for a given channel and applying a linear regression to the resulting data [18]. Extensive measurement campaigns by researchers over the past two decades have produced *n*'s for a plethora of propagation environments, and their results may be found in the relevant literature.

2.4.5 Total Multipath Power Gain

The total multipath power gain represents the total amount of power available at the receiver if all of the multipath were to be summed up [16], and is represented mathematically in Equation 2.50. Total Multipath Power Gain is a useful parameter for engineers, as it will

determine the effectiveness of the RAKE processing in CDMA systems or the amount of equalization required in TDMA systems [24].

$$G = \sum_k a_k^2 \tag{2.50}$$

Where: G is the total multipath power gain
a_i is the magnitude of the ith multipath signal

G can be calculated from the statistical moments of the Power Delay Profile, as shown in [16, 22, 23], and may be spatially averaged to create a function that depends upon the transmitter-receiver separation distance.

2.4.6 Doppler Spectrum and Spread

The Doppler spectrum is a plot of Doppler shifts associated with various multipath signals, and is useful in resolving the angle of arrival of multipath signals as well as the random FM imparted by a dynamic channel [7, 30]. The Doppler spectrum is found by first recording a series of *N* inphase and quadrature delay profiles over time. A particular multipath signal will then have a set of *N* inphase and quadrature values which vary with time. The Doppler spectrum for a particular multipath signal may be found by complex Fourier transforming the inphase and quadrature samples [7].

Additionally, the random FM modulation of the received signal may be characterized by the *Doppler Spread* and *coherence time* parameters.

The Doppler Spread, given in Equation 2.51, is a measure of the spectral growth due to the time-varying nature of a mobile radio channel [12].

$$BW_D = 2 f_m \tag{2.51}$$

Where: BW_D is the Doppler Spread
f_m is the maximum Doppler shift imparted by the channel

Buried in equation 2.51 is the fact that the amount of Doppler Spread is dependant upon the frequency of transmission, the velocity of the mobile user, and the angle between the direction of propagation of the signal and the direction of travel of the mobile user. The Doppler Spread will cause frequency errors in the transmission, as the instantaneous carrier frequency can vary from $f_c - f_d$ to $f_c + f_d$. This frequency deviation causes synchronization problems at the receiver as

well as false code phase transitions, meaning that degradation of the transmitted signal will occur unless the baseband bandwidth is larger than the Doppler Spread [12, 18].

Coherence time is the time-domain dual of the Doppler Spread, and represents the time duration for which the channel impulse response is essentially invariant; i.e. the time during which received signals have a strong level of amplitude correlation [12]. Therefore, if two signals arrive with a time separation greater than the coherence time, they will be affected differently by the channel. If coherence time is defined as the time for which two received signals have an amplitude correlation greater than 0.5, then it is approximately [28]:

$$T_c \approx \frac{9}{16p\ f_m} \tag{2.52}$$

Where: T_C is the Coherence Time

f_m is the maximum Doppler shift imparted by the channel

2.5 Conclusion

In this chapter, a brief overview of wireless propagation measurement theory and application was presented. The central concern lies in measuring the transfer function of a wireless channel, and three popular techniques for making this critical measurement were described. Additionally, the data directly available from the measurement system and its impact upon wireless transmissions was illustrated. This data can then be statistically analyzed [12] to provide a tremendous volume of information about the channel, including fading statistics and statistical channel models. Understanding this information is key to designing the high data rate communication systems demanded by today's users, and also provides the framework necessary to understand the concepts investigated in this thesis.

Chapter 3

Measurement System Design Issues

3.1 Overall System Constraints

In emerging ultrabroadband wireless communication systems (wireless communication systems which utilize bandwidths on the order of several hundreds of Megahertz) which will operate at millimeter-wave frequencies such as 38 and 60 GHz, one of the main limitations to achieving maximum data throughput will be channel impairments. Because millimeter wavelengths are so short, propagation becomes highly site-specific. For example, at 60 GHz the wavelength is only 5 mm. Compared to this wavelength, most reflective surfaces appear rough, and the incident wave will be scattered in both specular and non-specular directions [65]. Additionally, vegetation leaves appear as large random scatterers, causing attenuation, depolarization, and beam broadening [65]. Atmospheric effects such as rain and hail will cause excess attenuation and multipath propagation. Finally, the oxygen adsorption of RF frequencies peaks at 60 GHz, resulting in 15 dB/km attenuation in excess of free-space attenuation [64]. The result of all these effects is that the millimeter-wave propagation channel will vary based on the physical environment within which a communication system is operating.

In order to design and develop new ultrabroadband communication systems, engineers require measurement equipment capable of characterizing the millimeter-wavelength channels. Additionally, the equipment must be compact and portable, so that it can easily be transported to a variety of sites, or even integrated into the infrastructure in order to provide real-time feedback to communication systems.

The main objective of this Thesis was to upgrade and miniaturize the existing channel sounder at MPRG. The upgraded channel sounder will have the capability of making high-resolution magnitude and phase propagation measurements, as well as the portability to be easily set up at a variety of locations and versatility to study a wide range of channels. As discussed in Chapter 2, the chosen architecture for the measurement system described in this Thesis is a Sliding Correlator Channel Sounder, because of the processing gain, and noise/interference rejection inherent in spread spectrum signals. Additionally, the output of the Sliding Correlator Channel Sounder is time dilated by the slide factor k [12], which reduces the bandwidth and processing power requirements of the baseband data collection and post-processing equipment. To meet the needs of future researchers at MPRG, as well as engineers developing ultra-wideband communication systems, the upgraded channel sounder had to meet several constraints, summarized in Chapter 1, and detailed here:

- Miniaturize the channel sounder, making it compact, portable, and easily deployable, within certain budget limitations.
- Possess a native configuration that can characterize channels from 5.4 GHz to 94 GHz as well as the ability to be easily reconfigured for measurements at frequencies below 5.4 GHz.
- Utilize PN clock frequencies from 10 MHz to 450 MHz, yielding individual multipath resolution ranging from 100 nanoseconds down to 2.25 nanoseconds.
- Possess inphase and quadrature demodulation capability so that Power Delay Profiles, multipath phase information, and Doppler spectra can be measured.

3.1.1 Miniaturized Measurement System

The channel sounder previously in use at the Mobile and Portable Radio Research Group at Virginia Tech was large and unwieldy, requiring two large utility carts for transport (one for the transmitter and one for the receiver). The objective of this research was to reduce the size of the channel sounder to a unit that could be more easily transported, while maintaining a reasonable cost.

In order to miniaturize the existing channel sounder, several physically bulky subsystems had to be replaced with more compact but functionally equivalent units. Table 3.1 shows a list of subsystems, the equipment used to implement them on the previous channel sounder, and the suggested replacement units for the upgraded channel sounder. Three primary factors were

considered when finding replacement subsystems—size reduction, reducing unnecessary functionality, and minimizing the cost of implementing the upgraded channel sounder.

Table 3.1
Current Channel Sounder Subsystems and Suggested Replacements

Subsystem	Implemented Using	Suggested Replacement	Location: Transmitter, Receiver, or Both
PN Clock Generator	HP/Fluke Signal Generator	Phase Locked Oscillator on Printed Circuit Board	Both
Local Oscillators	HP Frequency Synthesizer	Dielectric Resonator Oscillator	Transmitter
Envelope Detector	Tektronix Spectrum Analyzer	I/Q Demodulation Unit on Printed Circuit Board	Receiver
Reference Signal	EFRATOM Rubidium Frequency Standard	GPS Disciplined Oscillator	Both
Data Acquisition	Tektronix Digital Oscilloscope	PCMCIA Data Acquisition Card	Receiver

As can be seen from Table 3.1, the suggested replacement parts make use of Printed Circuit Board (PCB) technology as an aid in the miniaturization process. Implementing devices on PCBs allows the use of lower-cost components in integrated circuit form, as well as to take advantage of MPRG's PCB rapid prototyping facility.

Additionally, many of the subsystems of the original channel sounder used heavy equipment, such as the spectrum analyzer, that had additional features that were unnecessary for operation in the channel sounder. Therefore, designing and implementing a device that was specifically geared toward operation in the channel sounder reduces the overall physical size by removing unnecessary functionality.

Lastly, cost minimization was highly important to upgrading the channel sounder. As cost minimization became the driving factor in the design process, many of the replacement subsystems were implemented with devices already available at MPRG or donated by various corporations.

3.1.2 Frequency Flexibility

In addition to being compact and portable, the upgraded channel sounder will have the capability to characterize wireless channels ranging from 5.4 GHz to 94 GHz, a necessary feature

caused by the demand for broadband wireless access which pushes the frequency of operation into the tens of Gigahertz where spectrum is more readily available. Frequency flexibility is accomplished by the use of a fixed intermediate frequency (IF) and interchangeable RF up/downconverters, described in greater detail in Chapters 4 and 5. It was also desirable for the channel sounder to be easily reconfigured to operate at frequencies below 5.4 GHz, an objective which is accomplished by changing transmitter and receiver mixers/amplifiers, and providing an appropriate local oscillator signal. The flexibility to characterize a wide variety of wireless channels using a single instrument makes the upgraded channel sounder a valuable measurement tool.

3.1.3 High Resolution of Multipath

In recent years, the size of wireless cells has decreased from kilometers to microcells and picocells with diameters of a hundred meters or less. In addition, as frequencies approach 60 GHz and higher, building walls attenuate signals so heavily that channel reuse in adjacent rooms becomes a possibility. In order to characterize these microcellular and picocellular environments, the channel sounder must have the capability of resolving the closely spaced multipath signals present in these environments, while maintaining the capability of characterizing the large cellular environments.

Since the channel sounder is implemented as a spread-spectrum communication system, realizing a high level of multipath resolution means implementing a PN generator that is capable of running at a higher clock frequency. The high PN clock frequency will yield an added benefit of transmitting an wideband signal, as the RF bandwidth of a PN signal is equal to twice its clock frequency [3].

The original objective was to design and implement a PN generator capable of operating at a clock frequency of 500 MHz, which would provide multipath resolution of 2 nanoseconds (2 feet [2]). Because of bandwidth limitations in some of the components used in the IF and baseband section of the receiver, in addition to PCB layout and fabrication constraints, the PN clock frequency requirement was reduced to implementing a PN generator capable of operating at up to 400 MHz, providing individual multipath resolution of 2.5 nanoseconds.

To provide further flexibility, a variable frequency PN clock generator was designed by Orndorff [58], which provides PN clock signals from 10 MHz to 400 MHz, with the capability to

provide up to a 500 MHz clock signal. The selectable frequency feature allows researchers to trade off the multipath resolution of the channel sounder with the amount of data they wish to gather about the channel. For example, in an outdoor macrocell environment, a slower PN clock frequency would be a more prudent choice, as multipath signals have excess path lengths of several kilometers or more. The same system could then be taken indoors, and a higher PN clock frequency selected in order to investigate the subtleties of a micro- or pico-cell environment. The use of a variable-frequency PN signal also means that the RF font-end bandwidth of the receiver must be sufficiently wide to accommodate the highest frequency PN signal the channel sounder will utilize. For a 400 MHz PN signal, the amplifiers, mixers, and filters must have an RF bandwidth of at least 800 MHz or the received signal will become distorted.

3.1.4 Magnitude and Phase Measurement Capability

As users of today's wireless services become increasingly mobile, Doppler induced effects caused by a time-varying channel will become a factor that determines their quality of service. Therefore, it is important that the upgraded channel sounder be capable of characterizing the Doppler Spectra of a channel (or Doppler Spectra of individual multipath), which is done via inphase and quadrature demodulation of the channel impulse response.

The objective for the upgraded channel sounder was to provide magnitude and phase measurement capability with a tolerance of ± 1 dB for the magnitude and ± 10° for the phase. Measuring the magnitude of the impulse response with such a tight tolerance requires utilizing highly linear amplifiers and mixers, and operating well within their linear range. Measuring the absolute phase of line-of-sight and multipath signals with such a high degree of accuracy is, however, a difficult endeavor, requiring the receiver to know a priori the phase of the signal generated by the transmitter. Any discrepancy between the transmitter and receiver, however slight, will cause erroneous phase and Doppler measurements. An in-depth discussion of the ways in which highly accurate phase measurements can be performed is contained in Section 3.3

3.2 PN Generator

In a Sliding Correlator Channel Sounder, the PN Generator is the heart of the measurement system, and determines many of the measurement system parameters. Table 3.2 shows the relationship between the system parameters and the PN Generator properties.

Table 3.2
Channel Sounder Dependence on Various PN Generator Properties

System Parameter	PN Generator Property	Dependence	Ref.
Time Domain Resolution of Multipath Signals	Clock frequency, f_c	$T_{\text{Res}} = \frac{1}{f_c}$ sec	[12]
Dynamic Range	Code Length, N_{PN}	$D_R = 20\log_{10}(N_{PN})$ dB	[34]
Maximum Resolvable Multipath Delay Time	Code Length and Clock frequency	$T_{\text{Max}} = \frac{N_{PN}}{f_c}$ sec	[12]
Process Gain	Slide factor, k, and Clock frequency	$G_P = 10\log\left(\frac{0.88 f_c}{k}\right)$ dB	[3]
Maximum Doppler Shift Resolution	Slide factor, Clock frequency, and Code length	$f_{D_{MAX}} = \frac{f_c}{2kN_{PN}}$ Hz	[30]
RF Bandwidth	Clock frequency	$BW = 2 f_c$ Hz	[12]

The Maximum Doppler Shift Resolution of the channel sounder is a particularly important parameter for a vector channel sounder, and its derivation is not immediately obvious.

Consider a spread spectrum sliding correlator channel sounder in an environment where only a single line-of-sight signal exists. Additionally, the line-of-sight signal experiences phase shifts due to motion of the transmitter, receiver, or objects in the channel. As discussed in Chapter 2, the PN code will repeat itself every $N_{PN}T_C$ seconds (N_{PN} is the PN code length, T_C is the PN chip rate). Because the inphase and quadrature delay profiles recorded by the measurement system are *time dilated*, they will repeat every $kN_{PN}T_C$ seconds (Figure 3.1).

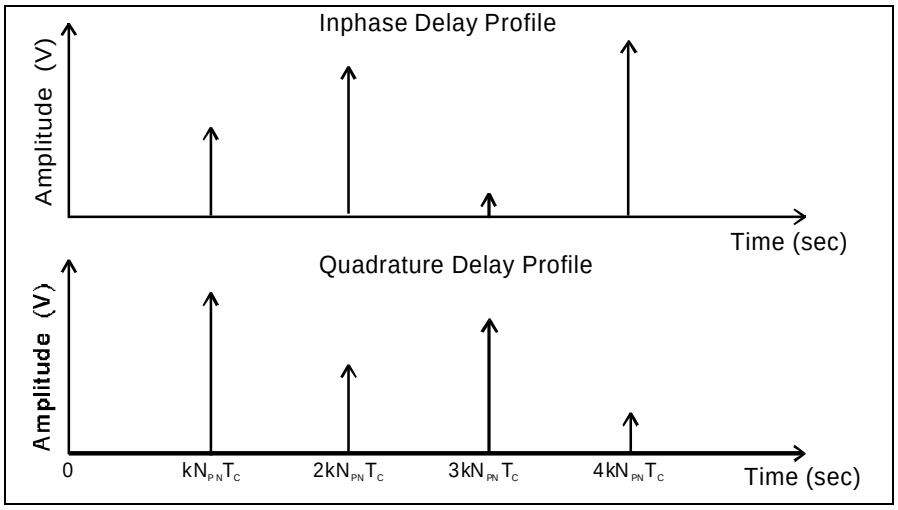

Figure 3.1: Repetition Rate of Inphase and Quadrature Delay Profiles

The Doppler Spectrum of a particular multipath signal (in this case, the single line-of-sight signal) is the Complex Fast Fourier Transform of its inphase and quadrature components. The Nyquist criteria, however, states that to reconstruct a waveform, it must be sampled at a rate equal to or greater than twice its maximum frequency. The sliding correlator is effectively sampling the Doppler shift of the line-of-sight signal at a rate of once every $kN_{PN}T_C$ seconds. Therefore, the maximum Doppler Shift that the channel sounder can resolve is:

$$f_D = \frac{Sampling\ Rate}{2}$$

$$f_D = \frac{\frac{1}{kN_{PN}T_C}}{2}$$

$$f_D = \frac{1}{2kN_{PN}T_C}$$

$$f_D = \frac{f_c}{2kN_{PN}} \qquad (3.1)$$

Where: f_D is the Maximum Doppler shift the channel sounder can resolve in Hz
N_{PN} is the PN code length
T_C is the PN chip rate in seconds
f_C is the PN clock frequency in Hertz

As can be seen from Table 3.2, a tradeoff exists between many of the PN Generator properties and the measurement system parameters. For example, a longer PN code will result in

a larger dynamic range and a longer maximum resolvable multipath delay time, but will result in a decrease in the maximum Doppler shift resolution of the channel sounder [30]. Therefore, a versatile measurement system must provide the end user with the ability to tradeoff these parameters to meet their needs. For this research, 11-bit and 18-bit PN generators were used in conjunction with variable PN clock signal generators and variable slide factors. The combination of variable PN clock frequency and two different PN code lengths provides the measurement system with the capability of emphasizing one or more of the system parameters or achieving a balance among all parameters, depending on the type of channel being evaluated.

The PN generators utilized in the channel sounder were developed as an undergraduate honors research project [6] and modified slightly (see Chapter 4) for use in this research. These generators are of the MLSR type discussed in Chapter 2, and are implemented with high-speed ECL logic circuits. Listed below are the design specifications for the PN generators.

- Operate at clock frequencies ranging from 10 – 450 MHz.
- Variable PN lengths of approximately $2^{11} - 1$ and $2^{18} - 1$.
- Implement PN Generators using Surface Mount Technology on Printed Circuit Boards to minimize their physical size.
- Design, fabricate, and assemble in-house using MPRG's PCB rapid prototyping facility.

3.2.1 PCB Layout and Fabrication Constraints

In order to facilitate rapid prototyping of various designs, MPRG acquired a PCB milling/drilling machine. The milling/drilling machine will mechanically mill a Printed Circuit Board from a single piece of double-sided copper-clad laminate in just a few hours, depending on the complexity of the design. The rapid fabrication time is advantageous in that PCB layouts can be quickly and cost-effectively fabricated and evaluated in-house, without the need to use an outside manufacturer. The use of the milling/drilling equipment does impart one major limitation: the board designer is limited to two layer microstrip circuit boards.

Because the PN Generator was implemented with high-speed ECL logic chips, the PCB layout was implemented using high-speed digital layout guidelines. The critical parameters for this particular layout results are summarized below and more details may be found in [6]. The resulting board layout is shown in Figure 3.2.

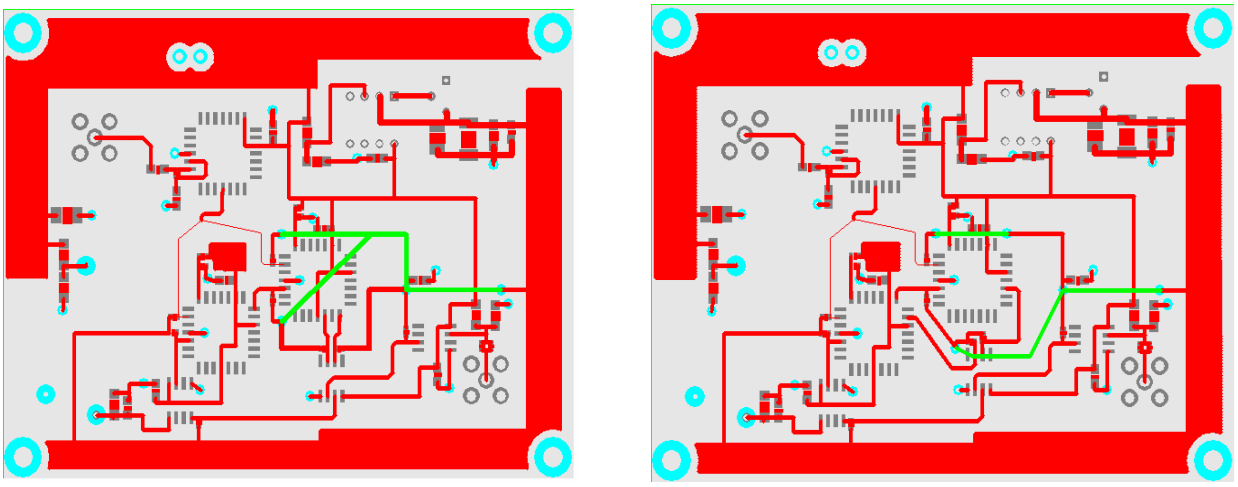

Figure 3.2: Board Layout for 11-bit (left) and 18-bit PN Generators

Ground Plane

High-speed digital circuits require a continuous ground plane underneath all signal traces, in order to minimize signal rise time and inductive coupling between traces (also known as "crosstalk"). In order to achieve a continuous ground plane with a simple two-layer PCB, all signal traces were constrained to the top layer. Traces that were absolutely necessary on the bottom layer were constrained to carry only DC and were routed as far away from critical signal traces as possible.

Propagation Delay

A key parameter for the operation of high-speed circuits is the propagation delay along signal traces that connect the various chips. The propagation delay is dependant on the length of the trace as well as the dielectric constant of the board substrate. In order to minimize propagation delay, Rogers 4003® High Frequency PCB Laminate, a PCB substrate with a very low dielectric constant ($\varepsilon_r = 3.38$), was utilized. Using Equation 3.2 [53] yielded a delay time of 125 picoseconsds/inch.

$$t_{PD} = 84.75\sqrt{0.45e_r + 0.67} \tag{3.2}$$

Where: t_{PD} is the propagation delay for Microstrip transmission lines in picoseconds/inch

e_r is the relative dielectric constant of the substrate

Timing Analysis

The PN Generator is composed of digital logic chips that implement a Linear Feedback Shift Register circuit (see Appendix A for the schematic). The circuit will produce a bit pattern based on the feedback configuration and at a rate determined by the PN Clock frequency. As the clock frequency is increased, the PN Generator will continue to produce the same bit pattern (although at a faster rate) until at some frequency the circuit fails because of the lack of setup time for the shift register chips. When clocked at or above the failure frequency, the circuit no longer produces the correct bit pattern and is said to have experienced *Timing Margin Failure* [53].

Timing Margin Failure can be prevented by intentionally clocking the circuit at less than its failure frequency, leaving a small positive timing margin under all operating conditions, which helps to protect the circuit against the effects of parasitic inductance/capacitance, noise, and crosstalk, all of which will slightly increase the edge transition times of digital signals, degrading the performance of the PN Generator.

For high-speed digital circuits, an appropriate amount of timing margin is usually a small percentage (10-15%) of the overall signal propagation delay through the circuit [53]. Timing margin is determined through the use of a timing budget analysis [53] and Table 3.3 below shows the analysis for the PN Generator used in this project. Data for the various ECL chips is taken from the datasheets in [70], and the circuit trace propagation delay is calculated using Equation 3.2. The maximum operating frequency of the PN Generator is simply the inverse of the total propagation delay through the circuit.

Table 3.3 **PN Generator Timing Budget Analysis**	
10E142 Shift Register	
Propagation Delay (typical)	800 ps
Setup and Hold Time (typical)	200 ps
Output-Output skew	75 ps
10EL07 High Speed XOR	
Gate Delay (typical)	260 ps
10EL01 High Speed OR	
Gate Delay (typical)	230 ps
Circuit Trace Propagation Delay	
125 ps/in x 2.14 in	268 ps
Circuit Subtotal	***1833 ps***
15% Timing Margin	275 ps
Total Delay	***2108 ps***
Theoretical Maximum Operating Frequency $f_{Max} = \frac{1}{Total\ Delay}$	***474 MHz***

To verify the theoretical data, the maximum operating frequency of the PN Generator was measured. The maximum operating frequency of the PN generator was defined as the maximum frequency at which the PN generator could operate before the autocorrelation of the PN sequence begins to differ from the ideal. Based on measurement data, the PN Generator can operate at a maximum frequency of 465 MHz, which is reasonably close to the theoretical maximum frequency from the analysis.

Characteristic Impedance

The use of 50 Ω characteristic impedances for the microstrip transmission lines with the chosen board material resulted in a tradeoff between the trace width and PCB substrate thickness. In order to populate the board as densely as possible (and therefore minimize the propagation delay time between logic elements), it was desired to utilize a narrow trace width. Narrow trace widths, however, necessitates the use of a thin PCB substrate material, which is more difficult to fabricate using the milling technique. Equations 3.2-3.5 shows the relationship between substrate thickness, trace width, and dielectric constant [53]. Experimentation

demonstrated that the optimal combination was a PCB substrate 12 mils thick, resulting in a trace width of 26.4 mils (1 mil = 0.001 inch).

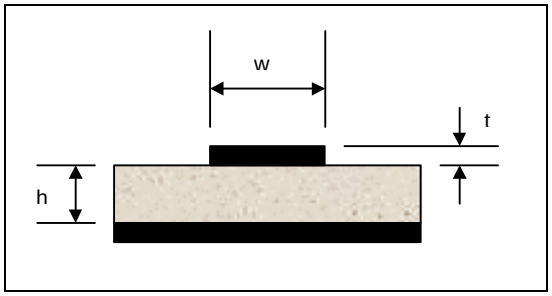

Figure 3.3: Cross-section of Microstrip Circuit Trace

For Narrow Traces $(w < h)$ [53]

$$Z_0 = 60 \ln\left[\frac{8h}{w_{eff-n}} + \frac{w_{eff-n}}{4h}\right] \tag{3.3}$$

Where w_{eff-s} is the effective trace width for narrow traces $(2p\,w < h)$

$$w_{eff-n} = w + \frac{1.25t}{p}\left[1 + \ln\left[\frac{4p\,w}{t}\right]\right] \tag{3.4}$$

For Wide Traces $(w > h)$ [53]

$$Z_0 = \frac{120p}{\frac{w_{eff-w}}{h} + 1.393 + .667 \ln\left[\frac{w_{eff-w}}{h} + 1.444\right]} \tag{3.5}$$

Where w_{eff-w} is the effective trace width for wide traces $(2p\,w > h)$

$$w_{eff-w} = w + \frac{1.25t}{p}\left[1 + \ln\left[\frac{2h}{t}\right]\right] \tag{3.6}$$

Where: Z_0 is the characteristic impedance of the microstrip transmission line
h is the thickness of the PCB substrate
t is the thickness of the microstrip transmission line
w is the width of the microstrip transmission line

Component Size

The physical size of passive components (Resistors, Capacitors, and Inductors) will have a number of different ramifications on the layout, assembly, and performance of the circuit board. Standard component package sizes range from the IPC 1206 to the IPC 0201, and a comparison of their relative sizes is given in Figure 3.4.

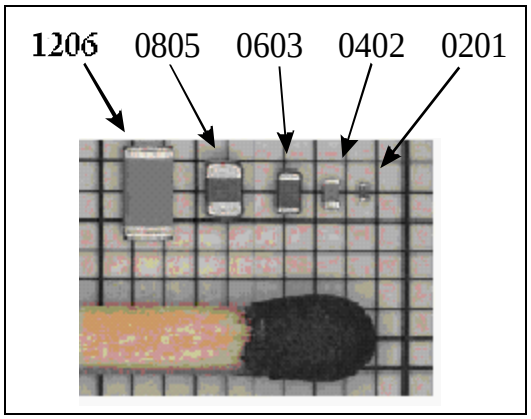

Figure 3.4: Comparison of Components Relative to the Head of a Match
From Apex 2001 CD-ROM [54]

When designing a circuit board, several tradeoffs between package size and component/board parameters must be taken into consideration, such as:

- Smaller component sizes allow for more densely populated circuit boards, minimizing circuit trace interconnects between components and reducing signal propagation delay.
- Power dissipation is inversely proportional to package size. For example, a typical 1206 sized resistor can dissipate $\frac{1}{8}$ Watt. An 0201 resistor, on the other hand, can only dissipate $\frac{1}{20}$ Watt. Therefore, careful analysis of the power handling requirements of passive components must be performed in order to prevent overloading.
- The size of the component also places constraints on the amount of capacitance and inductance that can be realized in a given package size. Capacitance, for example, is directly proportional to the area of two electrically conducting surfaces and inversely proportional to the distance between them. The maximum size of the conducting surfaces is dictated by the physical size of the component, and the manufacturing process determines the minimum separation distance as well as the breakdown voltage. Therefore, for a given component size and manufacturing process, there will be a limit to the maximum capacitance that can be achieved in the device.
- Smaller components present problems during board assembly—the process of attaching and soldering components to the circuit board. Smaller components are more difficult to assemble, and result in component misalignment and "tombstoning"—where one side of the component lifts up off the circuit board to a vertical or near vertical position (see Figure 3.5 below).

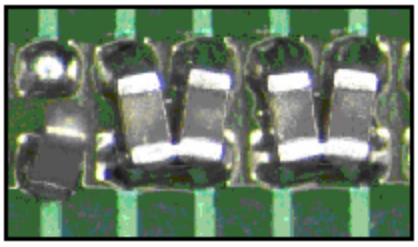

Figure 3.5: Component Tombstoning (far left) and Misalignment
From Electronic Packaging & Production Online Webcast [55]

- Smaller component packages require a smaller land pattern—the copper surface to which the component is attached. Smaller land patterns become increasingly difficult to fabricate with the milling machine, as the positioning resolution of the milling head is limited, as well as the size of the cutting tool.

After experimentation with a variety of components, the IPC 0603 component size was selected to be the standard size for the board. Larger sized components were used where higher power dissipation, larger capacitance/inductance were required, or where board area was non-critical, providing an acceptable tradeoff between board density, manufacturability, and ease of assembly.

3.3 Approaches to Measuring Magnitude and Phase

3.3.1 Discussion

The first researcher to demonstrate simultaneous magnitude and phase measurement of multipath signals using a sliding correlator channel sounder was Cox [7], who subsequently generated Power Delay Profiles as well as Doppler spectra plots. Measuring the phase of an incoming multipath signal relative to the phase of the signal at the transmitter is not a simple task, because the oscillators at the transmitter and receiver must be phase and frequency synchronized. Any frequency or non-constant phase offset will have a deleterious impact on the channel measurements. Mathematically, the impact of a frequency offset can be shown as follows:

Consider a spread-spectrum transmitter operating at a frequency of f_c MHz, and a receiver operating at a frequency of $f_c + \Delta f$ MHz (where the Δf represents either a frequency offset or non-stationary phase drift between the transmitter and receiver oscillators). The received I & Q signals are then:

$$f_I(t) = \left[x(t)\cos(2p\ f_c t) - y(t)\sin(2p\ f_c t)\right]\cos\left(2p\ (f_c + \Delta f)t\right) \tag{3.7}$$

$$f_Q(t) = \left[x(t)\cos(2p\ f_c t) - y(t)\sin(2p\ f_c t)\right]\sin\left(2p\ (f_c + \Delta f)t\right) \tag{3.8}$$

After some algebra and low pass filtering to remove higher order terms, the output of the measurement system is:

$$f_I(t) = \tfrac{1}{2}x(t)\cos\left(2p\Delta f t\right) + \tfrac{1}{2}y(t)\sin\left(2p\Delta f t\right) \tag{3.9}$$

$$f_Q(t) = -\tfrac{1}{2}\, y(t)\cos\left(2p\Delta ft\right) + \tfrac{1}{2}\, x(t)\sin\left(2p\Delta ft\right) \tag{3.10}$$

These baseband inphase and quadrature waveforms are markedly different from the waveforms that result from demodulation with a perfectly synchronized local oscillator. Of particular importance is the fact that the baseband PN waveforms, represented by $x(t)$ and $y(t)$ are now amplitude modulated by a cosine or sine function, which will yield an oscillating phase response of the channel, $q(t)$ at a rate equal to the frequency offset, Δf , between the transmitter and receiver, meaning that the phase response of the channel (and hence the Doppler spectra) will not yield any meaningful information about the channel. The critical issue, when designing a measurement system for characterizing the phase response and Doppler spectra of a channel becomes synchronization of the oscillators at the transmitter and receiver. First, however, it is important to understand the causes of the frequency offset and the limitations it places on the channel sounder.

The instantaneous frequency offset between the transmitter and receiver oscillators can be characterized as jitter. Jitter is defined by the International Telecommunications Union as "Short-term variations of the significant instants of a digital signal from their ideal positions in time" [41] (see Figure 3.6). More simply stated: the transitions of a digital signal never occur exactly where they should. Jitter is used as a way to characterize and quantify the random instantaneous frequency variance of a digital signal and is critical to understanding the performance of synchronous communication systems [41].

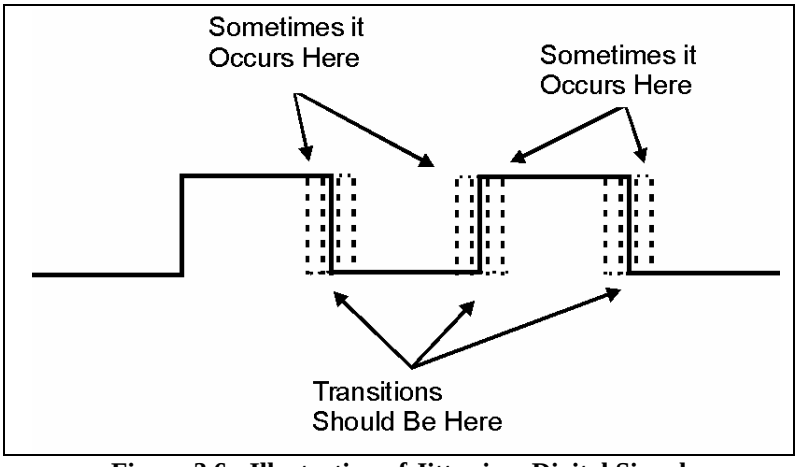

Figure 3.6: Illustration of Jitter in a Digital Signal

These random temporal variations of the digital clock edge will directly result in frequency instability of the oscillator, due to the dual time/frequency relationship. It is important to note the difference between frequency instability and frequency drift. Instability is, by its nature, random fluctuations in the instantaneous frequency of the oscillator; drift is a constant rate of change in the frequency of an oscillator. For example, an oscillator whose frequency changes by +0.5 Hz/day is a stable oscillator (since the rate of change is constant), however, it does experience drift.

One of the most useful ways to quantify jitter in a digital clock or frequency standard is by use of the *Allan Variance*, as defined in [61]. For example, assume a frequency standard produces a frequency output at f_0. Then, a series of measurements of the actual instantaneous frequency output, f_k, are recorded, with each measurement spaced t seconds apart. Because jitter is a random process, and positive and negative frequency deviation is possible, the average frequency error, $\overline{\Delta f_k}$, will be zero. The variance of Δf_k, however, provides insight as to how much the output will deviate from f_0.

Allan Variance is the IEEE and ITU recommended measure for the instability of an oscillator. To calculate the Allan Variance from a series of instantaneous frequency measurements spaced t seconds apart, first find the normalized average frequency difference for two successive sets of measurements (the change in frequency between two successive measurements divided by the time between measurements):

$$y_k = \frac{f_{k+1} - f_k}{f_0} \tag{3.11}$$

$$y_{k+1} = \frac{f_{k+2} - f_{k+1}}{f_0} \tag{3.12}$$

Where: y_k is the normalized average frequency deviation between intervals k and $k+1$ (the average frequency deviation over the measurement time t)
y_{k+1} is the normalized frequency difference between intervals $k+1$ and $k+2$
f_k 's are the instantaneous frequency error measurements of the oscillator
f_0 is the nominal output frequency of the oscillator

Note that y_k is unitless.

Then, the frequency instability from the first t interval to the second t interval is:

$$\Delta y_k = y_{k+1} - y_k \tag{3.13}$$

Figure 3.7 is a graphical representation of the procedure for determining the Δy_k's from the instantaneous frequency error measurements.

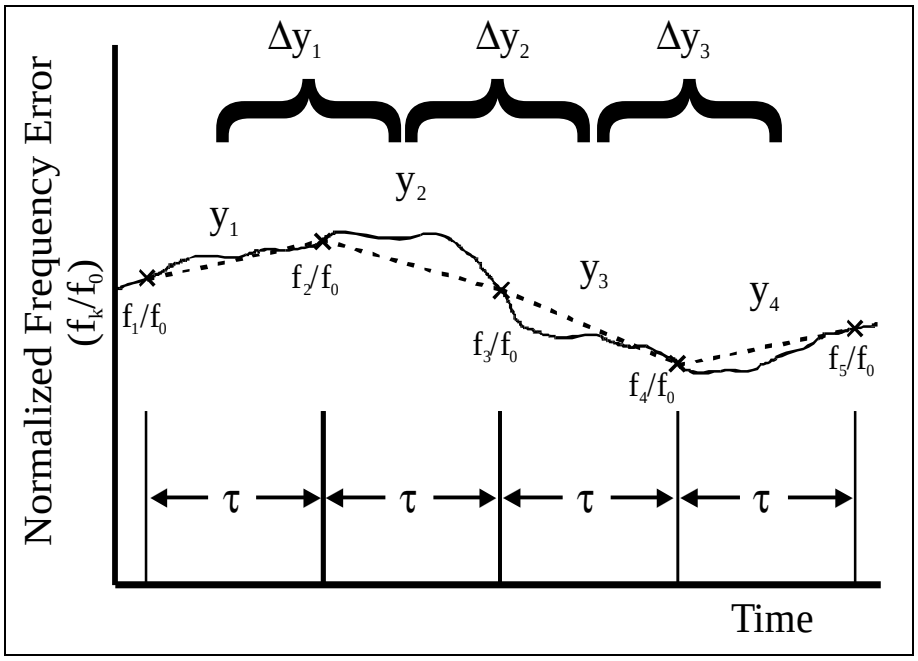

Figure 3.7: Graphical Representation of Determining Normalized Frequency Difference and Frequency Instability

An estimate of the two-sample variance may then be found from:

$$s_y^2(t) = \frac{1}{2(N-2)} \sum_{k=1}^{N-1} (\Delta y_k)^2 \tag{3.14}$$

For the case where the y_k's are random and uncorrelated and an infinite number of frequency error measurements are recoreded, Equation 3.14 becomes the Allan Variance [61]:

$$s_y^2(t) = \frac{1}{2} \left\langle (\Delta y)^2 \right\rangle \tag{3.15}$$

Where: $s_y^2(t)$ is the Allan Variance over a time interval t

$\langle \bullet \rangle$ denotes the expected value of the quantity inside the brackets.

Note that $s_y^2(t)$ ***is unitless.***

Note that the Allan Variance differs from the classical variance, in that the classical variance is based on the deviation of samples about the mean, whereas the Allan Variance is based on deviation from the previous sample. Additionally, the Allan Variance is always specified for a particular t time period, with typical t 's being 1 second, 1 minute, 1 hour, and 1 day. Also, the Fourier transform of the Allan Variance will provide the phase noise about the center frequency at a particular offset from the carrier (e.g., $s_y^2(t)=1\times10^{-11}$ for $t=1\text{sec}$ is equal to a phase noise of -90 dBc/Hz @ 1 Hz offset from the carrier). For the purpose of this Thesis, the interest is in achieving short-term stability, thus the Allan Variance will always be reported for a t =1 second time period.

In a sliding correlator channel sounder, knowing the effects of jitter on the Local Oscillators and PN Clock Generators are particularly important. Jitter in these signals will limit the performance of the measurement system in three important ways [30]:

1. Instability in the PN Clock generators will cause a relative shift in the timing of the PN code, so that multipath with the same propagation delay will no longer occupy the same time resolution bin. Jitter, therefore, limits the time over which the measurement system can resolve absolute propagation delay of incoming signals.
2. Frequency instability of the Local Oscillators will limit the phase angle resolution of incoming multipath and the length of time over which absolute phase may be measured.
3. Frequency instability of the Local Oscillators will determine the lowest Doppler shift frequency that can be unambiguously resolved. Essentially, instead of measuring the Doppler shift caused by the channel, the channel sounder will measure the frequency offset between the two oscillators.

Table 3.4 shows a comparison of commercially available frequency references, typical Allan Variances, and approximate price ranges. From this table, it can be seen that as the stability of an oscillator increases, the cost increases almost exponentially.

Table 3.4 **Comparison of Commercially Available Frequency Standards**		
Oscillator Type	**Typical $s_y^2(t)$ for t =1 sec**	**Price Range**
Ovenized Crystal Oscillator	1×10^{-9} — 5×10^{-11}	Under $1,000
Double Ovenized Crystal Oscillator	1×10^{-10} — 1×10^{-11}	$500 - $5,000
Rubidium Oscillator	1×10^{-10} — 7×10^{-12}	$1,000 - $10,000
Cesium Oscillator	1×10^{-11} — 3×10^{-12}	$20,000 - $50,000
Hydrogen Maser	5×10^{-12} — 1×10^{-13}	$65,000 - $250,000

Table 3.4 can be used in conjunction with the following analysis of the effects of jitter on the performance of the channel sounder, in order to determine (1) if a product that meets the requirements is commercially available and (2) if the desired accuracy merits the high expense of highly stable products.

Timing Shift of the PN Codes

A timing offset between the PN Sequence at the Transmitter and Receiver will cause a time bin shift between the two PN codes, causing multipath with identical propagation delays to occupy different time bins, as well as introducing errors into the measurement of absolute propagation delay [56]. If the PN clock signals experience a linear time shift with respect to each other, then the effects of the drift may be calibrated out of the measured data, with little to no loss of accuracy [56]. It is more likely, however, that the PN clock generators will experience a random timing jitter as described above, as the instantaneous frequency of any oscillator will always have a random component [61]. To prevent the effects of random jitter from introducing errors into the measurement system, the PN clock oscillators must have a stability (Allan variance) of:

$$s_y^2(t) \le \frac{T_C}{t_{meas}} \tag{3.16}$$

Where: $s_y^2(t)$ is the Allan Variance of the oscillator
T_C is the chip period of the PN generator in seconds
t_{meas} is the required measurement period in seconds

For example, if a channel sounder utilizes a 400 MHz PN generator and will be recording measurements over a 10 minute period then the required stability of the oscillators is:

$$s_y^2(t) = \frac{T_C}{t_{meas}} = \frac{2.5\times10^{-9}\,\text{sec}}{600\,\text{sec}} = 4.12\times10^{-12}$$

Note that if the oscillator stability and PN chip rate is known, Equation 3.16 can be rearranged to determine the maximum time that the system can operate before the PN codes slip one time bin:

$$t_{meas} = \frac{T_C}{s_y^2(t)} \tag{3.17}$$

Phase Measurement Limitations

Instability of the local oscillators in the transmitter and receiver will limit the ability of the channel sounder to measure the absolute phase of the incoming multipath. Here, "absolute phase" is defined as the phase of the multipath signal relative to the phase of the carrier signal at the transmitter. Essentially, the instability of the Local Oscillators represents a random time varying phase/frequency, which will be reflected in the phase of the demodulated signal.

To measure the phase angle of arriving multipath within θ degrees over a time period of t_{meas}, the required stability of the local oscillators is given by:

$$s_y^2(t) = \frac{\frac{q}{360^\circ}\cdot\frac{1}{f_c}}{t_{meas}} \tag{3.18}$$

Where: $s_y^2(t)$ is the Allan Variance of the local oscillator (unitless)

q is the desired absolute phase angle resolution of the measurement system in degrees

f_c is the carrier frequency used in the measurement system in Hz

t_{meas} is the required measurement period in seconds

For example, if a channel sounder is operating at 5.0 GHz, it will be recording measurements for a 10 minute period, and it is desired to be able to resolve the phase angles of the incoming multipath to within 10°, then the required stability of the local oscillators is:

$$s_y^2(t) = \frac{\frac{q}{360^\circ}\cdot\frac{1}{f_c}}{t_{meas}} = \frac{\frac{10}{360^\circ}\cdot\frac{1}{5.0\times10^9\,Hz}}{600\,\text{sec}} = 9.26\times10^{-15}$$

From Table 3.4, it is immediately obvious that no oscillator meets the required stability. In this case, the specification must be adjusted so that the required oscillator stability will fall within a

reasonable range. Equation 3.18 can be rearranged to yield a minimum phase angle resolution for a given oscillator stability:

$$q = 360^\circ \, f_c t_{meas} s_y^2(t) \tag{3.19}$$

Using the best available Hydrogen Maser, which has a stability of $s_y^2(t) = 1\times10^{-13}$, and a measurement time of 10 minutes, the phase angle resolution of the channel sounder is:

$$q = 360^\circ \, f_c t_{meas} s_y^2(t)$$
$$q = 360^\circ \left(5\times10^9 \, Hz\right)\left(600\text{sec}\right)\left(1\times10^{-13}\right)$$
$$q = 108^\circ = \pm 54^\circ$$

Therefore, from a practical standpoint, at a fixed operating frequency, a tradeoff exists between phase angle resolution, measurement time, oscillator stability, and cost.

Doppler Shift Limitations

A frequency offset in the Local Oscillators used in the channel sounder will result in a lower bound for the Doppler shift resolvable by the measurement system. The frequency offset is related to the oscillator stability by Equation 3.20.

$$f_{D_{MIN}} = s_y^2(t) \, f_c \tag{3.20}$$

Where: f_c is the carrier frequency used in the measurement system

Using the measurement system described above, with an oscillator stability of $s_y^2(t) = 4.12\times10^{-12}$, then the minimum Doppler shift that the system can resolve is 0.02 Hz.

3.3.2 Achieving Stability of Local Oscillators

In practice, there are a number of methods that may be utilized to achieve a high degree of frequency stability (or phase/frequency synchronization) between the transmitter and receiver oscllators, such as:

- Cable Connected
- Broadcast and Recover Carrier
- Atomic Master Oscillator
- Digital Downconversion
- GPS Disciplined Oscillators

Each of these options, along with their potential benefits, limitations, and design tradeoffs will be discussed below.

3.3.2.1 Cable Connected Method

The cable connected method utilizes a single Master Oscillator as the frequency reference at the transmitter and transmits the reference signal to the receiver through a fixed-length coaxial or optical fiber cable (See Figure 3.8). The transmitter and receiver oscillators are thus exactly phase and frequency synchronized to the same standard; therefore any instability in the frequency reference will be exactly replicated at both transmitter and receiver (provided the propagation delay through the air and the cable are equal), so that observed phase variations and Doppler spectra are caused only by the channel. The cable connected system is advantageous in that a high resolution of multipath phase angle and Doppler shift may be achieved by using a relatively inexpensive oscillator. The problem is that the Transmitter and Receiver must be physically connected together, making the cable connected method useful only for indoor or short-length outdoor measurements. The cable connected method was used in [16, 43, 45] because of the simplicity of the implementation and the absolute synchronization of transmitter and receiver oscillators it provides.

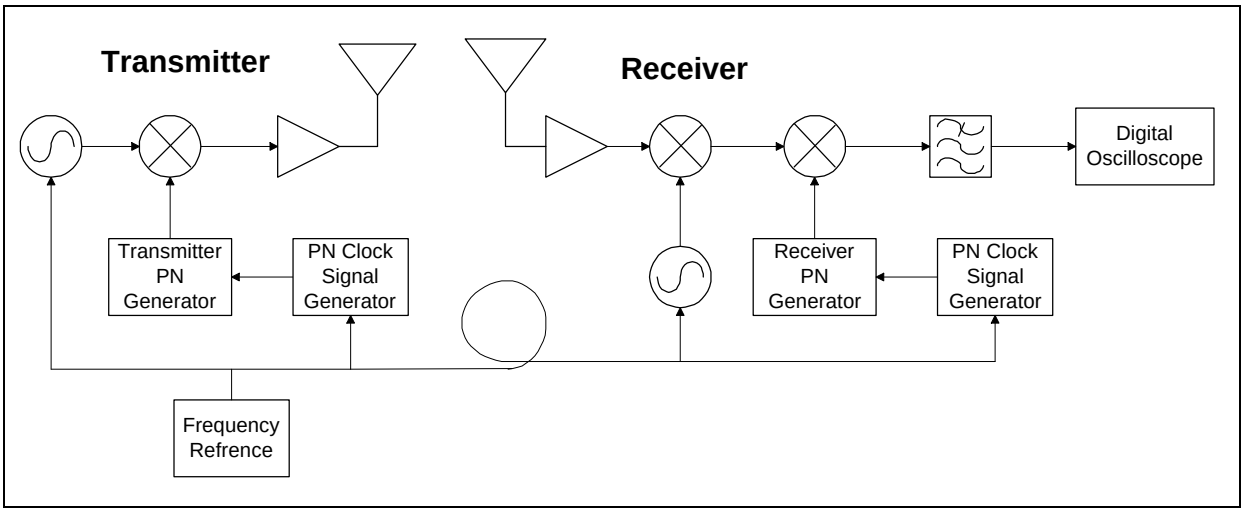

Figure 3.8: Block Diagram of a Fixed Length Cable Connected Channel Sounder

3.3.2.2 Broadcast and Recover Carrier Method

A slight modification of the Cable Connected Method transmits the RF carrier signal (or a subcarrier) across a fixed-length wireless link. The received carrier signal is filtered with an extremely tight bandpass filter to remove noise added by the channel, and is used as the local oscillator at the receiver (see Figure 3.9). As with the Cable Connected method, the local oscillators are exactly phase synchronized and the only phase perturbations occurring on the received signal are caused by the channel.

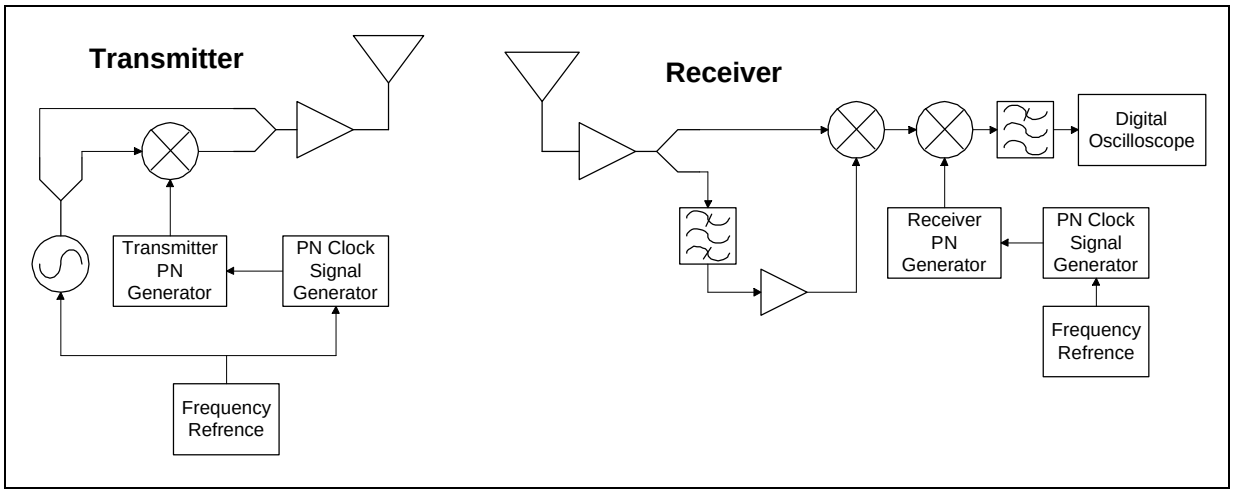

Figure 3.9: Block Diagram of a Broadcast and Recover Carrier Channel Sounder

The broadcast and recover carrier system is also advantageous in that it is relatively simple to implement, however it has some significant limitations, listed below:

- The channel sounder is not measuring "absolute phase" as defined in Section 3.3.1. Rather it is measuring the phase of the multipath relative to the phase of the received carrier, which may itself be affected by multipath signals in the environment. The channel sounder is also limited to non time-varying channels, as dynamic channels will result in a time varying amplitude and phase of the carrier signal.
- Very narrowband bandpass filters (1% Bandwidth or less) become increasingly difficult to implement (and increasingly expensive) as frequency increases, and result in large insertion losses [49]. While the use of SAW filters could alleviate the tight bandwidth/high insertion loss problem, at the current time none were available "off the shelf" with a 1% Bandwidth at the IF frequency of the channel sounder.
- The PN Generator at the Receiver requires a separate frequency generator from the one at the transmitter; therefore the broadcast and recover carrier method does not resolve the problem of the Timing Shift of the PN codes.

These limitations cause a significant degradation in the performance of the channel sounder. By referencing the phase of multipath signals to the phase of the carrier signal, the Doppler shift of multipath components can only be measured relative to the Doppler shift of the carrier. Additionally, even if a 1% bandwidth filter is utilized, 1% of a 1 GHz carrier is equal to a 10 MHz filter bandwidth; with a 60 GHz carrier, a 1% filter bandwidth is equal to 600 MHz filter bandwidth. Even though these filters are extremely tight, they still allow a tremendous amount of noise in with the desired carrier signal. The noise will manifest as phase noise of the carrier, significantly degrading the accuracy of the phase measurement.

3.3.2.3 Atomic Master Oscillator Method

The Atomic Master Oscillator (AMO) Method takes advantage of the high degree of stability obtainable with a Rubidium or Cesium based oscillator. With the AMO method, separate AMOs are used as frequency references at the transmitter and receiver. The use of separate frequency standards allow the measurement system to be synchronized at the start of the measurements, and then operated untethered for a period of time [7, 10] (See Figure 3.10).

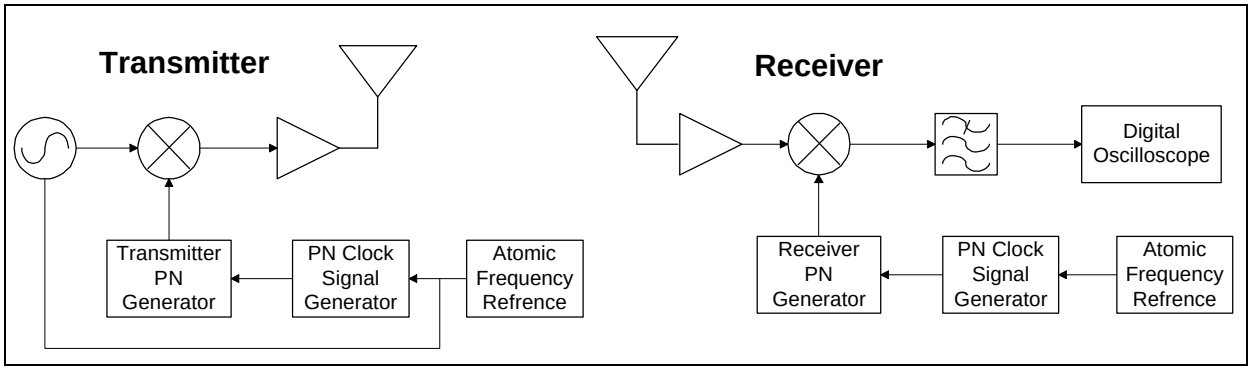

Figure 3.10: Block Diagram of an Atomic Master Oscillator Based Channel Sounder

Typical Cesium and Rubidium Oscillators have stabilities on the order of $s_y^2(t) = 3\times10^{-12}$ and $s_y^2(t) = 7\times10^{-12}$, respectively. Table 3.5 shows the performance of a channel sounder operating at 5.4 GHz with a 500 MHz PN code using these oscillators.

Table 3.5
Comparison of Rubidium and Cesium Oscillators at 5.4 GHz

Parameter	Rubidium Oscillator	Cesium Oscillator
Length of time before PN codes slip one chip (2 nanoseconds) (Equation 3.1 7)	285 sec	2000 sec
Phase Angle Resolution for measurement time periods of 30 and 60 seconds (Equation 3.1 9)	> 360° / > 360°	175° (±87°) / 350° (±175°)
Minimum Doppler shift that the measurement system can resolve (Equation 3.20)	0.04 Hz	0.02 Hz

From Table 3.5, it can be seen that the major limitation to the Atomic Master Oscillator method is the ability to make high resolution phase measurements. The poor resolution is caused by the frequency instability of the AMOs, which manifests as a slight frequency offset between the transmitter and receiver oscillators, limiting both the ability to resolve the phase of the incoming signal as well as the minimum Doppler shift that the system can resolve.

Stated another way, the frequency offset between the AMOs will result in a random phase drift of one with respect to the other. In the case of the Cesium oscillator, the drift will amount to a random phase shift of no more than ±87° during 30 seconds of operation, or ±175° during 60 seconds of operation. One way to improve the phase resolution is by measuring the phase of multipath signals relative to the phase of the line-of-sight (or first arriving multipath) signal, as the time to record a single power delay profile is significantly less than the time required to record multiple power delay profiles, although absolute phase as defined in section 3.3.1 is no longer being measured.

Note that at lower frequencies, the phase resolution of the system improves dramatically. Table 3.6 shows a dramatic improvement, however, the measurement time before the PN codes slip one time remains unchanged.

Table 3.6 **Comparison of Rubidium and Cesium Oscillators at 900 MHz**		
Parameter	Rubidium Oscillator	Cesium Oscillator
Length of time before PN codes slip one chip (2 nanoseconds) (Equation 3.17)	285 sec	2000 sec
Phase Angle Resolution for measurement time periods of 30 and 60 seconds (Equation 3.19)	68° (±34°) / 136° (±68°)	30° (±15°) / 60° (±30°)
Minimum Doppler shift that the measurement system can resolve (Equation 3.20)	0.0063 Hz	0.003 Hz

Table 3.7 lists a number of commercially available oscillators, suppliers, Allan Variances, and approximate price. The AMO type of system has been used by numerous researchers [2, 7, 44, 46] to measure Power Delay Profiles in a variety of propagation environments, as well as by [7] to measure Doppler Spectra. One final note is that Atomic Oscillators can be prohibitively expensive (particularly for Cesium oscillators, which are priced in the $40,000 range) and their use should only be considered when the cost can be reasonably justified.

Table 3.7 **Comparison of Commercially Available AMOs**			
Vendor	**Oscillator Type**	**Typical $s_y^2(t)$ for t =1 sec**	**Approx. Price**
Datum	Rubidium	3.0×10^{-11} — 2.0×10^{-11}	$1,500 — $3,000
Datum	Cesium	1×10^{-11} — 5×10^{-12}	$30,000 — $50,000
Datum	Hydrogen Maser	2×10^{-13}	> $100,000
FEI	Double Ovenized Quartz	1×10^{-11}	$2,000
C-MAC	Ovenized Quartz	2×10^{-11}	$500
Vectron	Double Ovenized Quartz	5×10^{-12}	$5,000
Corning	Double Ovenized Quartz	1×10^{-11}	$1,000
MTI	Double Ovenized Quartz	7×10^{-12}	$2,000
HP	Rubidium	1×10^{-11}	$18,000

3.3.2.4 Digital Downconversion

An alternative to the use of a standard superheterodyne receiver architecture is to bandpass sample the received RF signal, digitally down converting it directly to baseband. Digital downconversion may be done in two different ways: Direct I/Q Sampling and BandPass Sampling. The ability to digitally downconvert an RF signal is advantageous in that it reduces the complexity of the analog RF hardware required at the receiver in addition to eliminating the need to synchronize oscillators at the Transmitter and Receiver.

With Direct I/Q Sampling, the RF signal is directly sampled at a rate equal to at least 2 times the Nyquist rate (or at least 4 times the highest frequency signal), and the sampled signal is then decimated so that both the inphase and quadrature signals may be recovered [50, 51] (Figure 3.11).

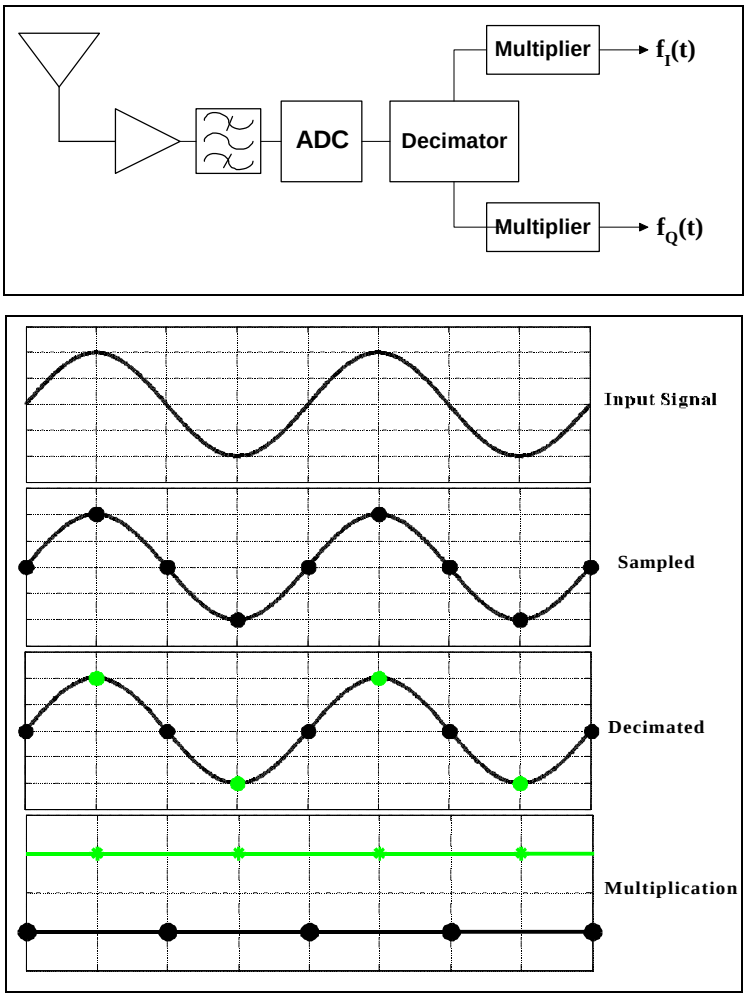

Figure 3.11: Illustration of Direct I/Q Sampling

Bandpass sampling of the received signal is used to significantly reduce the sampling rate requirement of the Analog to Digital Converter (ADC). Bandpass sampling, an application of the Sampling Theorem, works essentially the same way as Direct I/Q sampling, except that instead of sampling at twice the Nyquist frequency, the ADC need only sample at twice the information bandwidth. The signal of interest is intentionally aliased to a desired intermediate frequency or to baseband [47, 48] and the process of digital downconversion is depicted in Figure 3.12.

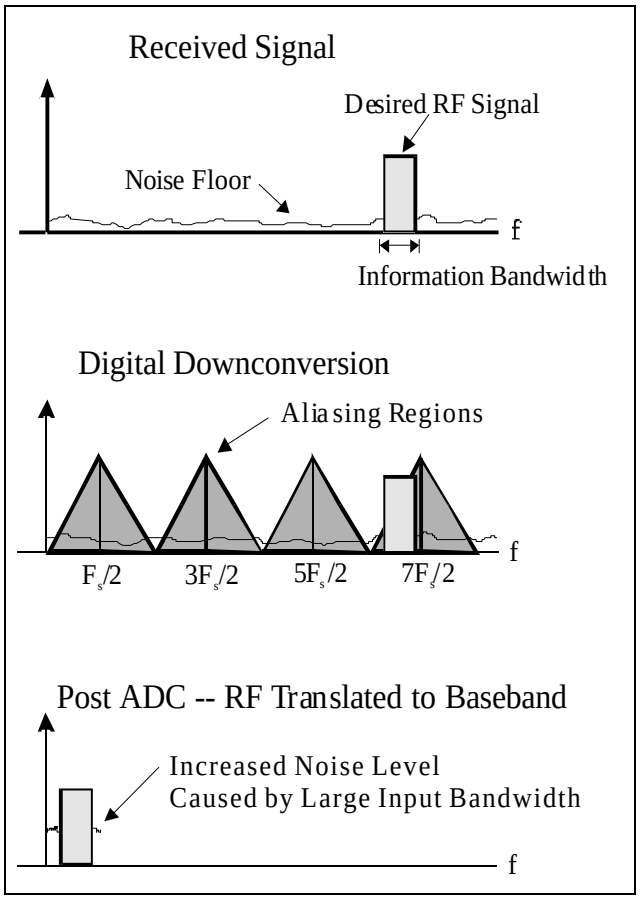

Figure 3.12: Bandpass Sampling Example from [47]

Unfortunately, the process of Digital Downconversion exhibits some significant limitations:

- As the RF frequency increases, Direct I/Q sampling becomes impossible. If the channel sounder is operating at a frequency of 5.0 GHz, then the RF signal would have to be sampled at a rate of 20 GHz to recover both I & Q signals, far beyond the capabilities of currently available ADCs.
- Bandpass sampling to downconvert the RF signal means that the Analog-to-Digital Converter must have an input bandwidth that can accommodate the desired RF signal as well as a sampling frequency sufficient to extract the desired information bandwidth, causing two additional problems.

  - If the Channel Sounder is operating at 5.0 GHz, then the ADC would have to have an Analog Input Bandwidth of at least 5.0 GHz. Analog Input Bandwidth is defined in [86] as the reconstructed output level drops 3 dB below the full-scale input. Such a high input bandwidth not only pushes the limits of currently available technology, but allows a large amount of noise into the system, degrading both the dynamic range and noise figure of the receiver [47].
  - In an Ultrabroadband Channel sounder utilizing a PN code rate of 400-500 MHz will result in an 800 MHz – 1 GHz RF Bandwidth. Such a wide RF bandwidth means that the sampling frequency of the ADC must be 1.6 GHz – 2.0 GHz, which is pushing the limits of currently available technology. Additionally, high speed ADCs usually have quantization limitations—typically around 8 bits quantization per sample. This limitation degrades the dynamic range of the channel sounder.

- The use of Low-IF or Zero-IF (downconverting the RF signal to a low frequency or baseband) relaxes the RF input bandwidth constraints on the ACD, but introduces other problems into the system.
  - Downconverting the RF signal to baseband will introduce jitter from the receiver local oscillator into the signal, reducing the phase measurement accuracy of the system.
  - To recover inphase and quadrature waveforms at baseband, the ADC must sample at twice the Nyquist rate. With a 500 MHz PN code, the ACD would have to sample at 2.0 GHz, pushing the limits of currently available technology.
- Even though digital downconversion negates the effect of jitter in the local oscillators, it is susceptible to sampling jitter, resulting in additive noise introduced into the system [40]. In the worst case, sampling jitter in the ADC causes an apparent drift in the phase of the digitized signal [52]. Additionally, a frequency offset in the sampling clock frequency will result in an effective frequency offset of the bandpass sampled signal (e.g. if the desired RF center frequency was 2 GHz, and the sampling clock frequency is 10.0001 MHz, then the actual RF center frequency downconverted by the ADC would be 2.02 GHz).
- The Dynamic Range of the system is limited by the number of quantization bits in the ADC. In commercially available ADC's the number of quantization bits decreases as the sampling frequency of the ADC increases [51].
- LO leakage across the mixer produces large DC offsets at baseband.

Table 3.8 provides a comparison of several commercially available high-speed ADC's. The cost of these ADCs is difficult to evaluate. The individual chips are reasonably inexpensive (less than $100 each), however, a PCB must be designed around the ADC—a labor intensive process. At GHz frequencies, proper PCB layout becomes critical, as even small amounts noise, crosstalk, or impedance mismatches can significantly degrade the quality of a signal and hence, the operation of the system. Therefore, the costs of creating a PCB around the ADC must be

factored into any price comparison between the Digital Downconversion method and any of the other methods discussed in this chapter.

Table 3.8
Comparison of Commercially High Speed ADC's

Vendor	Sampling Rate	Quantization Bits	Input Bandwidth
Rockwell Scientific	3.2 GS/s	6	8 GHz
Rockwell Scientific	1.0 GS/s	8	6 GHz
Amtel	2.0 GS/s	8	4 GHz
Maxim	1.5 GS/s	8	2.2 GHz

3.3.2.5 GPS Disciplined Oscillators

An alternative to the Atomic Master Oscillator method is to use ovenized, double-ovenized, or inexpensive rubidium oscillators synchronized to the 1 pulse-per-second (1 pps) signal broadcast by the Global Positioning System satellites in orbit around the earth. Ovenized oscillators have excellent short-term stabilities on the order of $s_y^2(t)=1\times10^{-11}$ over a period of one second, and the GPS signal is used to fine-tune their frequency to provide excellent long-term stability. The combination of the ovenized oscillator and GPS correction provides the stability of the cesium based oscillators on board the GPS satellites. Essentially, the GPS method operates similarly to the cable connected method, except that the frequency reference is now space-based and the signal is distributed to the transmitter and receiver through a wireless link. The transmitter/receiver oscillators are therefore constantly being retuned to synchronize with the GPS one pulse-per-second timing signal, thus when fully locked on to the GPS signal they will experience minimal fluctuations with respect to each other.

The GPS Disciplined Oscillator system is extremely versatile, as the GPS signals are available worldwide, and is a new method for implementing channel sounders to provide magnitude and phase information [59]. It does, however, have some significant limitations:

- The system is limited to operation only where the GPS signals can be received. In building operation is not possible unless the GPS antennas can be mounted outside the building and the signal fed through an open window or door. Additionally, if the weather is overcast or raining, signal level may be low, causing the receivers to frequently lose lock on the GPS signals, resulting in long-term oscillator instabilities, and prohibits propagation experiments during rain.

- Typical GPS receivers require 30 minutes to 1 hour to fully acquire the GPS 1 pps signal and synchronize the ovenized oscillator. Therefore, when the channel sounder is first set up, a warm up time will be required before measurements can be made. Additionally, if the GPS receiver loses lock for a significant period of time, the waiting period will again take effect when the signal is re-acquired.
- The stability of the ovenized oscillator is based on a long-term average of the GPS 1 pps signal, which reduces the effects of receiver noise and temporal errors of the GPS signal [87]. Additionally, stability is enhanced by tracking multiple satellite signals, as all signals can be averaged together to reduce the effects of errors in any particular signal.

Table 3.9 lists a number of commercially available GPS disciplined oscillators, suppliers, Allan Variances, and approximate price.

Table 3.9
Comparison of Commercially Available GPS Disciplined Oscillators

Vendor	Typical $s_y^2(t)$ for t =1 sec	Approx. Price
Datum	1.0×10^{-11} — 5.0×10^{-12}	\$2,000 — \$4,000
Absolute Time	1.0×10^{-11} — 7.0×10^{-12}	\$2,000
Temex Telecom	2.0×10^{-11} — 5.0×10^{-12}	\$2,500
Precision Test Systems	7×10^{-12}	\$5,500
Trimble	1×10^{-11}	\$2,000

3.3.2.6 Implementation

The method chosen for synchronizing transmitter and receiver local oscillators was the GPS Disciplined Oscillator Method with the Cable Connected method implemented as a backup. The GPS method was chosen to take advantage of a donation of Datum StarLoc II GPS disciplined oscillators to MPRG, which represents a cost reduction in the implementation of the new system. These oscillators have a stability of $s_y^2(t)=3\times10^{-12}$, and table 3.10 shows the performance of a channel sounder operating at 5.4 GHz with a 450 MHz PN code.

Table 3.10
Performance of GPS Disciplined Oscillators at 5.4 GHz with 450 MHz PN Code

Parameter	Channel Sounder Performance
Length of time before PN codes slip one chip (2.25 nanoseconds) (Equation 3.17)	750 sec
Phase Angle Resolution for measurement time periods of 30 and 60 seconds (Equation 3.19)	175° (±87.5°) / 350° (±175°)
Minimum Doppler shift that the measurement system can resolve (Equation 3.20)	0.02 Hz

As can be seen from the table, the use of the GPS disciplined oscillators provides the stability required so that phase and Doppler information could be measured—at least over a short measurement time period. From a practical perspective, if the channel sounder was recording a series of power delay profiles and phase measurements over a 30-second time period, then (assuming a static channel) the phase measurement of the last PDP in the series would differ from the phase of the first recorded PDP by ±11°. In the event that a higher accuracy or longer measurement time was required or if the GPS signals were unavailable, the cable connected method provides a secondary method for achieving highly accurate measurements.

3.4 I/Q Correlator Unit

As discussed in Chapter 2, the operational principle of the sliding correlator channel sounder is to correlate a PN sequence that is generated at the receiver with an incoming signal. The incoming signal is generated by the transmitter using an identical PN sequence, but which is clocked at a slightly different rate than the receiver sequence [3]. Correlation of these sequences is performed by multiplying the two signals together and then integrating the result over time, a process which may be performed by a low-pass filter. The process of correlation will generate a peak when the codes are aligned (caused by line-of-sight and multipath propagation) and pseudo-random noise when the codes are not aligned. A block diagram of the correlation process is shown in Figure 3.13

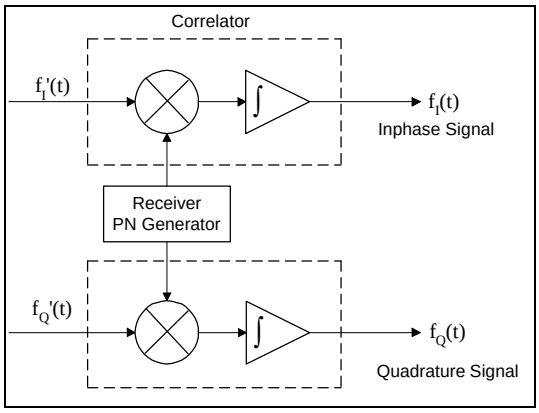

Figure 3.13: Functional Diagram of the I/Q Correlator Unit

The most important design parameter for the correlator unit is the bandwidth of the filter. Recall that the autocorrelation of a periodic signal is given by:

$$R_{ss}(t) = \int_{t_0}^{t_0+T_{PN}} s(t)s(t+t)\,dt \tag{3.21}$$

$$T_{PN} = \frac{N_{PN}}{f_c} \tag{3.22}$$

Where: $R_{ss}(t)$ is the autocorrelation of $s(t)$
T_{PN} is the period of the PN code
N_{PN} is the length of the PN code
f_c is the clock frequency (chip rate) of the PN code

In order to perform the integration properly, the bandwidth of the lowpass filter should be approximately $\frac{1}{T_{PN}}$. If the bandwidth is greater, then the integration time will be too short and will result in incomplete correlation, degrading the Signal-to-Noise (SNR) ratio [57].

In order to achieve the maximum SNR for the measurement, either the PN sequence length or the slide factor must be adjusted. The optimal filter bandwidth for a time-domain resolution of twice the chip length of the PN code is given by [57]:

$$B = 2(f_T - f_R) \tag{3.23}$$

Where: B is the bandwidth of the filter
f_T is the clock frequency of the transmitter PN signal
f_R is the clock frequency of the receiver PN signal

As stated above, for optimal SNR, the filter bandwidth should be equal to $\frac{1}{T_{PN}}$. For the maximal-length PN sequences used in this project, the length of the PN sequence is:

$$N_{PN} = 2^r - 1 \tag{3.24}$$

Where: N_{PN} is the length of the PN sequence
r is the number of shift registers in the PN generator circuit

Therefore, for a fixed PN sequence length and transmitter PN clock frequency, the receiver PN clock rate (and subsequently the slide factor) for optimal SNR can be calculated.

Using the 11-bit PN Generator used in this research, the sequence length is equal to 2048, and the clock frequency is 400 MHz. Therefore, the optimal low pass filter bandwidth is:

$$B = \frac{1}{T_{PN}} = \frac{f_c}{N_{PN}} = \frac{450\,MHz}{2047} = 195\,kHz$$

This bandwidth corresponds to a receiver PN clock rate of:

$$B = 2\left(f_T - f_R\right)$$
$$f_R = 400\,MHz - \frac{195\,kHz}{2}$$
$$f_R = 399.9\,MHz$$

And a channel sounder slide factor of:

$$k = \frac{f_T}{f_T - f_R} = \frac{400\,MHz}{400\,MHz - 399.9\,MHz} = 4000$$

3.5 Conclusion

In this chapter, a variety of issues concerning the design and implementation of the upgraded sliding correlator channel sounder were discussed. The objective was to create a compact and portable measurement system capable of characterizing a wide variety of wireless channels with user selectable time-domain multipath resolution ranging from 100 feet (for outdoor measurements) to 2.5 feet (for indoor measurements). In order to accomplish these objectives, several of the channel sounder's subsystems were implemented on printed circuit boards, and the design, layout, and manufacturing constraints were discussed.

The upgraded channel sounder would also have the capability to characterize the multipath phase response and Doppler spectrum of the channel via I&Q demodulation.

Measuring the absolute phase response of the channel with a high level of accuracy requires synchronization of the transmitter and receiver local oscillators, and a variety of methods for accomplishing synchronization were presented. I&Q demodulation also requires a properly designed correlator unit for maximal SNR and these design equations were also presented. Chapters 4 and 5 discuss the actual implementation of the upgraded channel sounder transmitter and receiver.

Chapter 4

Sliding Correlator Transmitter

4.1 Overview

The sliding correlator transmitter developed as part of this thesis is an upgrade of the millimeter-wave version developed by Xu and Rappaport [56, 64]. Three major changes were made to the channel sounder: GPS disciplined oscillators were used as frequency references, a 450 MHz PN generator was added, and a miniaturized PN clock signal generator was installed.

A block diagram of the implementation of the Sliding Correlator Channel Sounder Transmitter is shown in Figure 4.1. A GPS Disciplined Oscillator provides a highly stable 10 MHz reference signal which is input to the HP Frequency Synthesizer as well as the PN Clock Signal Generator; both of which phase lock the output signal to the 10 MHz reference signal. The HP Synthesizer provides the 5.4 GHz local oscillator and the PN Clock Signal Generator provides a 10 – 500 MHz user selectable clock signal for the PN Generator.

The output of the HP Frequency Synthesizer is then input to a power splitter. One of the resulting signals is input to the LO port of the Miteq mixer, and the other to the LO port of the HRL Upconverter. The output of the PN Generator is then input to the IF port of the with the Miteq mixer. This BPSK modulates the 5.4 GHz LO signal, which yields a signal spectrum with a $\left(\frac{\sin(x)}{x}\right)^2$ pattern with a null-null bandwidth equal to twice the clock frequency of the PN Generator. This modulated signal is then input to the IF port of an HRL Upconverter, where it is

then broadcast over the channel at 38 or 60 GHz. Images of the 38 and 60 GHz transmitters are given in Figure 4.2.

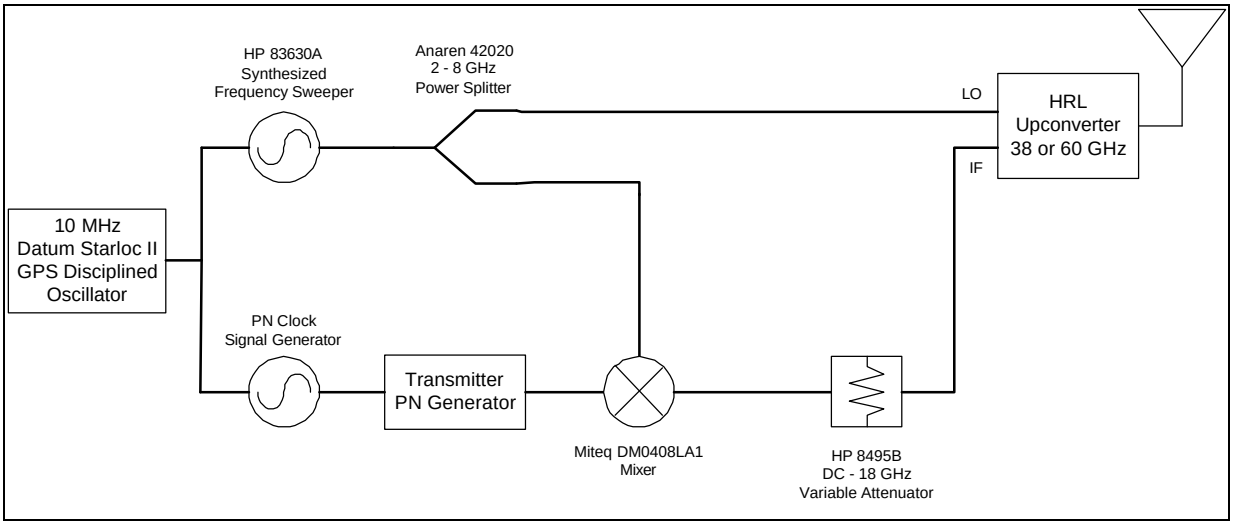

Figure 4.1: Transmitter Block Diagram

Figure 4.2a: 38 GHz Transmitter

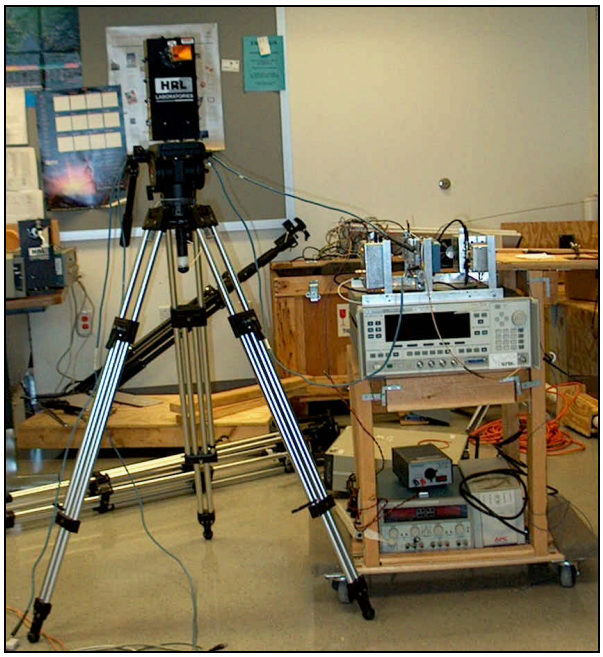

Figure 4.2b: 60 GHz Transmitter

Figure 4.2: Channel Sounder Transmitter Images

4.2 Implementation

4.2.1 GPS Disciplined Oscillator

The GPS Disciplined Oscillator is a Datum Starloc II™ ovenized oscillator. This unit contains an ovenized oscillator and is capable of tracking 8 GPS satellites, yielding a stability of $s_y^2(t) = 3 \times 10^{-12}$. In addition, it utilizes an advanced timing algorithm such that—after initial synchronization—only one GPS signal is necessary in order to maintain timing synchronization of the internal ovenized oscillator [62]. Table 4.1 shows the effects of the GPS disciplined oscillators on the performance of the channel sounder. Of particular importance is the maximum measurement time for a desired phase angle resolution of ±10°, ±90°, and ±180°. Essentially, this means that a series of delay profiles recorded within this time period will have the desired phase angle resolution; e.g., if 10 delay profiles were recorded at 38 GHz within 4.0 seconds, then the measured phase angle of a line-of-sight or multipath component would be within ±90° of the absolute phase of the signal.

Table 4.1
Performance of 38 & 60 GHz Channel Sounder with 400 MHz PN Code

Parameter	38 GHz Channel Sounder Performance	60 GHz Channel Sounder Performance
Length of time before PN codes slip one chip (2.25 nanoseconds) (Equation 3.17)	830 sec	830 sec
Maximum measurement time for phase angle resolution of ±10°, ±90°, and ±180° (Equation 3.19)	0.5 sec / 4.4 sec / 8.8 sec	0.3 sec / 2.8 sec / 5.6 sec
Minimum Doppler shift that the measurement system can resolve (Equation 3.20)	0.11 Hz	0.18 Hz

4.2.2 LO, Power Splitter, and Mixer

Local Oscillator

The local oscillator for the transmitter is provided by an HP 83630A Synthesized Frequency Sweeper. This instrument is capable of producing an output from 100 kHz to 26.5

GHz with a power level of +13 dBm, which is required to drive the mixer and upconverter. This provides the transmitter with a high degree of frequency versatility at the cost of bulk.

Power Splitter

The Anaren 42020 Power Splitter is tuned to operate over a frequency range of 2 – 8 GHz. The power splitter has an amplitude unbalance of ±0.4 dB and a phase unbalance of ±4 degrees. The phase unbalance is a particularly important specification, as it indicates how much of the inphase signal "leaks over" onto the quadrature channel. Essentially, if the signal input to the power splitter is

$$x(t) = \cos(2p\, f_c t) \tag{4.1}$$

Then the output of the power splitter will be

$$y\ (t) = \tfrac{1}{\sqrt{2}} A\cos(2p\, f_c t + q) \tag{4.2}$$

Where: $\frac{1}{\sqrt{2}}$ is the drop in signal amplitude caused by splitting the signal
A represents the amplitude unbalance
θ represents the phase unbalance

Fortunately, the amplitude and phase unbalance are caused by imperfections in the construction of the device, and hence will be constant for a given part. When using the channel sounder to make absolute phase measurements, the sum of all the phase unbalances in all power splitter used in the channel sounder will result in a small constant offset of the measured multipath phase relative to the actual multipath phase.

Mixer

A Miteq MD0408LA1 microwave mixer is used to BPSK modulate the 5.4 GHz LO with the PN sequence. This mixer accepts RF and LO inputs from 4 – 8 GHz and IF inputs from DC-600 MHz. The mixer requires an LO drive level of 7 – 10 dBm, and has a conversion loss of 5 dB.

4.2.3 PN Clock Signal Generator

The PN Clock Signal Generator was designed by Orndorff and a summary of its operation is included here. More detailed information about this device may be found in [58]. The PN Clock Signal Generator uses a Motorola 12430 high frequency PLL clock chip to phase

lock the 10 MHz input signal to a user selectable output signal. The MC12430 contains an integer-N PLL with output divider circuit that can produce outputs from 31.25 MHz to 500 MHz in when using a 10 MHz input signal. External circuits are used to program the MC12430 so that frequencies from 10 MHz to 500 MHz may be output from the Clock Signal Generator. Rotary Switches are used to allow the user to select output frequencies from 12.5 MHz -- 125 MHz in 12.5 MHz steps, from 50 – 500 MHz in 50 MHz steps, or to connect the 10 MHz reference signal to the output. The PCB layout for this device is shown in Figure 4.3, and an image of the implementation is shown in Figure 4.4.

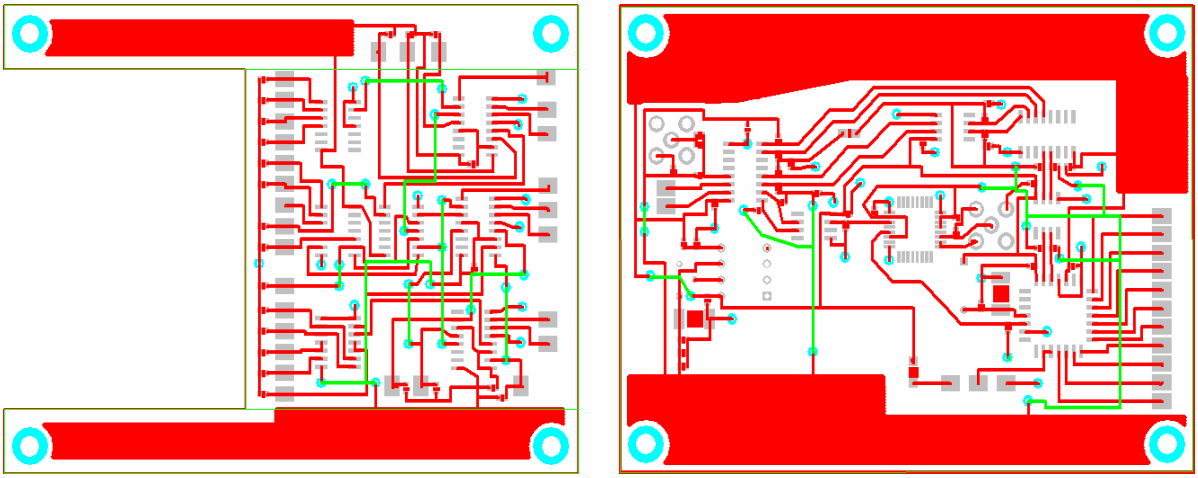

Figure 4.3: PN Clock Signal Generator PCB Layout [58]

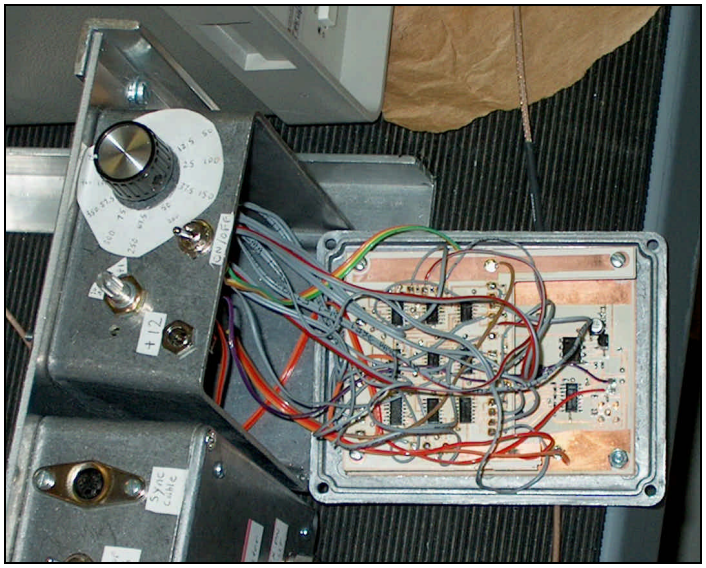

Figure 4.4: PN Clock Signal Generator Implementation [58]

Note that jitter on the output of the PN Clock Signal Generator will degrade the phase measurement resolution of the channel sounder, by causing instability in the timing of the PN sequence. Timing jitter of the PN sequence is on the order of the PN chip time will cause instability in the output of the correlator unit, as the points of maximal correlation (where the received multipath signals maximally correlate with the receiver PN sequence) will vary in time based on the timing jitter, and will result in erroneous phase measurements. If, however, the timing jitter is significantly less than the chip time of the PN sequence, the resulting timing offsets in the points of maximal correlation may be ignored for all practical purposes.

4.2.4 PN Generator

The PN Generator used in the channel sounder is either an 11-bit or 18-bit Maximal Length PN sequence generator and is slightly modified from the final version in [6], which was the precursor to this thesis project. The 11-bit version is feedback tapped at [11, 9] and operates at a maximum frequency of 450 MHz; while the 18-bit version is feedback tapped at [18, 7] and operates at a maximum frequency of 440 MHz. These boards can be quickly and easily interchanged to meet the requirements of a particular measurement campaign. The three primary design changes implemented in the PN generator are summarized below and the final schematic is located in Appendix A.

- The PN sequence startup and synchronize circuit was redesigned.
- The 10E107 XOR chip was replaced with a 10EL07 high-speed XOR chip.
- The PCB layout was altered slightly to provide a higher level of signal integrity.

PN Sequence Startup and Synchronize Circuit

The PN Sequence Startup and Synchronize Circuit is used to initialize the shift registers as well as to synchronize transmitter and receiver PN generators so that absolute propagation delay measurements can be made. Initially, this circuit utilized a toggle switch connected to a 10E131 R-S flip-flop to toggle between loading the shift registers and allowing the PN sequence to free-run. This circuit, however, failed to activate the PN sequence at clock frequencies above 200 MHz. After extensive troubleshooting, it was discovered that this combination produced significant transients on the output of the flip-flop, particularly for clock frequencies above 250 MHz. As the 10E131 was taking up a significant amount of board real estate, it was decided to

remove it entirely and use a simple toggle switch connected to a 10EL01 high-speed OR gate. Capacitors were placed on the input to the OR gate to reduce transients.

XOR Chip Replacement

The original XOR chip used in the PN generator was a 10E107 XOR chip, containing five separate XOR gates. This chip required a significant amount of board real estate and had a signal propagation delay of 600 picoseconds. Since only 2 of its 5 XOR gates were being utilized (one for the PN sequence feedback and one as an output buffer), it was decided to replace this chip with two 10EL07 high-speed single-gate XOR chips. These two chips require less board real estate than the 10E107 chip, which simplified routing the signal traces. In addition, this chip has a signal propagation delay of only 260 picoseconds, which increased the maximum operating frequency of the PN Generator.

PCB Layout Modification

The PCB layout for the PN Generator was modified from [6] in order to accommodate the design changes. Chip placement and signal traces were optimized to produce the minimum possible propagation delay, thus maximizing the operating frequency of the PN Generator. The trace that delivered the signal clock to the two shift register chips was adjusted to provide a nearly equal propagation delay to each chip, minimizing the clock skew. Lastly, ground pins were connected directly to the ground plane, rather than through thermal reliefs. (Thermal reliefs are used to prevent PCB warping in multilayer structures, but add parasitic inductance to ground, degrading the rise time of digital signals and limiting the maximum operating frequency of the circuit). The original PCB layout and the modified layout are presented in Figure 4.5, along with an image of the completed PN Generator PCB in Figure 4.6.

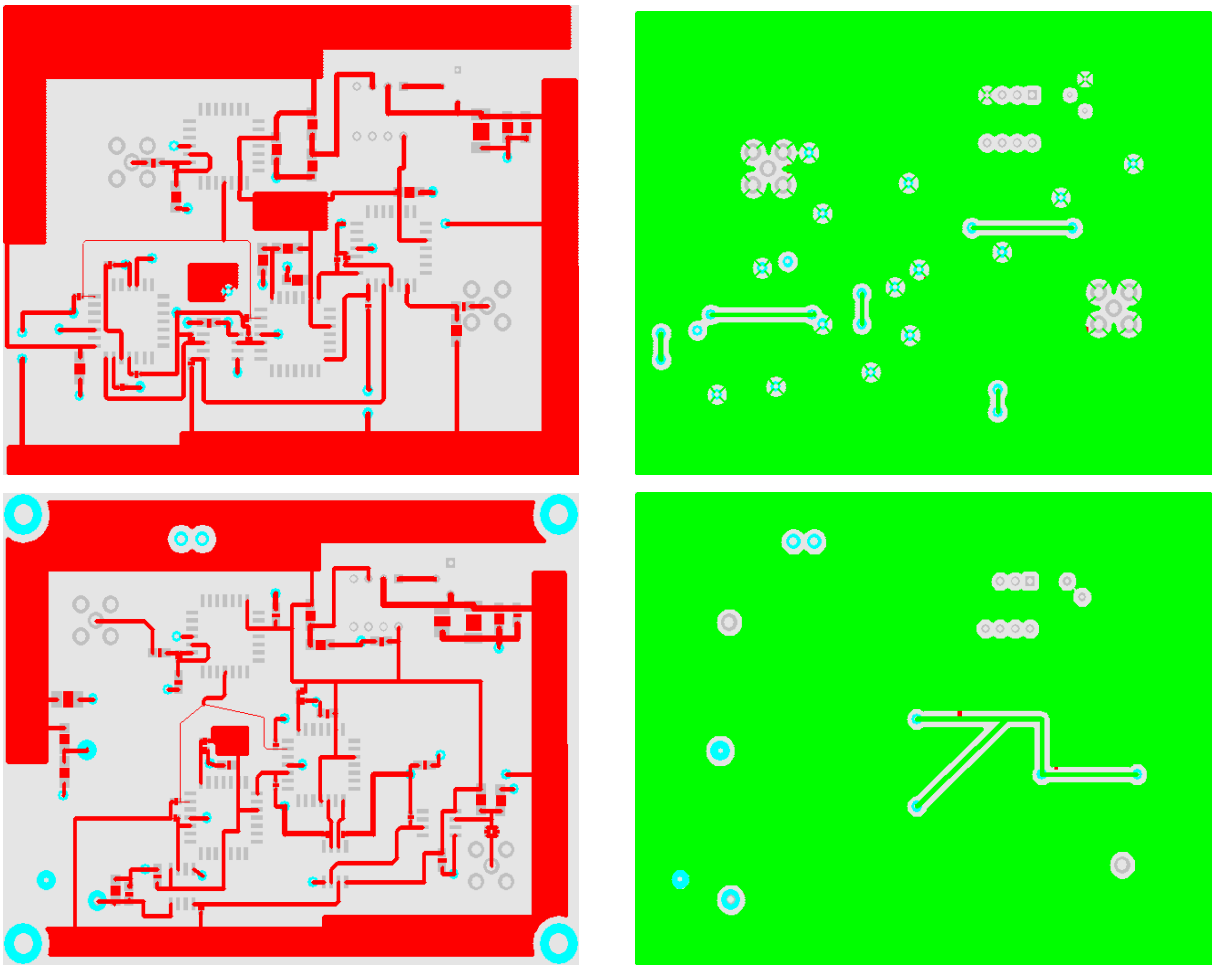

Figure 4.5: Comparison of Old 11-bit PN Generator Top and Bottom Layers (upper left and right) and New 11-bit PN Generator Top and Bottom Layers (lower left and right).

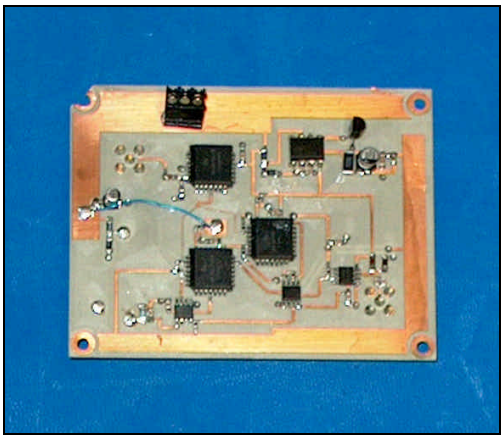

Figure 4.6: PN Generator PCB

4.2.5 Upconverters

The 38 and 60 GHz up/downconverters were manufactured by DBS Microwave/HRL Laboratories, and HRL provided these units to Professor Rappaport as a long-term loan. The up/downconverters are a single unit and Chapter 5 discusses the operation of the downconverter. A functional block diagram is shown in Figure 4.7, images of the upconverters are shown in Figure 4.8, and specifications are listed in Table 4.2.

The upconverters have two inputs, LO and IF. The LO signal is input to a phase-locked frequency multiplier, which generates an internal LO at 32.4 GHz (for the 38 GHz unit) or 54 GHz (for the 60 GHz unit). This internal LO is then mixed with the IF signal input, amplified and transmitted across the channel.

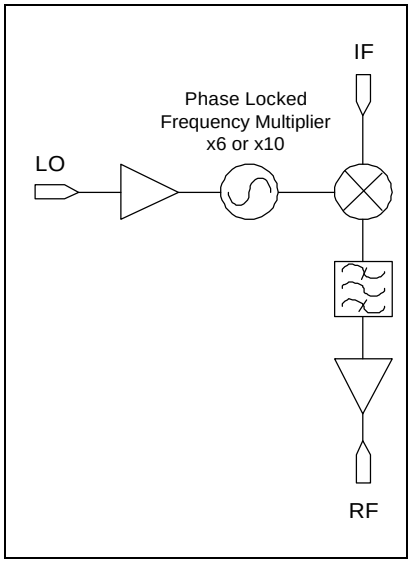

Figure 4.7: Block Diagram of Upconverter

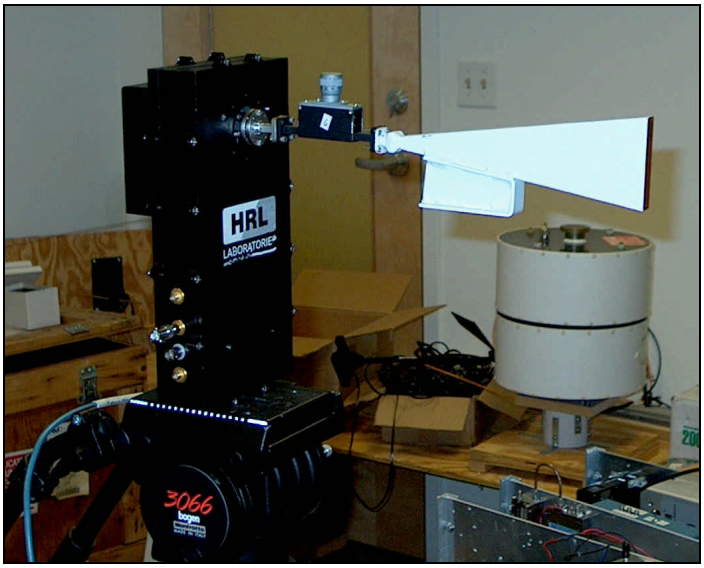

Figure 4.8a: 38 GHz Upconverter

Figure 4.8b: 60 GHz Upconverter

Figure 4.8: 38 GHz and 60 GHz Upconverters

Table 4.2: 38 and 60 GHz Upconverter Specifications

Specification	38 GHz Upconverter	60 GHz Upconverter
Output RF Frequency	37.8 ±0.5 GHz	59.4 ±1 GHz
Input IF Frequency	5.4 ±0.5 GHz	5.4 ±1 GHz
Input LO Power	+10 ±3 dBm	+10 ±3 dBm
Max Input IF Power	-20 dBm	-10 dBm
IF-RF Conversion Gain	20 dB	25 dB
Output Saturation Power Level	+27 dBm	+15 dBm
Antenna / Gain	Sector Horn / 19 dBi	Horn / 25 dBi

4.3 Conclusion

The upgraded ultrawideband channel sounder is capable of broadcasting a 10 – 450 MHz PN sequence at 38 or 60 GHz. Additionally, the implementation is flexible enough that other wireless channels could be characterized by constructing upconverters at a different operating frequency. A GPS disciplined frequency reference and a miniaturized PN clock signal generator were used to miniaturize the physical size of the transmitter, in order to create a smaller, more portable measurement system.

Chapter 5

Sliding Correlator Receiver

5.1 Overview

The sliding correlator receiver is based on the millimeter-wave channel sounder receiver developed by Xu, Kukshya, and Durgin under the direction of Professor Rappaport [63, 64, 65]. Several important design changes were made to implement a receiver capable of performing magnitude and phase channel measurements. The channel sounder subsystems that were added or improved are listed below:

- High-Speed PN Generator and PN Clock Signal Generator
- GPS Disciplined Oscillator
- Quadrature mixer
- I/Q Correlator Unit
- PCMCIA Digital Oscilloscope Card
- LabVIEW Data Postprocessing

A block diagram of the implementation of the Sliding Correlator Channel Sounder Receiver is shown in Figure 5.1. A GPS disciplined oscillator, identical to the one used at the transmitter, provides a 10 MHz reference signal to the CTI Microwave 50 MHz PLL, the HP 8648C signal generator, and to the PN Clock Signal Generator. The output of the CTI PLL is input to a Magnum Microwave Dielectric Resonator Oscillator (DRO), which provides a 5.4 GHz local oscillator signal. The output of the DRO is fed into a power splitter, with one of the resulting outputs connected to the LO port on the HRL downconverter unit and the other output amplified to the appropriate drive level and connected to the LO port on the Anaren quadrature

mixer. The IF output from the HRL downconverter is amplified and input to the RF port on the Anaren quadrature mixer. The Anaren mixer has two outputs, IF1 (the inphase signal) and IF2 (the quadrature signal). These two outputs are low-pass filtered and connected to the I/Q correlator unit.

The receiver has two separate PN generators, the "Receiver PN Generator" and the "Transmitter PN Generator." The Receiver PN Generator is clocked by the HP 8648C signal generator, and is run at a rate slightly slower than the transmitter PN generator. The output from the Receiver PN Generator is connected to the I/Q correlation unit, which performs the sliding correlation operation described in Chapter 2. The "Transmitter PN Generator" is an identical copy of the PN generator used at the transmitter, and their PN codes and clock frequencies are synchronized so that the receiver's "Transmitter PN Generator" (which will be referred to as the TX PN Generator to avoid confusion) will produce a PN sequence identical to the Transmitter PN Generator's PN sequence.

The Receiver PN Generator also contains a trigger pulse generator board. The trigger pulse generator board performs a sliding correlation operation on the PN sequences generated by the Receiver PN Generator and the TX PN Generator. When these two PN sequences are aligned, a pulse will be output from the trigger pulse generator board. The pulse is used to trigger a Data Acquisition (DAQ) card and corresponds to time zero at the transmitter, allowing absolute propagation delay measurements to be made.

The I/Q Correlator unit performs a sliding correlation operation on the inphase and quadrature signals from the Anaren mixer with the Receiver PN sequence. The output of I/Q Correlator unit is the inphase and quadrature delay profiles, which are digitized and recorded to disk using a PCMCIA DAQ card and laptop computer. Post-processing and statistical analysis of the recorded data is done in LabVIEW and Matlab. Images of the 38 and 60 GHz receivers are shown in Figure 4.2.

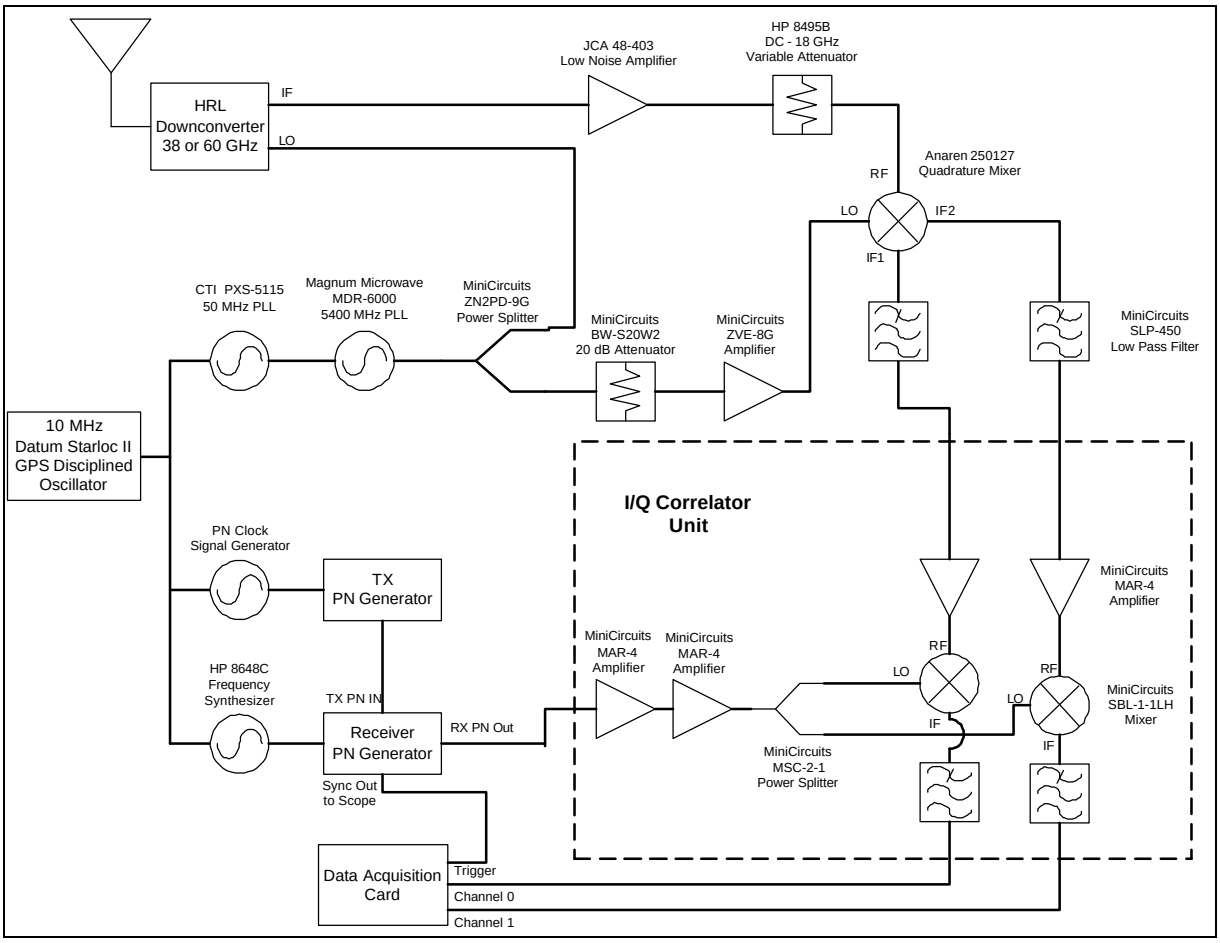

Figure 5.1: Receiver Block Diagram

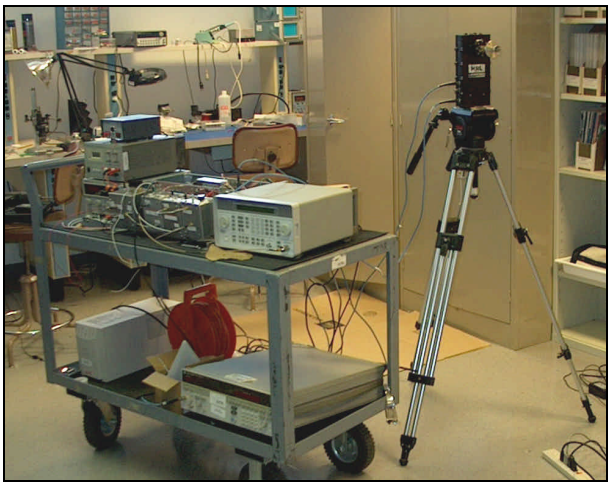

Figure 5.2a: 38 GHz Receiver

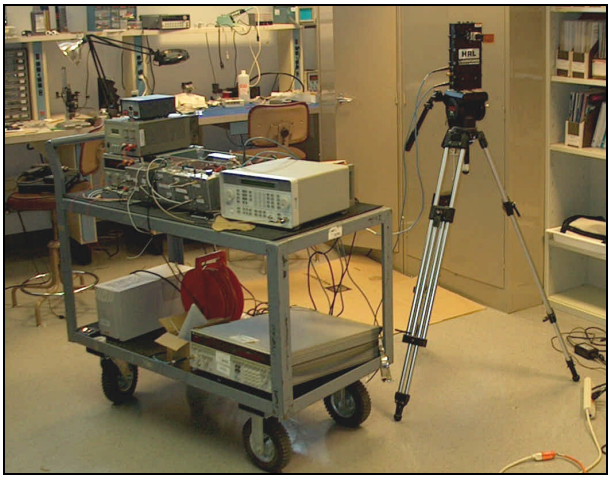

Figure 5.2b: 60 GHz Receiver

Figure 5.2: Channel Sounder Receiver Images

5.2 Receiver LO and Power Splitter

Local Oscillator

The Receiver local oscillator is composed of a CTI PXS-5115 50 MHz PLL and a Magnum Microwave MDR-6000 5400 MHz DRO. The CTI signal is phase-locked to the 10 MHz GPS oscillator, and the DRO is phase locked to the 50 MHz CTI oscillator. This double-PLL implementation was chosen because a DRO that phase-locks to a 50 MHz signal rather than a 10 MHz signal is less expensive. The DRO provides an output power level of +13 dBm at 5400 ±10 MHz, with its center frequency adjustable via a set screw on the front panel. The frequency stability of both the CTI and Magnum Microwave oscillators is equal to that of the reference signal; therefore providing a high-quality local oscillator signal for the receiver in a reasonably compact package. The disadvantage of the double-PLL design is that the LO signal is fixed (whereas at the transmitter it was variable) and in order characterize channels below 5.4 GHz a different oscillator would need to be installed.

Power Splitter

The output from the local oscillator is connected to a MiniCircuits ZN2PD-9G 1.7 GHz – 9 GHz power splitter. One of the power splitter's outputs provides the LO reference for the HRL downconverter and the other output provides the LO signal for the Anaren quadrature mixer. The power splitter has an amplitude unbalance of ±0.6 dB and a phase unbalance of ±4 degrees.

5.3 Downconverters

The 38 and 60 GHz downconverters were manufactured by DBS Microwave/HRL Laboratories and are the counterpart to the upconverters used at the transmitter. The downconverters have the same form factor as the upconverters discussed in Chapter 4. A functional block diagram is shown in Figure 5.3, specifications are listed in Table 5.1, and images of the downconverters are shown in Figure 5.4.

The downconverters use the 5.4 GHz LO signal generated by the receiver as an input to an internal phase-locked frequency multiplier, generating an internal LO signal. The received RF signal is amplified and then mixed with the internal LO. The resulting 5.4 GHz IF signal is then output to the IF port of the downconverter.

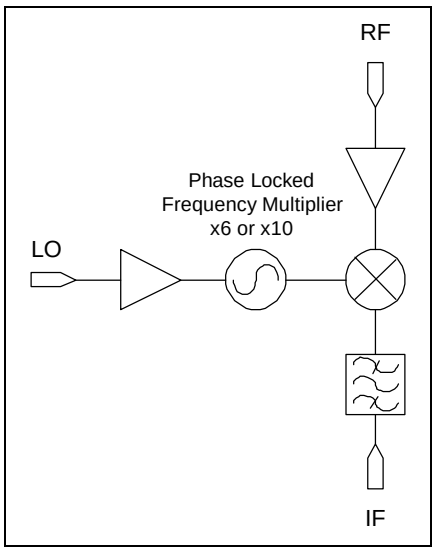

Figure 5.3: Block Diagram of Downconverter

Figure 5.4a: 38 GHz Downconverter

Figure 5.4b: 60 GHz Downconverter

Figure 5.4: 38 and 60 GHz Downconverters

Table 5.1: 38 and 60 GHz Downconverter Specifications		
Specification	**38 GHz Downconverter**	**60 GHz Downconverter**
Input RF Frequency	37.8 ±0.5 GHz	59.4 ±1 GHz
Output IF Frequency	5.4 ±0.5 GHz	5.4 ±1 GHz
Input Dynamic Range	-60 to -20 dBm	-60 to -20 dBm
Input LO Power	+10 ±3 dBm	+10 ±3 dBm
RF-IF Conversion Gain	20 dBm	25 dB
Noise Figure	8.0 dB	7.0 dB
Antenna / Gain	Parabolic Reflector / 39 dBi	Horn / 25 dBi

An external JCA 48-403 low-noise amplifier is used to boost the IF signal level in order to overcome conversion losses in the subsequent mixers. This amplifier provides 35 dB of gain, a 19 dBm compression point, and a 1.5 dB noise figure over a 4—8 GHz frequency range. Multiple amplifiers may be connected in series in order to provide enough gain to overcome high levels of path loss experienced during rain, snow, or other channel phenomenon.

5.4 Receiver PN Generator and Trigger Pulse Generator

The Receiver PN Generator is composed of two Printed Circuit Boards, the receiver PN generator board and the trigger pulse generator board. The receiver PN generator board is a slightly modified version of the transmitter PN generator design—a second PN output was added and connected to the trigger pulse generator board. Except for this change, the layout and operation of the PN generator board is identical to the Transmitter PN Generator. An HP 8634B signal generator provides the clock signal for the PN generator. The use of the 8634B adds bulk to the receiver, but provides a large degree of flexibility in choosing the operating frequency for the PN generator (and hence the slide factor). One possible replacement for the 8634B is a fractional-N phase lock loop (PLL) frequency synthesizer, which would be capable of producing a wide variety of PN clock frequencies. The fractional-N PLL approacch, however, has two major disadvantages:

1. A high-quality bandpass filter would be needed to remove the reference spurs from the output of the PLL. In order to avoid placing significant restrictions on the range of output frequencies the PLL could produce, the bandpass filter would have to be implemented digitally.
2. A fractional-N PLL works by “swallowing” pulses from the output, meaning that the instantaneous output frequency is either slightly higher or lower than the desired

output frequency [71]. Because precise timing is critical for measuring the magnitude and phase of the channel impulse response, the effects of "pulse swallowing" on the PN generator output as well as the resolution of the channel sounder would need to be investigated.

Because the 8634B was already available in the lab, it was decided that its inclusion in the channel sounder was worth the increase in bulk and decrease in development time.

The trigger pulse generator board was designed to trigger a DAQ card to begin recording data. If zero propagation delay exists, then the maximum voltage of the delay profile output from the I/Q Correlator unit will occur at exactly the same time as the sync pulse. With signal propagation delay, the maximum voltage of the delay profile will occur at some time offset relative to the sync pulse, and the actual delay can be measured to a resolution equal to the chip period of the PN sequence.

The trigger pulse generator board mixes and low-pass filters the PN sequence from the Receiver PN generator with the PN sequence from the TX PN Generator, and its design is based on the oscilloscope triggering technique described in [10]. The operation of the trigger pulse generator board is simple: a MiniCircuits MAR-7SM amplifies the receiver PN signal to the appropriate LO drive level for the MiniCircuits UNCL-L1H Mixer. The TX PN generator signal is input to the RF port of the Mixer, and the IF output is low-pass filtered (time integrated) and connected to the 'Sync Out to Scope' output of the Receiver PN Generator.

Figures 5.5-5.7 shows the board layout for the 11-bit and 18-bit Receiver PN generator boards and trigger pulse generator board. Figure 5.8 shows the completed Receiver PN generator board and trigger pulse generator board. Schematics may be found in Appendix A.

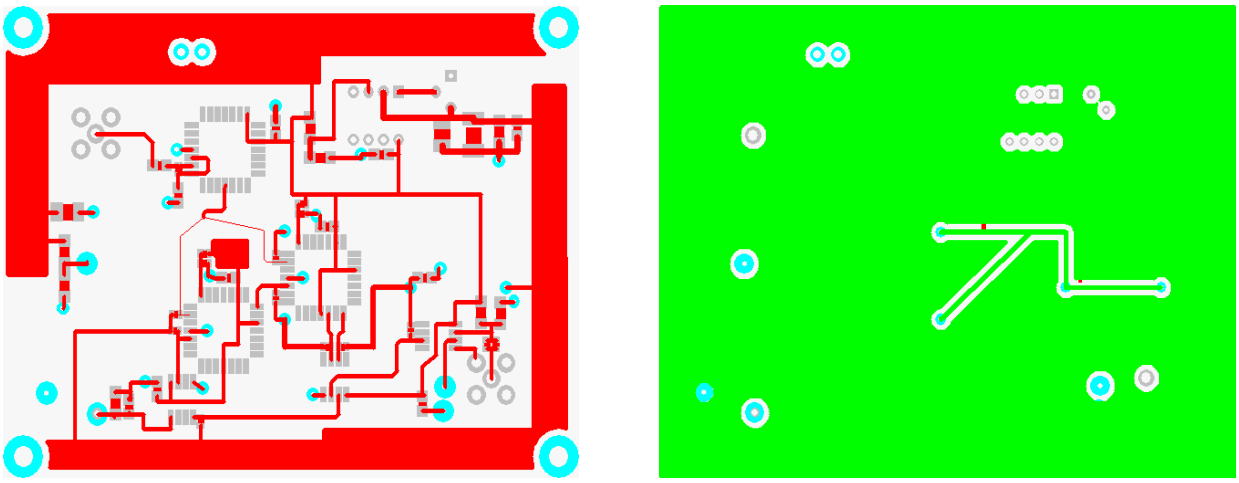

Figure 5.5: 11-bit Receiver PN Generator Board Top and Bottom Layers

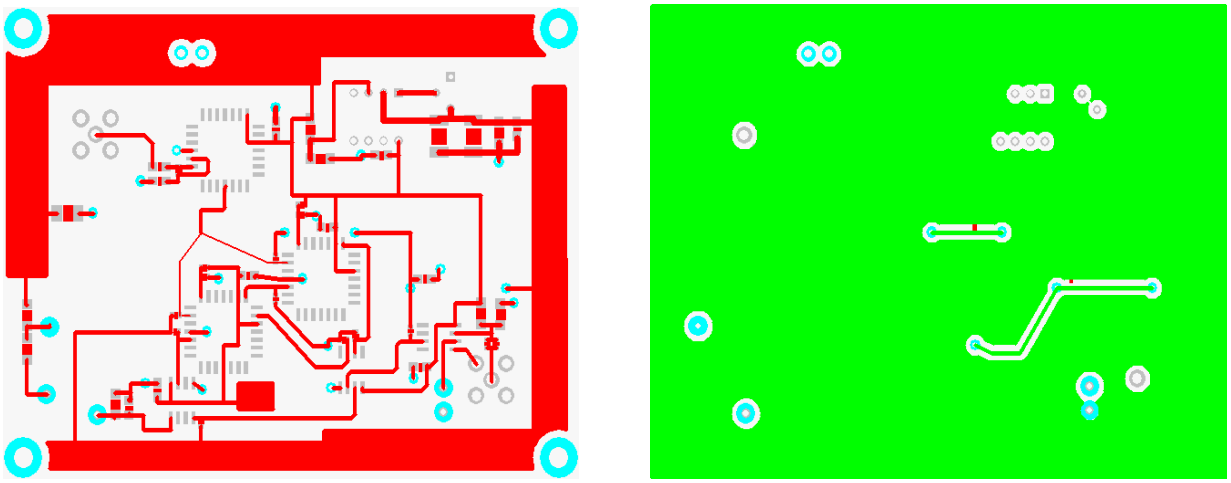

Figure 5.6: 18-bit Receiver PN Generator Board Top and Bottom Layers

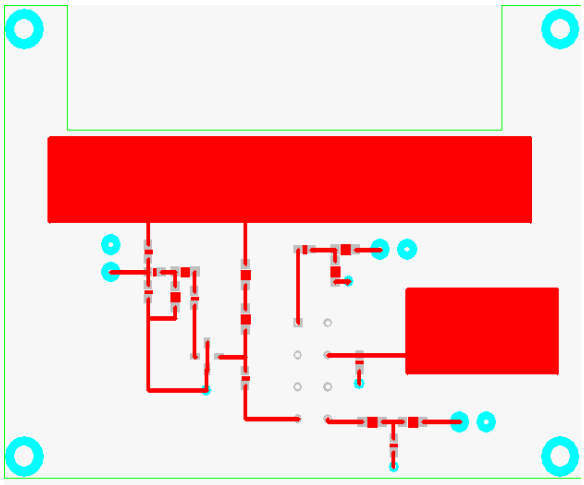

Figure 5.7: Receiver PN Trigger Pulse Generator Board

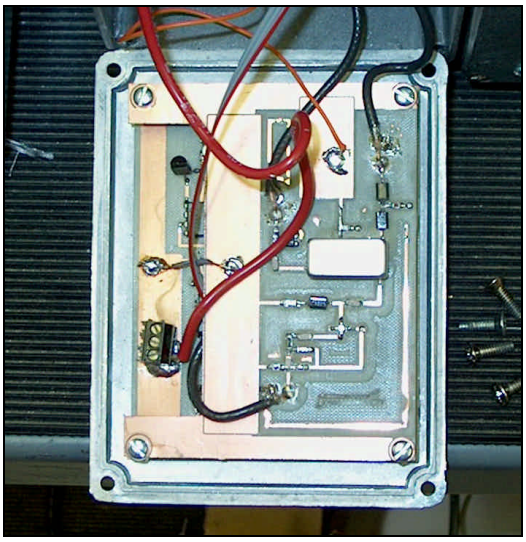

Figure 5.8: Receiver PN Generator and Trigger Pulse Generator

5.5 I/Q Demodulation

I/Q Demodulation is carried out by the receiver in two stages—the quadrature mixer and the I/Q Correlator. The quadrature mixer generates inphase and quadrature baseband signals from the 5.4 GHz IF signal, which the I/Q Correlator uses to create the inphase and quadrature delay profiles.

5.5.1 Quadrature Mixer

The inphase and quadrature baseband signals are generated by the Anaren 250127 Quadrature IF mixer. The mixer has an RF/LO Bandwidth ranging from 4 – 8 GHz and an IF Bandwidth of DC — 400 MHz, with a 10 dB conversion loss, required LO drive level of +13 dBm, and a 1 dB compression point on the RF input of +10 dBm. A MiniCircuits ZVE-8G amplifier is used to provide the appropriate signal level. While the use of this amplifier is actually overkill (it has a 1 dB compression point of +30 dBm and an IP3 of +40 dBm), it was left over from a previous measurement campaign and was used to reduce the cost of implementing the receiver.

The IF1 and IF2 (inphase and quadrature) outputs from the quadrature mixer have a rated amplitude/phase unbalance of ±1.2 dB / ±10°. These IF outputs are filtered using MiniCircuits SLP-450 low pass filters, which bandlimits the output baseband waveforms and reduces the noise bandwidth of the resulting signals.

5.5.2 I/Q Correlation Design

The I/Q Correlator unit (Figure 5.9) performs a sliding correlation operation between the inphase and quadrature baseband signals and the Receiver PN sequence. Central to the design of the correlator unit is the mixer/low-pass filter combination that performs the correlation operation, as the mixer and filter characteristics determine the dynamic range and linearity of the measurement system.

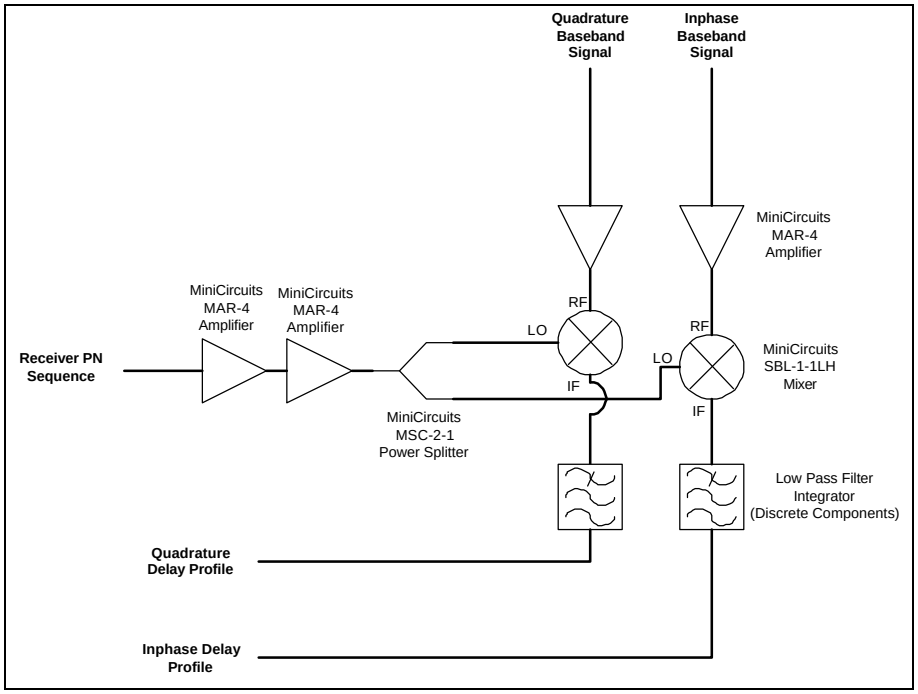

Figure 5.9: I/Q Correlator Unit Block Diagram

Mixer Selection

The mixer utilized in the Correlator unit is the MiniCircuits SBL-1-1LH, which provides an LO/RF bandwidth from 0.2—400 MHz and an IF bandwidth of DC—400 MHz. This mixer requires an LO drive level of +10 dBm, has a 1 dB compression point on the RF input of +5 dBm, and a RF/LO conversion loss of 5 dB. The SBL-1-1LH was chosen because it provides a reasonable tradeoff between LO drive level and the maximum RF input signal level (as determined by the 1dB compression point). The tradeoff between LO drive level and RF compression point is important because the output from the Receiver PN Generator is only 3.0 dBm and must be amplified to meet the LO drive level specification of the mixer. The use of the SBL-1-1LH meant that inexpensive low-power amplifiers could be used to amplify the Receiver

PN Generator output to the appropriate level. Unfortunately, the compression point specification limits the maximum RF signal level that can be input to the mixer, in turn limiting the dynamic range of the receiver. A mixer that would be capable of handling stronger RF signals requires an LO drive level of +13 to +21 dBm, necessitating the use of more expensive medium-power amplifiers. In order to keep costs down the MiniCircuits SBL-1-1LH was chosen for use in the I/Q Correlator Unit.

The Receiver PN Generator produces a PN sequence at a power level of +2 dBm, and the MiniCircuits MSC-2-1 power splitter has an insertion loss of 3.5 dB. In order to provide the appropriate LO drive level for the SBL-1-1LH mixer, MiniCircuits MAR-4 amplifiers were used to amplify the PN sequence. These amplifiers have a gain of 7 dB, and a 1 dB compression point of +14 dBm, therefore two amplifiers operating in series were required to provide the appropriate LO drive level for the mixer.

Low Pass Filter Design

As discussed in Chapter 3, the bandwidth of the low-pass filter following the mixer (see Figure 5.9) is critically important to ensuring that the maximum SNR is achieved by the channel sounder. Equation 5.1 shows the relationship between low pass filter bandwidth, PN clock frequency, and PN code length. Since the channel sounder was designed to operate with PN clock rates ranging from 10 MHz to 400 MHz, the maximum and minimum filter bandwidths were calculated for the 11-bit and 18-bit PN sequences and the results are listed in Table 5.2.

$$B = \frac{1}{T_{PN}} = \frac{f_{PN}}{2^r - 1} \tag{5.1}$$

Where: B is the bandwidth of the low pass filter
T_{PN} is the period of the PN code
f_{PN} is the clock frequency of the transmitter PN signal
r is the number of shift registers in the PN generator circuit

Table 5.2: Correlator Low Pass Filter Bandwidth Required for Maximum and Minimum PN Clock Rate

PN Sequence	Minimum Required Bandwidth (10 MHz PN Code)	Maximum Required Bandwidth (400 MHz PN Code)
11-bit	4.88 kHz	195 kHz
18-bit	38 Hz	1.53 kHz

From Table 5.2, it is obvious that a great disparity exists between the minimum and maximum bandwidth requirements. The choice of a filter bandwidth that is too large will result in a higher noise level in the delay profiles; however, a filter bandwidth that is too narrow will distort the shape of the delay profile [60]. In practice, the filter bandwidth requirements are less stringent, and may be set to approximately twice the frequency offset between transmitter and receiver PN sequences with minimal impact on the noise level and signal distortion [60].

The channel sounder was designed primarily to characterize ultrawideband channels using the 11-bit PN Generator running at a clock speed of 400 MHz. From Table 5.2, the corresponding low-pass filter bandwidth necessary to achieve maximum SNR in the Correlator is 195 kHz. Provisions were made on the circuit board layout so that a tighter filter could be implemented if a different PN code length/clock frequency combination was desired.

The low pass filter was implemented with a 3-element butterworth low-pass filter, as this configuration provides a maximally flat response in the passband. The frequency response for the filter is shown in Figure 5.10.

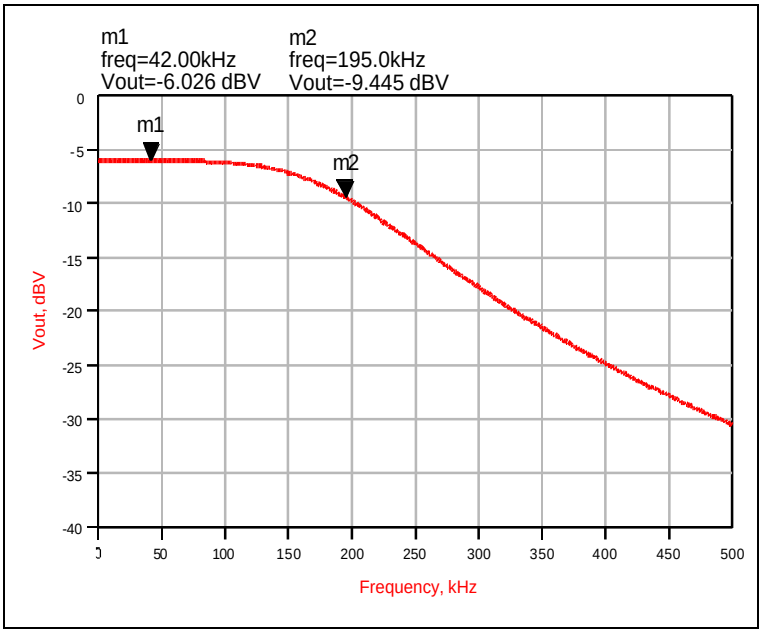

Figure 5.10: I/Q Correlator Low-Pass Filter Frequency Response

Organization of the Correlator

The correlator as a whole was split into two separate halves, one for the inphase channel and one for the quadrature channel. Each half performs an identical mixing and low-pass

filtering operation on either the inphase or quadrature baseband signal. The receiver PN sequence is input to a MiniCircuits MSC-2-1 Power Splitter and amplified to the appropriate drive level using MiniCircuits MAR-4 surface mount amplifiers. These amplifiers provide 7 dB of gain from DC — 1 GHz and have a 1dB compression point of 12.5 dBm. The amplifiers are also used to give an added boost to the inphase and quadrature baseband signals.

5.5.3 I/Q Correlator PCB Layout

In order to facilitate the miniaturization of the channel sounder, the I/Q Correlator unit was implemented on a Printed Circuit Board. The substrate used was Rogers TMM 6, which has a dielectric constant of $e_r = 6$. A board thickness of 20 mils yields a microstrip trace width of 28.9 mils for a 50 O characteristic impedance, which was a reasonable tradeoff between board manufacturability and simplicity of board layout.

For the PN generator board layout, the primary concern was minimizing the signal propagation delay through the network, to maximize the frequency at which it could operate. For the correlator, the emphasis was on preventing noise and crosstalk from corrupting the inphase and quadrature signals. Since the board was divided into two halves, a ground strip was placed in the center of the board, in order to provide increased isolation between the two sides. Additionally, power supply bypass capacitors and filtering inductors were used throughout the board to reduce coupling along the power supply rail. The final board layout is shown in Figure 5.11, and an image of the finished Correlator unit is shown in Figure 12.

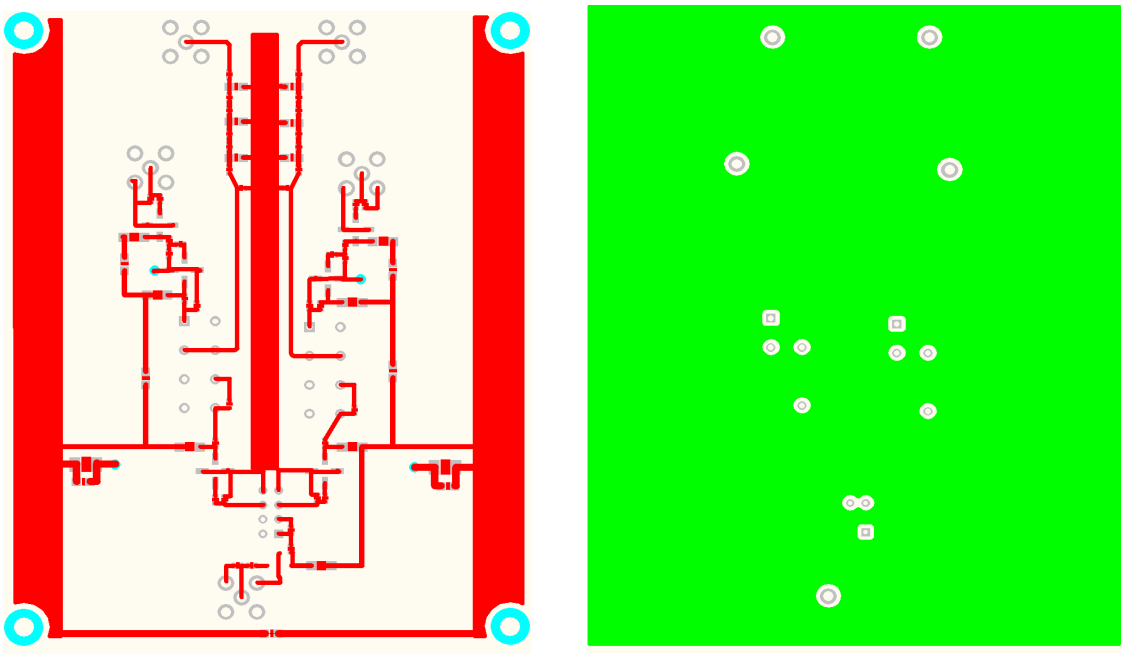

Figure 5.11: I/Q Correlator Board Layout Top (left) and Bottom Layers

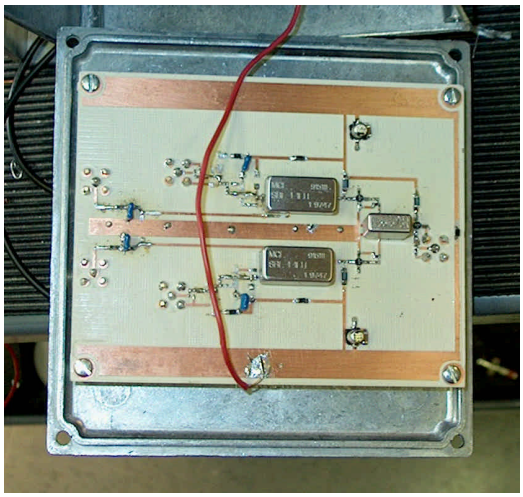

Figure 5.12: I/Q Correlator Implementation

5.5.4 Data Acquisition and Post Processing

Data Acquisition

In the previous version of the channel sounder, data acquisition was performed with a Textronix TDS-784C Digital Oscilloscope connected to a laptop via a GPIB interface. This instrument added a significant amount of size and bulk to the receiver, and it was decided to replace it with a National Instruments 5102 PCMCIA digitizing oscilloscope card. The DAQ card is used to digitize the inphase and quadrature delay profiles output from the I/Q Correlation

Unit. The DAQ software was implemented in LabVIEW by Orndorff [58], and has three primary features: real-time display, system calibration, and data logging.

As seen in Figure 5.13, the user interface was designed to look and function similarly to a digital oscilloscope. The design was chosen to ease in the transition from the Textronix oscilloscope/GPIB data acquisition system.

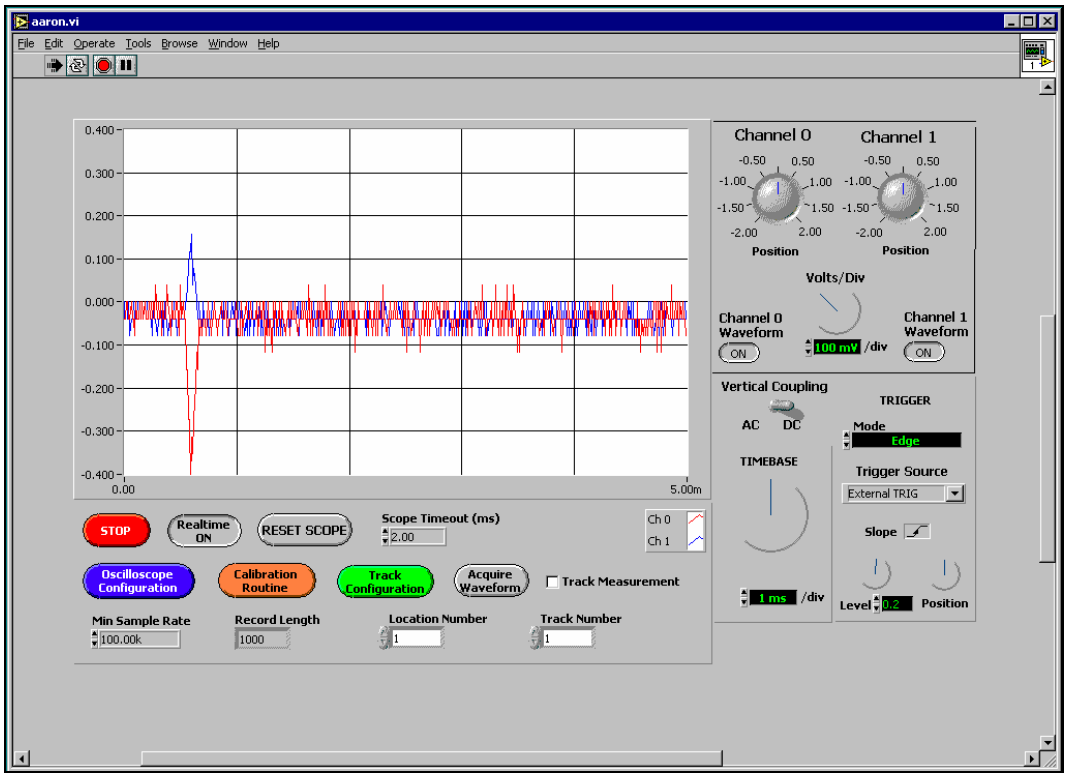

Figure 5.13: LabVIEW Channel Sounder Data Acquisition System from [58]

Data Post-Processing

Separate LabVIEW and Matlab programs are used to post-process the recorded delay profiles. The Matlab Channel Imaging Analysis Suite was used in previous versions of the channel sounder to perform a variety of statistical analyses on the recorded waveforms [63, 65]. Because the Analysis Suite was designed to be used with the original DAQ software (which was only capable of recording magnitude power delay profiles), a LabVIEW overlay was written in order to maintain compatibility between the new DAQ software and the Analysis Suite. Additionally, LabVIEW analysis software was written to supplement the capabilities of the Analysis Suite.

LabVIEW Analysis Software

The LabVIEW post-processing software (Figures 5.14—5.15) generates magnitude power delay profiles, Doppler spread, and multipath phase plots using the recorded inphase and quadrature delay profiles. Individual or spatially averaged magnitude PDPs can be displayed on screen and/or recorded to disk as a text file compatible with the Analysis Suite. The ability to record data as text files also allows the results from channel measurements to be compared with simulations such as ray tracing, an example of which is shown in Figure 5.16.

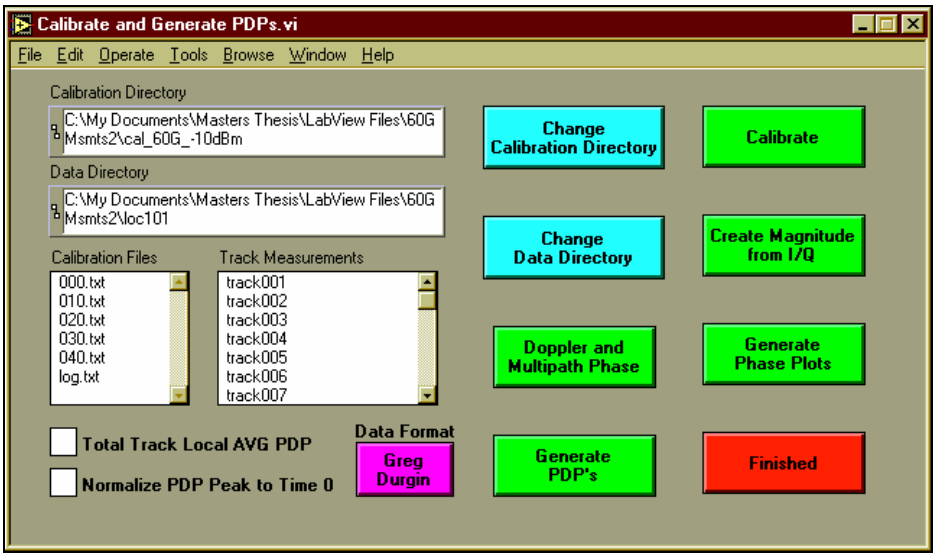

Figure 5.14: LabVIEW Data Postprocessing System

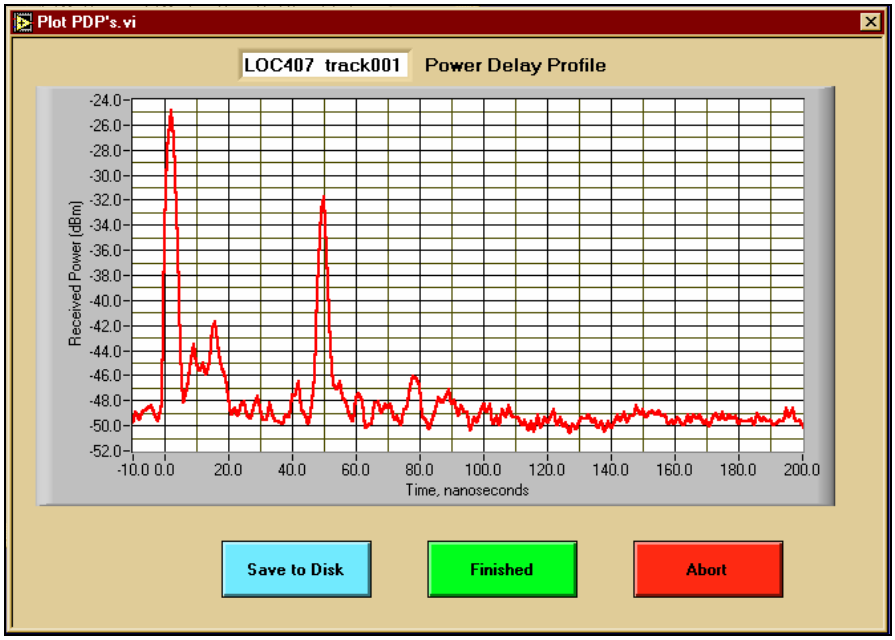

Figure 5.15: LabVIEW Data Postprocessing Power Delay Profile

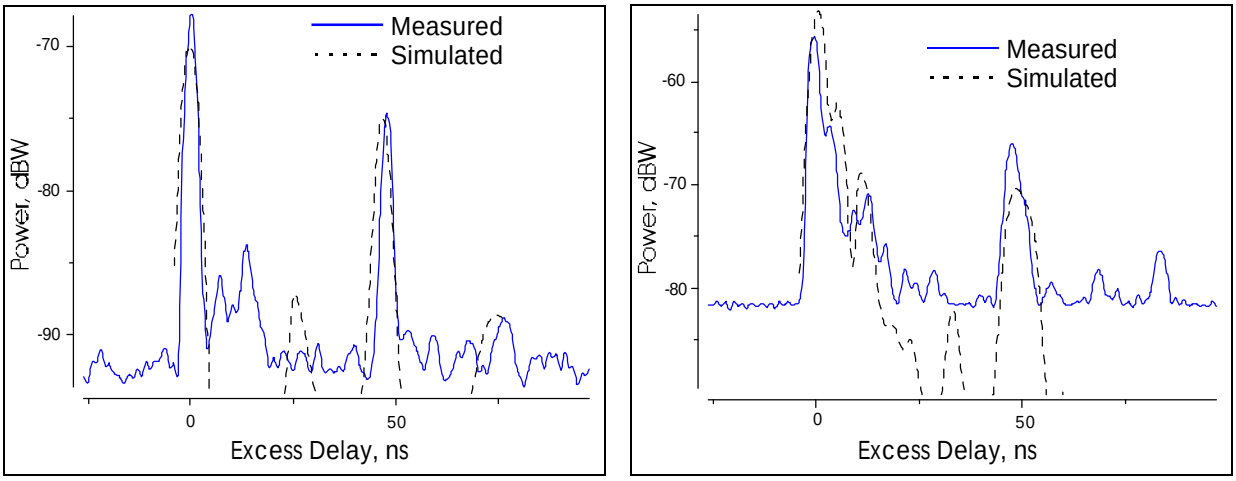

Figure 5.16: Comparison of Measured PDPs with Ray Tracer Simulated PDPs from [66]

In addition to the PDPs, the Doppler spread and multipath phase plots can be generated by the LabVIEW software, displayed on screen, and recorded to disk for further analysis (Figure 5.17—18). These graphs are used to obtain a more complete picture of the channel transfer function, as well as to determine statistical parameters such as coherence time.

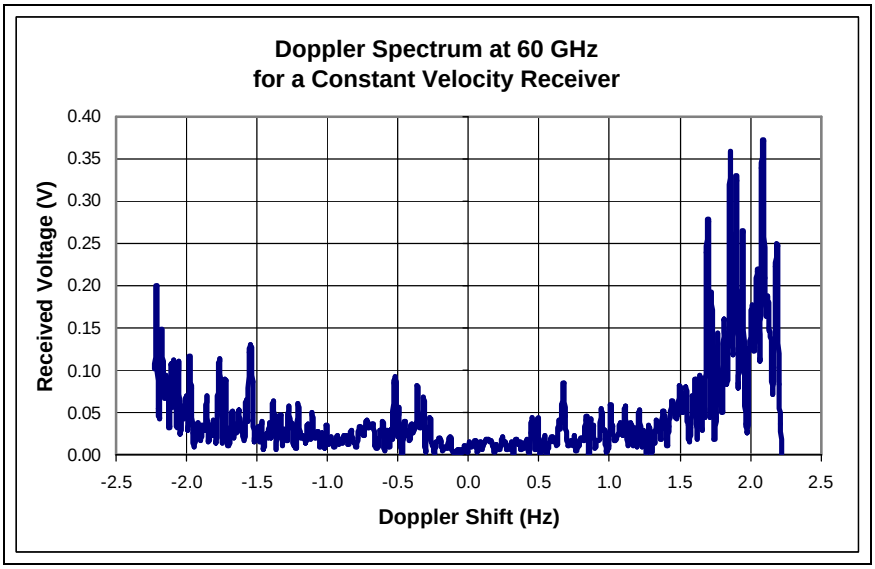

Figure 5.17: Doppler Spectrum Example for a 60 GHz Receiver Moving at a Constant Velocity of 0.01 m/s

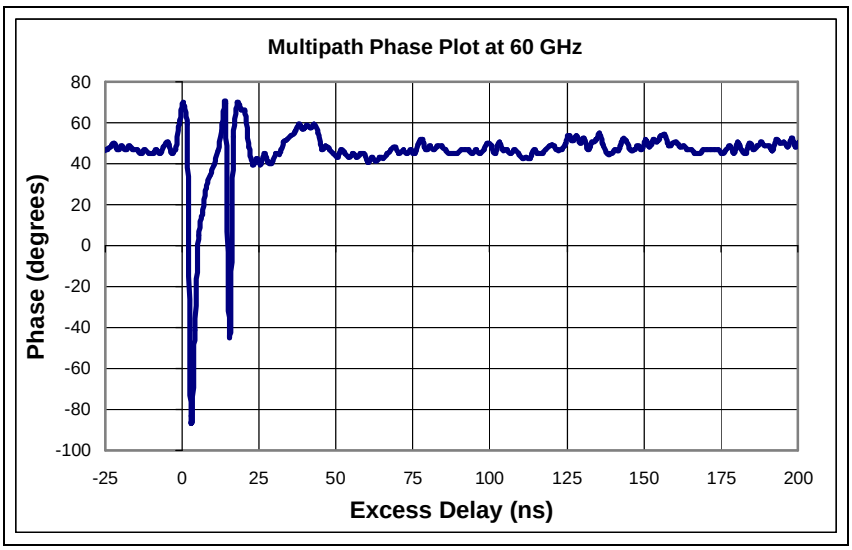

Figure 5.18: Multipath Phase Plot Example

Matlab Channel Imaging Analysis Suite

The Channel Imaging Analysis Suite, originally developed by Steger and Durgin and later modified by Kukshya [63, 65], is used to visualize, analyze and compute statistics from sets of measured power delay profiles. The power of the Analysis Suite is its ability to be used in combination with an automated receiver positioning system in order to analyze track and spin measurements.

Track measurements consist of a series of power delay profiles taken with the receiver antenna at a different track position, with each position separated from the others by a regular interval. The Analysis Suite then uses the track data to generate an accurate description of the small scale fading of the received power in a given location. Spin measurements, on the other hand, consist of a series of power delay profiles taken from different antenna azimuthal angles at a fixed track position. Spin measurements at a series of track positions can be analyzed to identify small position-dependant changes in the propagation characteristics at a particular location, or averaged together to remove the effects of small-scale fading and provide a local average description of the propagation characteristics. Figure 5.19 shows example track and spin plots from a measurement campaign conducted by Durgin [63].

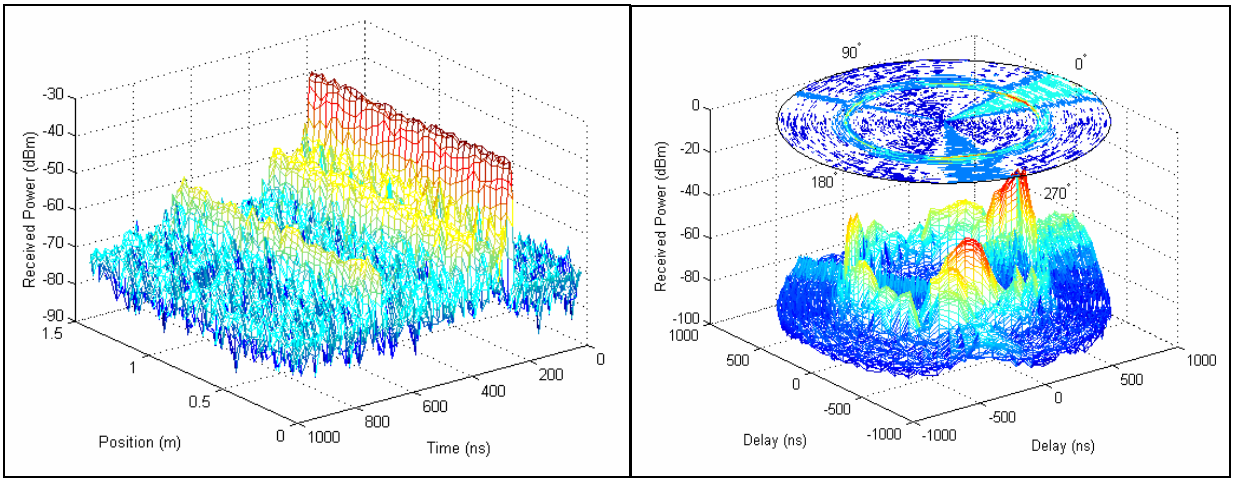

Figure 5.19: PDP Snapshots Along a Linear Track and Azimuthal Sweep from [63]

5.6 Conclusion

The upgraded ultrawideband channel sounder is capable of receiving a 10—400 MHz PN sequence at 38 or 60 GHz, providing a time domain resolution of multipath signals of 2.25 nanoseconds. The receiver implementation is flexible enough that other wireless channels could be characterized by constructing downconverters at a different operating frequency. A GPS disciplined oscillator (identical to the one at the transmitter) provides a highly stable frequency reference so that multipath phase may be measured via a miniaturized I/Q Correlator unit and LabVIEW DAQ program. Recorded delay profiles may be post-processed using the LabVIEW Data Post Processing software or the Matlab Channel Imaging Analysis Suite, allowing users to gather a variety of statistical information about the channel.

Chapter 6

Measurement System Verification and Calibration

6.1 Overview

Prior to performing measurements, the channel sounder was thoroughly evaluated to ensure that all cables, hardware, and software were in proper operating condition. Also, channel sounder subsystems were analyzed to ensure they were operating within their designed specifications.

Calibration of the channel sounder allows the user to validate the proper functioning of the system hardware and software as a whole. Calibration accounts for the effects of amplifiers, cables, attenuators, and upconverters, ensuring that received power levels recorded by the channel sounder are reported accurately. At lower frequencies, calibration is performed by disconnecting the antennas and connecting transmitter and receiver back-to-back through a set of fixed and variable attenuators. At millimeter-wave frequencies, the back-to-back method becomes impractical; therefore, the transmitter and receiver antennas are placed in a free-space environment with known separation distance and antenna heights [64]. In either case, received voltages are recorded at various receiver attenuation settings, plotted to determine the linear operating range of the channel sounder, and mapped to a received power level.

6.2 Equipment Verification

Verification of the channel sounder ensured that all subsystems are operating within their designed specifications. Anomalies in the operation of these subsystems as well as potential operating problems were noted. Below is the list of subsystems that were evaluated:

- PN Clock Signal Generator
- PN Generator
- GPS Disciplined Oscillators
- Transmitter IF Modulation
- Receiver I/Q Demodulation
- I/Q Correlator Unit

6.2.1 PN Clock Signal Generator

The PN Clock Signal Generator at both transmitter and receiver were evaluated to ensure they were producing a square wave output with peak-peak amplitude in the range of 0.5 – 1.0 Volts and frequency equal to the dial setting on the top of the unit (Figure 6.1). Two potential problems were identified when evaluating with this unit.

1. When the output has the proper voltage level but does not match the frequency on the dial setting, then the frequency reference input signal amplitude is incompatible with the MC12430 PLL chip. The MC12430 requires a CMOS level input in order to achieve phase lock, and the input signal should be amplified to the appropriate level.

2. When the square wave output appears jagged or blurred, the most likely cause of the problem is a bad cable or loose connection. All cables and connections should be evaluated to ensure signal continuity.

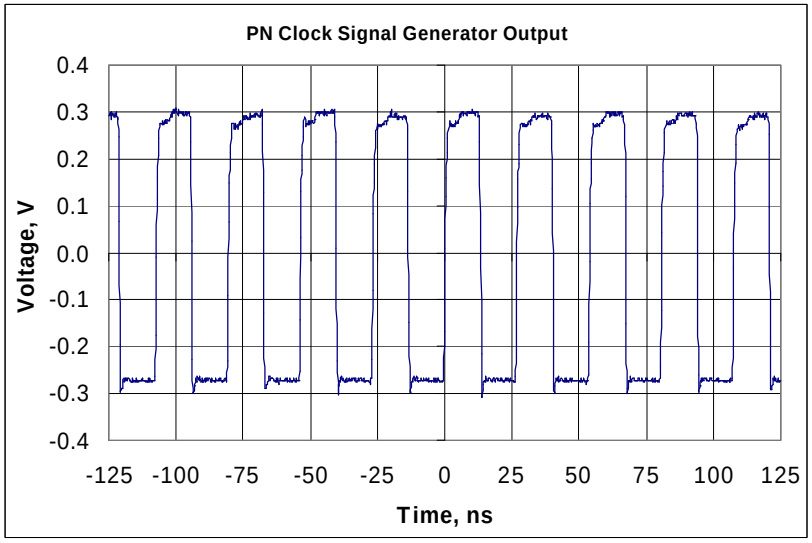

Figure 6.1: PN Clock Signal Generator Output

6.2.2 PN Generator

The three PN Generators utilized by the channel sounder were evaluated to confirm that they operated at a clock frequency of 450 MHz, and produced an antipodal pseudo-random bit sequence, with peak-peak signal amplitude between 0.5 and 1.0 Volts (Figure 6.2). When operating properly, the spectrum of this signal has a $\left(\frac{\sin(x)}{x}\right)^2$ shape, with the nulls occurring at integer multiples of the PN Generator Clock Frequency (Figure 6.3) [3]. Small spikes in the spectrum which occur at the nulls are caused by harmonics of the PN clock that couple into the output and/or code asymmetry resulting from clock skew (shift registers which are clocked at slightly different times). When the PN Generators are operated at a frequency which exceeds their maximum operating frequency, where the PN Generator experiences *Timing Margin Failure*, the output PN sequence will contain bit errors (which will cause false correlation peaks in the autocorrelation waveform) and at a high enough clock frequency the PN sequence will become distinctly periodic (Figure 6.4).

Even though the PN Generator is capable of operating at 450 MHz, due to bandwidth limitations in the Anaren Quadrature mixer, the maximum useable frequency of the PN Generator is limited to 400 MHz.

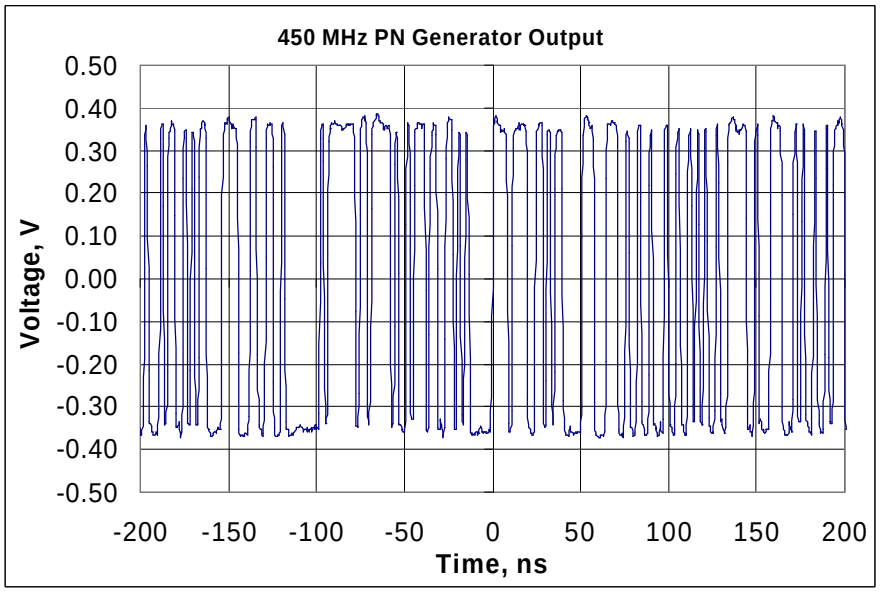

Figure 6.2: 450 MHz PN Generator Output Waveform

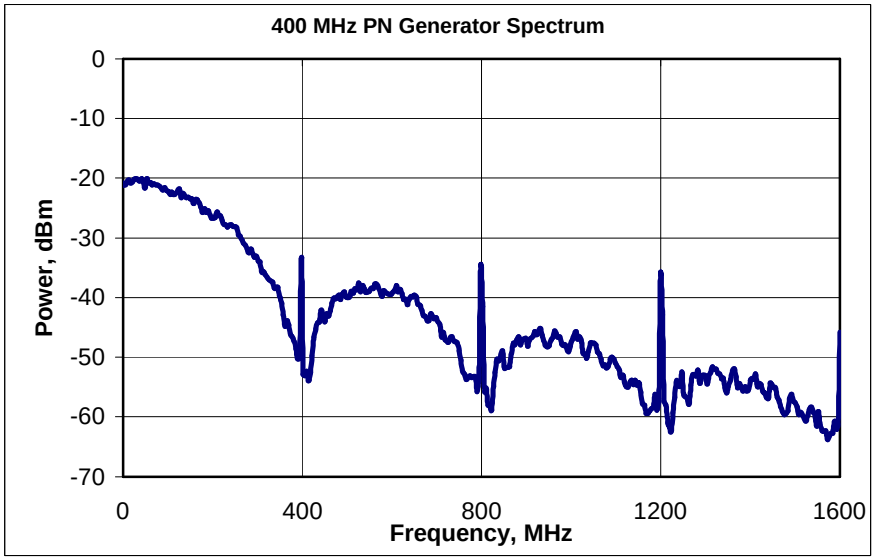

Figure 6.3: 400 MHz PN Generator Output Spectrum

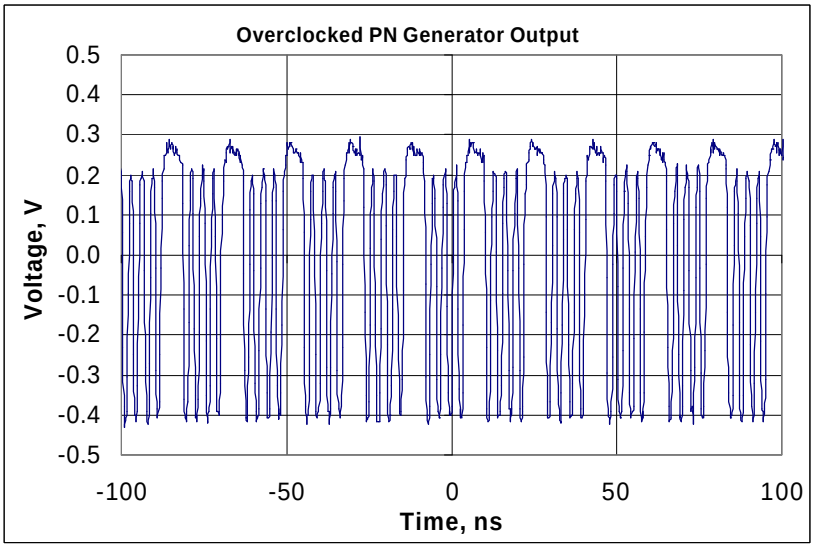

Figure 6.4: Overclocked PN Generator Output

6.2.3 GPS Disciplined Oscillators

In order to produce a 10 MHz signal that is locked to the GPS one pulse-per-second timing signal, the GPS Disciplined Oscillators require a minimum warm-up period of 1 — 3 hours. To determine when the signals from the oscillators were fully locked on to the GPS signal, the 10 MHz output signals were monitored on an oscilloscope. The transmitter oscillator output was connected to Channel 1, the receiver oscillator output was connected to Channel 2, and the scope was set to trigger on Channel 1. When the oscillators were not locked, the waveform on Channel 2 drifted with respect to the waveform on Channel 1. As the oscillators begin to warm up and track the GPS signal, the rate of drift slowed until the waveform on Channel 2 eventually became stationary, although it exhibited a phase offset from the waveform on Channel 1.

The oscillators were also evaluated using the StarLoc II™ Operations and Management Software, which communicates to the oscillators via a RS-232 null modem cable. The Operations and Management Software provided information about the number of satellites each oscillator tracked, the quality of the GPS signal, as well as the status of any correction applied to the oscillator output.

6.2.4 Transmitter Modulation

Depending on the frequency the channel sounder is configured for, either the IF or RF spectrum should be evaluated to ensure that the transmitter as a whole is operating properly. When using the millimeter-wave upconverters, it is more practical to evaluate the IF spectrum of the transmitter, whereas at lower PCS or Cellular frequencies it may be possible to evaluate the RF spectrum.

When the channel sounder transmitter is operating properly, the spectrum will have a $\left(\frac{\sin(x)}{x}\right)^2$ shape centered on the RF or IF carrier frequency (Figure 6.5). An asymmetric spectrum indicates a bad connection, a bandwidth limitation in one of the components, or interference between subsystems through power supply connections.

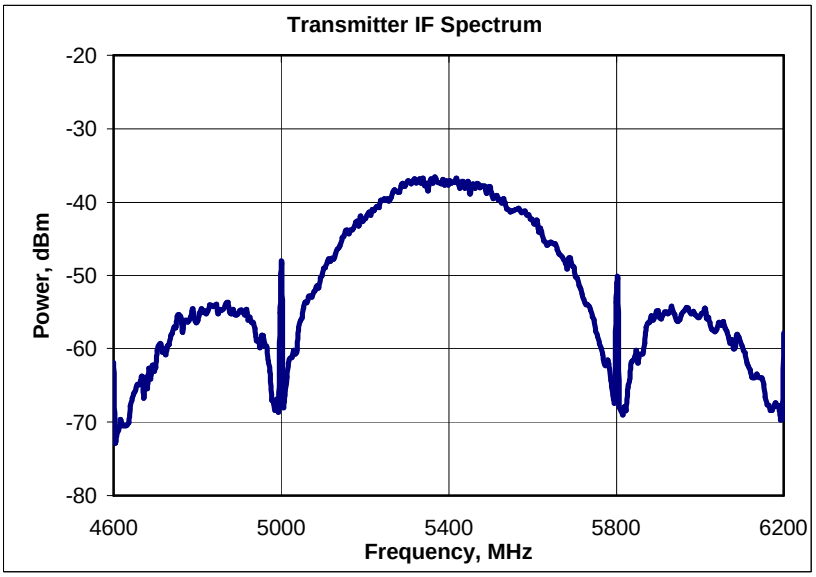

Figure 6.5: Transmitter IF Spectrum with 400 MHz PN Code

6.2.5 Receiver Demodulation

To determine whether the receiver was operating properly, the transmitter IF output and the receiver IF input were connected back-back via a cable and a fixed attenuator, with the value of the attenuator chosen so as to avoid overdriving any of the components in the receiver.

With transmitter and receiver connected together, the Anaren Quadrature mixer produces baseband PN waveforms on both the inphase and quadrature outputs. If the GPS oscillators are

not fully locked or if the local oscillators at transmitter and receiver are not exactly the same frequency, the PN waveforms observed on either the inphase or quadrature outputs will be amplitude modulated at a frequency equal to the offset between the transmitter and receiver local oscillators (Figure 6.6).

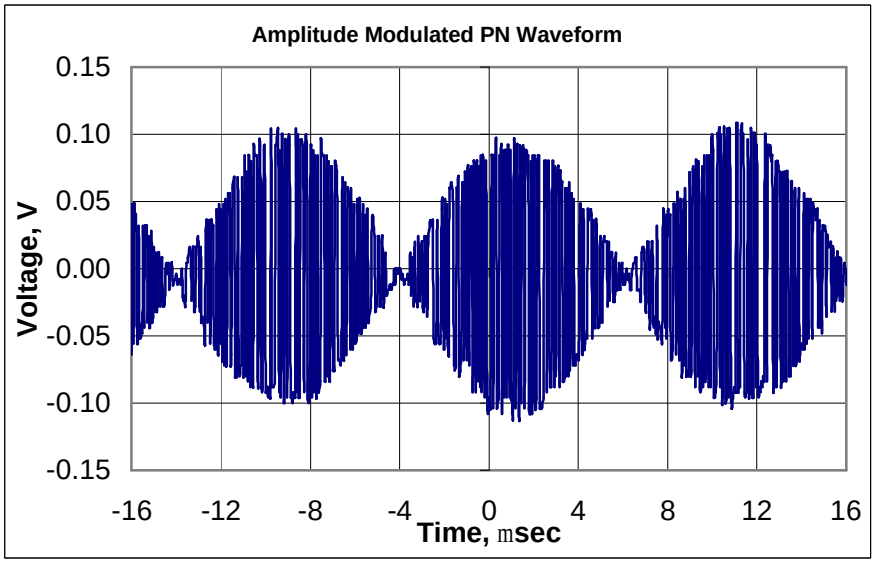

Figure 6.6: Effect of Offset of Local Oscillators on Received Signal

6.2.6 I/Q Correlator Unit

The operation of the I/Q Correlator unit was evaluated in two ways. First, the output from the TX PN Generator was attenuated and connected to the I and Q baseband input on the Correlator unit. The Receiver PN Generator was also connected to the Correlator unit, and was clocked slightly slower than the TX PN Generator. The outputs from the Correlator unit were then displayed on an oscilloscope, and the resulting waveform is the crosscorrelation of the TX and Receiver PN sequences (Figure 6.7). As discussed in Section 6.2.2, if either or both PN Generators are operated at a frequency higher than their maximum operating frequency, their crosscorrelation will have false peaks (Figure 6.8) and will result in erroneous delay profiles when recording measurements.

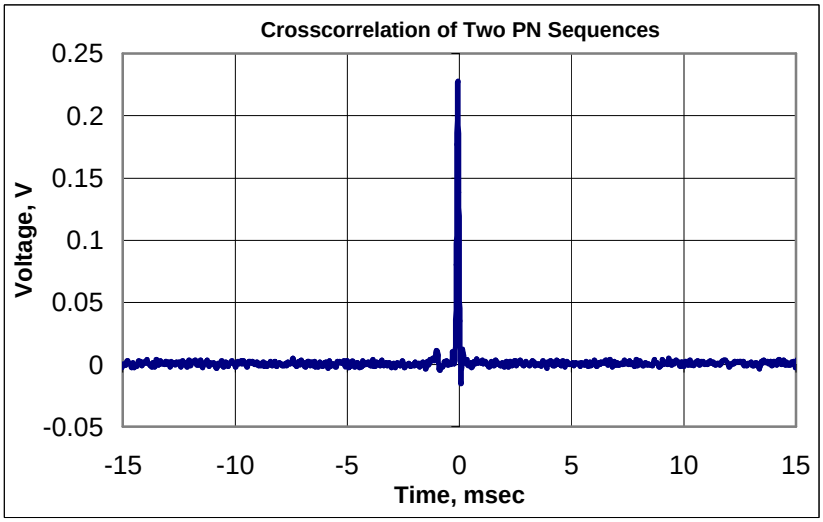

Figure 6.7: Crosscorrelation of Two PN Sequences

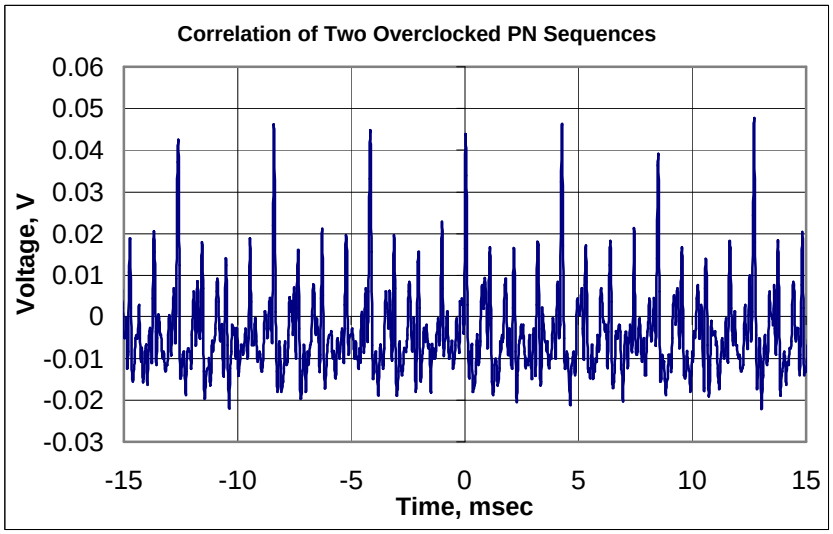

Figure 6.8: Crosscorrelation of Two Overclocked PN Sequences

With the IF output from the transmitter connected via a cable and the fixed attenuator to the receiver IF input, the next step in evaluating the Correlator unit was to disconnect the TX PN Generator and connect the inphase and quadrature baseband waveforms output from the Anaren quadrature mixer to the inputs of the Correlator unit. The outputs from the Correlator unit were connected to an oscilloscope, and the resulting waveforms represent the Crosscorrelation of the I&Q baseband PN sequences (from the output of the Anaren quadrature mixer) with the receiver PN sequence (Figure 6.9). Note that a large correlation peak occurs on the inphase channel and a small correlation peak occurs on the quadrature channel. Because the system is cable connected, the quadrature waveform should be zero; however, due to the phase imbalance of the various

power splitters and mixers (as discussed in Chapter 4) a small correlation peak appears on the quadrature channel [30]. A correlation peak on the quadrature channel may also be observed when a phase offset exists between transmitter and receiver local oscillators.

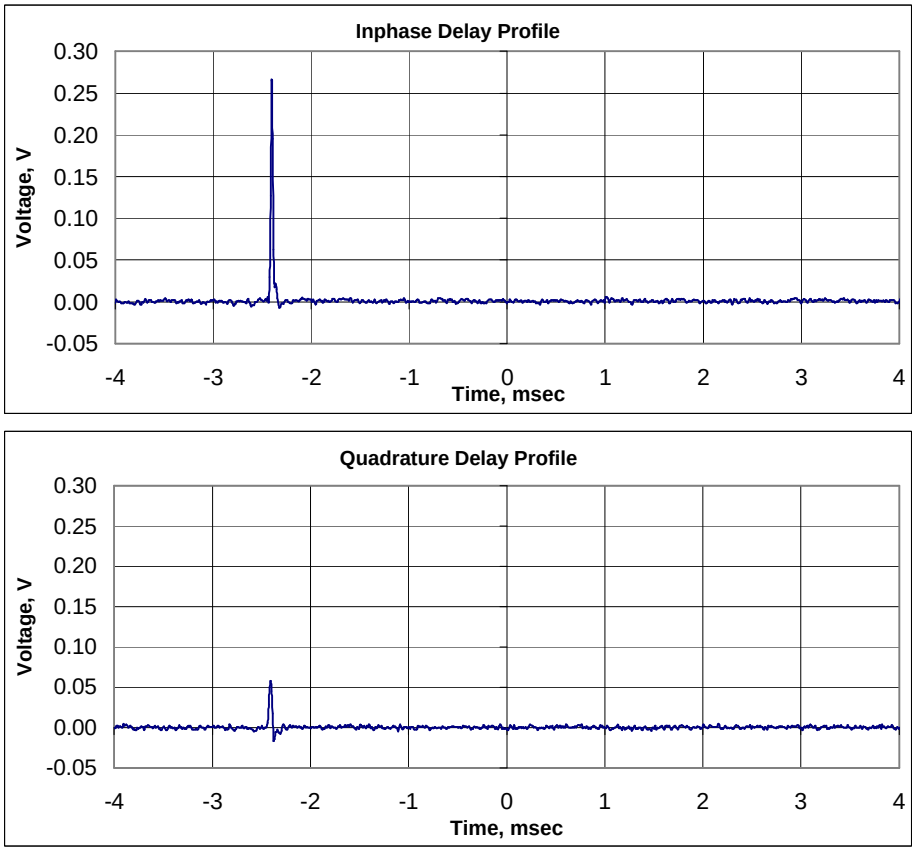

Figure 6.9: Inphase and Quadrature Voltage Delay Profiles

6.3 System Calibration and Repeatability Evaluation

6.3.1 Calibration

Calibration of the channel sounder prior to recording measurements is necessary so that a power delay profile can be generated from the inphase and quadrature voltage delay profiles recorded by the data acquisition card, and is based on the procedure described in [65]. Two techniques for performing calibration exist, depending on the operating frequency of the channel sounder, known as the *free space method* and the *cable connected method.*

6.3.1.1 Equipment Setup

Free Space Calibration Equipment Setup

For free space calibration, the transmitter and receiver antennas are placed in a benign environment without stationary or mobile reflectors, allowing the equipment to operate free from the influence of multipath components reflected from the ground, walls, or nearby objects. The antennas are separated by a distance equal to or greater than the Fraunhofer distance, (Equation 6.1) [12, 65] ensuring that they are operating in the far field. The separation distance should also be large enough to ensure that free space path loss will be sufficient to prevent exceeding the receiver's maximum allowable input signal level.

$$d_f = \frac{2D^2}{l} \tag{6.1}$$

Where: d_f is the Fraunhofer distance
D is the largest linear dimension of the antenna
l is the signal wavelength

The separation of the transmitter and receiver antennas is also affected by the Fresnel Zone clearance. Fresnel zones represent regions where secondary waves have path lengths which are $\frac{nl}{2}$ greater than the line of sight path length, causing constructive and destructive interference to the received signal [12]. For the free space calibration setup of the channel sounder, the radius of the n^{th} Fresnel zone in a plane located between transmitter and receiver (Figure 6.10) is expressed in Equation 6.2.

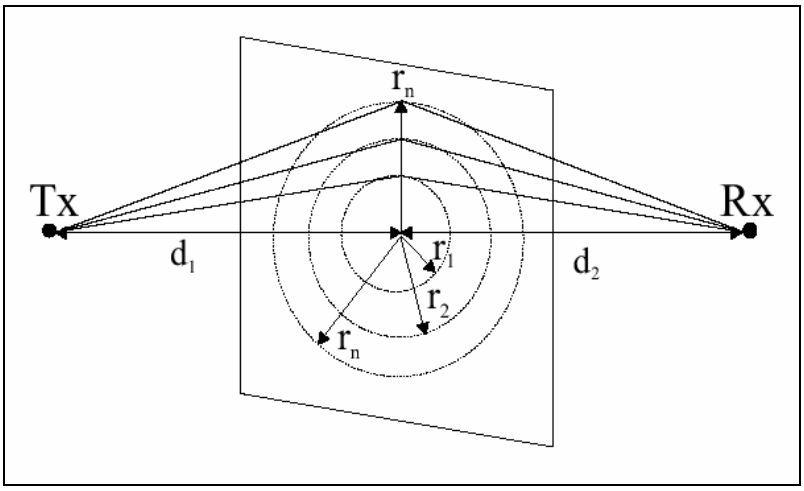

Figure 6.10: Fresnel Zone Boundaries, from [64]

$$r_n = \sqrt{\frac{n l d_1 d_2}{d_1 + d_2}} \tag{6.2}$$

Where: r_n is the radius of the nth Fresnel Zone in meters
d_1 is the distance from the transmitter to the plane in meters
d_2 is the distance from the receiver to the plane in meters
l is the signal wavelength in meters

Based on Equations 6.1 and 6.2, the transmitter and receiver separation distance must be carefully chosen so that the antennas are operating in the far field and the first Fresnel zone remains unobstructed [64, 65]. For example, the antennas used on the 60 GHz upconverters are rectangular horns with a diagonal length of 5.8 cm. At 60 GHz, the signal wavelength is 0.5 cm, and the corresponding Fraunhofer distance is 1.34 meters. If the antennas are separated by a total of 40 meters, then the radius of the first Fresnel zone at a point midway between transmitter and receiver ($d_1 = d_2 = 20\,m$) is 0.23 meters. Therefore, the antenna heights and positions should be chosen such that a clear line-of-sight signal exists from transmitter to receiver with no obstructions in the first Fresnel zone.

Cable Connected Calibration Equipment Setup

For cable connected calibration, the transmitter and receiver antennas are disconnected and the output from the transmitter is connected through a fixed attenuator to the input of the receiver. The actual attenuation value is dependant on the transmitter output power and the

maximum input power the receiver can tolerate. Also, the attenuator should have a rated power handling capacity equal to or greater than the transmitter output power.

6.3.1.2 Calibration Measurements

After transmitter and receiver are setup, they should be powered on and operated for a period of at least 30 minutes, allowing the losses, gains, and other system parameters which depend on operating temperature to reach a steady-state value. Measurements should not be made until the GPS receivers lock on to the GPS signal and the 10 MHz output signals stabilize, which may require several hours of warm-up time.

For accurate calibration of the channel sounder, two parameters must be determined so that voltages digitized by the data acquisition software can be accurately mapped to received powers: the *transmitter output power* and the *reference attenuation*.

The *transmitter output power* is measured at the point where the antenna is connected to the transmitter, i.e., the power input to the antenna. In the event that it is impractical to make this measurement, the power should be measured at the most convenient point in the transmitter chain, and all gains and losses between that point and the antenna should be accurately characterized and combined into the reference attenuation.

The *reference attenuation* parameter is the amount of attenuation that exists between the transmitter and receiver. In the cable connected method, this parameter is simply the value of the fixed attenuator plus any additional cable losses. For the free space calibration method, the reference attenuation is the path loss experienced from transmitter to receiver (Equation 6.3). Note that the path loss value is a calculated value under the assumption of free-space propagation, and is based on the frequency of operation and transmitter-receiver separation distance.

$$ATTEN_{ref} = -10\log_{10}\left(\frac{g_T g_R \lambda^2}{(4\pi d)^2}\right) \tag{6.3}$$

Where: $ATTEN_{REF}$ is the reference attenuation in dB
λ is the wavelength in meters
g_T is the transmitter antenna gain in linear ratio
g_R is the receiver antenna gain in linear ratio
d is the transmitter-receiver separation distance in meters

After determining the transmitter power and reference attenuation, the calibration is recorded using the following procedure:

1. At the receiver, the HP8495B Variable Attenuator is set at either 0 dB or a level necessary to prevent overloading of the amplifiers, mixers, etc. that follow. The laptop data acquisition program is configured to record a calibration measurement and the reference attenuation and transmitter power parameters are entered into the program [58].
2. The level of excess attenuation is set to correspond to the setting of the HP8495B. The laptop will then record a magnitude delay profile to disk.
3. The setting of the HP8495B is increased and step 2 is repeated. This process continues until the peak value of the delay profile falls below the noise floor of the receiver.

6.3.1.3 Processing Calibration Measurements

Data post-processing is used to map the voltage delay profiles recorded by the channel sounder into power delay profiles. A linear relationship exists between the recorded voltage and the received power level in dBm, as shown in [10, 63, 65, 69], and is expressed in Equation 6.4.

$$P_{rec} = a \log_{10}(V) + b \tag{6.4}$$

Where: P_{rec} is the received power level in dBm at the output of the receiver antenna
V is the voltage level recorded on a delay profile
a, b are system constants determined by the calibration process, and represent slope and intercept of the linear operating region of the channel sounder.

Determining α and β is based on the procedure developed in [63, 65]. First, a collection of receiver attenuation values and peak voltage levels from the recorded magnitude delay profiles is compiled, an example of which is shown in Table 6.1.

Table 6.1 **Example of Calibration Data Points**		
Receiver Attenuation (dB)	**Peak Voltage (Volts)**	**$\log_{10}$(Peak Voltage)**
20	2.17	.337
30	2.07	.318
40	1.88	.274
50	1.70	.230
60	1.53	.186
70	1.48	.170

Plotting the values from Table 6.1, it can be seen that two regions of non-linearity exist (Figure 6.10). The first region is for low receiver attenuation values, caused by saturation of mixers and amplifiers in the receiver. The second region is for high levels of receiver attenuation where the received signal drops below the system noise floor.

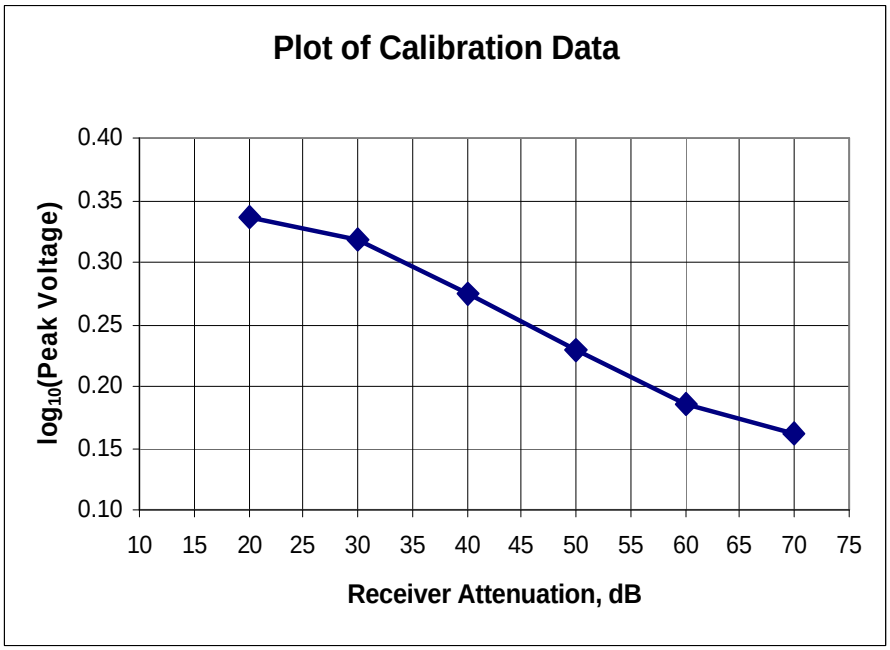

Figure 6.11: Plot of Example Calibration Data

From Figure 6.10, it is evident that the linear operating region for the channel sounder exists when the receiver attenuation setting is between 30 and 60 dB. The dynamic range for the measurements recorded by the channel sounder is the difference between these two points, in this case 30 dB.

Once the linear range has been established, the voltages can be mapped into received powers using the transmitter power and reference attenuation parameters (Equation 6.5).

$$P_{RX} = P_{TX} - ATTEN_{ref} - ATTEN_{RX} \tag{6.5}$$

Where: P_{RX} is the received power level at the output of the receiver antenna in dBm
P_{TX} is the transmitter power in dBm
$ATTEN_{ref}$ is the reference attenuation in dB
$ATTEN_{RX}$ is the receiver attenuation setting in dB

For example, if the system in Table 6.1 had a transmitter output power of 20 dBm and a reference attenuation level of 30 dB, then over the linear operating range of the channel sounder, the received power levels would map into the output voltages as shown in Table 6.2 and Figure 6.11.

Table 6.2
Example of Calibration Voltage-Power Data

Receiver Attenuation (dB)	Received Power Level (dBm)	$\log_{10}$(Peak Voltage)
30	-40	.318
40	-50	.274
50	-60	.230
60	-70	.186

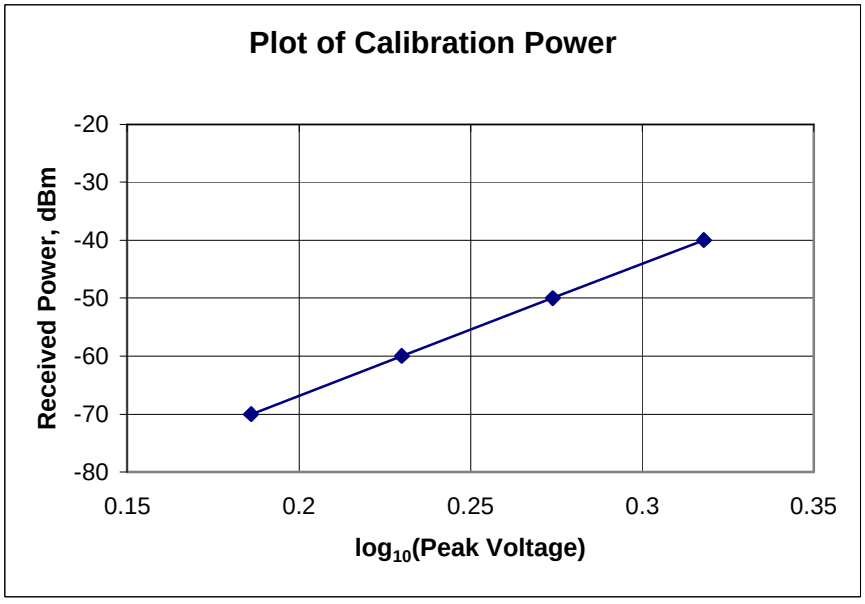

Figure 6.12: Plot of Received Voltage vs. Power Using Example Calibration Data

A linear regression [63, 65] is then applied to the data in Table 6.2 and determines the system constants α & β from Equation 6.4. Once these constants are known, any output voltage (so long as it is within the linear range of the channel sounder) can be mapped into a received power. Therefore, the recorded voltage delay profiles can then be mapped into power delay profiles via Equation 6.5.

6.3.2 Repeatability Testing

While calibration determines how accurately the channel sounder can measure received power levels, repeatability testing characterizes the variance in measurements recorded over a period of time. That is, if a measurement is recorded at time t_0, and another measurement is recorded at time $t_0 + \Delta t$, the two recorded measurement values will differ by some Δx. Repeatability testing determines how much Δx can be expected.

Repeatability evaluation simply involves placing the channel sounder in a benign environment free from multipath and recording N power delay profiles over a particular time period. Then, the $3s$ variance of the peaks of the recorded power delay profiles represents the maximum expected variation between any two measurements. Table 6.3 is an example repeatability analysis for 10 power delay profiles, which has a $3s$ variance of 0.76 dB or ±0.38 dB. Therefore, measurements made in the field which have amplitude variation within the $3s$ range may be regarded as essentially equal, as it is impossible to determine whether the variation was caused by the channel or the measurement system.

Table 6.3 **Example Repeatability Analysis**	
Measurement Number	**Power Delay Profile Peak Power (dBm)**
1	-25.1
2	-25.0
3	-24.9
4	-25.3
5	-24.8
6	-25.1
7	-24.6
8	-25.1
9	-25.5
10	-24.9
3s variance	±0.76 dB

6.4 System Calibration and Repeatability Evaluation for 60 GHz Channel Sounder Configuration

6.4.1 Channel Sounder Calibration

System calibration at 60 GHz was performed in a large, empty parking lot outside Durham Hall at Virginia Tech. Transmitter and Receiver were separated by a distance of 7.0 meters. The first Fresnel zone radius at a point midway between transmitter and receiver ($d_1 = d_2 = 3.5\,m$) for this setup is significantly less than 1 meter; therefore the antenna heights were set at 1.5 meters to provide sufficient clearance. Table 6.4 contains the link budget for the 60 GHz Calibration Setup.

Table 6.4 **Link Budget for 60 GHz Calibration**	
Desired Received Power Level at IF	-20 dBm
Receiver Downconverter Gain	25 dB
Receiver Antenna Gain	25 dB
7.0 m Free Space Path Loss at 60 GHz (excluding antenna gains)	-85 dB
Transmitter Antenna Gain	25 dB
Required Transmitter Power Level at RF	-10 dBm
Required Transmitter Power Level at IF	-35 dBm

A –20 dBm signal power level was desired at the receiver IF input to provide sufficient tuning range for calibration, meaning that the received power level at the output of the receiver antenna would be –45 dBm. Free space path loss over a 7.0 meter link at 60 GHz (excluding antenna gains) is 85 dB. The reference attenuation used for the calibration is equal to the free space path loss plus the transmitter and receiver antenna gains, or 35 dB. Therefore, the desired power level at the output of the transmitter is –10 dBm. The channel sounder was powered on and allowed to warm up for a period of 2 hours to allow the GPS disciplined oscillators to stabilize. Free-space calibration measurements were then performed in accordance with the procedure outlined in Section 6.3.1.2. Figure 6.12 is a plot of the peak voltages versus receiver attenuation settings for the 60 GHz setup, which shows that the channel sounder has a measurement dynamic range of 30 dB.

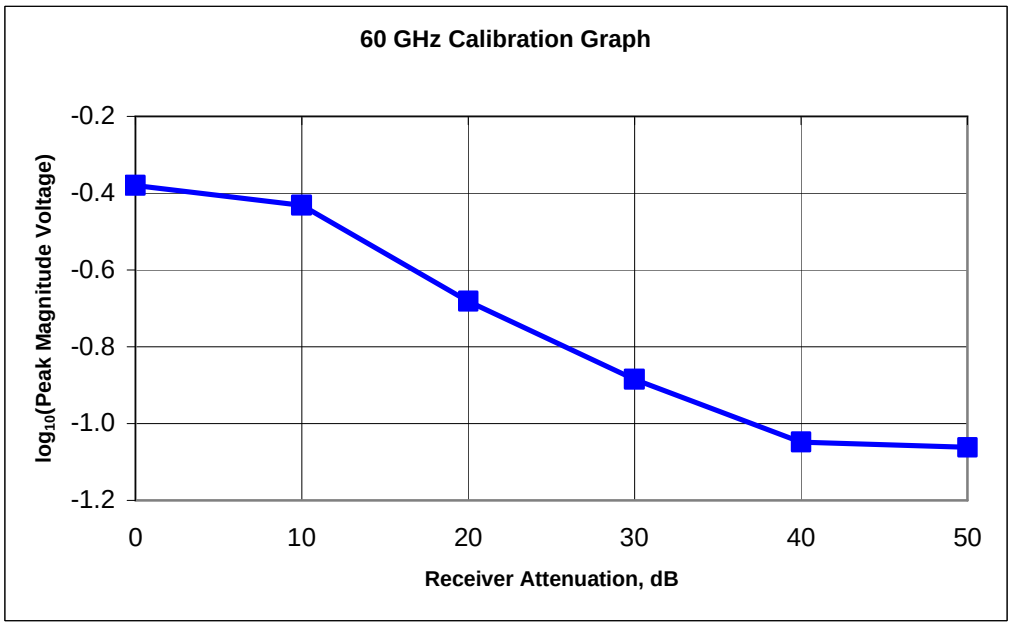

Figure 6.13: 60 GHz Voltage vs. Receiver Attenuation Calibration Plot

Performing a linear regression on the 60 GHz calibration data yields $a = 48.2$ and $b = -6.30$. Figure 6.13 is a comparison of the received power calculated using Equation 6.4 and the received power based on the linear regression. The error between the actual power and the linear regression is ±1.2 dB, which is reasonably close to the channel sounder design

specification to provide magnitude power delay profile measurements with an accuracy of ±1 dB.

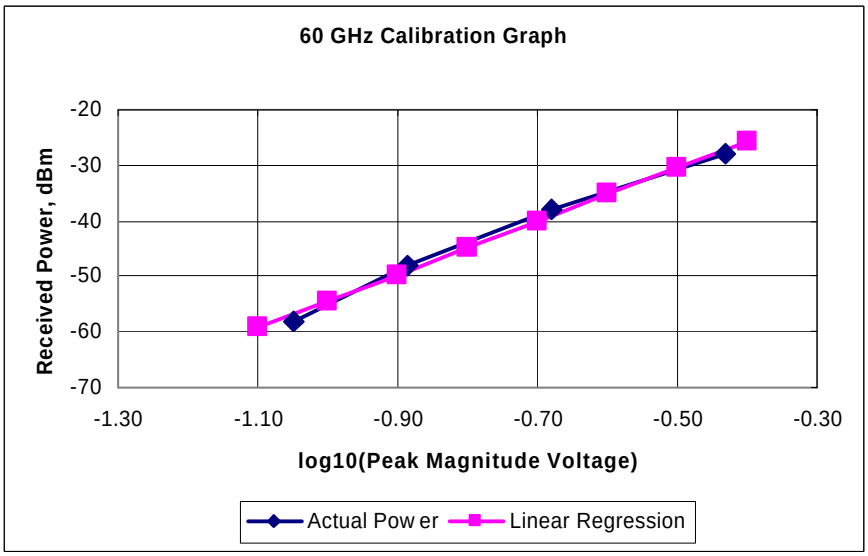

Figure 6.14: Comparison of Actual Received Power Levels with Linear Regression from Calibration

6.4.2 Channel Sounder Repeatability Evaluation

After performing calibration measurements, a repeatability evaluation was performed on the channel sounder. A set of 20 power delay profiles were recorded over a 20 minute time period. Table 6.5 contains the repeatability analysis for the 60 GHz channel sounder configuration, and shows that the $3s$ variance is equal to ±1.3 dB.

Table 6.5
Repeatability Analysis for
60 GHz Channel Sounder Configuration

Measurement Number	Power Delay Profile Peak Power (dBm)
1	-57.0
2	-57.6
3	-54.9
4	-55.5
5	-54.5
6	-55.2
7	-54.4
8	-56.2
9	-55.2
10	-55.5
11	-56.4
12	-56.7
13	-55.5
14	-55.8
15	-55.6
16	-56.4
17	-56.5
18	-56.0
19	-55.8
20	-54.5
3σ variance	2.6 dB (±1.3 dB)

6.5 Conclusion

The operation and functionality of the various channel sounder subsystems were evaluated to ensure that they met the design specifications presented in Chapter 3. Problems that may cause some of the subsystems to operate improperly were noted, along with anomalies in the operation of these subsystems. The general channel sounder calibration procedure was discussed, as well as specific results from the 60 GHz configuration. A comparison of the received power based on the linear regression and the actual received power illustrated that when the channel sounder is operating within is linear region; the measurement accuracy is within ±1.2 dB, which is very close to meeting the ±1 dB specification, along with a measurement repeatability of ±1.3 dB.

1

Chapter 7

Indoor Measurements at 2.5 and 60 GHz

7.1 Measurement Scope

Characterization of wireless channels is an important part in the development of new wireless communication standards. As discussed in Chapter 2, multipath signals can have many detrimental effects on a communication system; therefore, knowledge of the multipath structure for a given propagation environment is key to developing a robust communication link.

In recent years, there has been an increasing interest in designing and deploying in-building wireless networks in the unlicensed 2.4 GHz and 60 GHz bands [72]. As part of this research, a measurement campaign was conducted on the 4th floor of Durham Hall at Virginia Tech. These measurements look specifically at the wideband propagation effects that may be encountered in a typical laboratory or office building, with transmitter and receiver locations chosen to provide line-of-sight (LOS), non line-of-sight (NLOS), and cluttered propagation environments.

7.2 Measurement Plan

7.2.1 Channel Sounder Setup

The channel sounder was configured for operation using the 11-bit PN code running at 400 MHz and with GPS disciplined oscillators providing the frequency reference at transmitter and receiver. Two different RF chains were then utilized, one for the 60 GHz measurements and

the other for the 2.5 GHz measurements. For both configurations, transmitter and receiver antenna heights were nominally set at 1.2 meters (with exceptions noted).

60 GHz Configuration

For the 60 GHz measurements, the channel sounder was configured as described in Chapters 4 and 5. Both transmitter and receiver utilized horn antennas which had a gain of 25 dBi and first-null beamwidths of 50°. E- and H-plane antenna patterns are shown below in Figure 7.1. Transmitter output power (as measured at the base of the antenna) was set at -10 dBm in order to avoid driving the receiver into compression at short link distances, as well as to approximate expected transmitter power for future single-cell-per-room wireless networks.

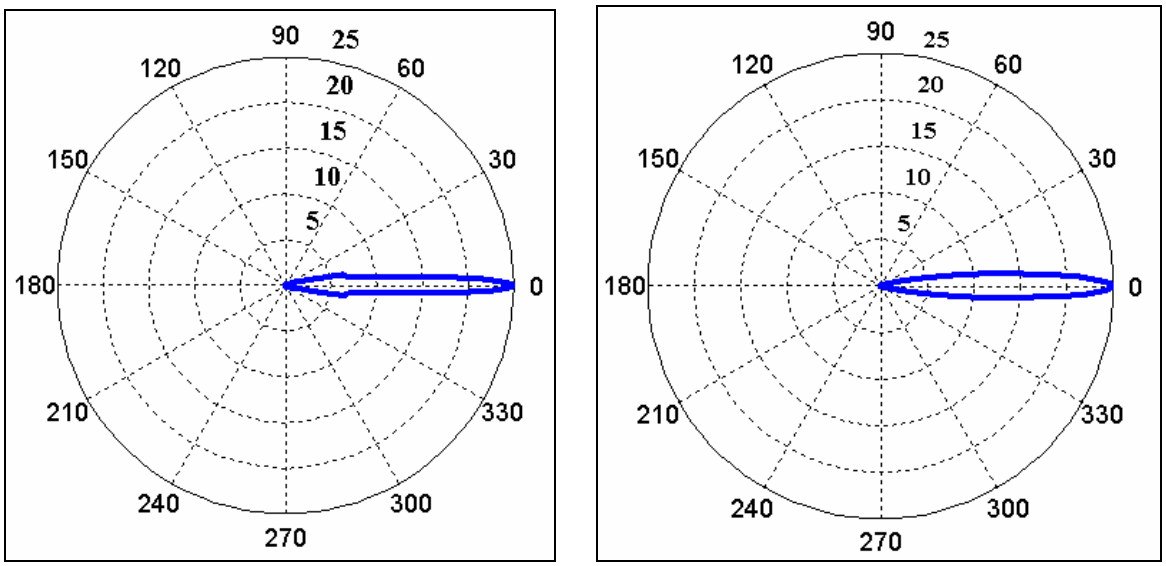

Figure 7.1: Azimuth (left) and Elevation Antenna Patterns for the 60 GHz Configuration

2.5 GHz Configuration

For the 2.5 GHz measurements, it was necessary to reconfigure the RF front end of the channel sounder (detailed instructions for reconfiguring the channel sounder for operation below 5.4 GHz may be found in Appendix C). A block diagram of the 2.5 GHz configuration is shown below in Figure 7.2. Transmitter output power was set at 0 dBm, and both transmitter and receiver used omnidirectional biconical antennas which had a 6 dBi gain and omnidirectional radiation pattern. E- and H-plane antenna patterns are shown below in Figure 7.3.

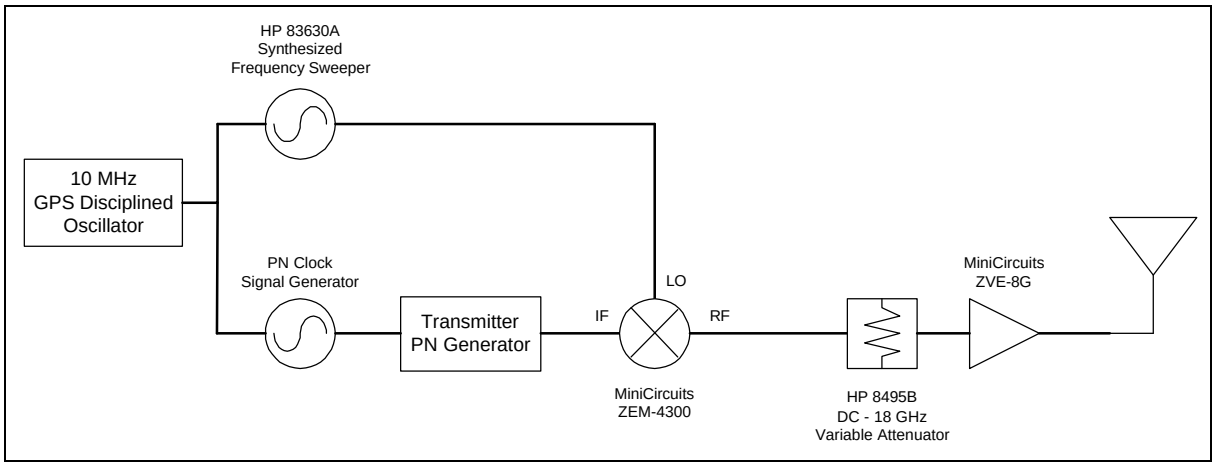

Figure 7.2a: 2.5 GHz Channel Sounder Transmitter

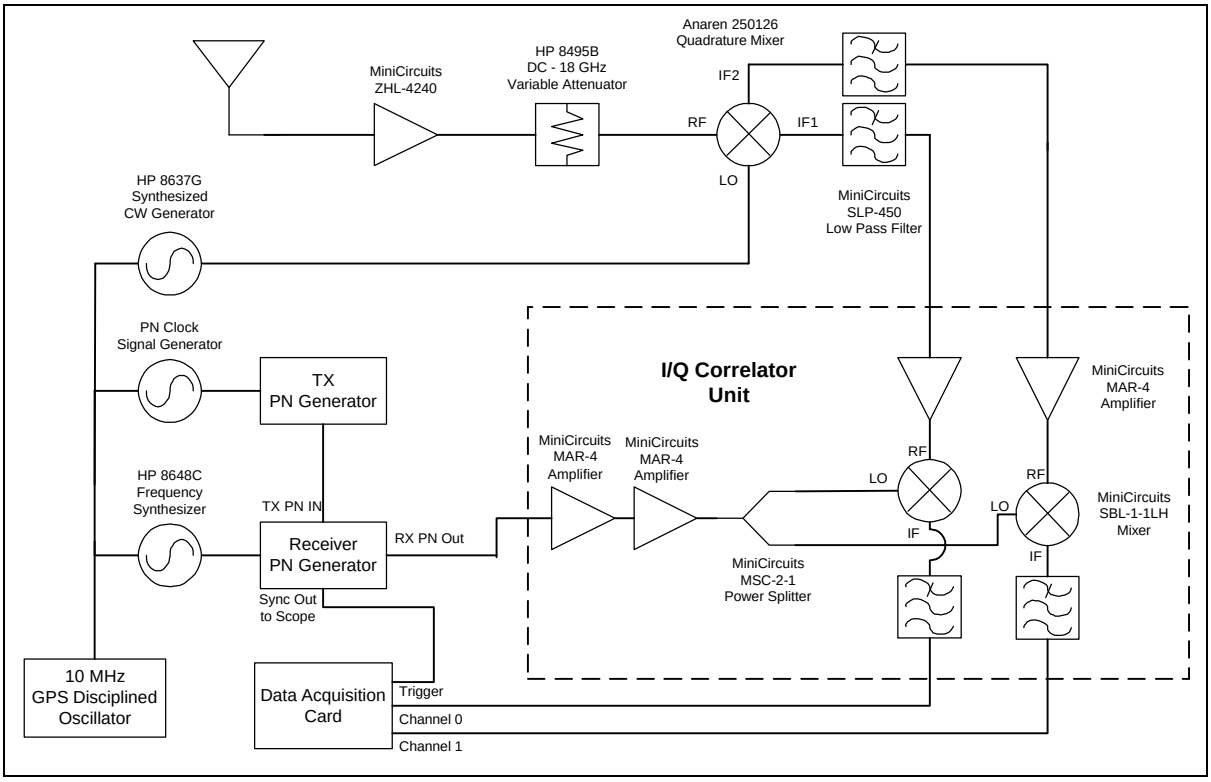

Figure 7.2b: 2.5 GHz Channel Sounder Receiver

Figure 7.2: 2.5 GHz Channel Sounder Block Diagram

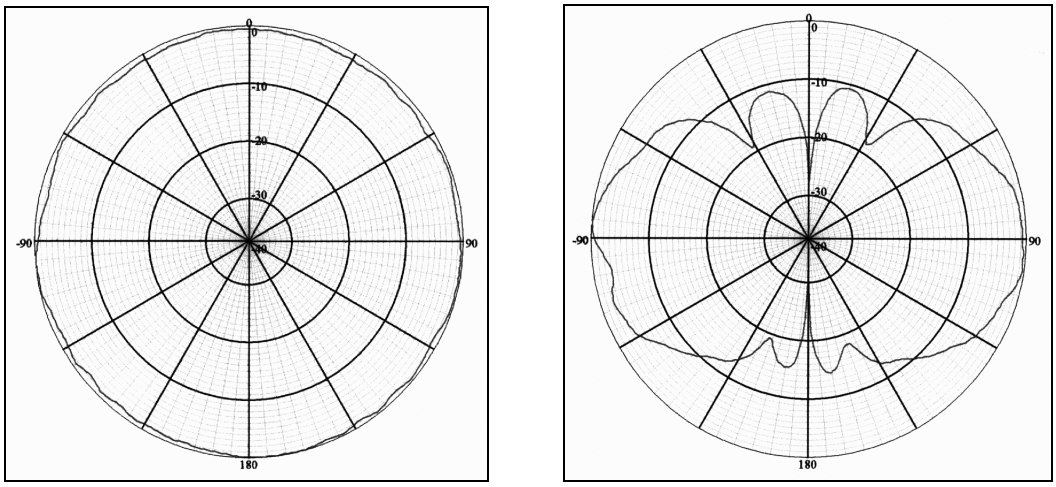

Figure 7.3: Azimuth (left) and Elevation Antenna Patterns for the 2.5 GHz Configuration. Antenna Pattern has been Normalized to the Maximum Gain

7.2.2 Measurement Procedure

Eight separate transmitter and 22 separate receiver locations were selected on the 4th floor of Durham Hall on the Virginia Tech campus (Figure 7.2). In this measurement campaign, a series of power delay profiles were recorded along a linear measurement track (Figure 7.3). The track positioning accuracy is less than one millimeter [69], which is critically important because at 60 GHz the wavelength is only 5 millimeters.

Figure 7.4: Map of the 4th Floor of Durham Hall at Virginia Tech

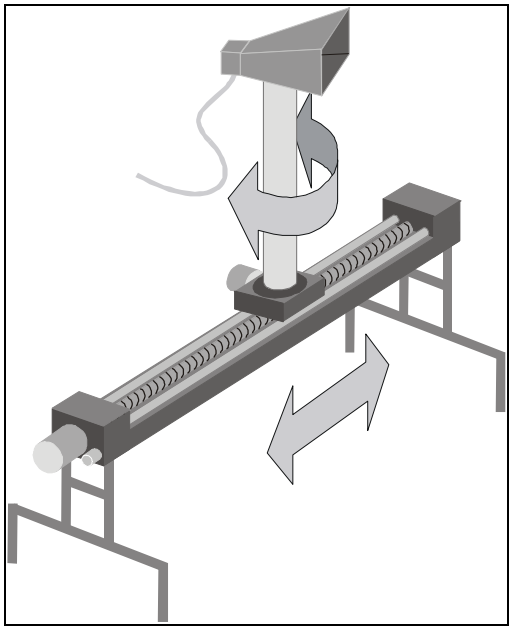

Figure 7.5: Automated Track Measurement System, from [63]

For both 2.5 GHz and 60 GHz, two types of track measurements were performed, a parallel track measurement and a perpendicular track measurement:

- *Parallel Track Measurements* consisted of orienting the track parallel to the LOS path from transmitter to receiver (or the direct path from transmitter to receiver in the case where they were separated by an obstruction). Power delay profiles were then recorded at 40 positions along the track with a separation between successive measurements of $\frac{l}{4}$, so that the receiver traveled a total distance of 10 l .
- *Perpendicular Track Measurements* consisted of orienting the track perpendicular to the LOS path from transmitter to receiver (or the direct path from transmitter to receiver in the case where they were separated by an obstruction). Power delay profiles were then recorded at 40 positions along the track with a separation between successive measurements of $\frac{l}{4}$, so that the receiver traveled a total distance of 10 l .

Additionally, at 60 GHz a second set of parallel and perpendicular track measurements were performed where power delay profiles were recorded at 10 positions along the track with a separation between successive measurements of 10 l , so that the receiver traveled a total distance of ½ meter (100 l).

Power delay profiles from a given track measurement were then linearly averaged together to create a local average power delay profile. A compilation of the power delay profiles from this measurement campaign as well as photographs of the measurement locations may be found in Appendix B.

7.2.3 Site Descriptions and Maps

Transmitter location 1 was chosen to study NLOS propagation from a room to another room, and from a room to a hallway (Figure 7.4). The transmitter and receivers were separated by drywall containing metal studs, where the studs have a 16 inch center-to-center separation distance. The transmitter was located in a small laboratory. Receiver locations 1.1 – 1.3 were in adjacent rooms, whereas receiver location 1.4 was in an adjacent hallway. Additionally, for locations 1.1 – 1.3, standard office dry-erase "whiteboard" was located on the wall separating the transmitter and receiver.

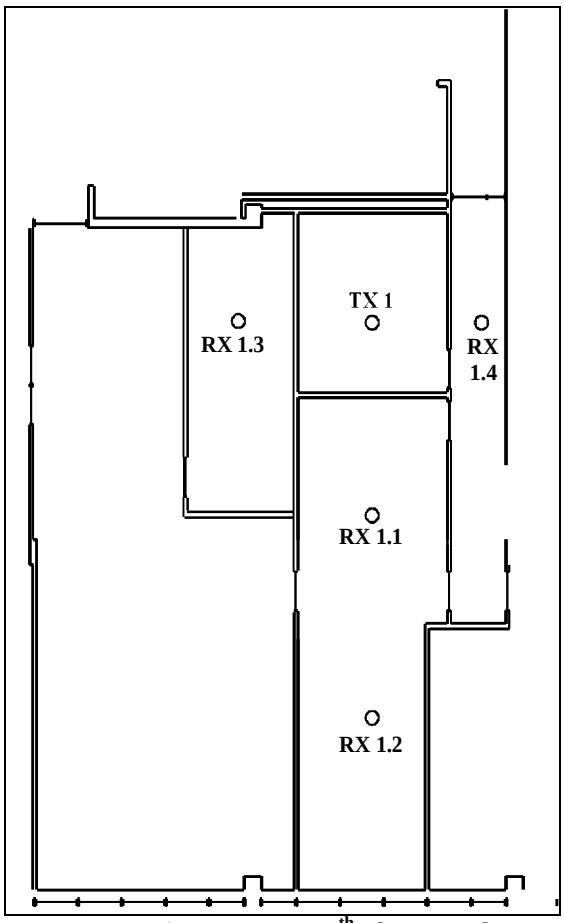

Figure 7.6: Measurement Locations 1.1 – 1.4, 4th Floor, Durham Hall, Virginia Tech. The transmitter is located in Room 475, Receivers 1.1 and 1.2 are located in Room 471; Receiver 1.3 is in the conference room in the 476 computer lab, and Receiver 1.4 is located in the hallway adjacent to 475.

Transmitter locations 2 and 3 represent a typical line-of-sight hallway environment (Figure 7.5). At location 2, the transmitter was positioned at the end of the hallway, whereas at location 3 the transmitter was positioned near the middle of the hall. Several receiver positions were chosen at distances from 7 meters to 27 meters.

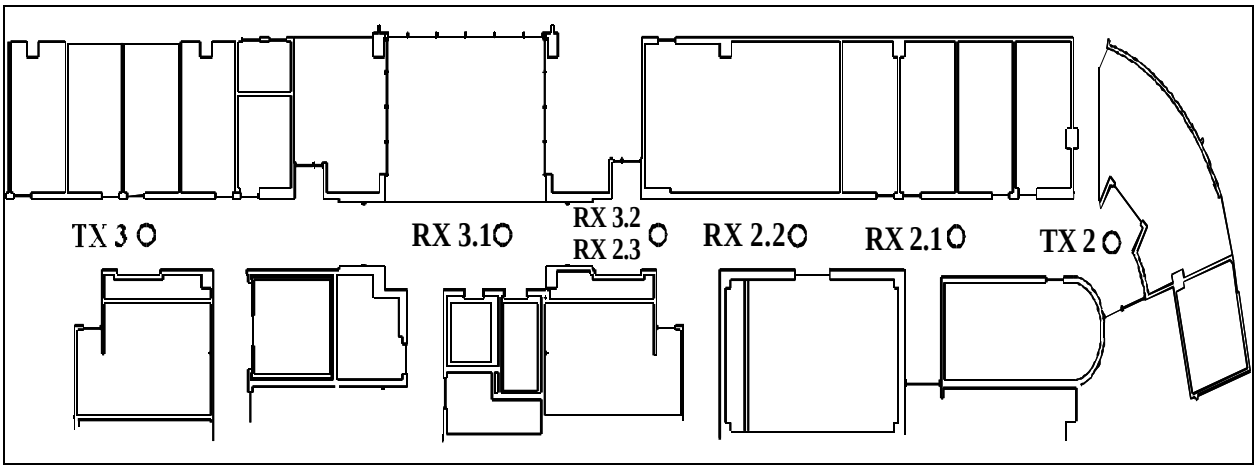

Figure 7.7: Measurement Locations 2.1—2.3 and 3.1 – 3.2, 4th Floor, Durham Hall, Virginia Tech. Transmitter 2 is located outside of Room 450, Transmitter 3 is located adjacent to Room 412. Receivers are at various positions in the hallway.

Transmitter location 4 is a medium sized room containing standard office cubicles (Figure 7.6). Because cubical partitions are made out of metal, the transmitter antenna height was set at 2.4 meters, with the antenna aimed down toward the receiver. Receiver antenna height was maintained at 1.2 meters. Receiver location 4.1 is NLOS propagation through drywall containing metal studs into a conference room. Receiver locations 4.2 and 4.3 are LOS propagation in and around cubicles. Receiver location 4.4 investigates the propagation through drywall containing metal studs into the hallway.

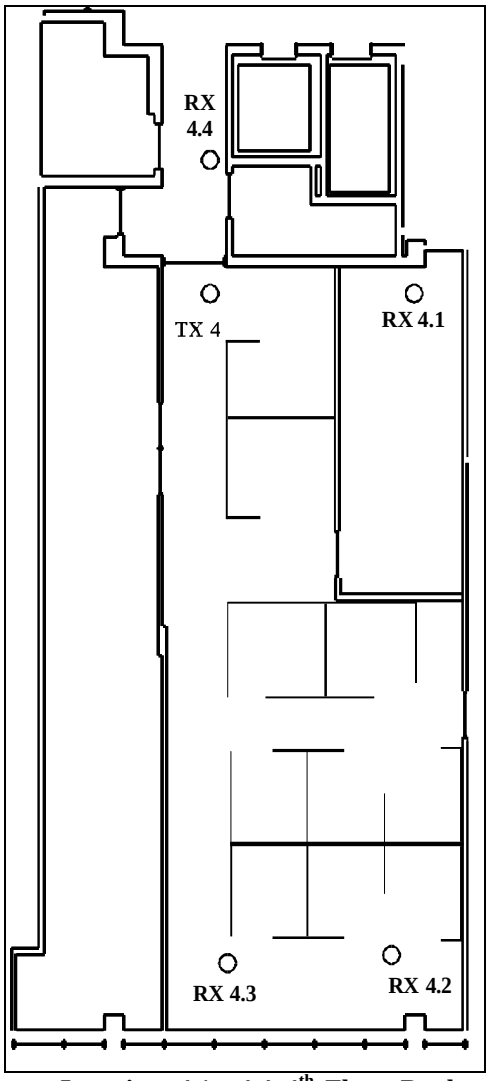

Figure 7.8: Measurement Locations 4.1 – 4.4, 4th Floor, Durham Hall, Virginia Tech. The Transmitter is located just inside the entrance to Room 476. Receiver locations are at various positions in 476, as well as the adjacent hallway.

Transmitter location 5 represents a typical office reception area containing a single cubicle, chairs, and office plants (Figure 7.7). Receiver location 5.1 investigates NLOS propagation through drywall containing metal studs into an office. Receiver locations 5.2 & 5.3 are on the opposite side of a large clear glass window partially obscured by office plants, and receiver location 5.4 is on the opposite side of a large clear glass door.

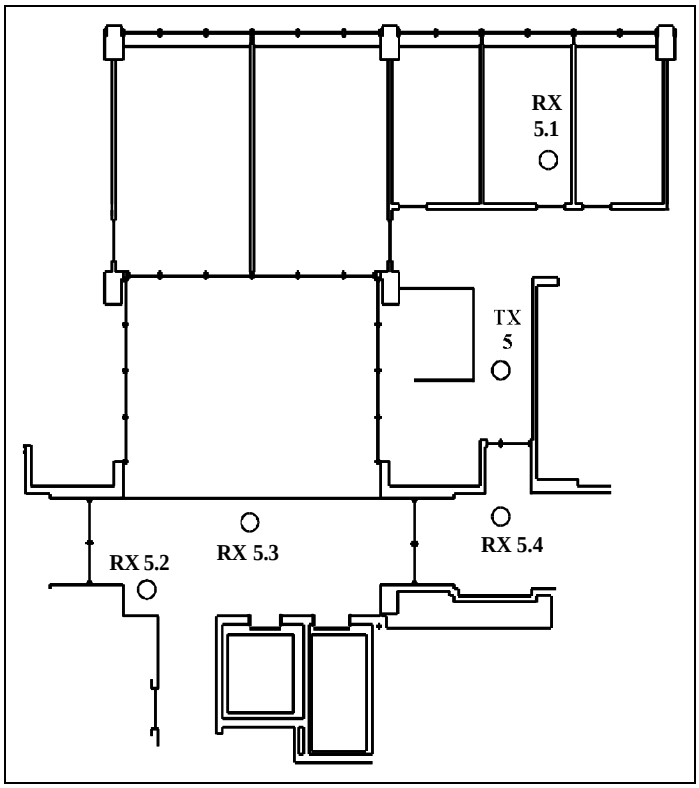

Figure 7.9: Measurement Locations 5.1 – 5.4, 4th Floor, Durham Hall, Virginia Tech. The Transmitter is located next to the receptionist's desk in Room 432. Receiver location 5.1 is in room 433, Receiver locations 5.2 and 5.3 are in the atrium next to the elevators, and Receiver location 5.4 is in the hallway next to 432.

Transmitter locations 6, 7, and 8 investigate propagation through glass doors (Figure 7.8). At locations 6 and 7 the glass is reinforced with a 24 gauge wire mesh, while at location 8 the glass is clear. For location 7, the transmitter was positioned approximately 3 meters away from the door, while at location 6 the transmitter was positioned approximately 7.5 meters away from the door—in order to determine if there were any differences caused by the relative position of the door in the transmitter-receiver link.

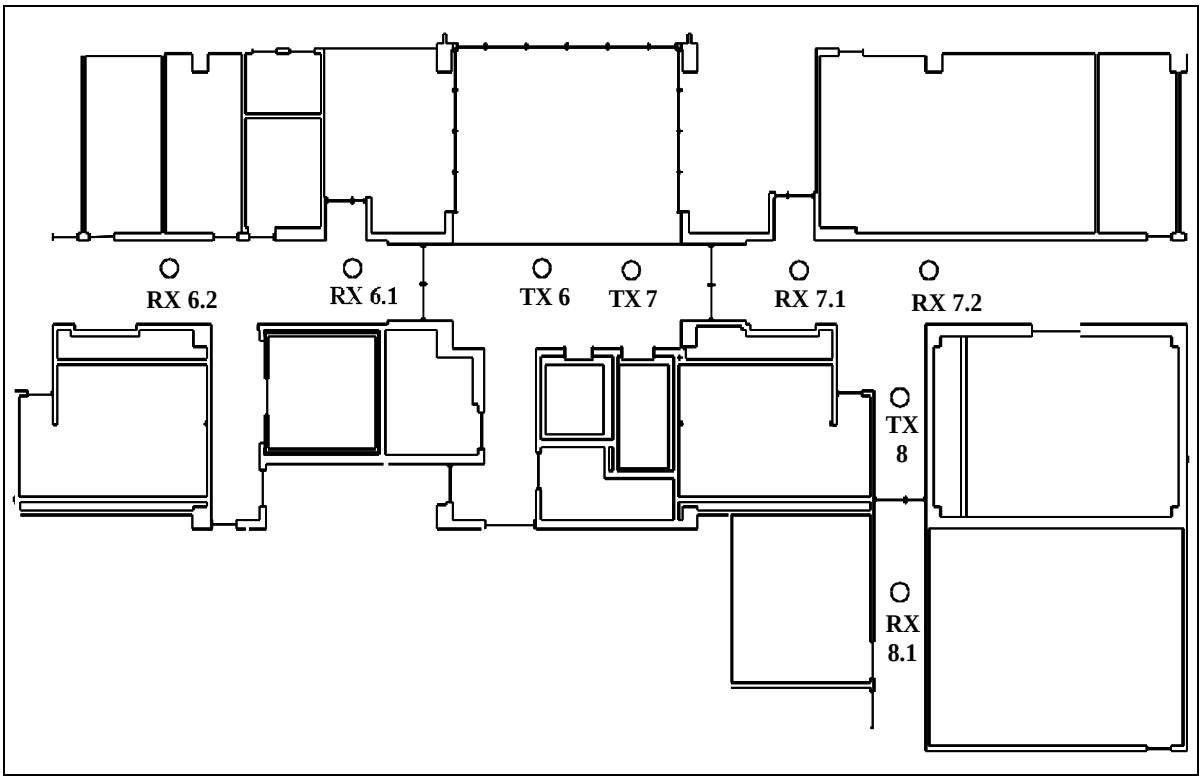

Figure 7.10: Measurement Locations 6.1 – 6.2, 7.1—7.2, and 8.1, 4th Floor, Durham Hall, Virginia Tech. Transmitters 6 and 7 are located in the atrium next to the elevators, while Transmitter 8 is located in a side hallway adjacent to the Women's Restroom. Receiver locations 6.1, 6.2, 7.1, and 7.2 are at various positions in the main hallway. Receiver location 8.1 is in the hallway next to Room 475.

7.3 Measurement Results

7.3.1 Summary Results Table

Tables 7.1 and 7.2 summarize the results of the 39,600 power delay profiles recorded during this measurement campaign. The tables are ordered by link number. For these measurements, partitions that existed between transmitter and receiver were placed in five separate categories, with the number of each type of partition noted in the table:

1. *Drywall*: 2 sheets of standard ½ inch thick sheetrock wallboard.
2. *Office Whiteboard*: Standard office dry-erase melamine whiteboard, attached to ½ inch thick plywood backing.
3. *Clear Glass*: ⅛ inch thick clear glass which is untextured and unreinforced.
4. *Mesh Glass*: ⅛ inch thick glass which has been reinforced with interlacing 24 gauge wires configured in a rectangular grid with openings of ½ inch × ½ inch.
5. *Clutter*: Objects that encroached into the first Fresnel zone but did not directly block the LOS signal from transmitter to receiver.

Also listed in the tables are the *Free Space Path Loss, Local Area Average Path Loss, Local Area Min/Max Path Loss, Local Area Max Excess Delay t_{max} (10 dB),* and *Local Area Max Excess Delay t_{max} (20 dB).* *Free Space Path Loss* is the expected path loss between transmitter and receiver, assuming free space propagation and excluding antenna gains, and is calculated using Equation 7.1.

$$PL_{FS} = 20\log\left(\frac{4p\,d}{l}\right) \tag{7.1}$$

Where: PL_{FS} is the free-space path loss in dB
l is the wavelength in meters
d is the transmitter-receiver separation distance in meters

Local Area Average Path Loss is the measured path loss averaged over all receiver positions (for both parallel and perpendicular track measurements) at a given measurement location, and is a spatial average value for path loss at that measurement location. Because the channel sounder records wideband power delay profiles, it is necessary to calculate the equivalent narrowband received power level using the method described in [73]. However, the measured received power includes the effects of the transmitter and receiver antenna gains. To provide a meaningful comparison with the free-space path loss calculated from Equation 7.1, the antenna gains must be subtracted out from the measured received power. Subtracting out the antenna gains provides path loss values as if isotropic antennas were used to measure the channel, even though directional antennas were actually employed on the channel sounder. The *Local Area Average Path Loss* is then given by Equation 7.2:

$$PL_{LA} = P_T - \left(P_{REC} - G_T - G_R\right)$$
$$PL_{LA} = P_T + G_T + G_R - P_{REC} \quad (7.2)$$

Where: PL_{LA} is the measured Local Area Average Path Loss (in dB) for a particular measurement location
P_T is the transmitter power level in dBm
G_T is the transmitter antenna gain in dBi
G_R is the receiver antenna gain in dBi
P_{REC} is the measured narrowband received power level in dBm

Local Area Min/Max Path Loss is the minimum and maximum path loss among all PDPs recorded at a particular receiver location. Similarly, the *Local Area Min/Max/Avg* s_t is the minimum, maximum, and average RMS delay spread (calculated from Equation 2.40) among all PDPs recorded at a particular measurement location.

Local Area Max Excess Delay t_{max} *(10 dB)* is the maximum excess delay [12] at which multipath power falls 10 dB below the PDP maximum. Similarly, the *Local Area Max Excess Delay* t_{max} *(20 dB)* is the maximum excess delay at which multipath power falls 20 dB below the PDP maximum. The values reported in the table are the largest excess delays observed among all PDPs recorded at a particular measurement location.

Figures 7.9 and 7.10 are scatter plots of all measured path loss values versus distance for the 2.5 GHz and 60 GHz measurements. A Minimum Mean Square Error analysis [12] was applied to the measured data to determine the path loss exponent (defined in Equation 2.48). The resulting path loss exponent for 2.5 GHz was $n = 2.4$, with a standard deviation of $s = 5.8$dB and for 60 GHz the path loss exponent was $n = 2.1$ with $s = 7.9$dB, which are within the ranges for in-building same-floor propagation reported in [12, 73, 64, 74, 85].

Table 7.1
2.5 GHz & 60 GHz Single Floor Office Building Path Loss

Frequency (GHz)	Number of Measurement Locations	n	s (dB)
2.5	22	2.4	5.8
60	22	2.1	7.9

Table 7.2
Summary of 2.5 GHz Measurement Results on a Single Floor of a Modern Office Building

Location	Link Distance (m)	Obstruction Type					Free Space Path Loss (dB)	Local Area Average Path Loss (dB) Excluding antenna gains	Local Area Min / Max Path Loss (dB) Excluding antenna gains	Local Area Min / Max / Avg σ_τ (ns)	Local Area Max Excess Delay τ_{max} (10 dB) (ns)	Local Area Max Excess Delay τ_{max} (20 dB) (ns)
		Drywall	Office White-board	Clear Glass	Mesh Glass	Clutter						
1.1	5.4	1	1	0	0	0	55	64	63 / 64	31.5 / 41.5 / 36.5	97	97
1.2	9.2	1	1	0	0	0	60	64	64 / 65	23.1 / 28.8 / 26.0	52	100
1.3	4.7	1	1	0	0	0	54	55	54 / 56	24.4 / 27.5 / 26.0	32	100
1.4	3.5	1	1	0	0	0	51	54	53 / 54	18.5 / 21.7 / 20.1	15	50
2.1	7.8	0	0	0	0	0	58	62	60 / 64	15.5 / 24.4 / 20.0	5	35
2.2	16.2	0	0	0	0	0	65	63	61 / 65	7.2 / 18.5 / 12.9	3	31
2.3	22.9	0	0	0	0	0	68	67	67 / 68	21.2 / 22.0 / 21.6	3	32
3.1	18.2	0	0	0	0	0	66	63	62 / 64	37.1 / 48.3 / 42.7	128	150
3.2	27.4	0	0	0	0	0	69	66	64 / 68	25.7 / 36.1 / 30.9	3	135
4.1	6.0	1	0	0	0	0	56	64	64 / 65	16.9 / 33.3 / 25.1	32	125
4.2	13.0	0	0	0	0	1	63	65	64 / 65	21.6 / 31.7 / 26.7	42	55
4.3	13.6	0	0	0	0	1	63	64	63 / 65	21.4 / 22.1 / 21.8	18	55
4.4	4.7	1	0	0	0	0	54	64	64 / 65	29.7 / 31.1 / 30.4	15	110
5.1	4.5	1	0	0	0	0	54	54	53 / 54	19.9 / 20.2 / 20.1	9	105
5.2	12.2	0	0	1	0	1	62	73	72 / 73	18.0 / 23.8 / 20.9	3	60
5.3	7.7	0	0	1	0	1	58	72	71 / 72	27.2 / 27.5 / 27.4	3	78
5.4	3.9	0	0	1	0	0	52	55	55 / 56	17.8 / 18.3 / 18.1	3	40
6.1	7.6	0	0	0	1	0	58	68	67 / 68	15.8 / 16.2 / 16.0	4	49
6.2	17.1	0	0	0	1	0	65	68	67 / 68	24.2 / 30.4 / 26.3	4	150
7.1	5.5	0	0	0	1	0	55	67	66 / 68	15.8 / 16.3 / 16.0	4	75
7.2	10.4	0	0	0	1	0	61	68	67 / 68	9.1 / 9.7 / 9.4	4	25
8.1	5.5	0	0	1	0	0	55	64	63 / 64	21.0 / 21.3 / 21.2	15	75

Table 7.3
Summary of 60 GHz Measurement Results on a Single Floor of a Modern Office Building

Location	Link Distance (m)	Obstruction Type					Free Space Path Loss (dB)	Local Area Average Path Loss (dB) Excluding antenna gains	Local Area Min / Max Path Loss (dB) Excluding antenna gains	Local Area Min / Max / Avg σ_τ (ns)	Local Area Max Excess Delay τ_{max} (10 dB) (ns)	Local Area Max Excess Delay τ_{max} (20 dB) (ns)
		Drywall	Office White-board	Clear Glass	Mesh Glass	Clutter						
1.1	5.4	1	1	0	0	0	83	98	97 / 99	14.8 / 20.2 / 17.5	35	51
1.2	9.2	1	1	0	0	0	87	103	101 / 105	17.9 / 22.0 / 20.2	24	80
1.3	4.7	1	1	0	0	0	81	93	91 / 94	15.7 / 18.3 / 16.8	30	60
1.4	3.5	1	1	0	0	0	79	82	81 / 83	1.0 / 3.7 / 2.5	5	5
2.1	7.8	0	0	0	0	0	86	73	72 / 74	2.5 / 7.6 / 5.6	3	5
2.2	16.2	0	0	0	0	0	92	78	76 / 87	7.2 / 8.5 / 7.9	3	13
2.3	22.9	0	0	0	0	0	95	98	95 / 104	6.0 / 9.1 / 7.5	3	28
3.1	18.2	0	0	0	0	0	93	89	88 / 90	11.0 / 16.5 / 13.8	3	3
3.2	27.4	0	0	0	0	0	97	99	97 / 100	7.7 / 11.6 / 9.4	3	12
4.1	6.0	1	0	0	0	0	84	94	89 / 98	9.8 / 15.8 / 11.4	3	3
4.2	13.0	0	0	0	0	1	90	99	97 / 101	9.1 / 17.9 / 13.6	12	25
4.3	13.6	0	0	0	0	1	91	91	89 / 97	10.2 / 18.8 / 14.5	18	26
4.4	4.7	1	0	0	0	0	81	89	88 / 90	5.5 / 22.4 / 12.9	3	13
5.1	4.5	1	0	0	0	0	81	81	76 / 83	5.8 / 11.5 / 7.9	3	15
5.2	12.2	0	0	1	0	1	90	96	94 / 97	2.9 / 11.5 / 7.8	3	12
5.3	7.7	0	0	1	0	1	86	87	85 / 87	5.2 / 10.4 / 8.0	3	13
5.4	3.9	0	0	1	0	0	80	80	73 / 83	2.9 / 5.9 / 3.9	3	17
6.1	7.6	0	0	0	1	0	86	89	88 / 91	2.0 / 12.0 / 5.8	3	4
6.2	17.1	0	0	0	1	0	93	103	97 / 107	19.2 / 30.0 / 25.3	37	75
7.1	5.5	0	0	0	1	0	83	94	93 / 95	8.9 / 14.2 / 11.9	3	22
7.2	10.4	0	0	0	1	0	88	99	97 / 99	6.2 / 12.1 / 9.2	3	20
8.1	5.5	0	0	1	0	0	83	85	84 / 86	16.9 / 24.1 / 19.1	37	73

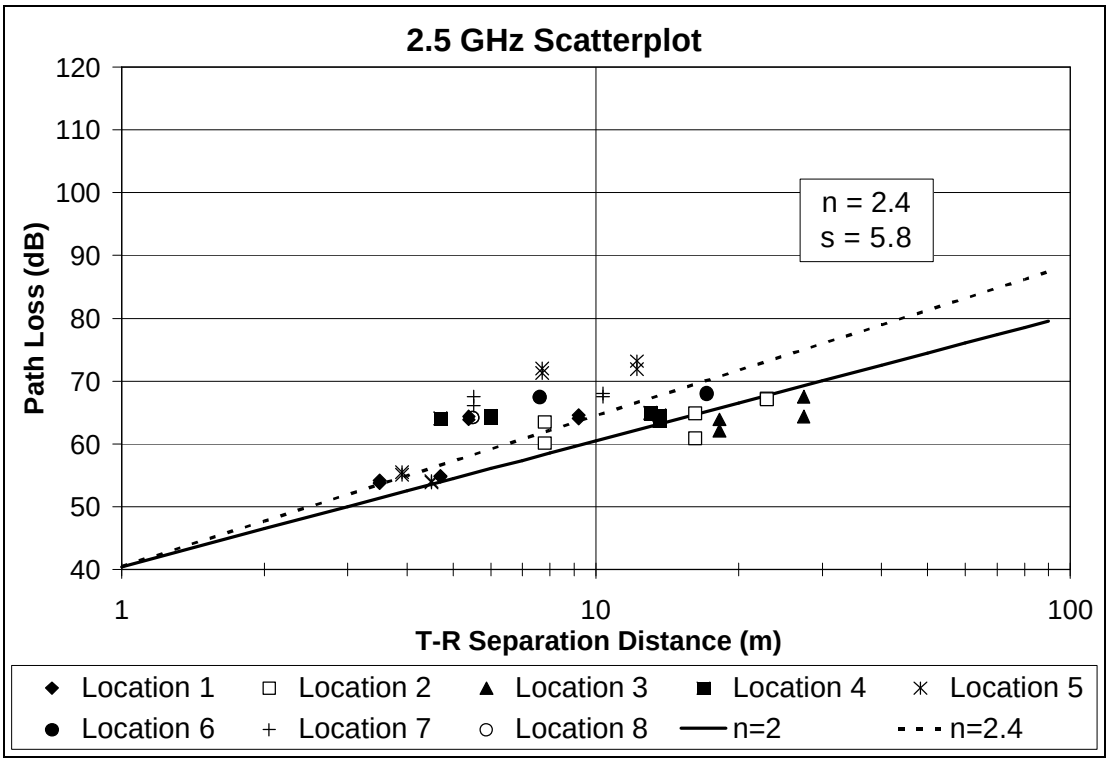

Figure 7.11: Scatterplot of all Measured Path Loss Values (Excluding Antenna Gains) at 2.5 GHz on a Single Floor of a Modern Office Building. Transmitter and Receiver use Omnidirectional Biconical Antennas with 6dBi Gain.

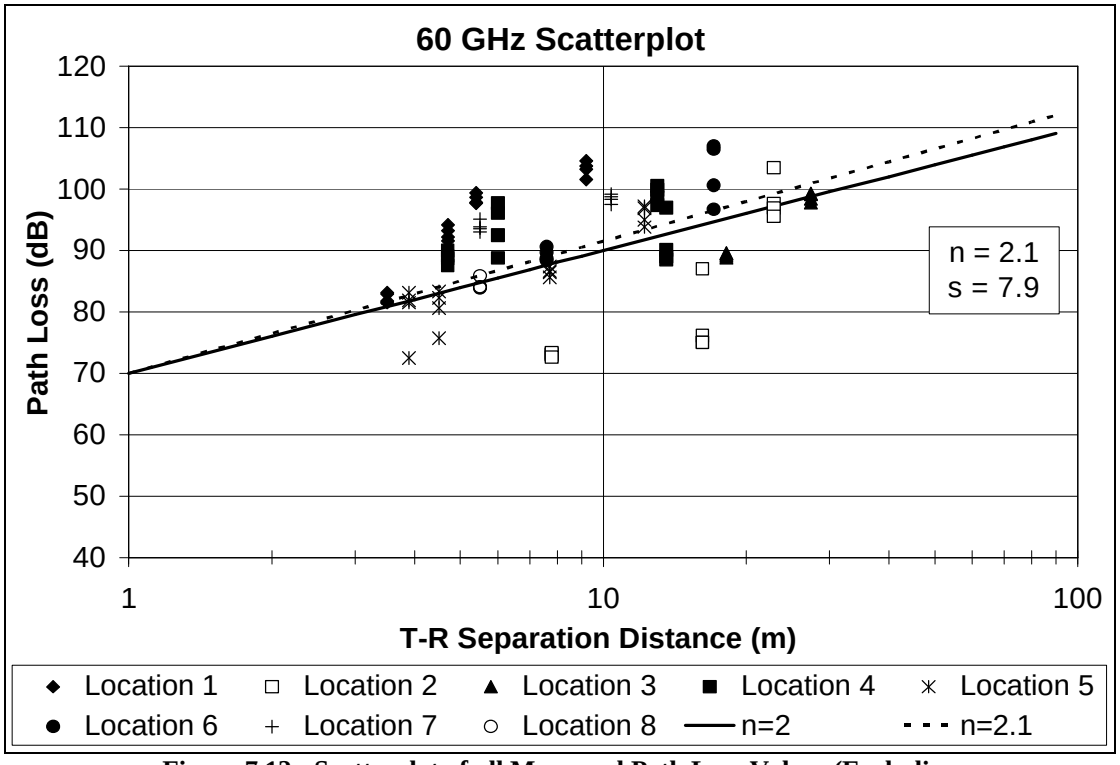

Figure 7.12: Scatterplot of all Measured Path Loss Values (Excluding Antenna Gains) at 60 GHz on a Single Floor of a Modern Office Building. Transmitter and Receiver use Pyramidal Horn Antennas with 25dBi Gain and 50° First-Null Beamwidth.

7.3.2 Partition Based Path Loss Analysis

In propagation analysis the path loss exponent, *n*, is useful for predicting large-scale propagation effects. However, the path loss exponent model is inadequate at predicting site-specific propagation effects, such as reflection, diffraction, or penetration losses caused by a particular building layout, construction materials, furniture, etc. A more refined model uses *partition-dependant attenuation factors* [75, 82], which assumes free space propagation (*n=2*) with additional path loss incurred based on the number and type of objects (such as walls or doors) intersected by a single ray drawn from transmitter to receiver. Then, the path loss is given by Equation 7.3 [75]. Note that in the case of free space propagation with no partitions between transmitter and receiver, path loss calculated from Equation 7.3 will be identical to path loss calculated from Equation 7.1.

$$PL(d) = 20\log_{10}\left(\frac{4p\,d}{l}\right) + aX_a + bX_b + \ldots \tag{7.3}$$

Where: $PL(d)$ is the path loss in dB

d is the transmitter—receiver separation distance in meters

l is the wavelength in meters

$X_a, X_b, \ldots$ are the attenuation values in dB for the partitions between transmitter and receiver

$a, b, \ldots$ are the number of times the ray intersects each type of partition (i.e. a intersections with partition X_a, b intersections with partition X_b, and so forth).

For measurement data at a particular site, the only unknowns in Equation 7.3 are the individual partition attenuation factors, $X_a, X_b, \ldots$, which may be found by applying a Minimum Mean Square Error analysis of measured versus predicted path loss using the procedure in [75]. Table 7.3 shows the resulting partition attenuation factors at 2.5 GHz and 60 GHz, respectively, for the five types of partitions studied in this measurement campaign. Tables 7.5 and 7.6 list partition loss values for drywall and plywood reported in the literature at a variety of frequencies, and Table 7.7 lists partition values reported in the literature for several miscellaneous building materials at several frequencies. To ensure that path loss values for similar materials could be compared in a meaningful way, all path loss values were normalized to dB per centimeter of material thickness.

Table 7.4
Measured Partition Losses at 2.5 GHz and 60 GHz on a Single Floor of a Modern Office Building

Material	Number of Measurements at Each Frequency	Material Thickness (cm)	2.5 GHz			60 GHz		
			Average Measured Attenuation (dB)	Measurement Standard Deviation (dB)	Normalized Average Attenuation (dB/cm)	Average Measured Attenuation (dB)	Measurement Standard Deviation (dB)	Normalized Average Attenuation (dB/cm)
Drywall ½ inch thick sheetrock (2 Sheets Total)	7	2.54	5.4	2.1	2.1	6.0	3.4	2.4
Whiteboard ¼ inch thick Melamine whiteboard with ½ inch thick plywood backing.	4	1.91	0.5	2.3	0.3	9.6	1.3	5.0
Clear Glass **8** inch thick smooth, clear glass	4	0.32	6.4	1.9	20.0	3.6	2.2	11.3
Mesh Glass **8** inch thick smooth, clear glass Reinforced with a 24 gauge wire mesh	4	0.32	7.7	1.4	24.1	10.2	2.1	31.9
Clutter Objects which encroached on the first Fresnel Zone but did not block LOS	4	--	2.5	2.2	--	1.2	1.8	--

Table 7.5
Reported Partition Losses for Drywall Type Material

Material Name	Thickness (cm)	Frequency (GHz)	Reported Attenuation (dB)	Normalized Attenuation (dB/cm)	Ref.
Plaster Walls	1.3*	5.8	4.7	3.6	[75]
Sheetrock	1.9	9.6	2.0	1.1	[12]
Plasterboard Wall	2.6*	17	4.3	1.7	[79]
Sheetrock	1.6	17.5	1.3	0.8	[80]
Sheetrock	1.9	28.8	2.0	1.1	[12]
Plasterboard Wall	2.6*	37.2	4.4	1.8	[90]
Sheetrock	1.9	57.6	5.0	2.6	[12]
Plasterboard	2.4	60	6.5	2.7	[78]
Plasterboard Wall	2.6*	60	13.2	5.1	[79]
Plasterboard	1.4	60	2.8	2.0	[76]
Plasterboard	1.0	60	2.1	2.1	[76]
Plasterboard	--	60	--	1.5	[77]
Composite Wallboard	2.6*	60	8.8	3.4	[64]

Table 7.6
Reported Partition Losses for Plywood Type Material

Material Name	Thickness (cm)	Frequency (GHz)	Reported Attenuation (dB)	Normalized Attenuation (dB/cm)	Ref.
Plywood	0.4	5.0	0.9	2.3	[81]
Dry Plywood	1.9	9.6	1.0	0.5	[12]
Dry Plywood	3.8	9.6	4.0	1.1	[12]
Plywood	1.3	17.5	2.9	2.2	[80]
Dry Plywood	1.9	28.8	4.0	2.1	[12]
Dry Plywood	3.8	28.8	6.0	1.6	[12]
Dry Plywood	1.9	57.6	8.0	4.2	[12]
Dry Plywood	3.8	57.6	14.0	3.7	[12]
Wooden Panel	1.9	60	8.6	4.5	[76]
Wooden Panel	1.2	60	7.6	6.3	[76]
Wooden Joint Panel	1.6	60	7.6	4.8	[76]
Wood	--	60	--	4.2	[77]

*Thickness of plasterboard not reported, a standard thickness of ½ inch (1.3 cm) per sheet is assumed

Table 7.7
Reported Partition Losses for Miscellaneous Building Materials

Material Name	Thickness (cm)	Frequency (GHz)	Reported Attenuation (dB)	Normalized Attenuation (dB/cm)	Ref.
Clear Glass	0.3	17.5	1.3	4.1	[80]
Glass Door	0.4	37.2	0.56	1.4	[90]
Smooth, Clear Glass	0.2	60	1.7	8.5	[76]
Smooth, Clear Glass	0.4	60	2.4	6.0	[76]
Smooth, Clear Glass	0.6	60	3.1	5.2	[76]
Smooth, Clear Glass	0.8	60	3.1	3.9	[76]
Glass	--	60	--	6.1	[77]
Glass Door	0.4	60	2.5	6.3	[64]
Rough Glass	0.4	60	4.5	11.3	[76]
Glass Door with Wire Mesh	--	17	0.9	--	[79]
Glass Door with Wire Mesh	--	60	4.2	--	[79]
Wooden Home Siding	1.3	5.8	8.8	6.8	[75]
Wood Fiberboard	1.2	60	3.4	2.8	[76]
Wooden Chipboard	1.3	60	6.2	4.8	[76]
Wooden Chipboard	1.6	60	8.3	5.2	[76]
Wood	--	60	--	4.2	[77]
Chipboard	--	60	--	5.2	[77]
Concrete Pillar	30.0	17	22.4	0.8	[79]
External Concrete Wall	75.2	37.2	43.0	0.6	[90]
Concrete Pillar	30.0	60	= 20	--	[79]
Concrete	1.0	60	6.7	6.7	[77]
Concrete	5.0	60	= 30	--	[76]
Concrete Wall	15.0	60	36.0	2.4	[91]
Aerated Concrete	1.0	60	3.7	3.7	[77]
Aerated Concrete	5.0	60	18.9	3.8	[76]
Concrete (1 week cure time)	3.0	57.5	73.6	24.5	[83]
Concrete (5 week cure time)	3.0	57.5	46.5	15.5	[83]
Concrete (14 month cure time)	3.0	57.5	28.1	9.4	[83]

In Figures 7.11 and 7.12, the partition loss from Tables 7.4 and 7.5 for drywall and plywood, as well as the measured partition loss for drywall and whiteboard from Table 7.3, were plotted to determine if any correlation existed between transmission frequency and material attenuation.

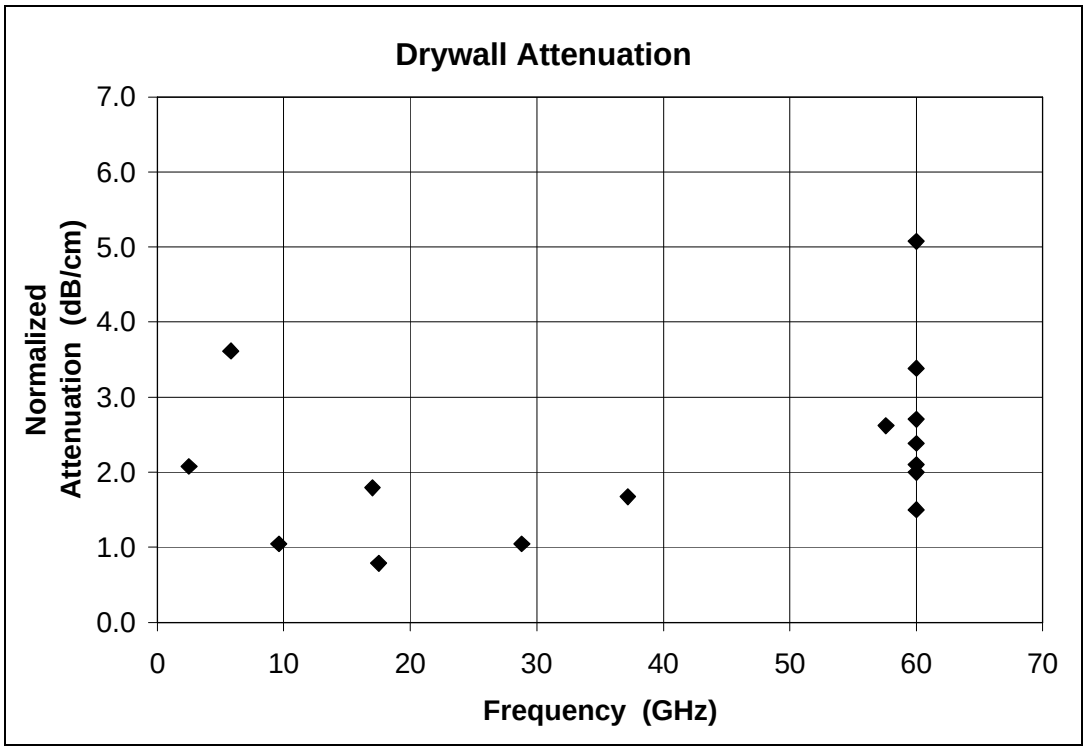

Figure 7.13: Normalized Attenuation of Drywall vs. Frequency, from Measured and Reported Data.

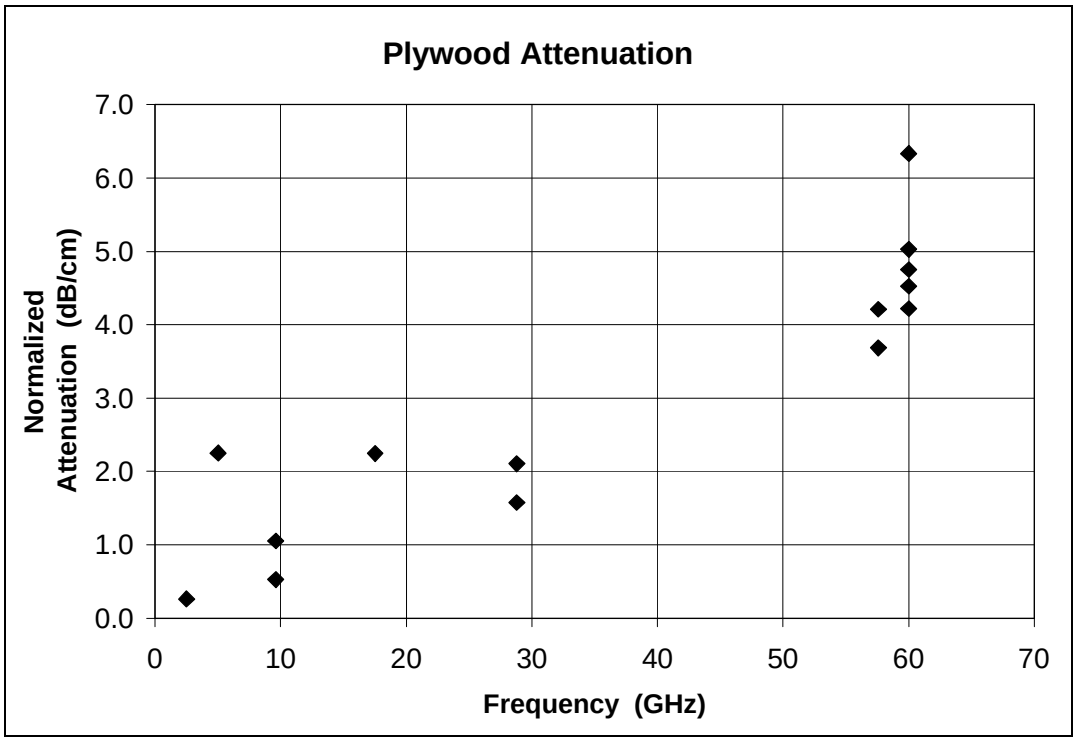

Figure 7.14: Normalized Attenuation of Plywood vs. Frequency, from Measured (Values for Whiteboard Used) and Reported Data.

7.3.3 Discussion of Results

Comparing Figures 7.9 and 7.10, it can be seen that when using highly directional antennas at 60 GHz, the large-scale mean path loss is very close to free-space; however, the spread of values about the mean is higher than at 2.5 GHz. Also it must be noted that the RMS Delay Spread at 2.5 GHz is significantly higher than at 60 GHz, which was caused by the use of omnidirectional antennas at 2.5 GHz and horn antennas at 60 GHz. Additionally at 2.5 GHz, very little difference exists between the minimum and maximum path loss measured in a local area, due to minimal fading of multipath signals over a small local area [12]. At 60 GHz, the difference between the minimum and maximum path loss is somewhat greater, caused by the influence of the ½ meter track measurements. With the combination of the ½ meter track measurements and highly directional antennas, the receiver would frequently move out of the spatial region where the transmitter and receiver antennas were maximally aligned, resulting in a drop in the received power due to antenna misalignment.

Comparing the measured partition losses for 2.5 GHz and 60 GHz in Table 7.3, the attenuation of drywall, whiteboard, and mesh glass increases from 2.5 GHz to 60 GHz, however the attenuation of clear glass and clutter decreases. The reason for the decrease in attenuation from clutter is intuitive, since the first Fresnel zone at 60 GHz is significantly smaller than at 2.5 GHz; therefore, fewer objects in the environment are capable of perturbing the LOS signal. It is not known why the attenuation of Clear Glass decreases from 2.5 GHz to 60 GHz.

Looking at the reported attenuation values for various types of concrete also demonstrates the idea that material composition may play a role in the amount of attenuation. At 60 GHz, the attenuation of Aerated Concrete is significantly less than for regular concrete. Additionally, the attenuation of concrete decreases as it cures, decreasing from 24.5 dB/cm at a 1 week cure time to 9.4 dB/cm after a 14 month cure time. As concrete cures, its physical properties change due to water desiccation and hydration, requiring more than a year before the water content in concrete fully stabilizes [83]. Research in [83] has shown that the dielectric properties of concrete (which determine the transmission coefficient) are strongly correlated with the water content. The decrease in attenuation of concrete during its cure time means that a 60 GHz network installed in a new building will experience an increase in coverage as the concrete cures, which is an important consideration for engineers deploying these networks.

From Figure 7.11, it can be seen that a nonlinear relationship exists between transmission frequency and attenuation of Drywall, a phenomenon also observed in [84]. In Figure 7.12, it appears that a linear relationship does exist between transmission frequency and attenuation of Plywood; however, the lack of data between 30 GHz and 50 GHz prevents generalizing this trend. Another observation is that, for both drywall and plywood, the range of attenuation values at 60 GHz is rather large, indicating that not only does the material type (drywall, wood, brick, etc.) affect transmission properties, but other factors that influence the material's dielectric properties (and therefore the transmission coefficient), such as material composition and structure may play an important role as well.

7.4 Conclusion

This chapter presents the results of a measurement campaign and detailed analysis of in-building 2.5 GHz and 60 GHz channels. Measurements were analyzed in context with site-specific information, and results include local average power delay profiles, received signal power, and partition loss values for a variety of materials encountered in an office or laboratory building. Measurements of partition loss in several types of partitions indicate that material type as well as composition and structure may play an important role in determining transmission loss as well as multipath structure. The measured path loss exponents and partition losses agree well with results published in the literature. These measurement results provide important information for engineers designing and deploying wireless local area networks, in addition to providing a better understanding of radio wave propagation.

Chapter 8

Conclusions

8.1 Summary of Findings

In microcellular and picocellular environments, the performance of a wireless network becomes increasingly site-specific, particularly for millimeter-wavelength frequencies. This thesis has presented the design and implementation of a miniaturized ultrawideband channel sounder with the capability to measure the magnitude and phase response of a wireless channel. Additionally, a portable, reconfigurable measurement system provides engineers with a tool that can be easily used to characterize a variety of wireless links, and data post-processing software provides an abundance of statistical information about the channel. A 2.5 GHz and 60 GHz measurements campaign was conducted on the 4th floor of Durham Hall at Virginia Tech, and channel models were developed from the results of these measurements.

8.1.1 Miniaturized Channel Sounder

The primary focus of this thesis was designing and implementing an upgraded ultrawideband channel sounder. Many of the large and bulky subsystems on the channel sounder were replaced with smaller, more compact but functionally equivalent systems. GPS disciplined oscillators provided a highly stable frequency reference at transmitter and receiver so that multipath phase measurements could be recorded. A variable frequency PN Generator provides multipath resolution as high as 2.5 nanoseconds, so that the characteristics of indoor propagation environments may be studied in greater detail. The channel sounder is also capable of utilizing a

linear positioning track so that variations in the received signal over a local area in space may be investigated. Accuracy of the power delay profiles recorded by the channel sounder is ±1.2 dB, with a repeatability of ±1.3 dB. The accuracy of the phase measurement depends upon the operating frequency the channel sounder is configured for as well as the time duration over which measurements are recorded.

8.1.2 Data Post Processing Software

The combination of the LabVIEW Data Analysis software and the Matlab Channel Imaging Analysis Suite generate Power Delay Profiles, multipath phase angle plots, Doppler Spectra, and statistical information about the structure of the Power Delay Profile. The results from the post processing analysis can then be used to develop highly accurate site-specific channel models, improving the accuracy and reliability of siteplanning tools as well as channel simulations such as ray-tracing.

8.1.3 Indoor Measurements at 2.5 GHz and 60 GHz

An extensive measurements campaign was undertaken at 2.5 GHz and 60 GHz to investigate short-range in-building communication links. Power Delay Profiles at a variety of locations on the 4^{th} floor of Durham Hall at Virginia Tech were recorded along a linear track and then averaged together to generate a local average power delay profile. Additionally, narrowband received power was calculated from the power delay profiles, and used to analyze the partition losses of several objects commonly found in a office or laboratory environment. The results of these measurements will provide future researchers with the detailed channel models they require to design, develop, and implement future generations of wireless networks.

8.2 Further Research

Even though this research has resulted in a smaller, more compact channel sounder, many improvements can be implemented that will further reduce the size of the channel sounder as well as increase its functionality. The printed circuit boards used in various channel sounder subsystems were constrained to two copper layers, and as a result many subsystems had to be installed in separate enclosures. Utilizing multilayer printed circuit boards would allow all subsystems implemented on two-layer boards to be implemented on a single printed circuit board

and placed in a single enclosure. Additionally, many of the discrete components (such as the I/Q mixer at the receiver) are available in integrated circuit form and could be included on the same board, further reducing the size of the channel sounder.

Another advantage of multilayer boards is the implementation of more complex digital logic circuits. The primary limitation to two-layer boards is the lack of board real estate to route signal traces. With a multilayer board this problem is significantly reduced, because the number of layers available to route traces is increased. For example, a higher speed PN generator as well as the clock signal generator circuit could be implemented on the same board, reducing the size of the channel sounder and increasing its functionality.

In addition to further decreasing the size of the channel sounder, the phase measurement accuracy could also be improved. Many high-stability oscillators have a voltage control that allows a user to adjust the frequency of the oscillator. Conceivably, a pilot signal could be transmitted from the channel sounder transmitter to the channel sounder receiver over a fixed-length wireless link. The pilot signal could then be used to synchronize the receiver's oscillator to the exact frequency of the transmitter's oscillator, similar to how a CDMA cell phone synchronizes itself to the pilot signal transmitted by the base station. Synchronizing the oscillators will result in a reduced Alan variance, and hence a higher accuracy in the phase measurement.

Finally, it would be interesting to extend the measurements campaign to a wider variety of building layouts, containing a larger number of partition types. The results from these measurements could be used in the development of more accurate and reliable ray-tracing algorithms, more detailed channel models, and to verify the hypothesis that not only does the material type affect its transmission of radio waves, but also its composition and structure.

8.3 Conclusion

This research has studied the development of wireless measurement equipment to investigate the effects of radio wave propagation at a wide variety of frequencies and in a variety of propagation environments. Additionally, an in-building measurement campaign was conducted in two frequency bands (2.5 GHz and 60 GHz), which have become popular for the design and deployment of current and future generations of wireless networks.

This research shows that for indoor applications, the propagation environment affects the multipath structure. Additionally, partition loss through different materials has been shown to have a loose correlation between frequency and material type, composition, and structure. As a result, engineers must account for these factors when developing the next generation of wireless networks.

The enormous amount of spectrum available at millimeter-wavelength frequencies has the potential to deliver the real-time voice, video, and data traffic that today's consumer demands. This thesis has provided a research tool to more fully evaluate these channels, as well as fundamental research into the nature of propagation at these frequencies.

Appendix A

Schematics

A.1 11 bit Transmitter PN Generator Schematic
A.2 18 bit Transmitter PN Generator Schematic
A.3 11 bit Receiver PN Generator Schematic
A.4 18 bit Receiver PN Generator Schematic
A.5 Trigger Pulse Generator Board Schematic
A.6 I/Q Correlator Board Schematic

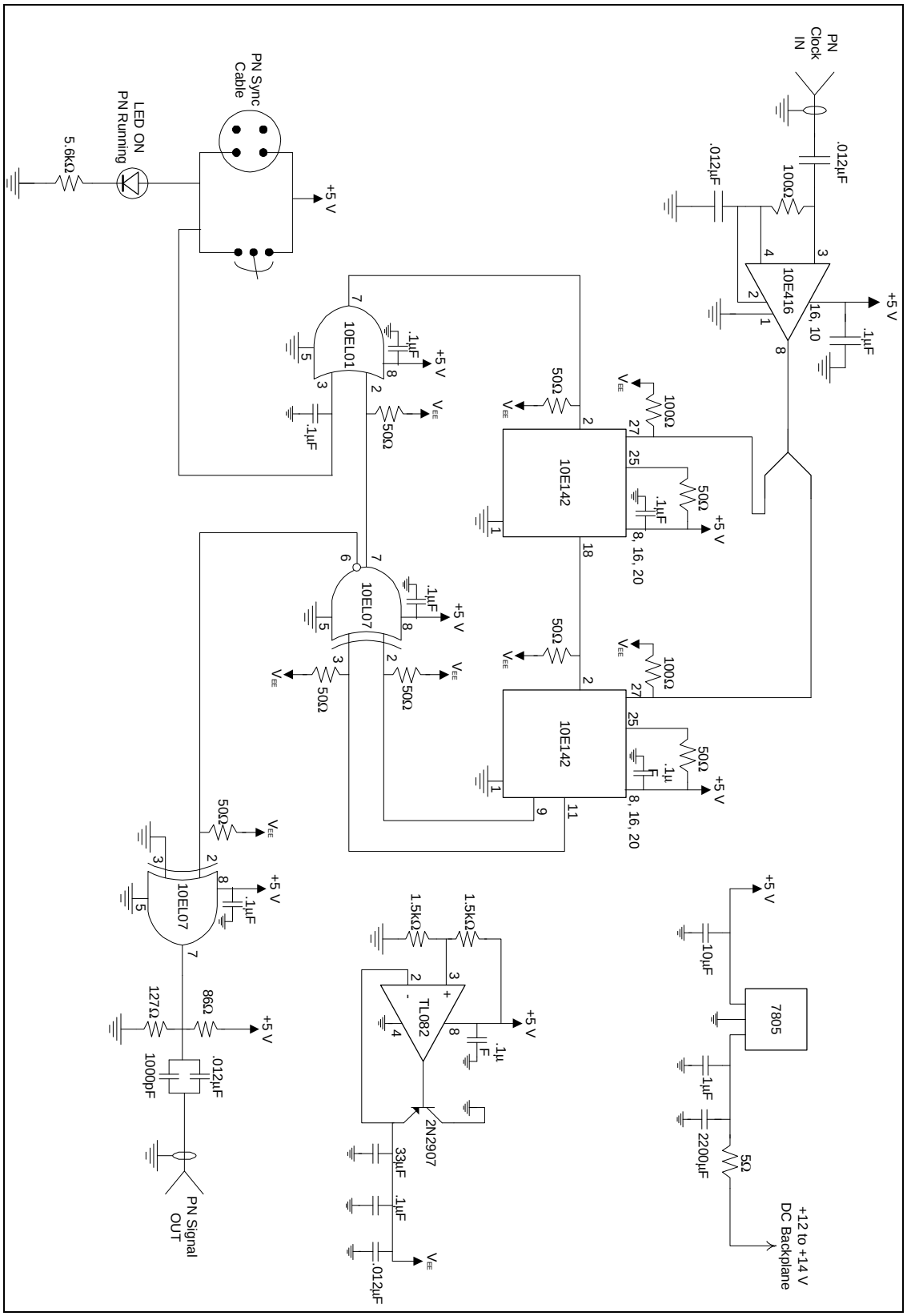

Figure A.1: 11-Bit Transmitter PN Generator Schematic

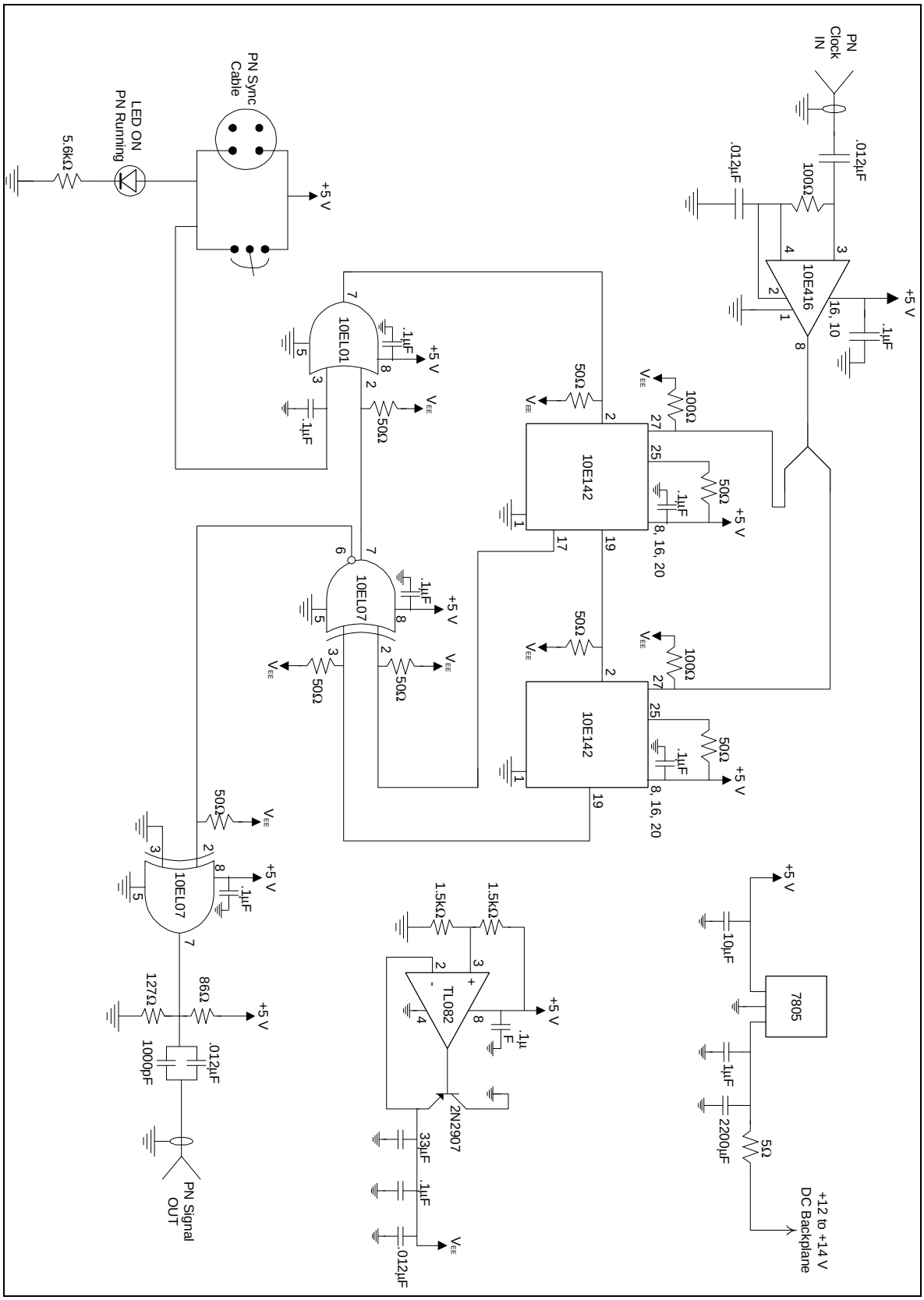

Figure A.2: 18-Bit Transmitter PN Generator Schematic

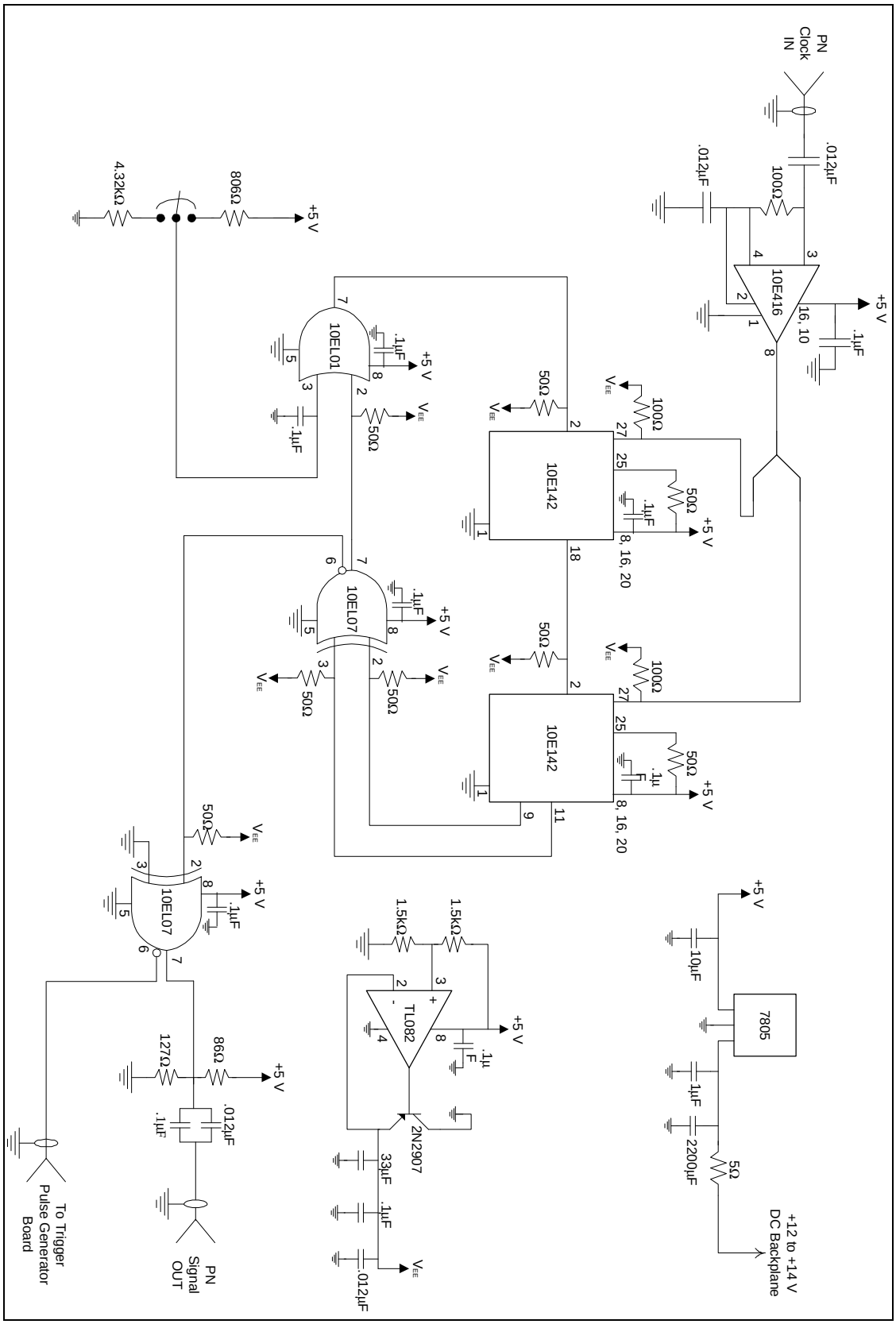

Figure A.3: 11-Bit Receiver PN Generator Schematic

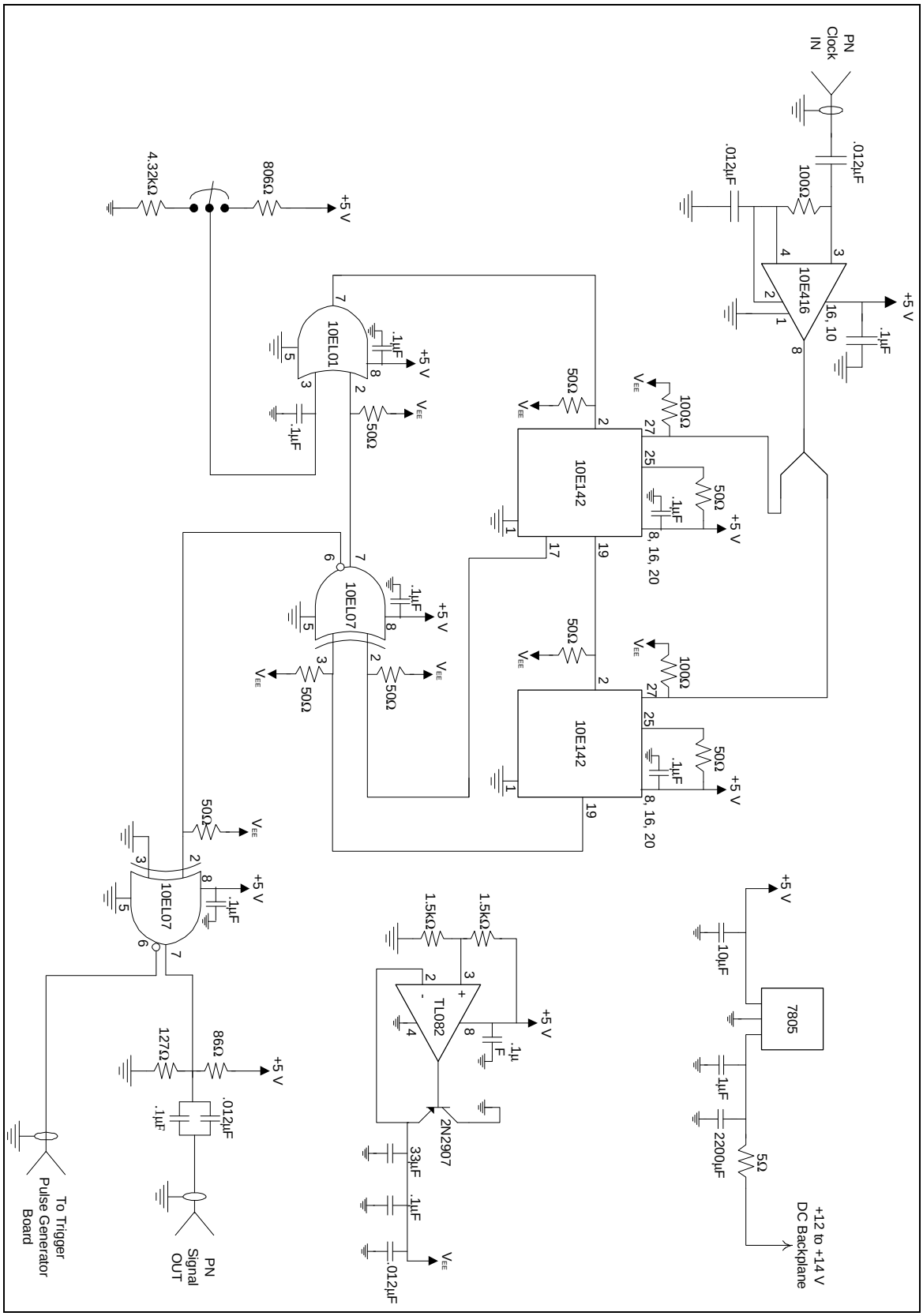

Figure A.4: 18-Bit Receiver PN Generator Schematic

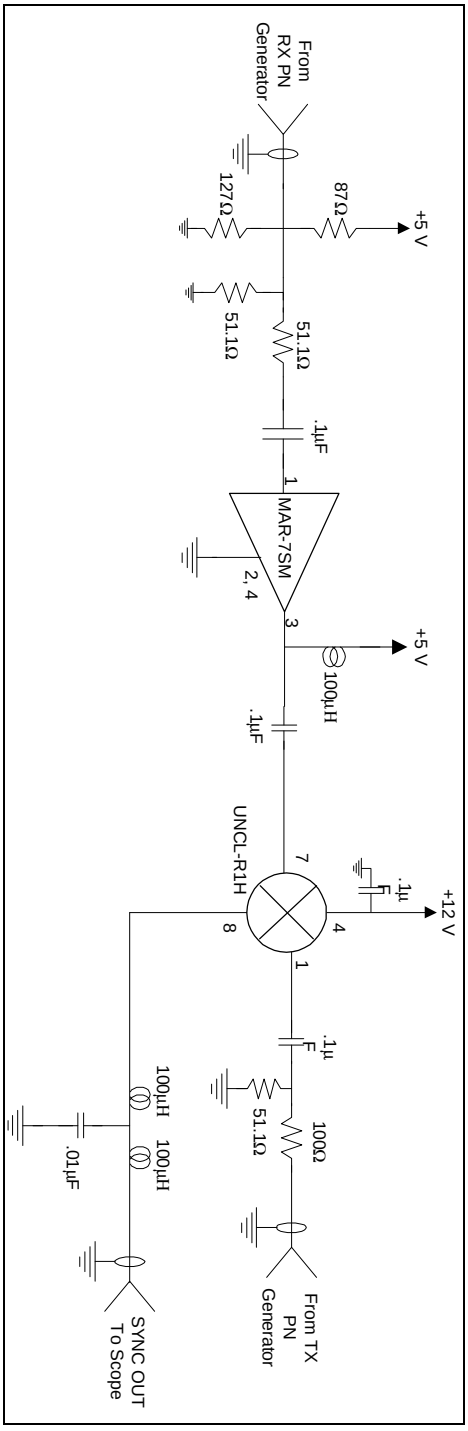

Figure A.5: Trigger Pulse Generator Schematic

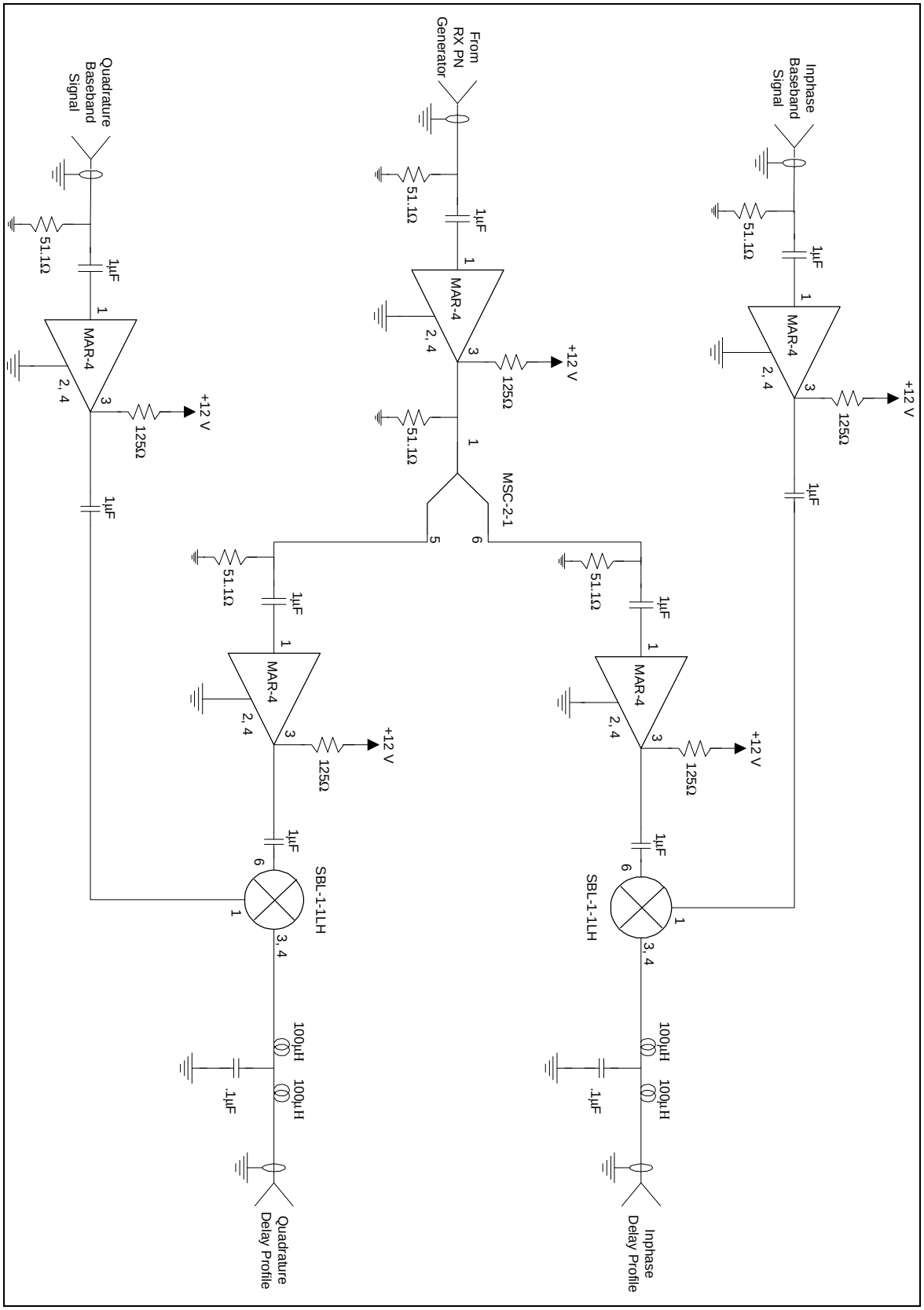

Figure A.6: I/Q Correlator Board Schematic

Appendix B

Power Delay Profiles and Site Photos for 2.5 & 60 GHz Measurements

The following figures show local average PDPs for all 22 measurement locations. For both 2.5 GHz and 60 GHz, two types of track measurements were performed, a parallel track measurement and a perpendicular track measurement:

- 10 l *Parallel Track Measurements* consisted of orienting the track parallel to the LOS path from transmitter to receiver (or the direct path from transmitter to receiver in the case where they were separated by an obstruction). Power delay profiles were then recorded at 40 positions along the track with a separation between successive measurements of $\frac{l}{4}$, so that the receiver traveled a total distance of 10 l .

- 10 l *Perpendicular Track Measurements* consisted of orienting the track perpendicular to the LOS path from transmitter to receiver (or the direct path from transmitter to receiver in the case where they were separated by an obstruction). Power delay profiles were then recorded at 40 positions along the track with a separation between successive measurements of $\frac{l}{4}$, so that the receiver traveled a total distance of 10 l .

Additionally at 60 GHz, a second set of parallel and perpendicular track measurements were performed:

- *½ meter Parallel Track Measurements* consisted of orienting the track parallel to the LOS path from transmitter to receiver (or the direct path from transmitter to receiver in the case where they were separated by an obstruction). Power delay profiles were then recorded at 10 positions along the track with a separation between successive measurements of 10 l , so that the receiver traveled a total distance of 100 l .

- *½ meter Perpendicular Track Measurements* consisted of orienting the track perpendicular to the LOS path from transmitter to receiver (or the direct path from transmitter to receiver in the case where they were separated by an obstruction). Power delay profiles were then recorded at 10 positions along the track with a separation between successive measurements of 10 l , so that the receiver traveled a total distance of 100 l .

All power delay profiles from a given track measurement were then linearly averaged together to create a local average power delay profile.

For the 2.5 GHz measurements, two PDPs are shown:

10l **Parallel Local Average PDP—**the local average power delay profile calculated from the *10 l Parallel Track Measurements*.

10l **Perpendicular Local Average PDP—**the local average power delay profile calculated from the *10 l Perpendicular Track Measurements*.

For the 60 GHz measurement, four PDPs are shown:

10l **Parallel Local Average PDP—**the local average power delay profile calculated from the *10 l Parallel Track Measurements*.

10l **Perpendicular Local Average PDP—**the local average power delay profile calculated from the *10 l Perpendicular Track Measurements*.

½ meter Parallel Local Average PDP—the local average power delay profile calculated from the *½ meter Parallel Track Measurements*.

½ meter Parallel Local Average PDP—the local average power delay profile calculated from the *½ meter Perpendicular Track Measurements*.

All PDPs for a given measurement location should roughly agree in overall shape and number of multipath components, within the limits introduced by noise, interference, and channel transients.

Finally, photographs of the transmitter and receiver setup at each measurement location are provided for reference.

B.1 2.5 GHz Power Delay Profiles

B.1.1 2.5 GHz Location 1 PDPs, 4th Floor Durham Hall, Virginia Tech

Receiver Location 1.1

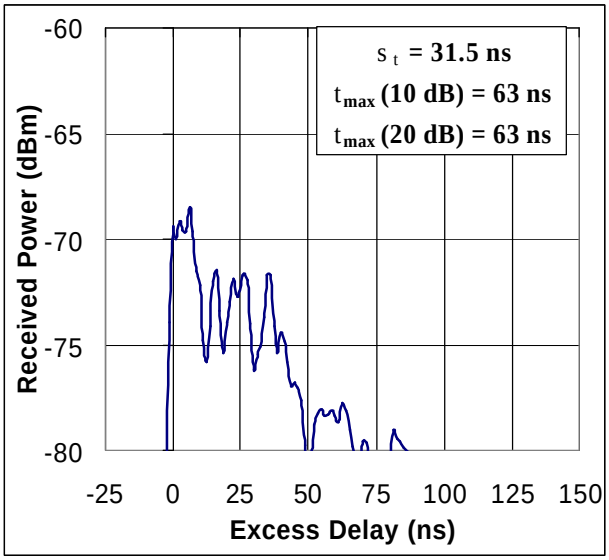

10l Parallel Local Average PDP

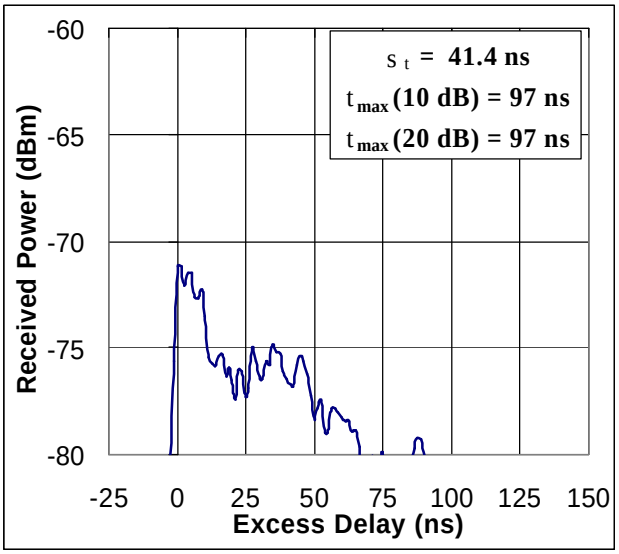

10l Perpendicular Local Average PDP

Figure B.1: 2.5 GHz Location 1.1 Power Delay Profiles

Receiver Location 1.2

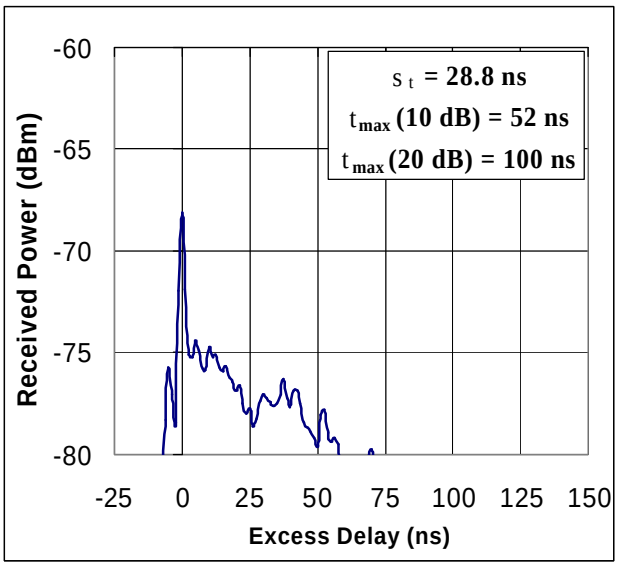

10l Parallel Local Average PDP

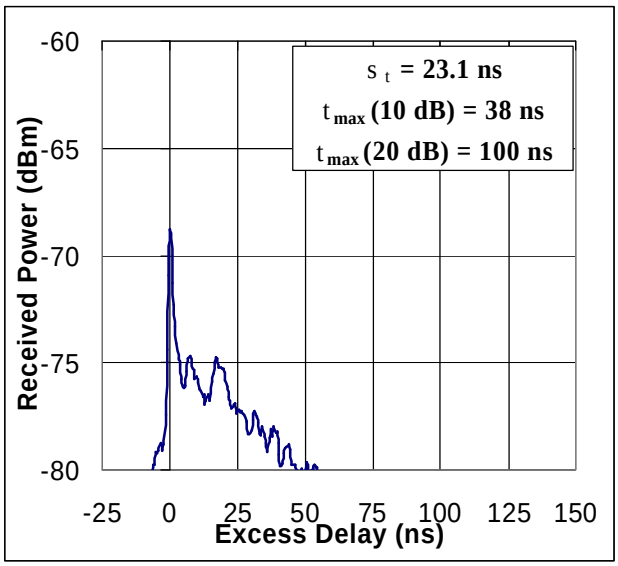

10l Perpendicular Local Average PDP

Figure B.2: 2.5 GHz Location 1.2 Power Delay Profiles

Receiver Location 1.3

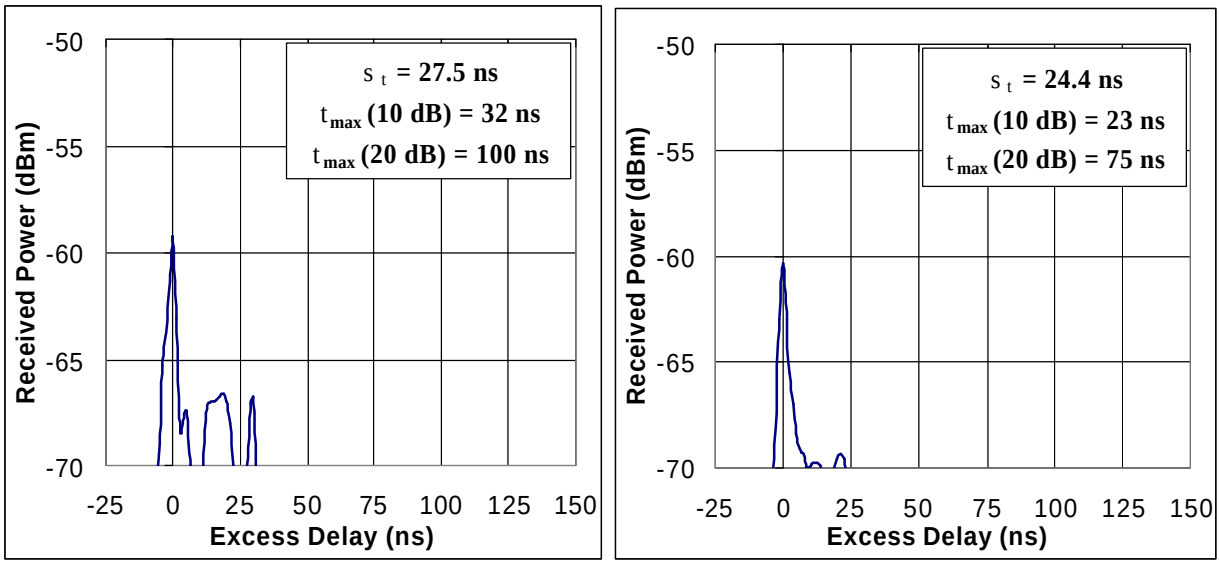

10° Parallel Local Average PDP **10° Perpendicular Local Average PDP**

Figure B.3: 2.5 GHz Location 1.3 Power Delay Profiles

Receiver Location 1.4

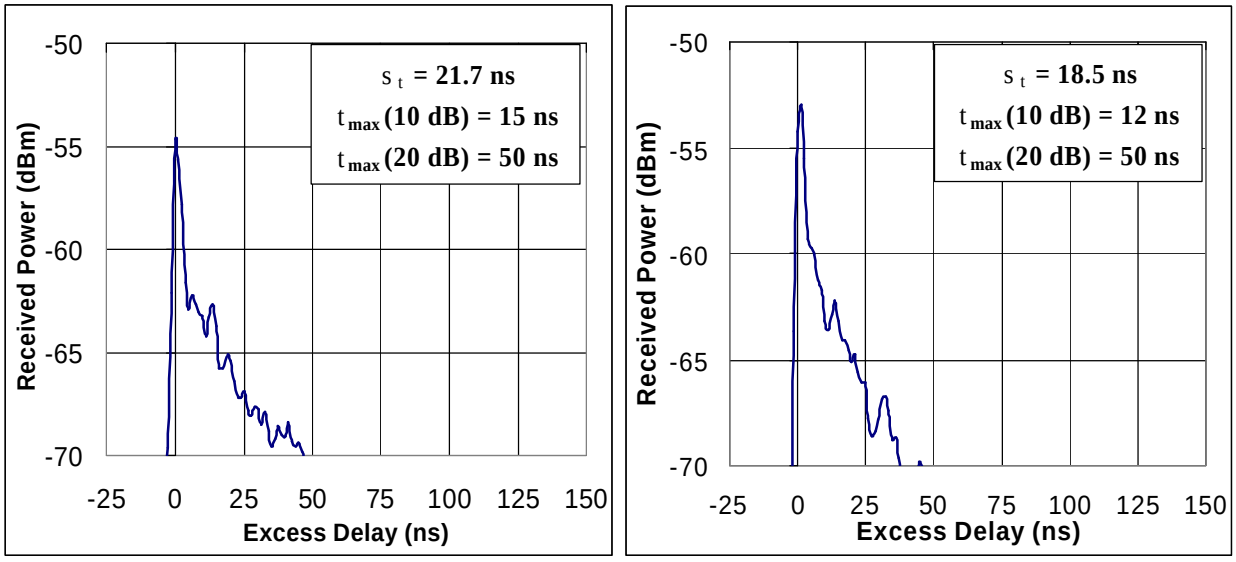

10° Parallel Local Average PDP **10° Perpendicular Local Average PDP**

Figure B.4: 2.5 GHz Location 1.4 Power Delay Profiles

B.1.2 2.5 GHz Location 2 PDPs, 4th Floor Durham Hall, Virginia Tech

Receiver Location 2.1

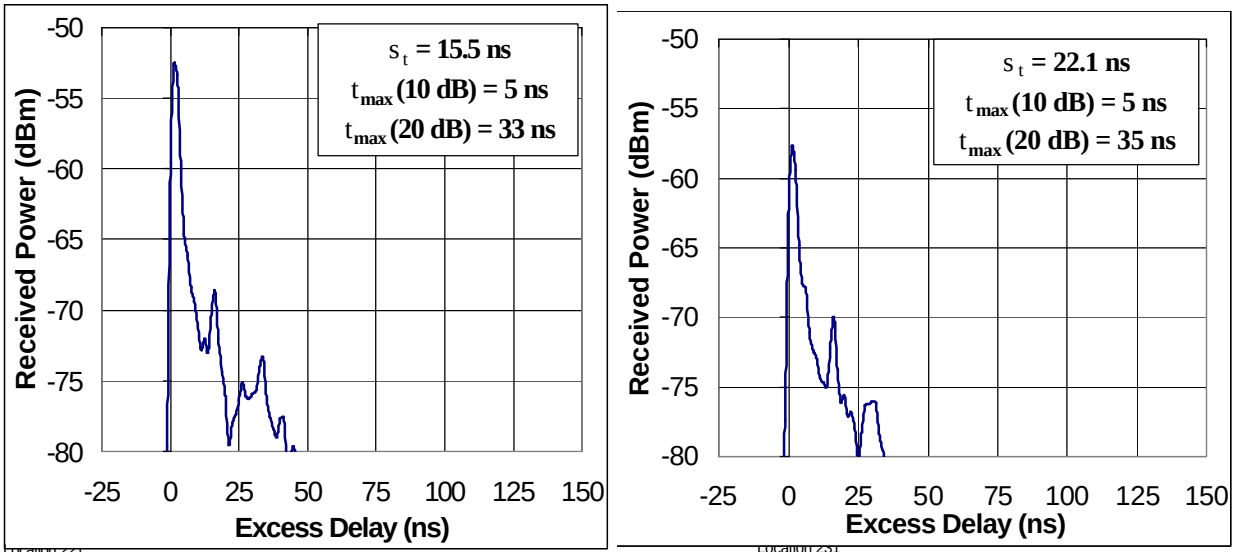

10l Parallel Local Average PDP 10l Perpendicular Local Average PDP

Figure B.5: 2.5 GHz Location 2.1 Power Delay Profiles

Receiver Location 2.2

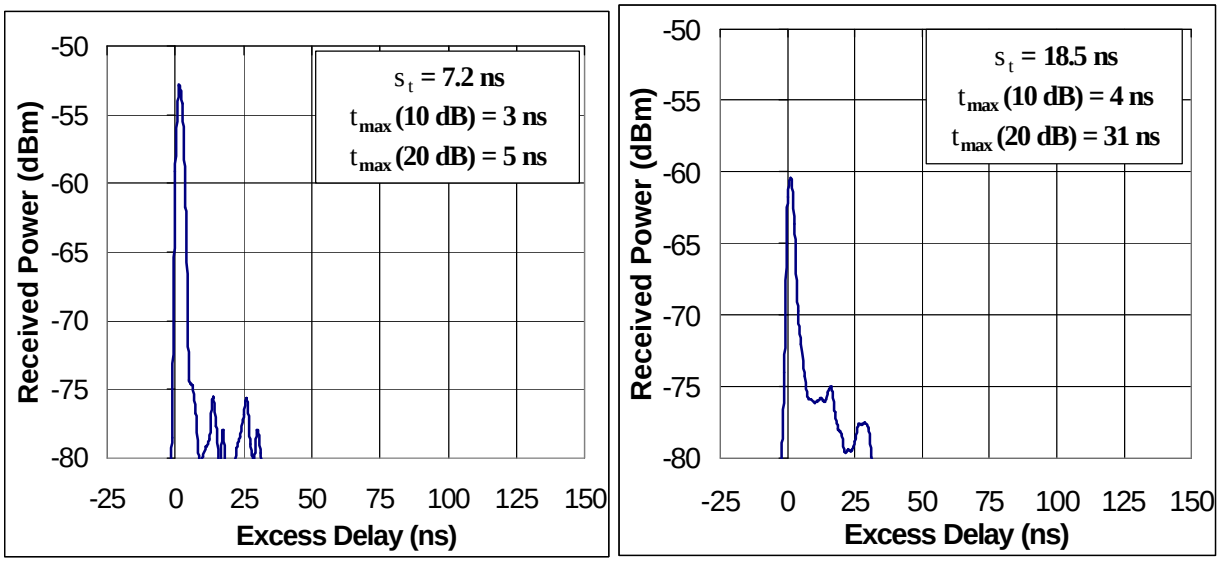

10l Parallel Local Average PDP 10l Perpendicular Local Average PDP

Figure B.6: 2.5 GHz Location 2.2 Power Delay Profiles

Receiver Location 2.3

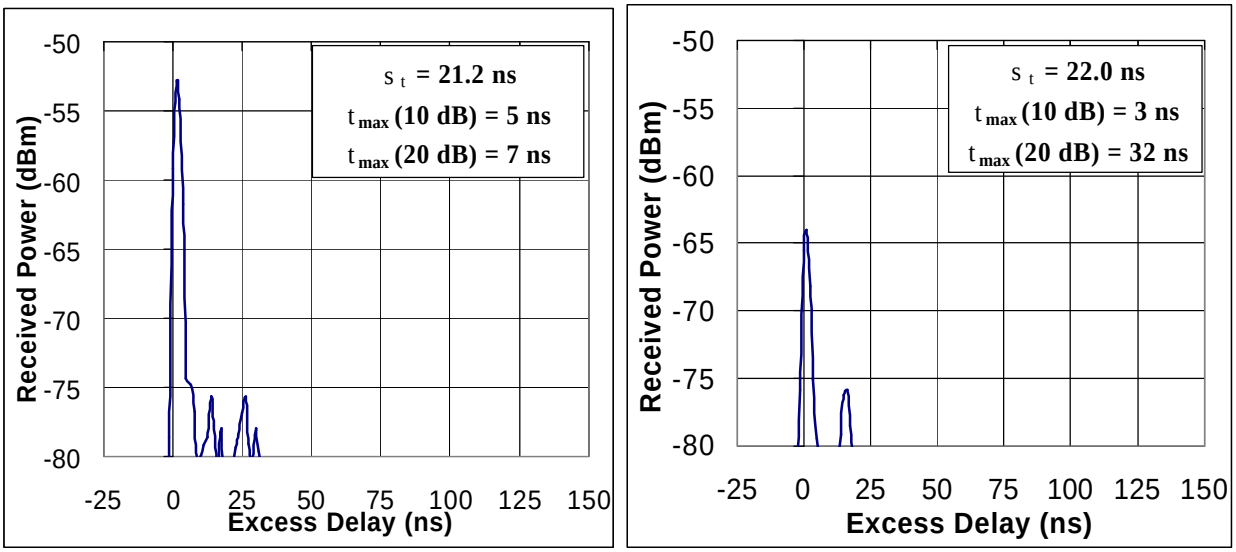

10° Parallel Local Average PDP **10° Perpendicular Local Average PDP**

Figure B.7: 2.5 GHz Location 2.3 Power Delay Profiles

B.1.3 2.5 GHz Location 3 PDPs, 4th Floor Durham Hall, Virginia Tech

Receiver Location 3.1

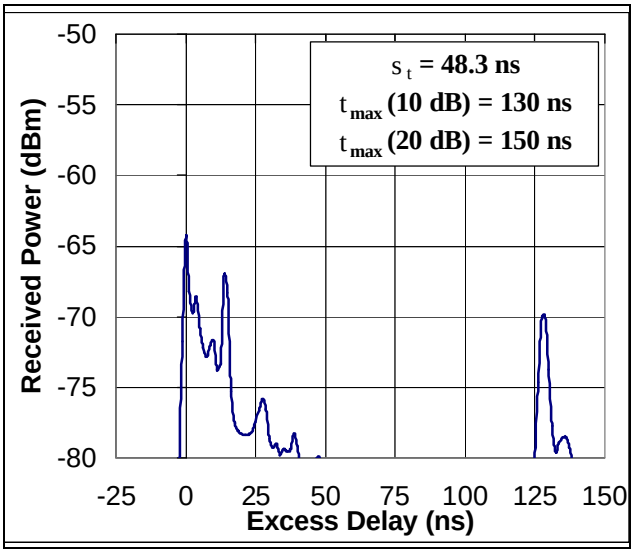

10l Parallel Local Average PDP

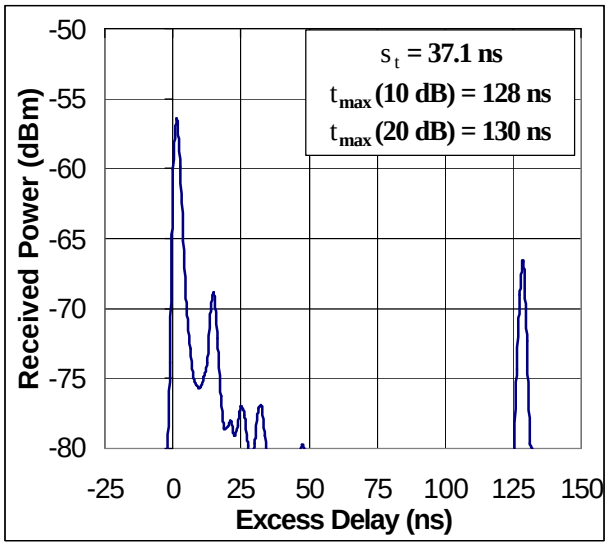

10l Perpendicular Local Average PDP

Figure B.8: 2.5 GHz Location 3.1 Power Delay Profiles

Receiver Location 3.2

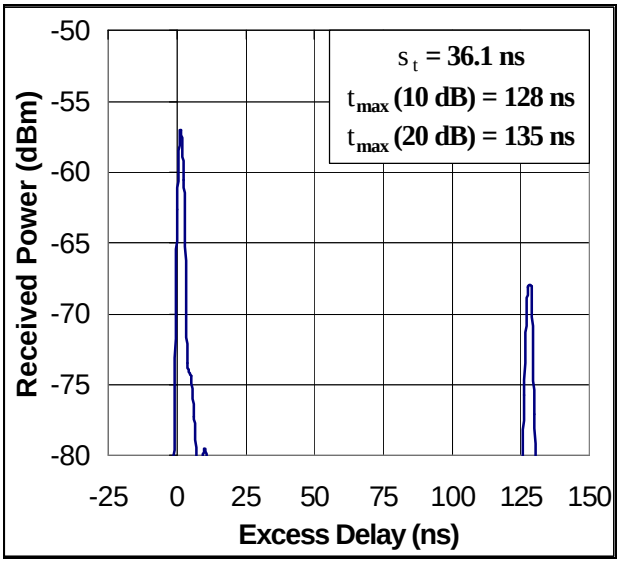

10l Parallel Local Average PDP

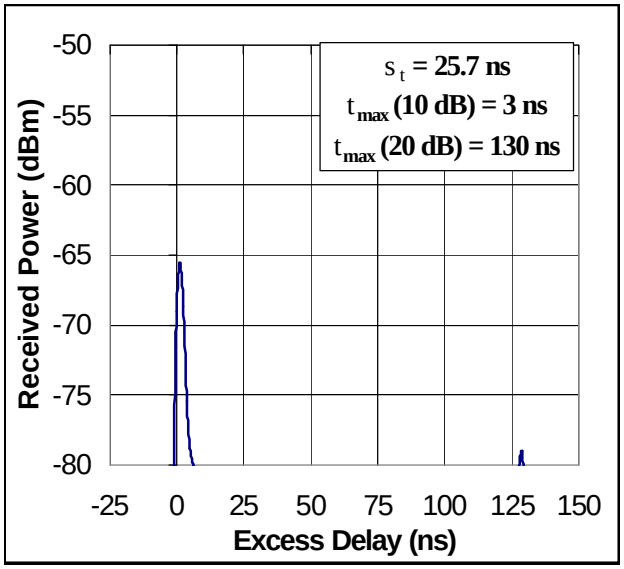

10l Perpendicular Local Average PDP

Figure B.9: 2.5 GHz Location 3.2 Power Delay Profiles

B.1.4 2.5 GHz Location 4 PDPs, 4th Floor Durham Hall, Virginia Tech

Receiver Location 4.1

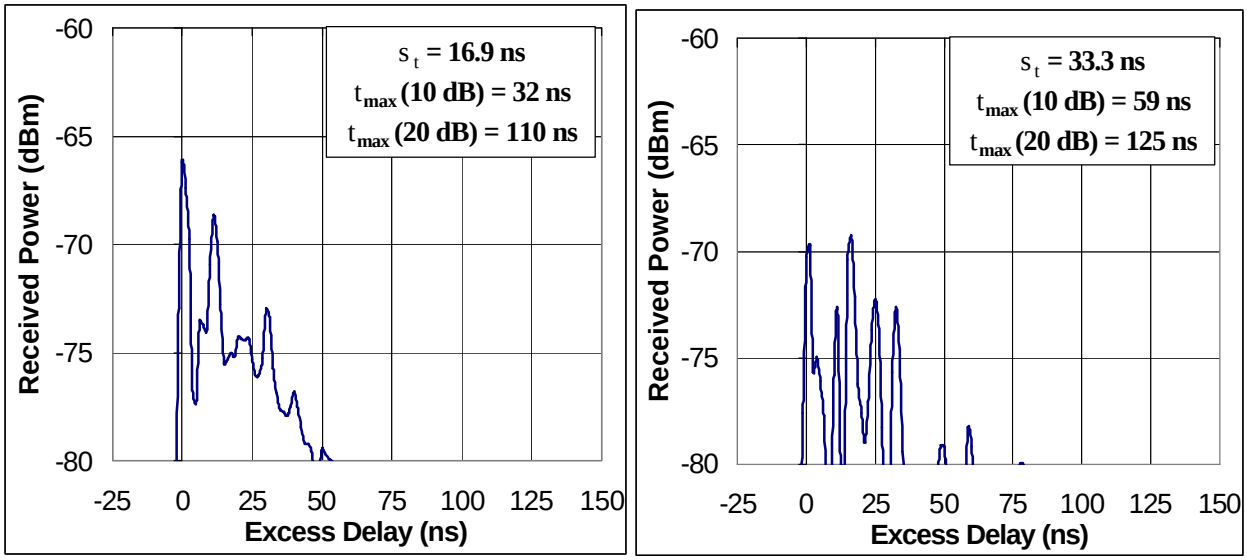

10° Parallel Local Average PDP 10° Perpendicular Local Average PDP

Figure B.10: 2.5 GHz Location 4.1 Power Delay Profiles

Receiver Location 4.2

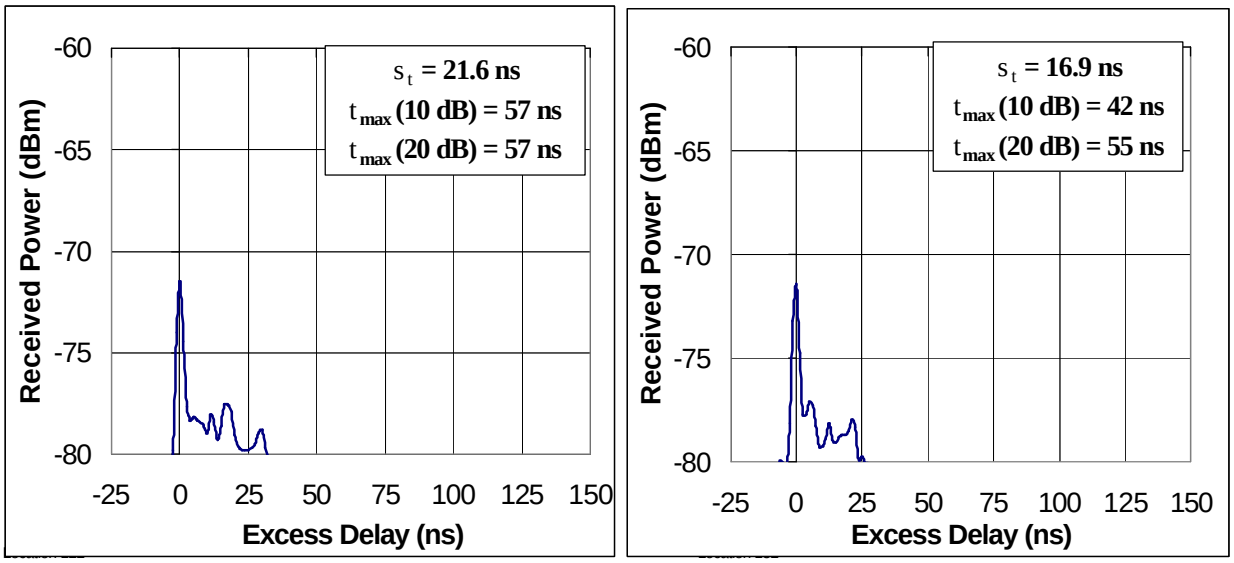

10° Parallel Local Average PDP 10° Perpendicular Local Average PDP

Figure B.11: 2.5 GHz Location 4.2 Power Delay Profiles

Receiver Location 4.3

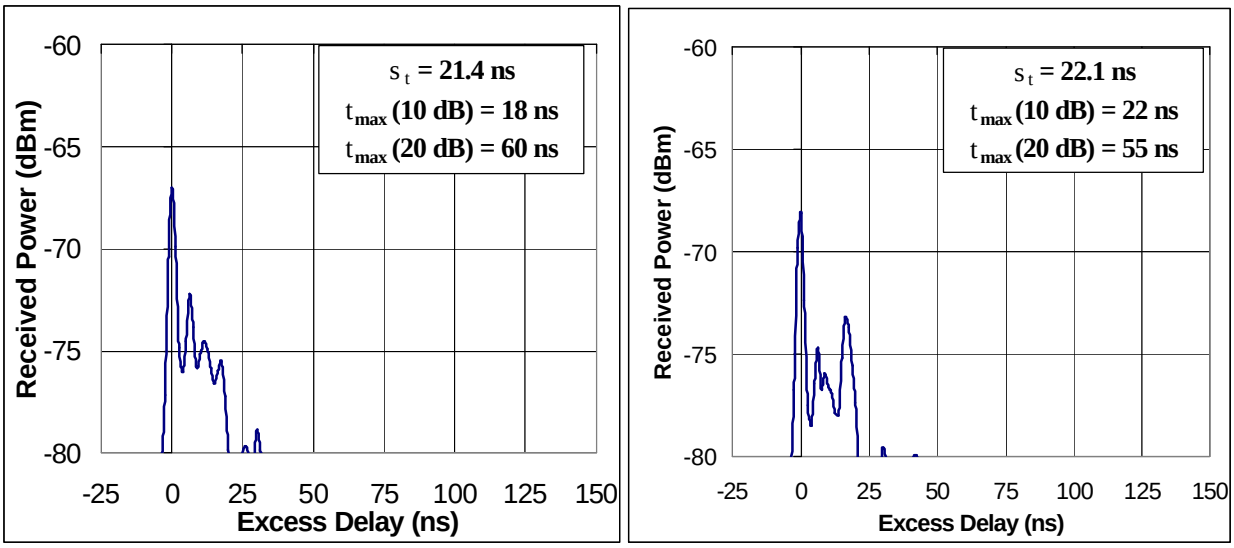

10° Parallel Local Average PDP **10° Perpendicular Local Average PDP**

Figure B.12: 2.5 GHz Location 4.3 Power Delay Profiles

Receiver Location 4.4

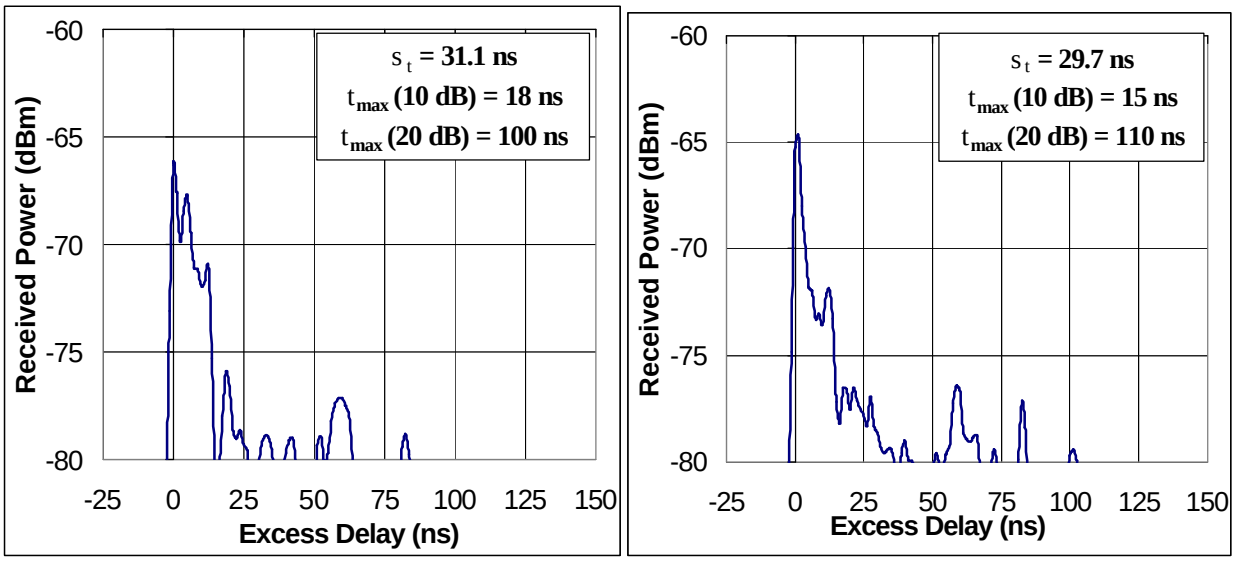

10° Parallel Local Average PDP **10° Perpendicular Local Average PDP**

Figure B.13: 2.5 GHz Location 4.4 Power Delay Profiles

B.1.5 2.5 GHz Location 5 PDPs, 4th Floor Durham Hall, Virginia Tech

Receiver Location 5.1

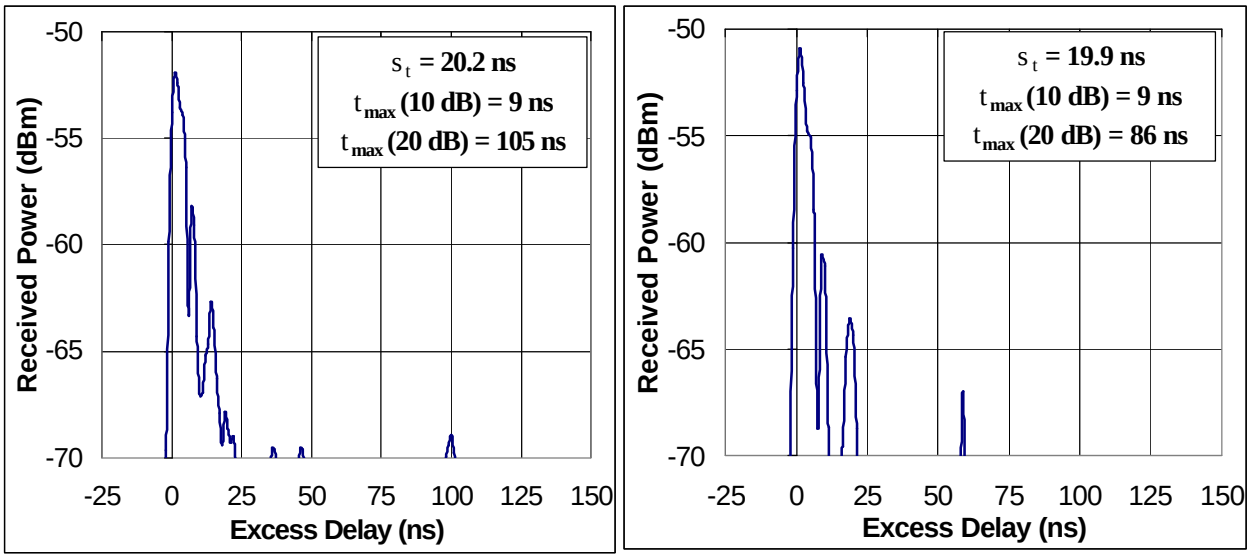

10l Parallel Local Average PDP 10l Perpendicular Local Average PDP

Figure B.14: 2.5 GHz Location 5.1 Power Delay Profiles

Receiver Location 5.2

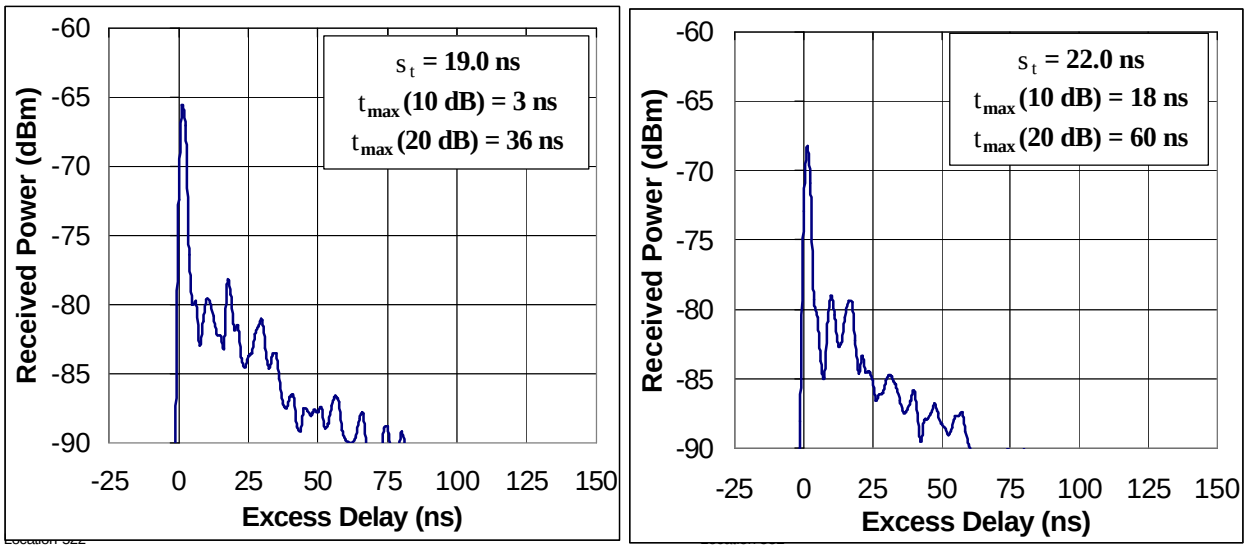

10l Parallel Local Average PDP 10l Perpendicular Local Average PDP

Figure B.15: 2.5 GHz Location 5.2 Power Delay Profiles

Receiver Location 5.3

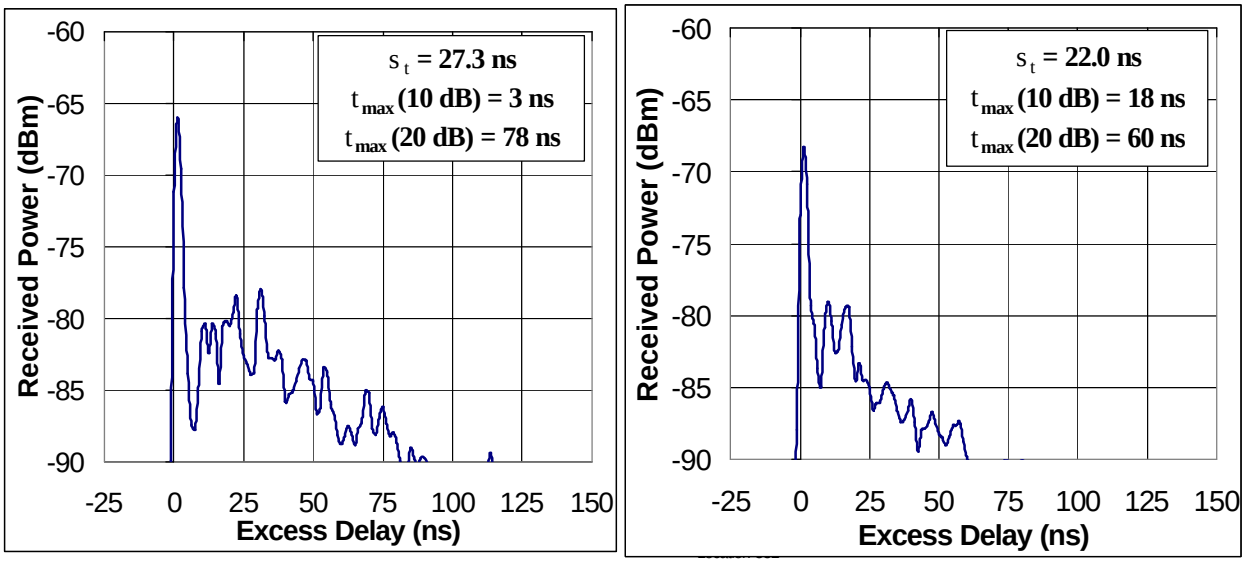

10l Parallel Local Average PDP 10l Perpendicular Local Average PDP

Figure B.16: 2.5 GHz Location 5.3 Power Delay Profiles

Receiver Location 5.4

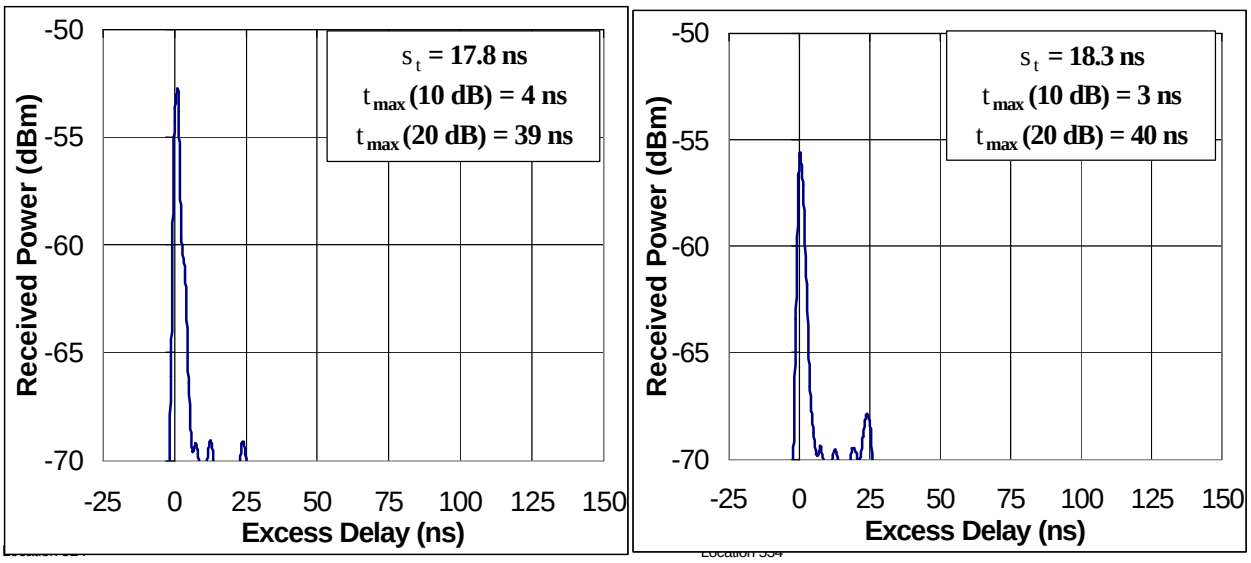

10l Parallel Local Average PDP 10l Perpendicular Local Average PDP

Figure B.17: 2.5 GHz Location 5.4 Power Delay Profiles

B.1.6 2.5 GHz Location 6 PDPs, 4th Floor Durham Hall, Virginia Tech

Receiver Location 6.1

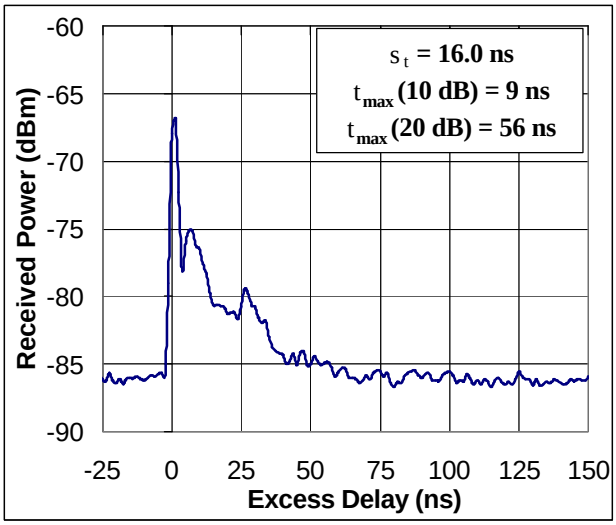

10l Parallel Local Average PDP

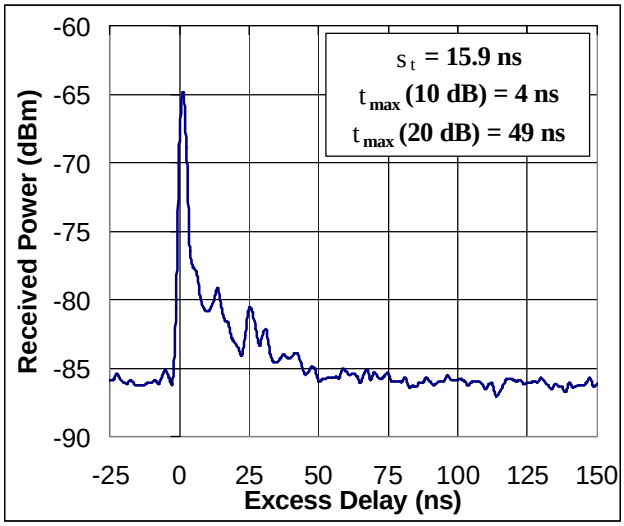

10l Perpendicular Local Average PDP

Figure B.18: 2.5 GHz Location 6.1 Power Delay Profiles

Receiver Location 6.2

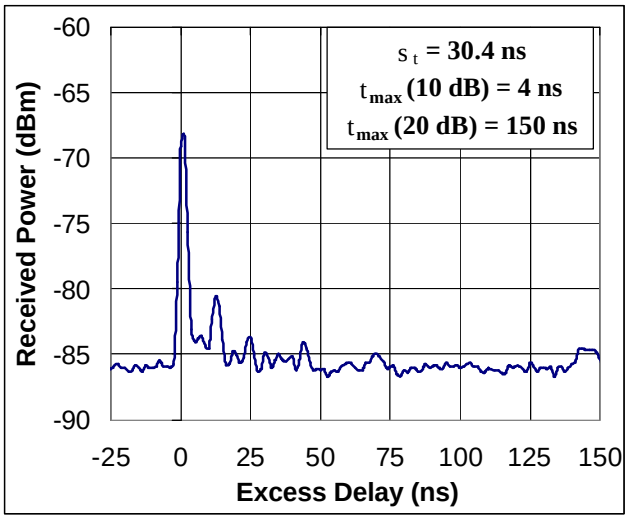

10l Parallel Local Average PDP

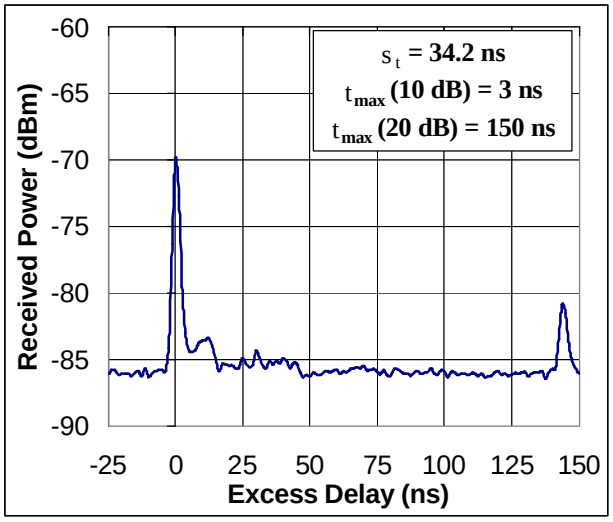

10l Perpendicular Local Average PDP

Figure B.19: 2.5 GHz Location 6.2 Power Delay Profiles

B.1.7 2.5 GHz Location 7 PDPs, 4th Floor Durham Hall, Virginia Tech

Receiver Location 7.1

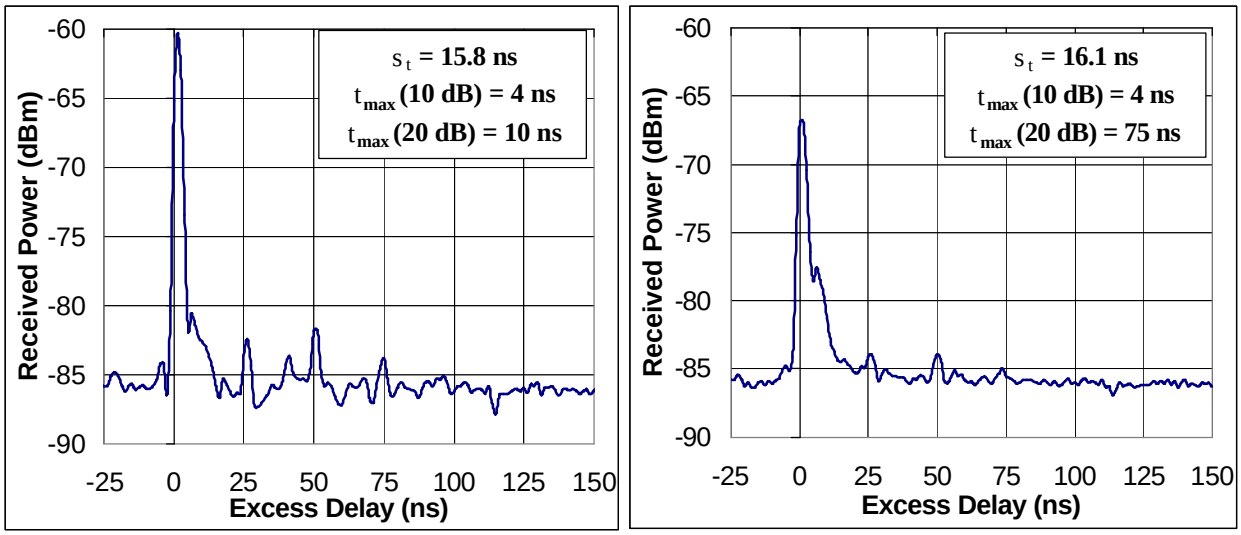

10l Parallel Local Average PDP 10l Perpendicular Local Average PDP

Figure B.20: 2.5 GHz Location 7.1 Power Delay Profiles

Receiver Location 7.2

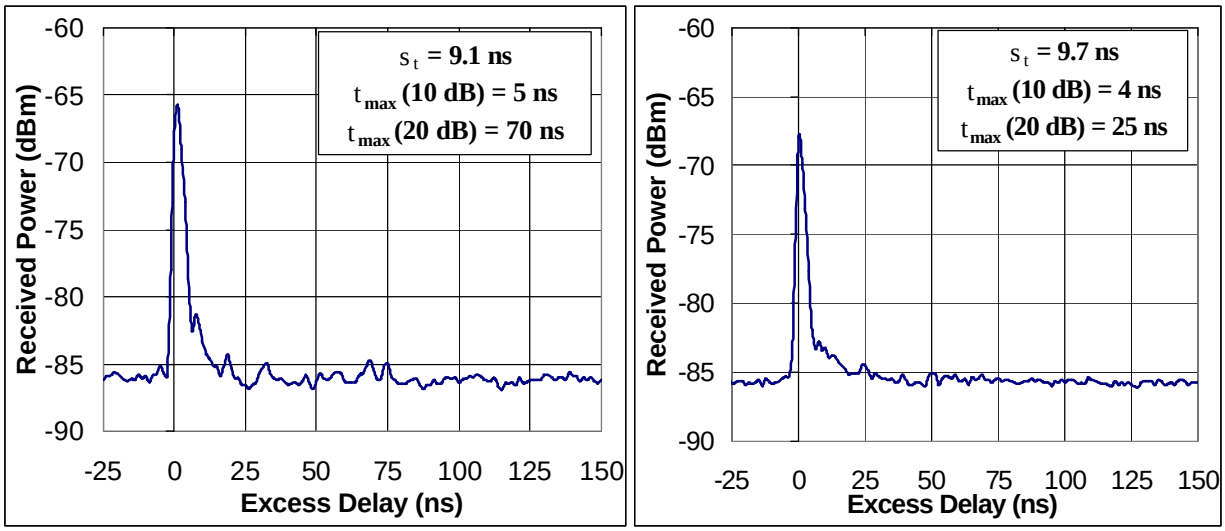

10l Parallel Local Average PDP 10l Perpendicular Local Average PDP

Figure B.21: 2.5 GHz Location 7.2 Power Delay Profiles

B.1.8 2.5 GHz Location 8 PDPs, 4th Floor Durham Hall, Virginia Tech Receiver Location 8.1

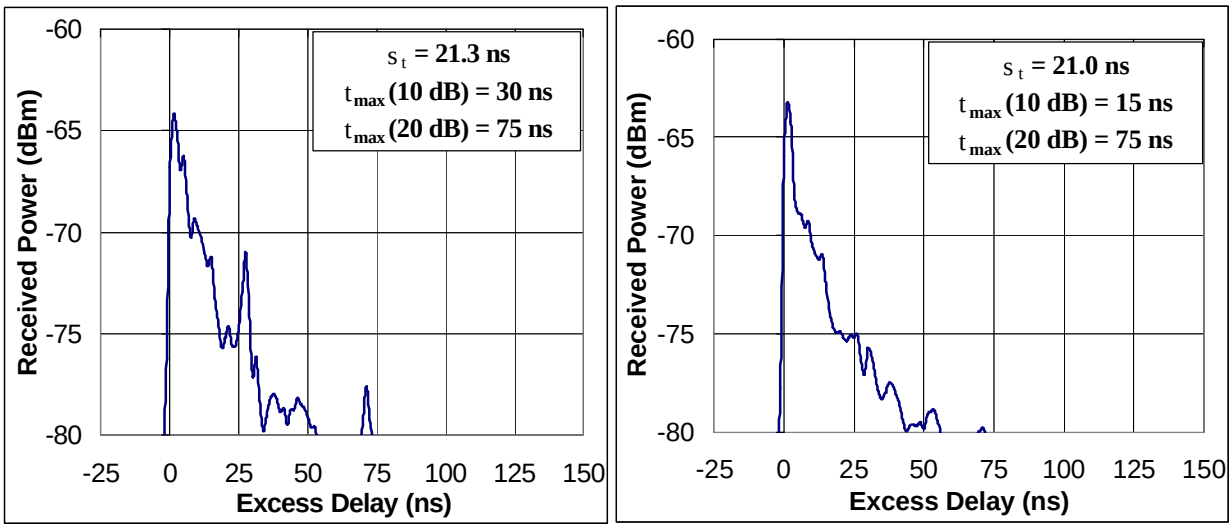

10° Parallel Local Average PDP **10° Perpendicular Local Average PDP**

Figure B.22: 2.5 GHz Location 8.1 Power Delay Profiles

B.2 60 GHz Power Delay Profiles

B.2.1 60 GHz Location 1 PDPs, 4th Floor Durham Hall, Virginia Tech Receiver Location 1.1

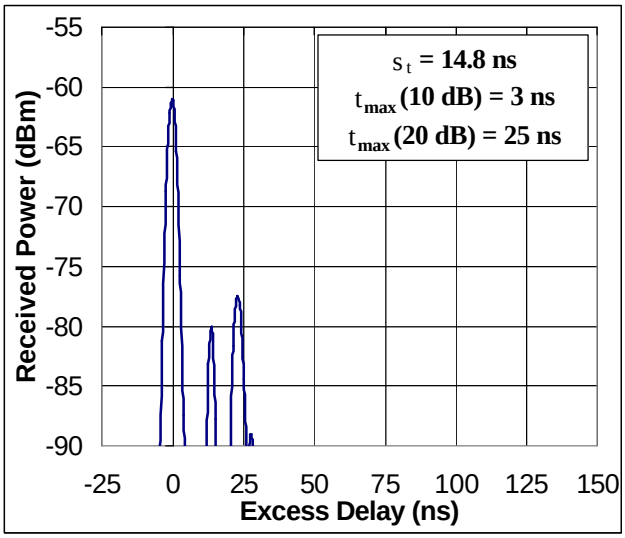

10° Parallel Local Average PDP

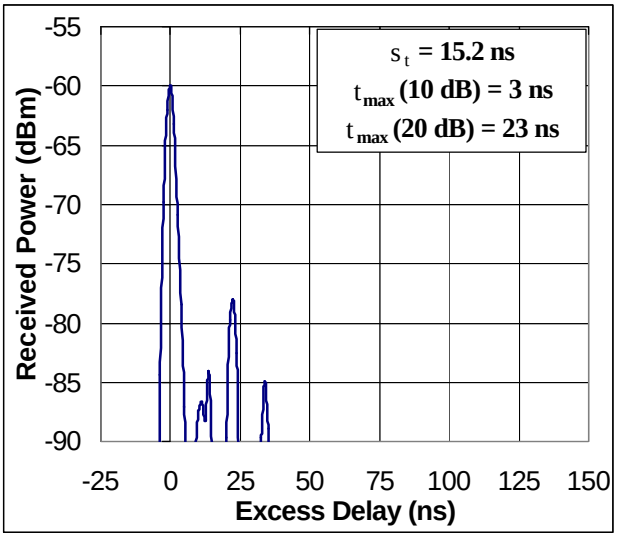

10° Perpendicular Local Average PDP

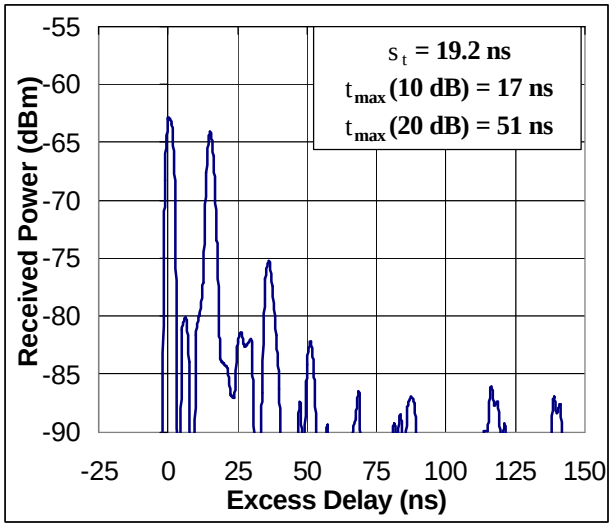

½ meter Track Parallel Local Average PDP

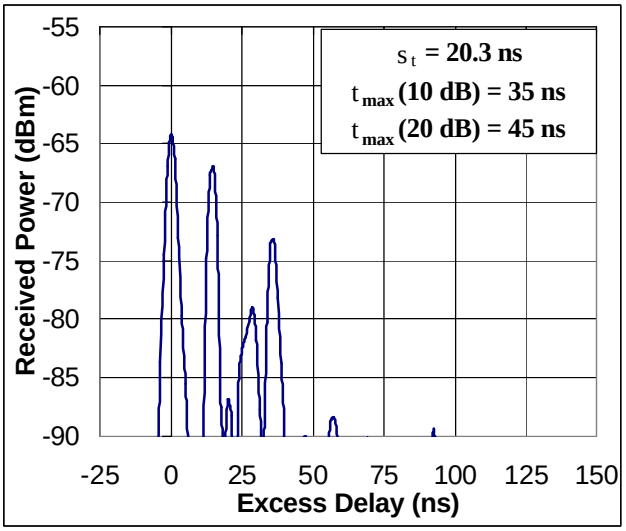

½ meter Track Perpendicular Local Average PDP

Figure B.23: 60 GHz Location 1.1 Power Delay Profiles

Receiver Location 1.2

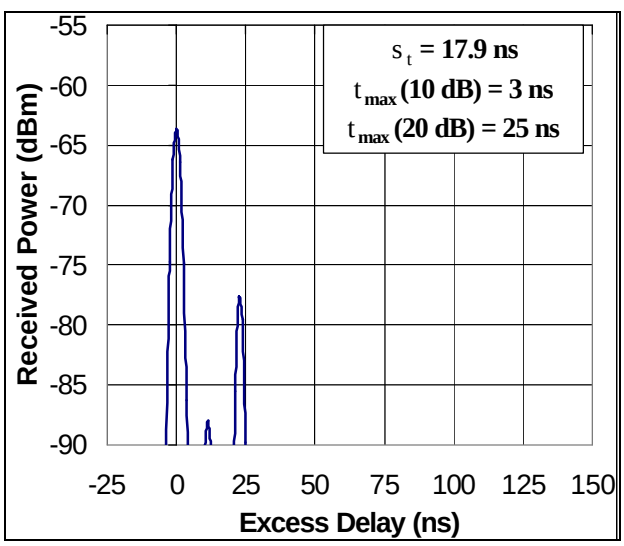

10° Parallel Local Average PDP

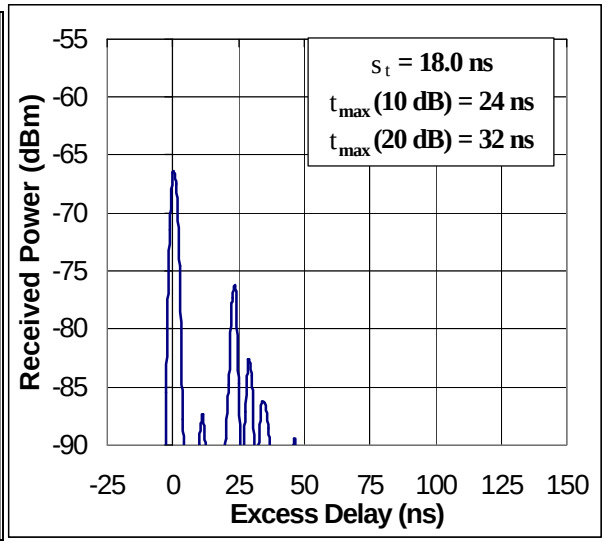

10° Perpendicular Local Average PDP

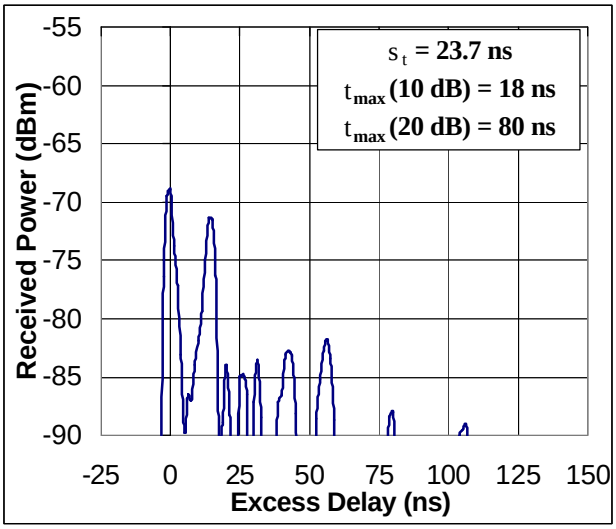

½ meter Track Parallel Local Average PDP

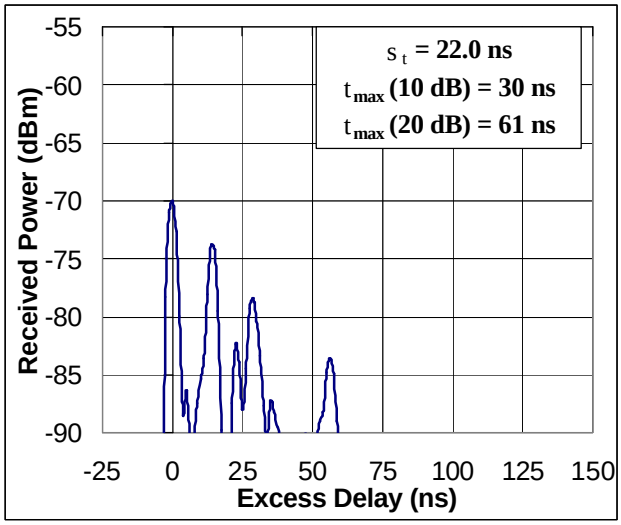

½ meter Track Perpendicular Local Average PDP

Figure B.24: 60 GHz Location 1.2 Power Delay Profiles

Receiver Location 1.3

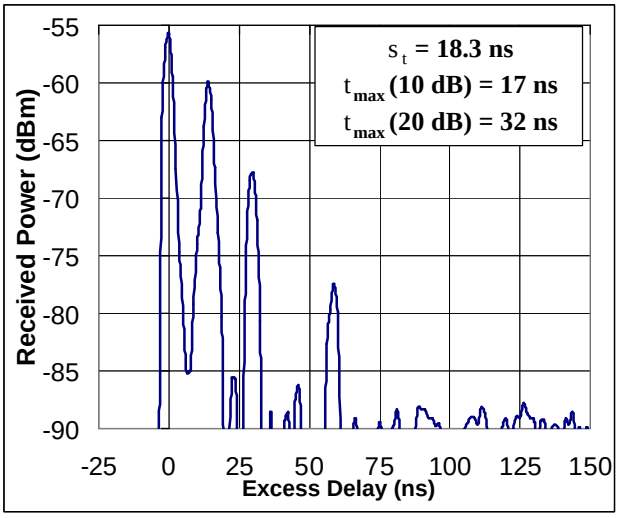

10° Parallel Local Average PDP

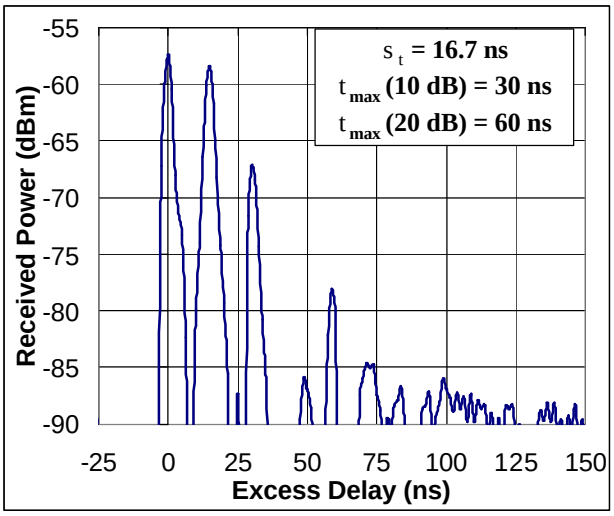

10° Perpendicular Local Average PDP

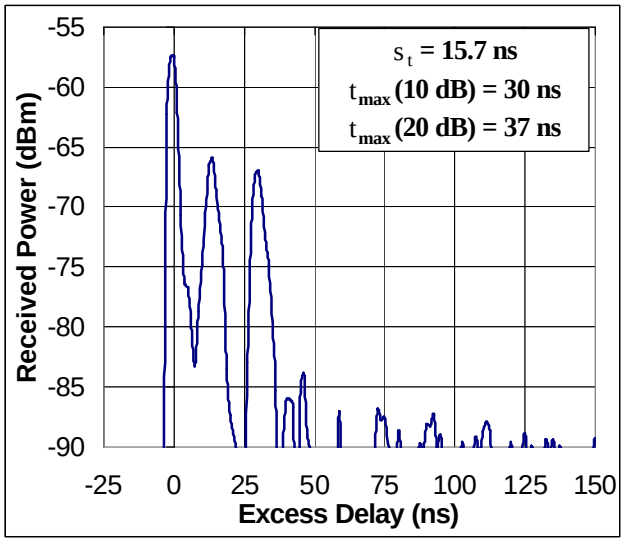

½ meter Track Parallel Local Average PDP

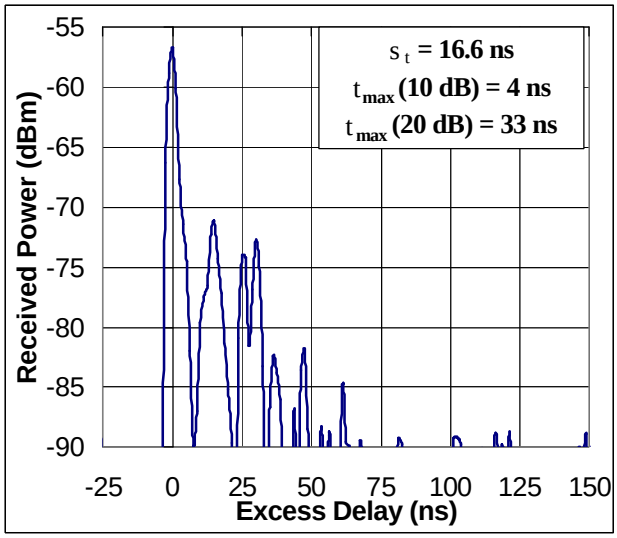

½ meter Track Perpendicular Local Average PDP

Figure B.25: 60 GHz Location 1.3 Power Delay Profiles

Receiver Location 1.4

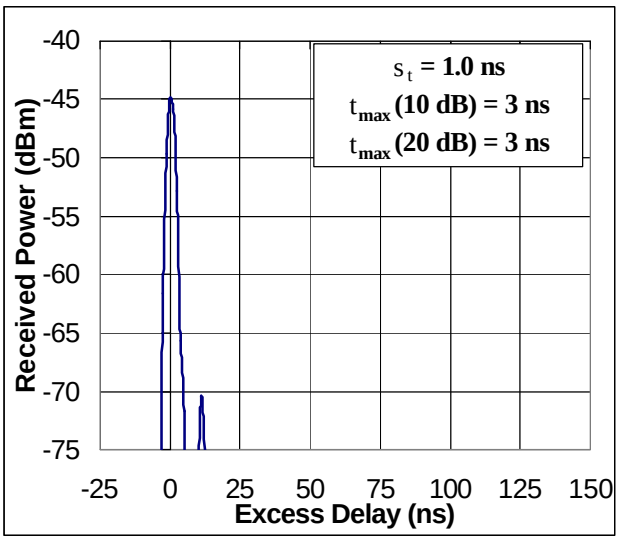

10° Parallel Local Average PDP

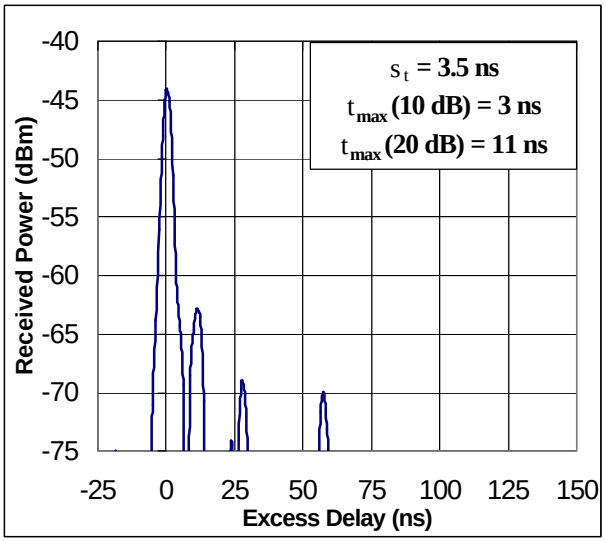

10° Perpendicular Local Average PDP

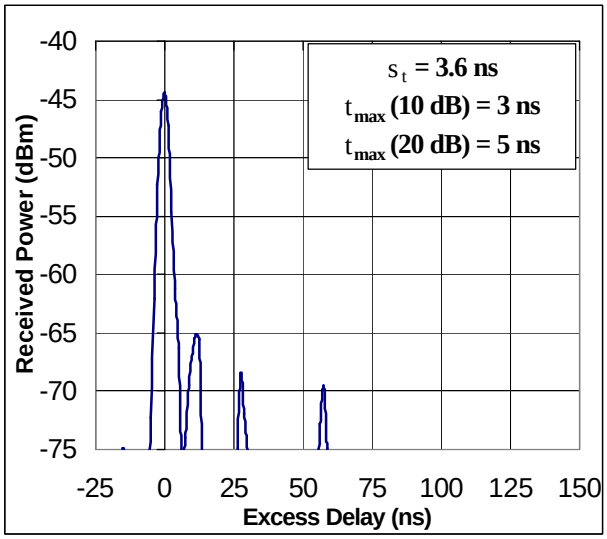

½ meter Track Parallel Local Average PDP

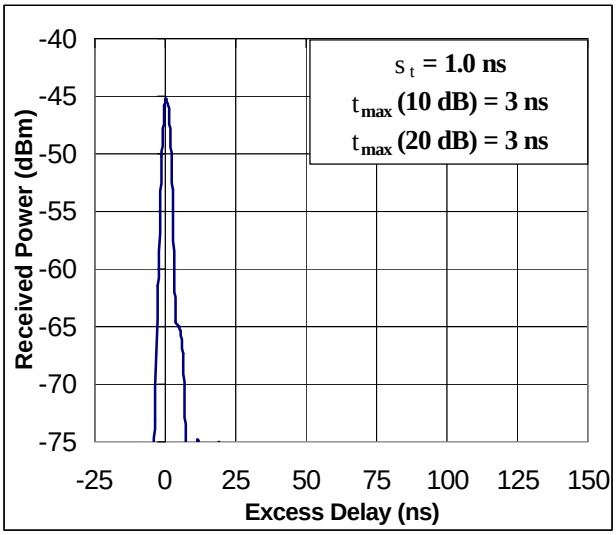

½ meter Track Perpendicular Local Average PDP

Figure B.26: 60 GHz Location 1.4 Power Delay Profiles

B.2.2 60 GHz Location 2 PDPs, 4th Floor Durham Hall, Virginia Tech

Receiver Location 2.1

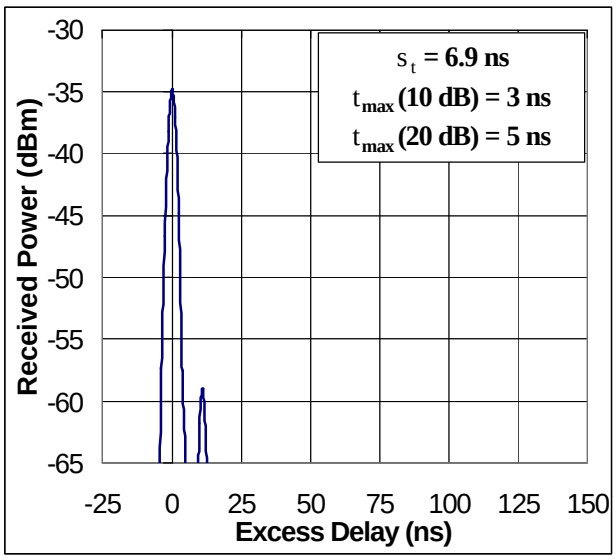

10° Parallel Local Average PDP

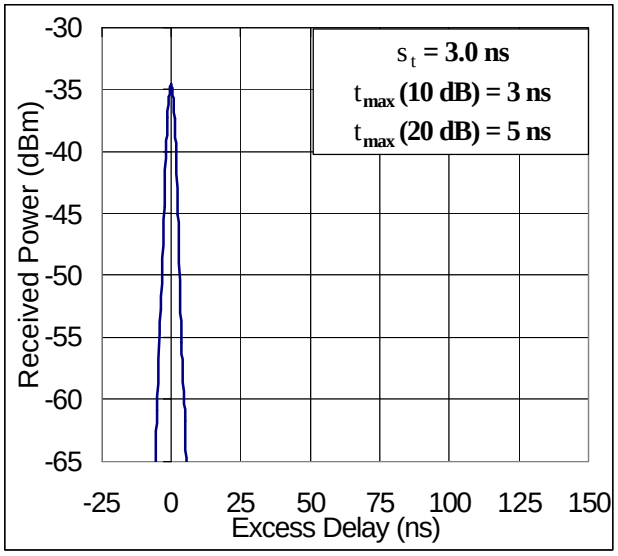

10° Perpendicular Local Average PDP

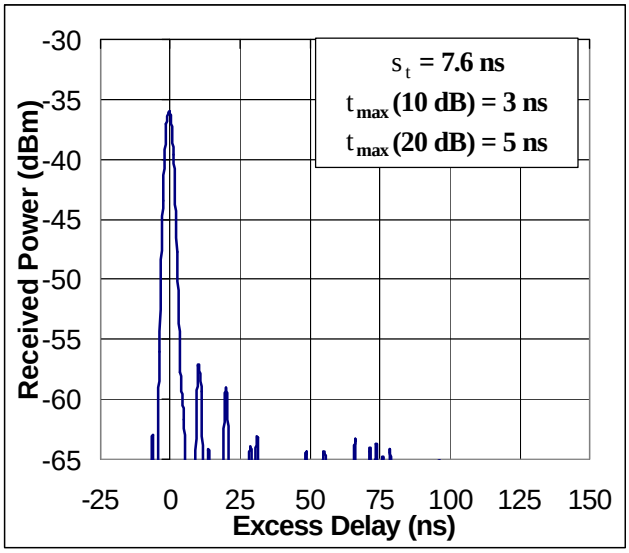

½ meter Track Parallel Local Average PDP

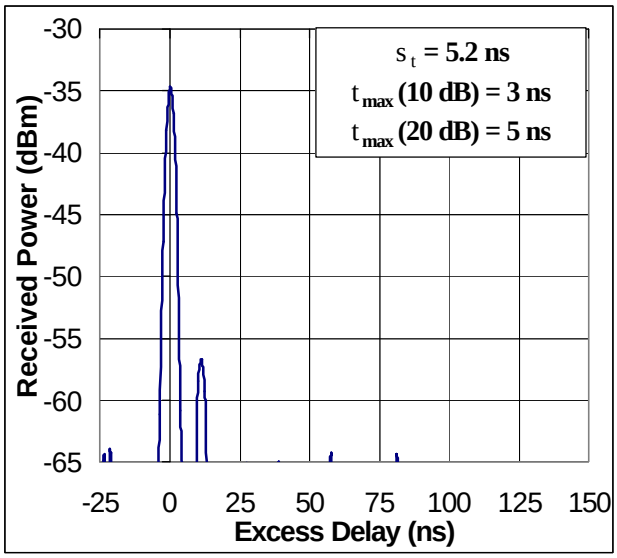

½ meter Track Perpendicular Local Average PDP

Figure B.27: 60 GHz Location 2.1 Power Delay Profiles

Receiver Location 2.2

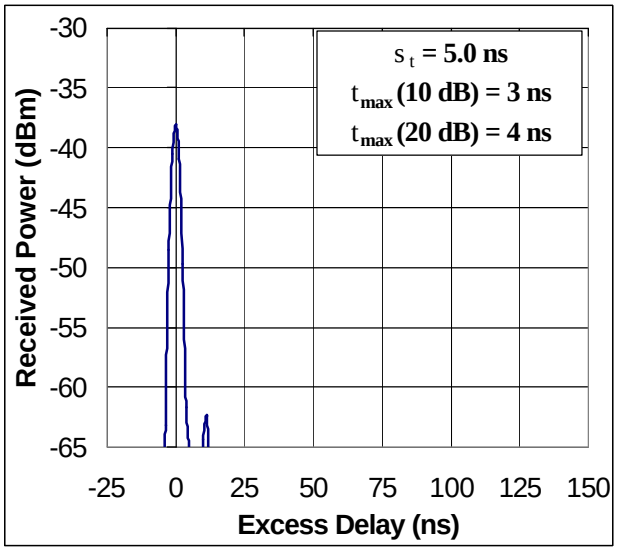

10° Parallel Local Average PDP

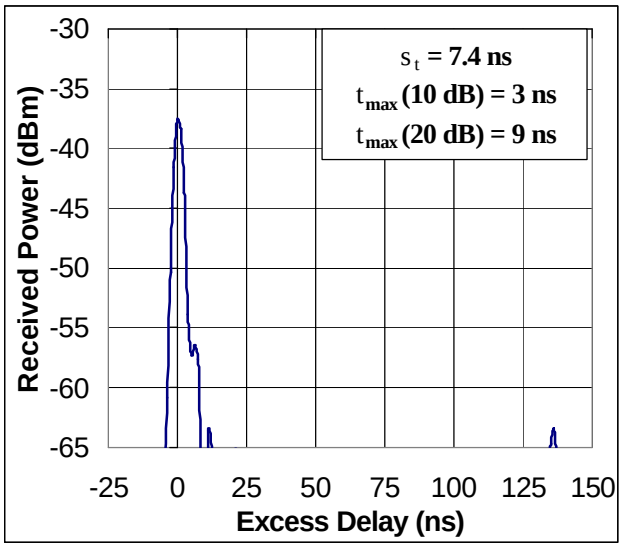

10° Perpendicular Local Average PDP

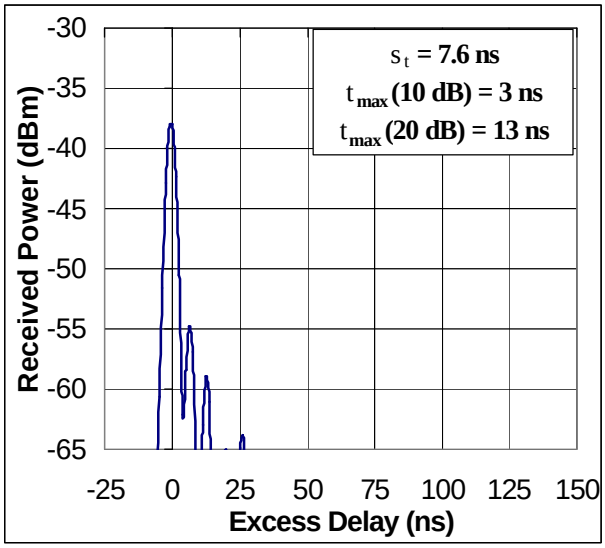

½ meter Track Parallel Local Average PDP

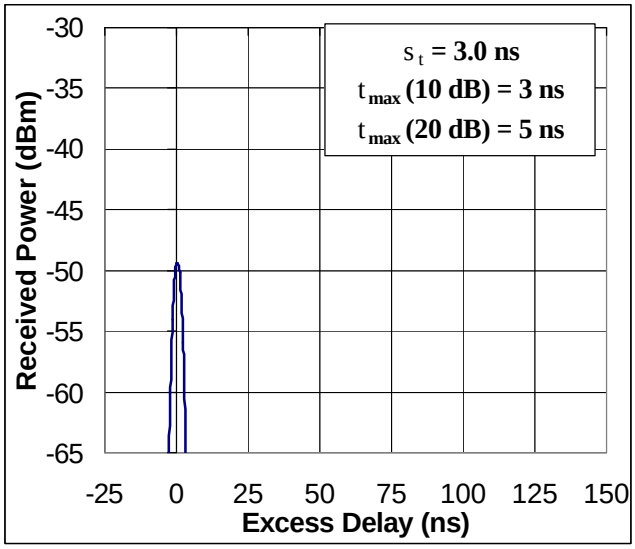

½ meter Track Perpendicular Local Average PDP

Figure B.28: 60 GHz Location 2.2 Power Delay Profiles

Receiver Location 2.3

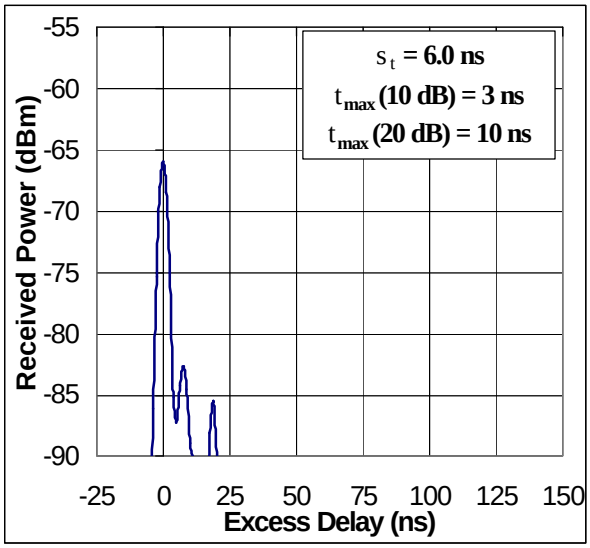

10l Parallel Local Average PDP

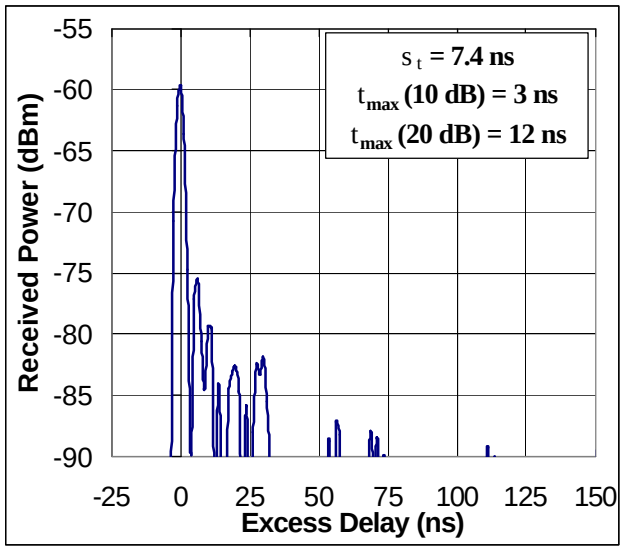

10l Perpendicular Local Average PDP

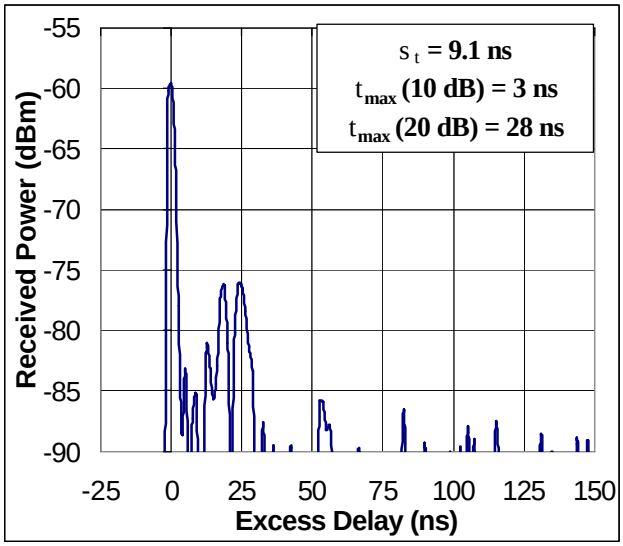

½ meter Track Parallel Local Average PDP

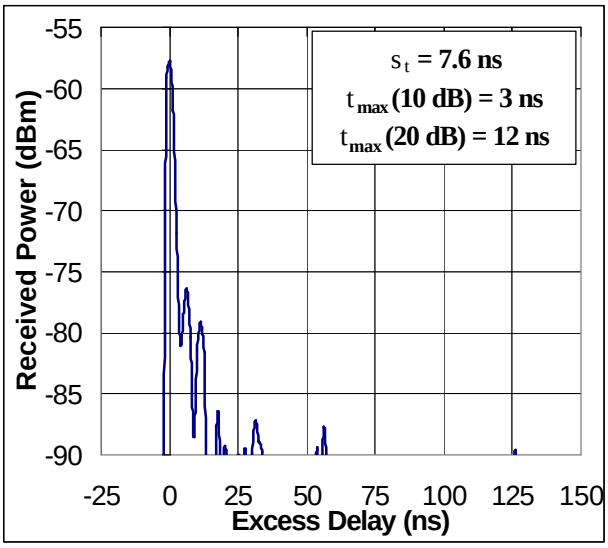

½ meter Track Perpendicular Local Average PDP

Figure B.29: 60 GHz Location 2.3 Power Delay Profiles

B.2.3 60 GHz Location 3 PDPs, 4th Floor Durham Hall, Virginia Tech

Receiver Location 3.1

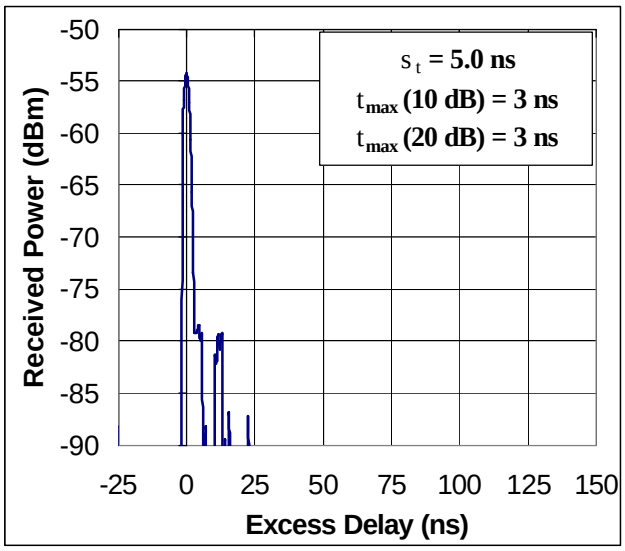

10λ Parallel Local Average PDP

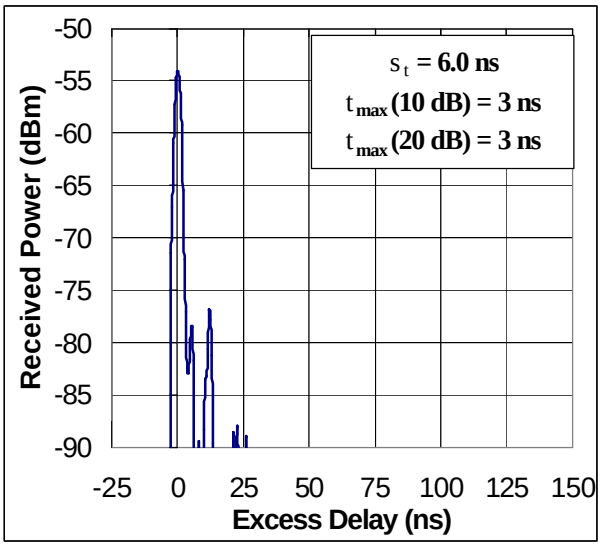

10λ Perpendicular Local Average PDP

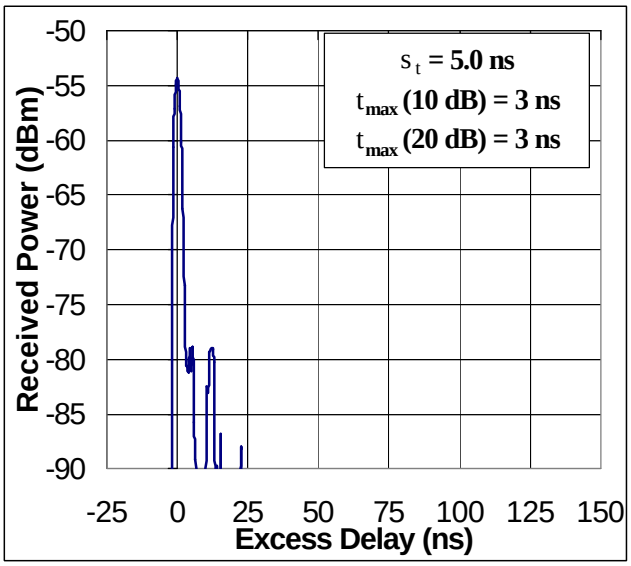

½ meter Track Parallel Local Average PDP

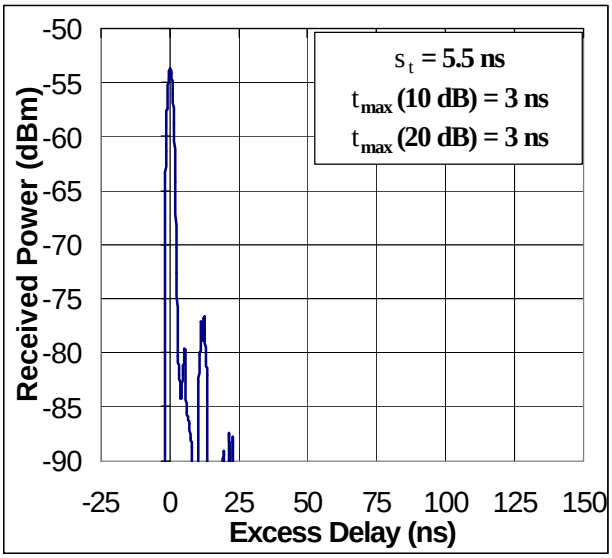

½ meter Track Perpendicular Local Average PDP

Figure B.30: 60 GHz Location 3.1 Power Delay Profiles

Receiver Location 3.2

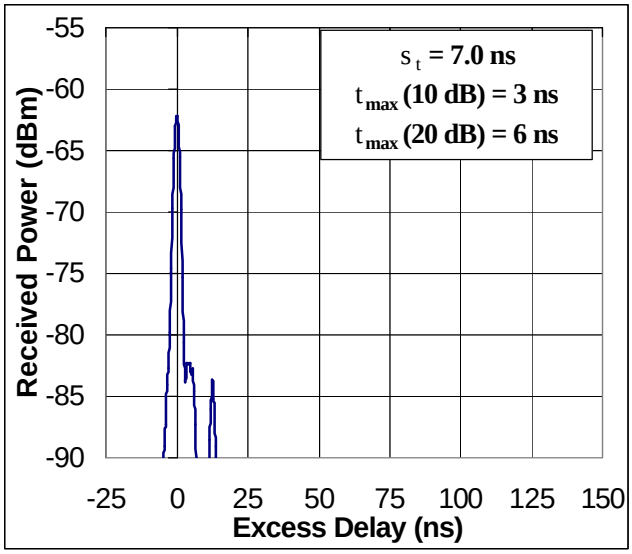

10° Parallel Local Average PDP

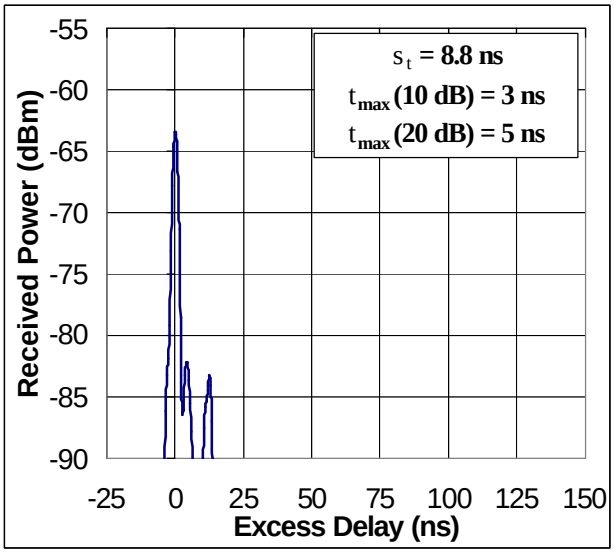

10° Perpendicular Local Average PDP

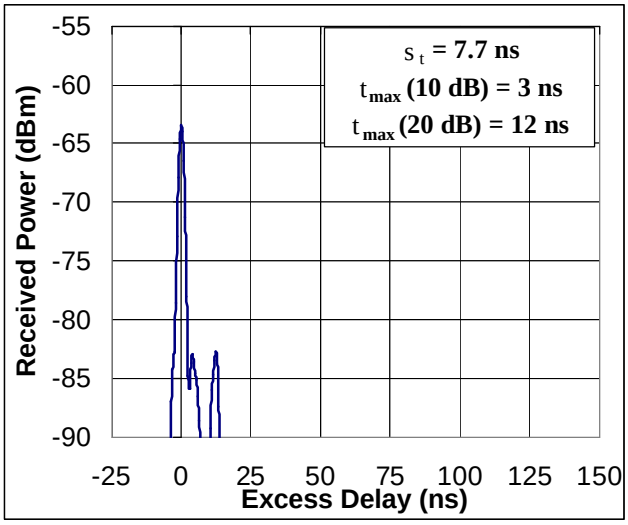

½ meter Track Parallel Local Average PDP

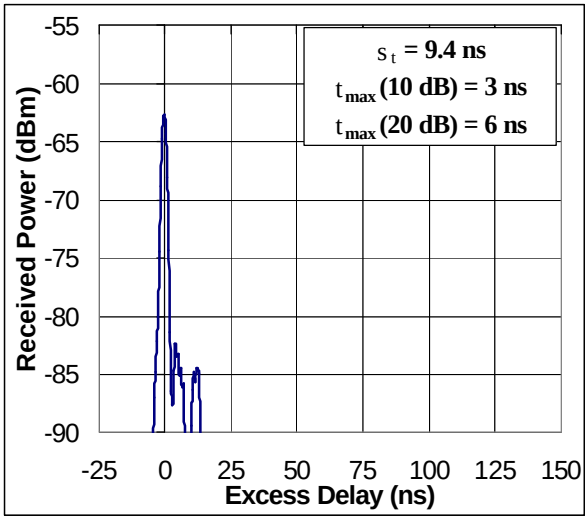

½ meter Track Perpendicular Local Average PDP

Figure B.31: 60 GHz Location 3.2 Power Delay Profiles

B.2.4 60 GHz Location 4 PDPs, 4th Floor Durham Hall, Virginia Tech

Receiver Location 4.1

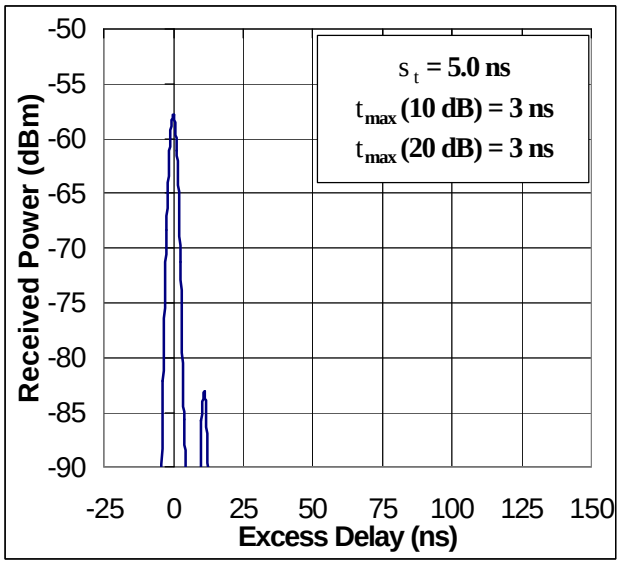

10l Parallel Local Average PDP

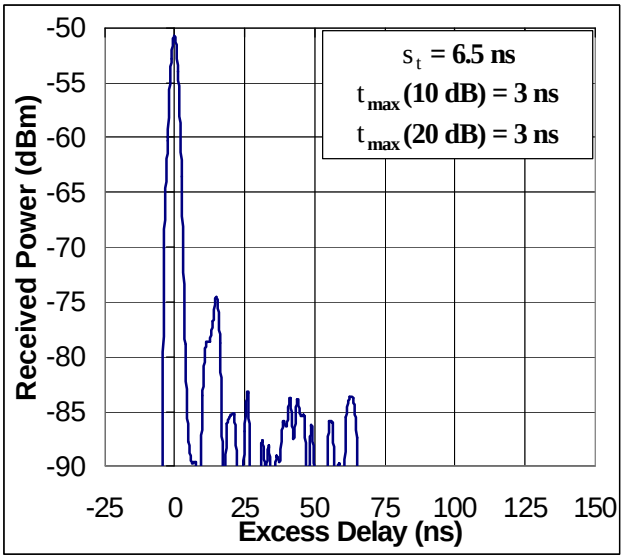

10l Perpendicular Local Average PDP

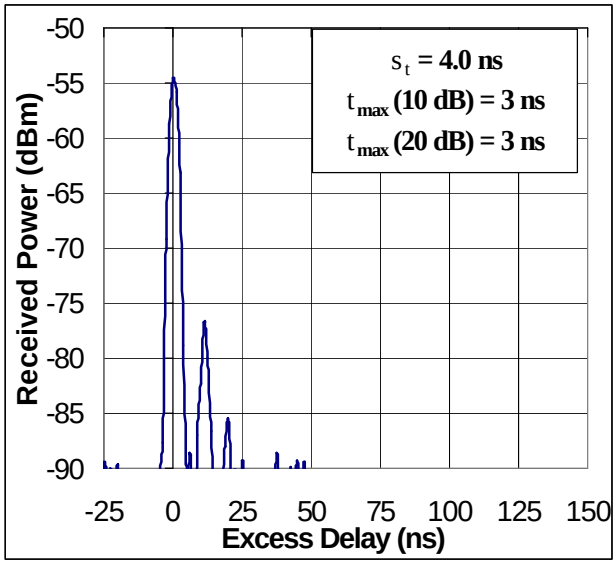

½ meter Track Parallel Local Average PDP

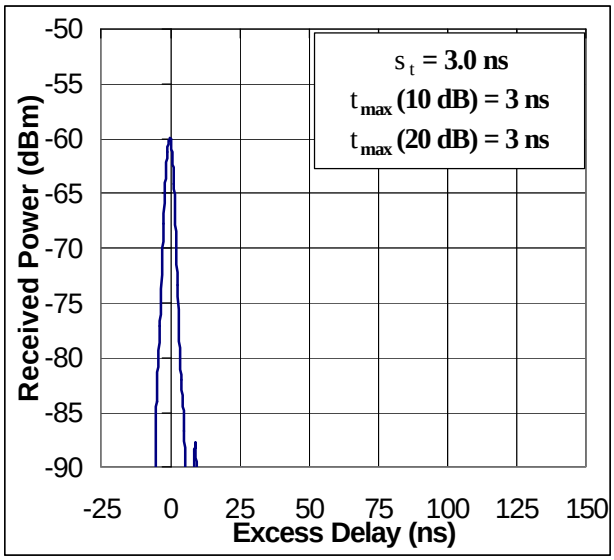

½ meter Track Perpendicular Local Average PDP

Figure B.32: 60 GHz Location 4.1 Power Delay Profiles

Receiver Location 4.2

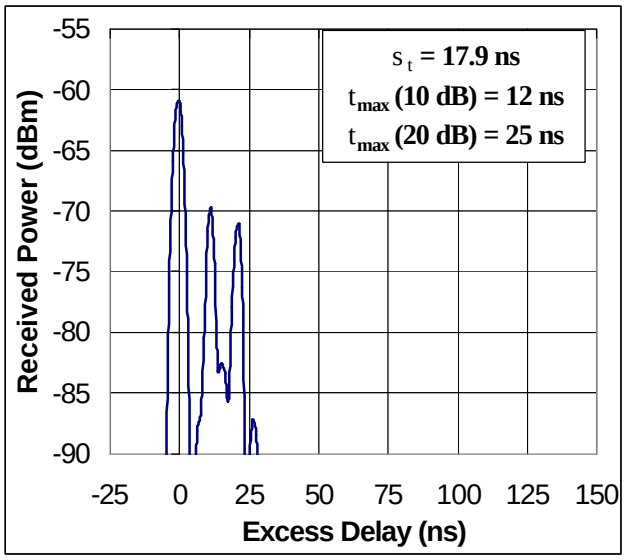

10° Parallel Local Average PDP

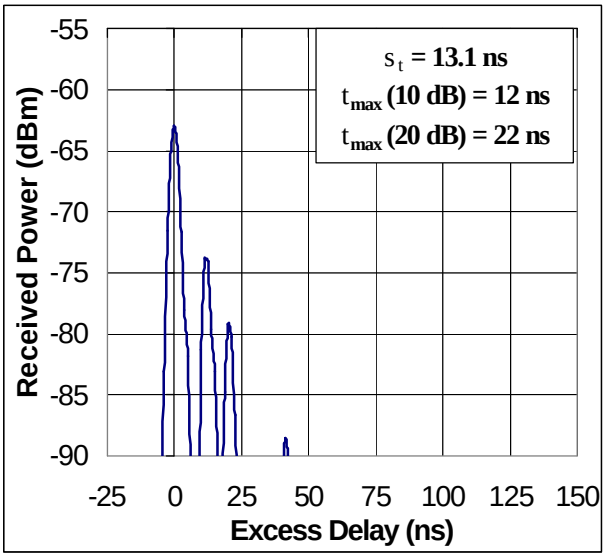

10° Perpendicular Local Average PDP

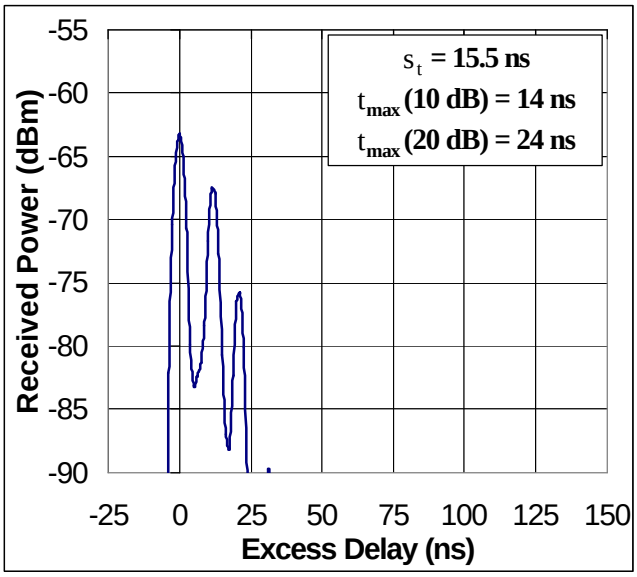

½ meter Track Parallel Local Average PDP

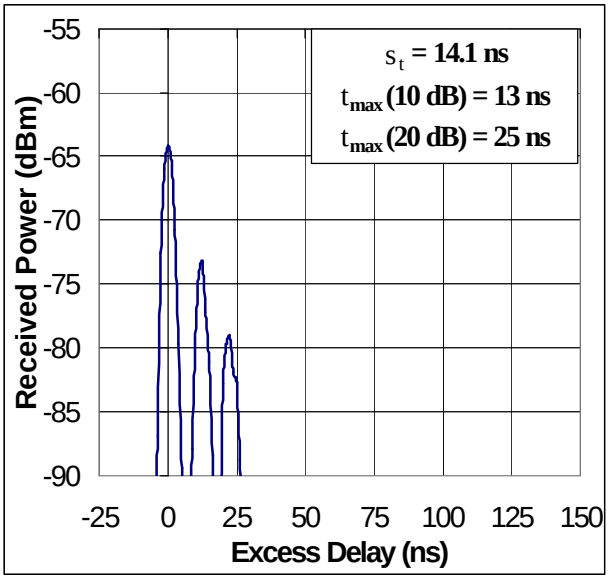

½ meter Track Perpendicular Local Average PDP

Figure B.33: 60 GHz Location 4.2 Power Delay Profiles

Receiver Location 4.3

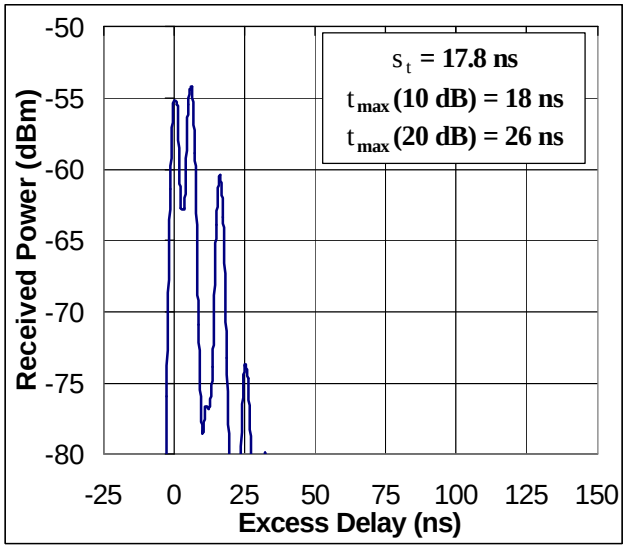

10° Parallel Local Average PDP

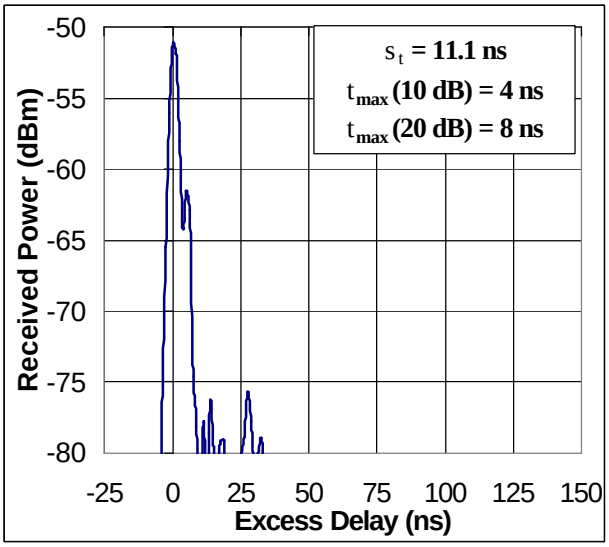

10° Perpendicular Local Average PDP

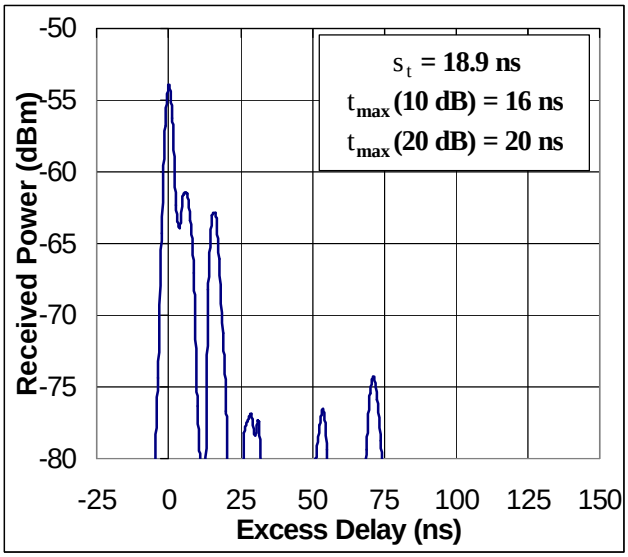

½ meter Track Parallel Local Average PDP

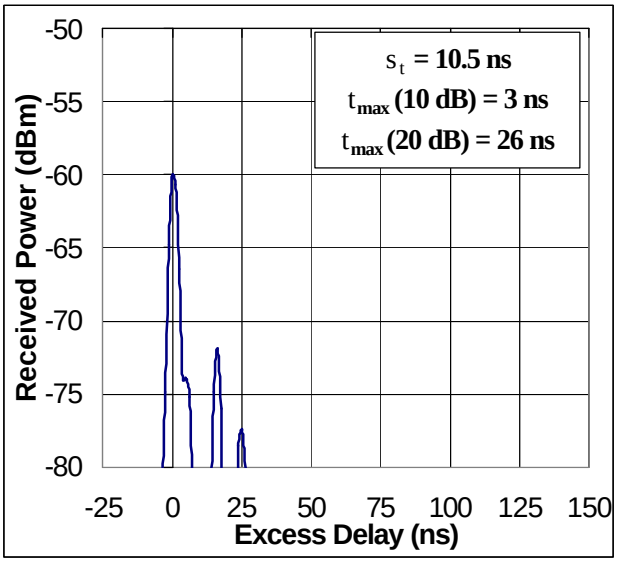

½ meter Track Perpendicular Local Average PDP

Figure B.34: 60 GHz Location 4.3 Power Delay Profiles

Receiver Location 4.4

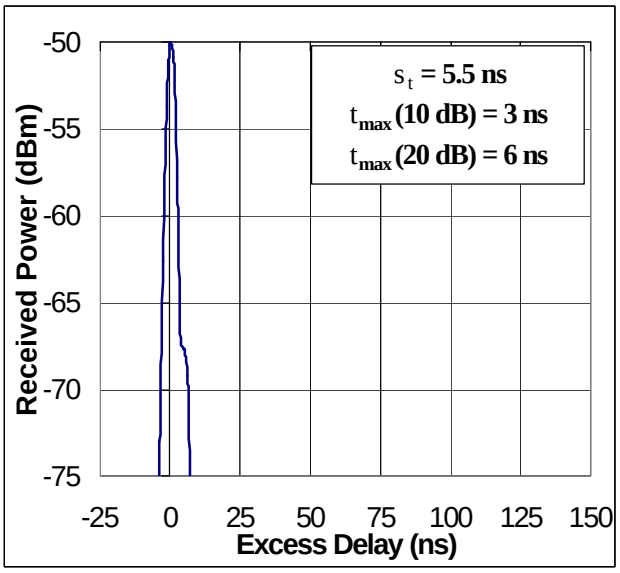

10° Parallel Local Average PDP

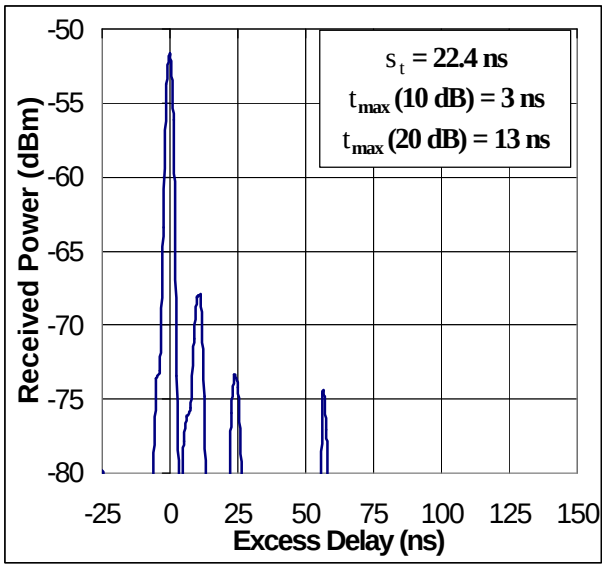

10° Perpendicular Local Average PDP

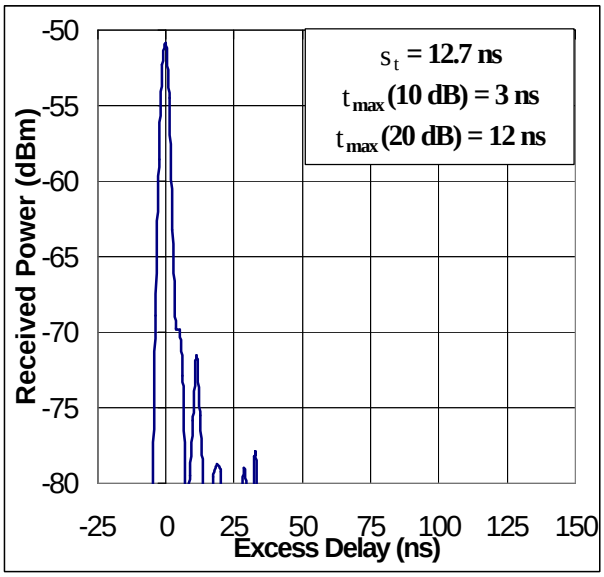

½ meter Track Parallel Local Average PDP

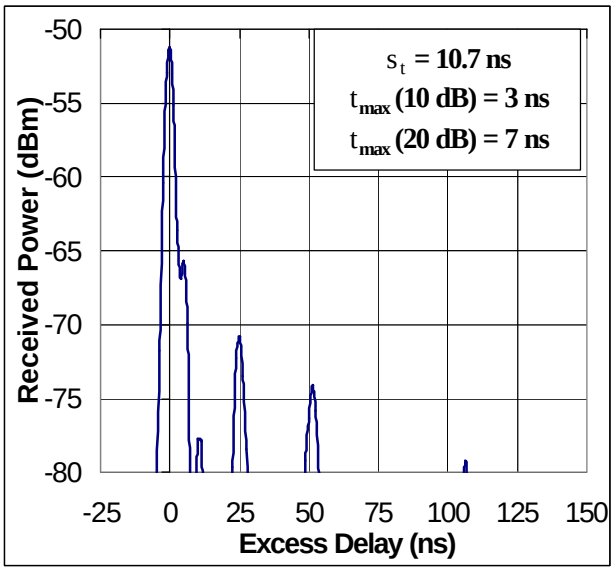

½ meter Track Perpendicular Local Average PDP

Figure B.35: 60 GHz Location 4.4 Power Delay Profiles

B.2.5 60 GHz Location 5 PDPs, 4th Floor Durham Hall, Virginia Tech

Receiver Location 5.1

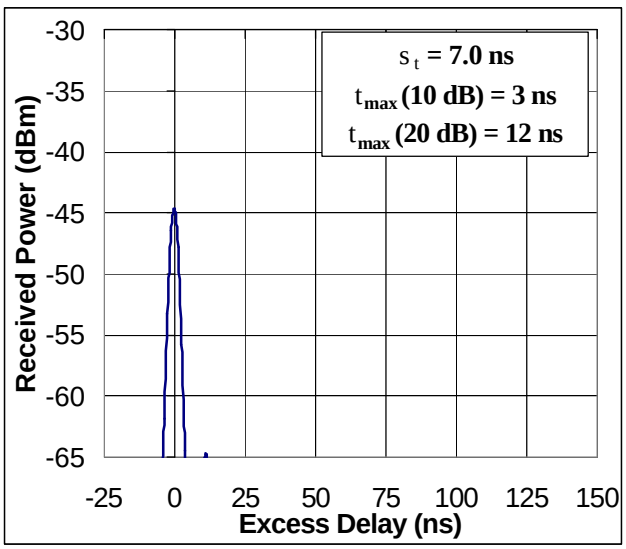

10° Parallel Local Average PDP

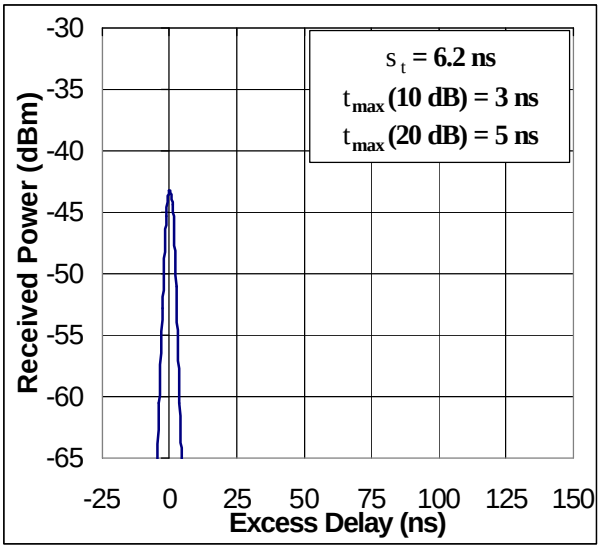

10° Perpendicular Local Average PDP

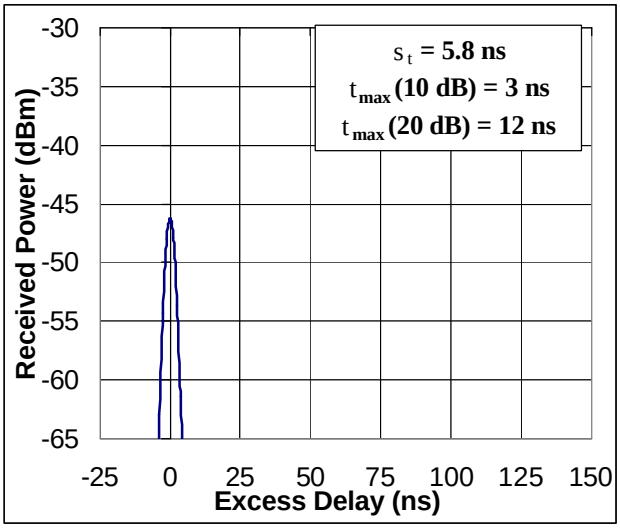

½ meter Track Parallel Local Average PDP

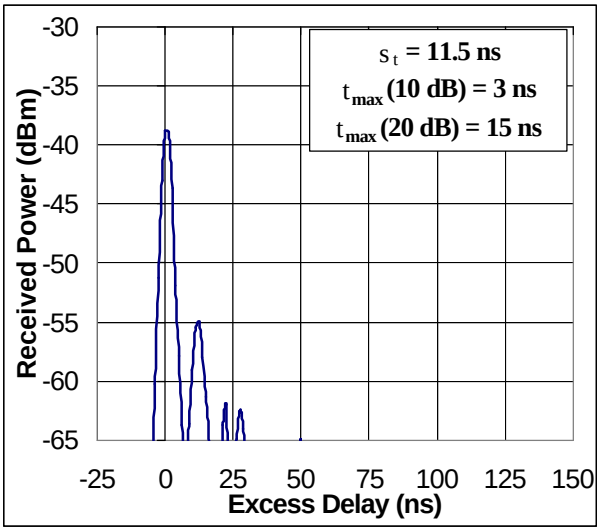

½ meter Track Perpendicular Local Average PDP

Figure B.36: 60 GHz Location 5.1 Power Delay Profiles

Receiver Location 5.2

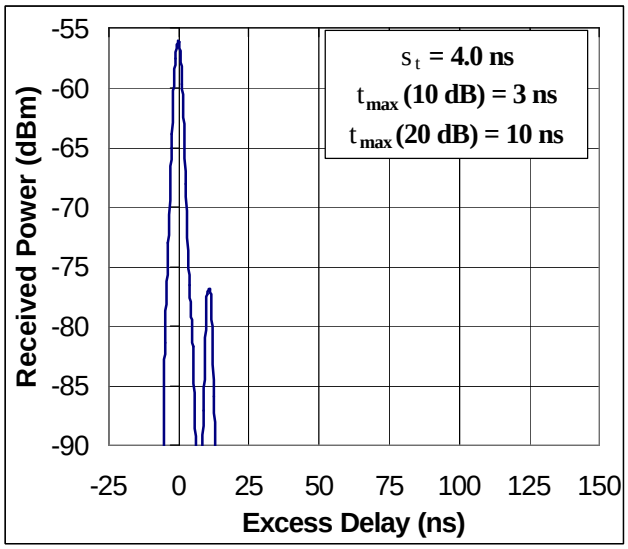

10° Parallel Local Average PDP

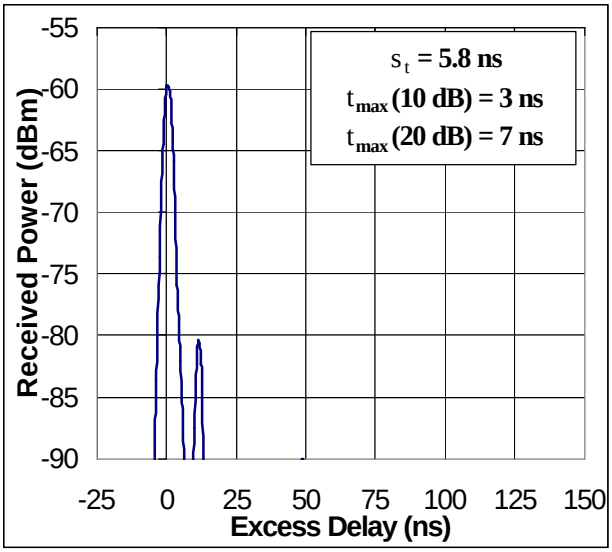

10° Perpendicular Local Average PDP

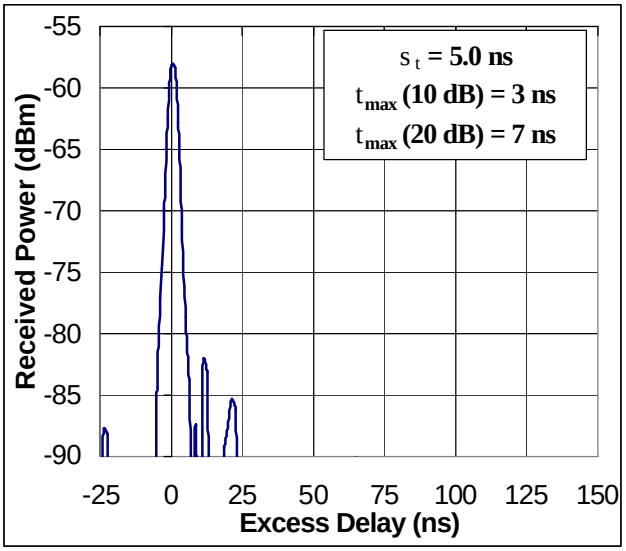

½ meter Track Parallel Local Average PDP

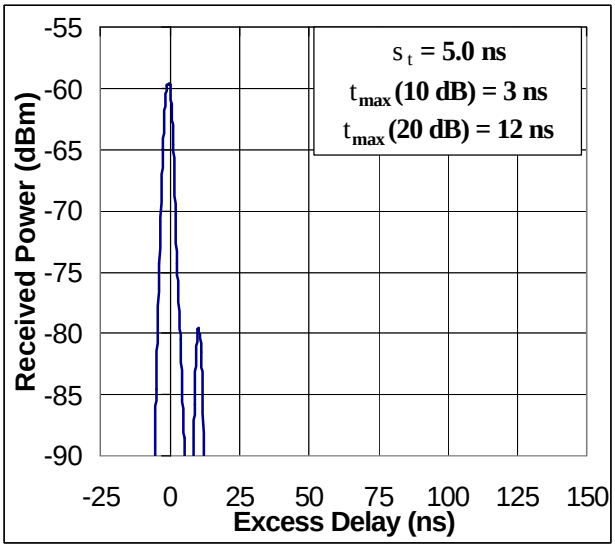

½ meter Track Perpendicular Local Average PDP

Figure B.37: 60 GHz Location 5.2 Power Delay Profiles

Receiver Location 5.3

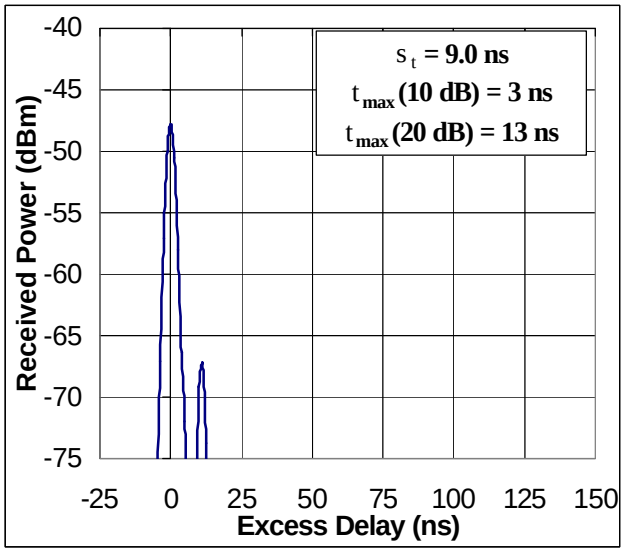

10° Parallel Local Average PDP

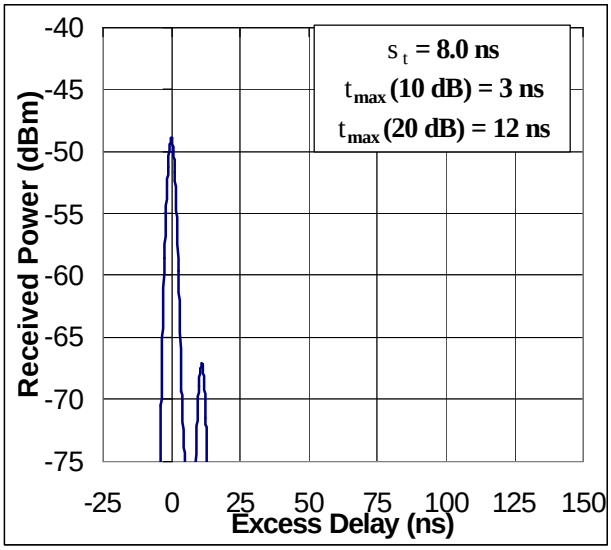

10° Perpendicular Local Average PDP

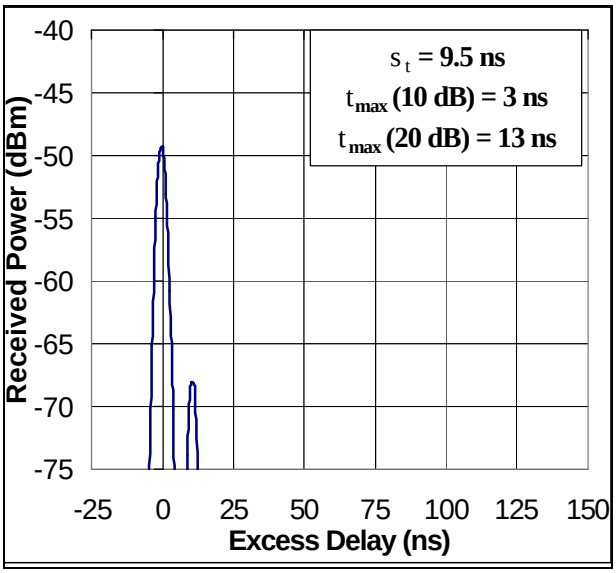

½ meter Track Parallel Local Average PDP

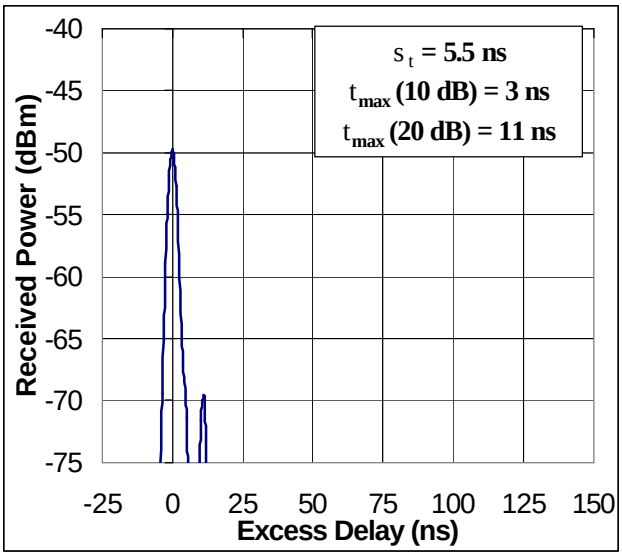

½ meter Track Perpendicular Local Average PDP

Figure B.38: 60 GHz Location 5.3 Power Delay Profiles

Receiver Location 5.4

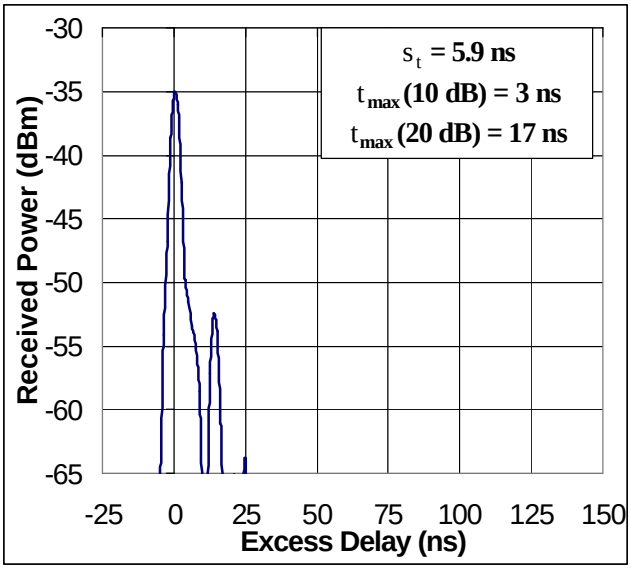

10° Parallel Local Average PDP

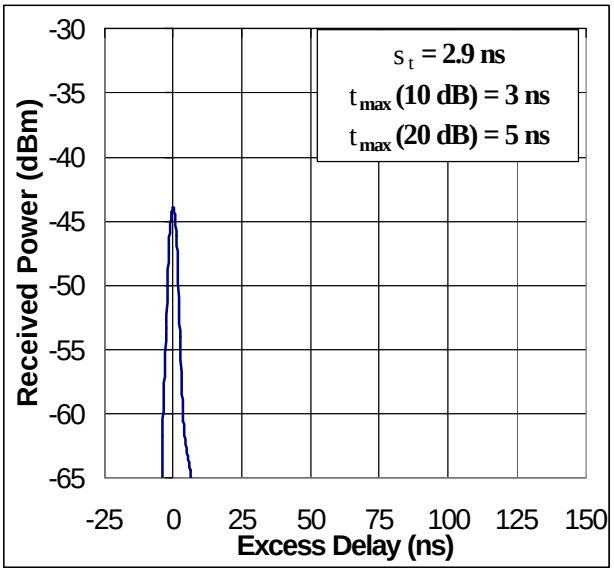

10° Perpendicular Local Average PDP

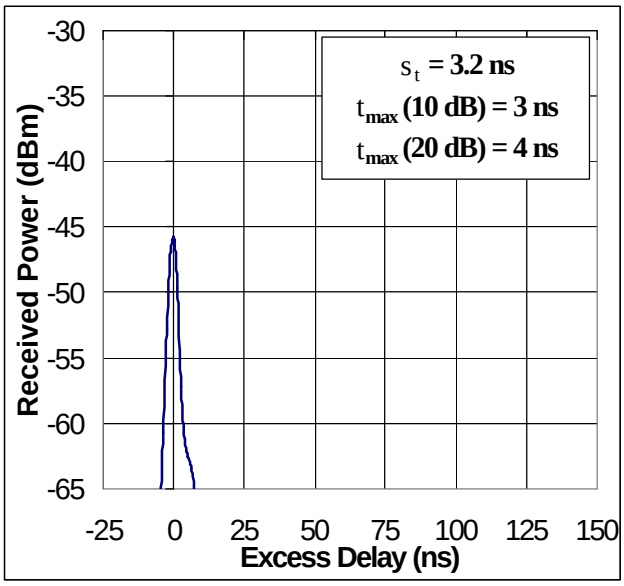

½ meter Track Parallel Local Average PDP

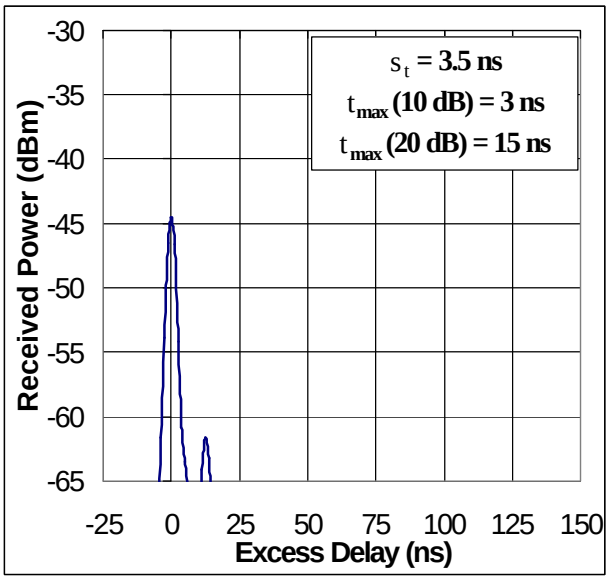

½ meter Track Perpendicular Local Average PDP

Figure B.39: 60 GHz Location 5.4 Power Delay Profiles

B.2.6 60 GHz Location 6 PDPs, 4th Floor Durham Hall, Virginia Tech

Receiver Location 6.1

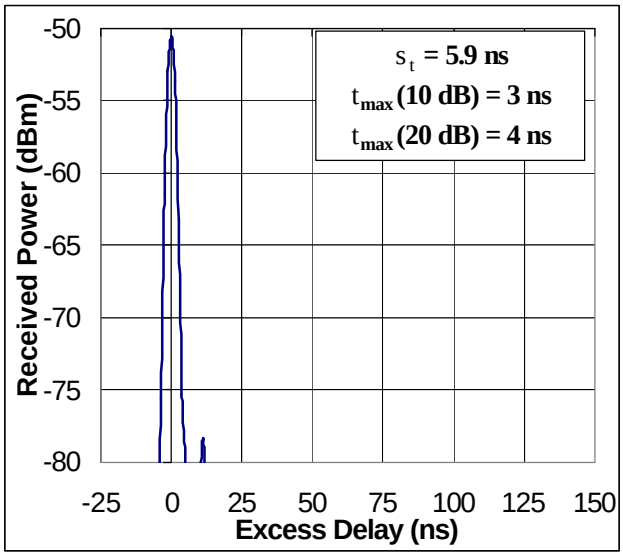

10 Parallel Local Average PDP

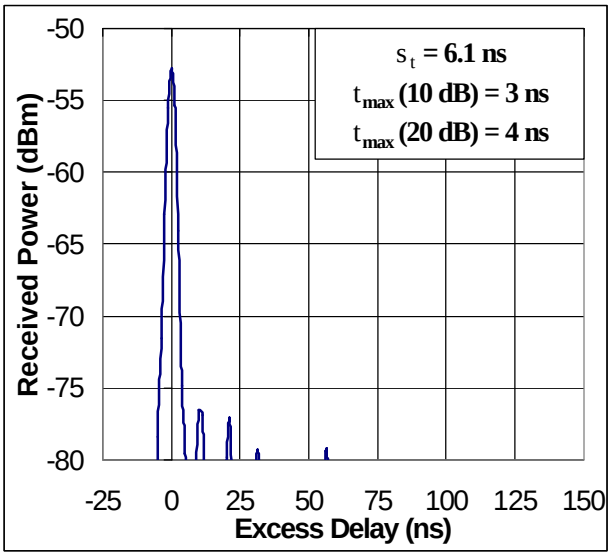

10 Perpendicular Local Average PDP

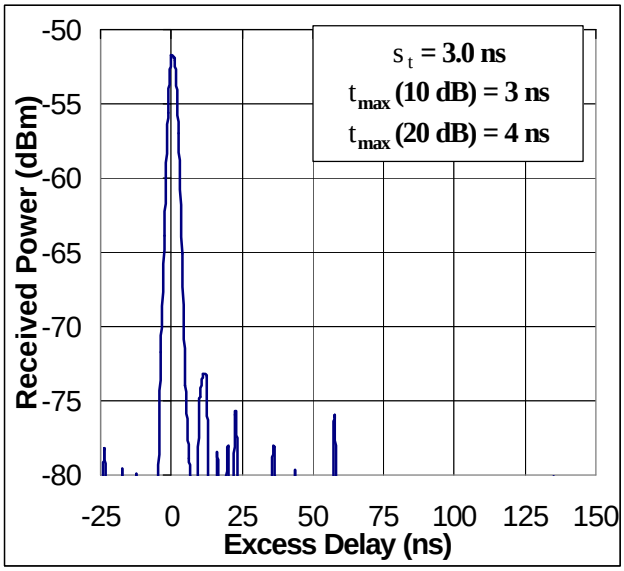

½ meter Track Parallel Local Average PDP

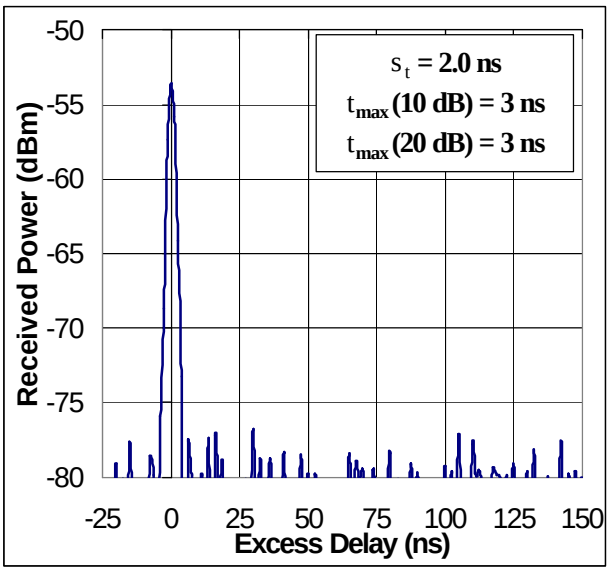

½ meter Track Perpendicular Local Average PDP

Figure B.40: 60 GHz Location 6.1 Power Delay Profiles

Receiver Location 6.2

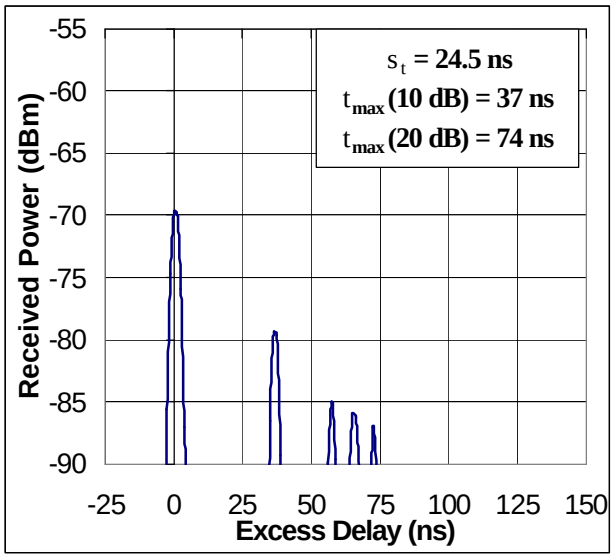

10° Parallel Local Average PDP

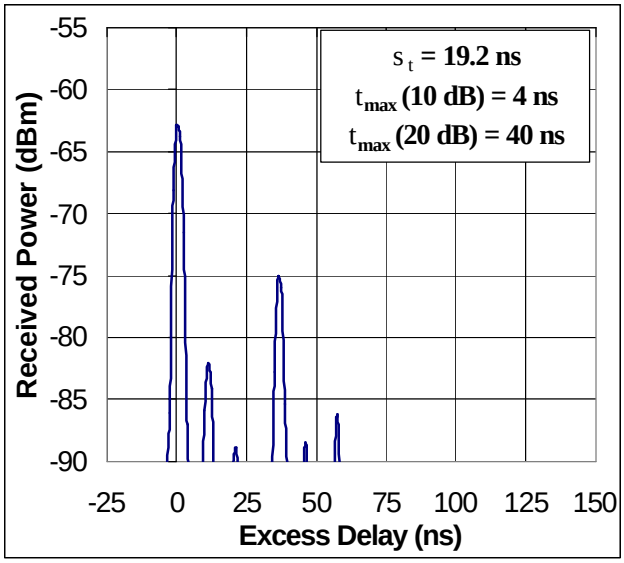

10° Perpendicular Local Average PDP

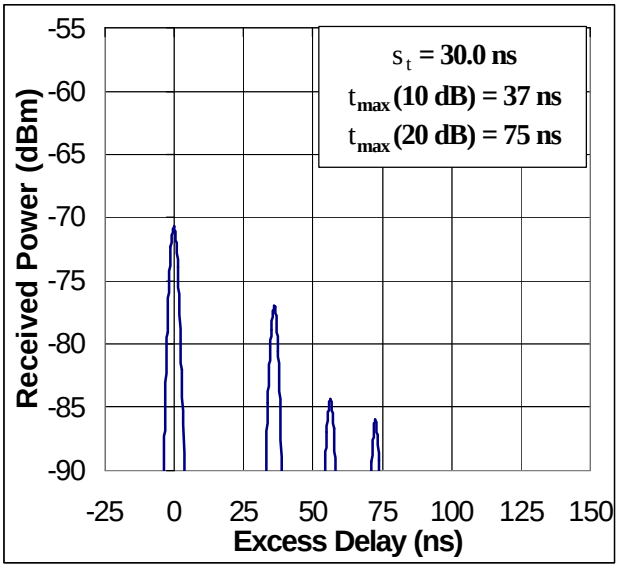

½ meter Track Parallel Local Average PDP

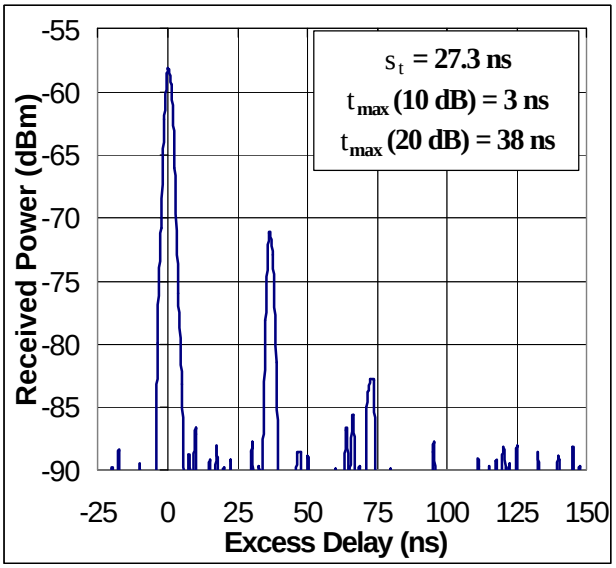

½ meter Track Perpendicular Local Average PDP

Figure B.41: 60 GHz Location 6.2 Power Delay Profiles

B.2.7 60 GHz Location 7 PDPs, 4th Floor Durham Hall, Virginia Tech

Receiver Location 7.1

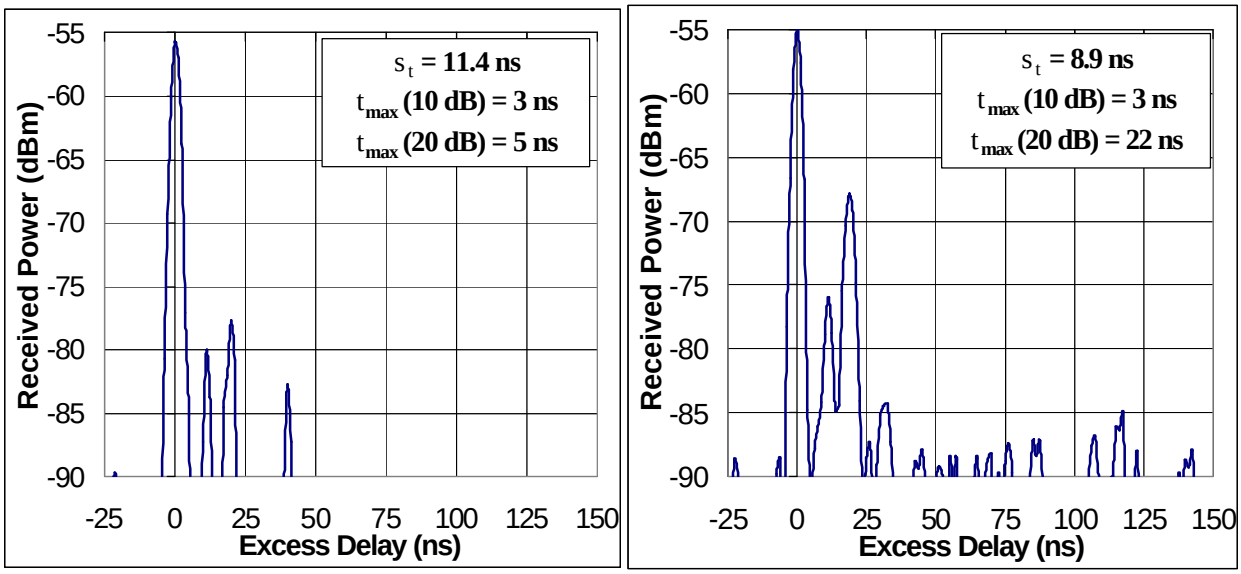

10l Parallel Local Average PDP **10l Perpendicular Local Average PDP**

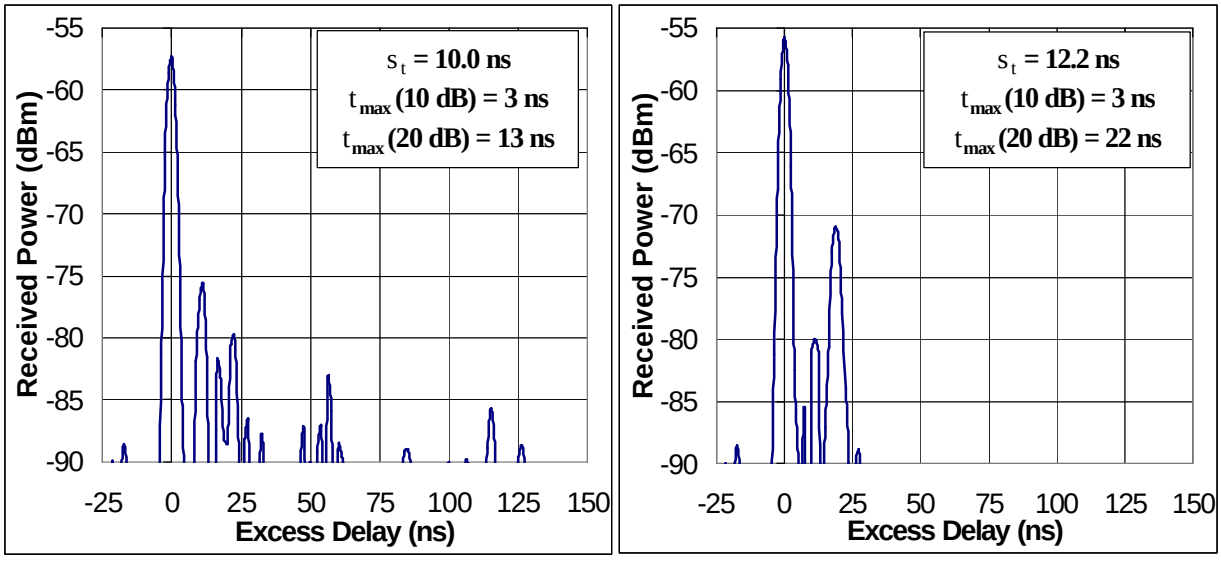

½ meter Track Parallel Local Average PDP **½ meter Track Perpendicular Local Average PDP**

Figure B.42: 60 GHz Location 7.1 Power Delay Profiles

Receiver Location 7.2

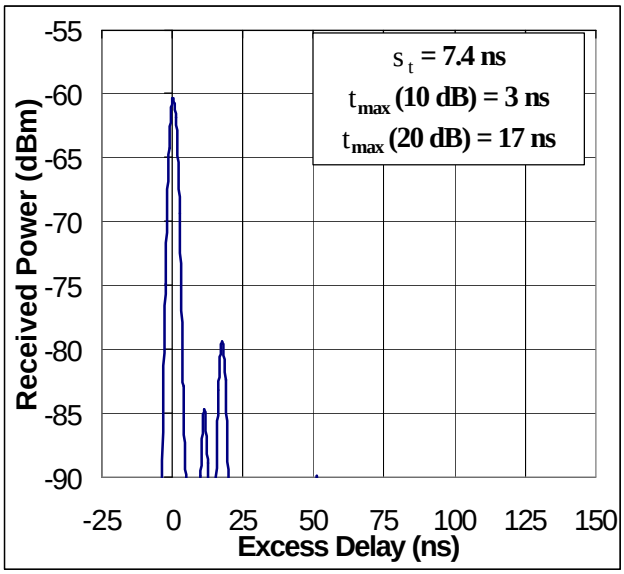

10° Parallel Local Average PDP

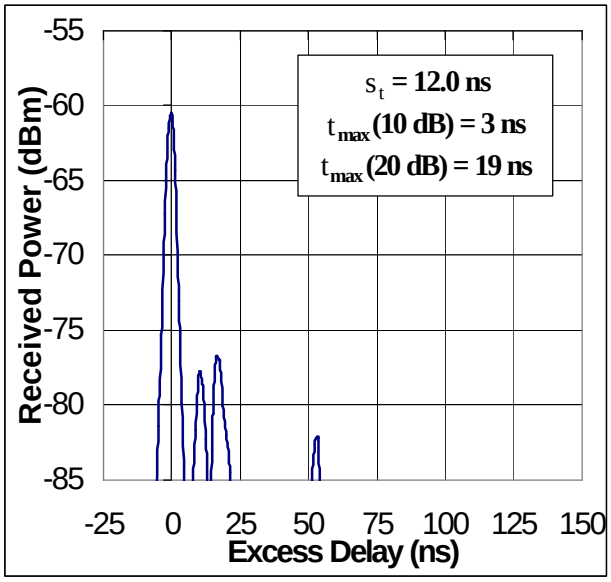

10° Perpendicular Local Average PDP

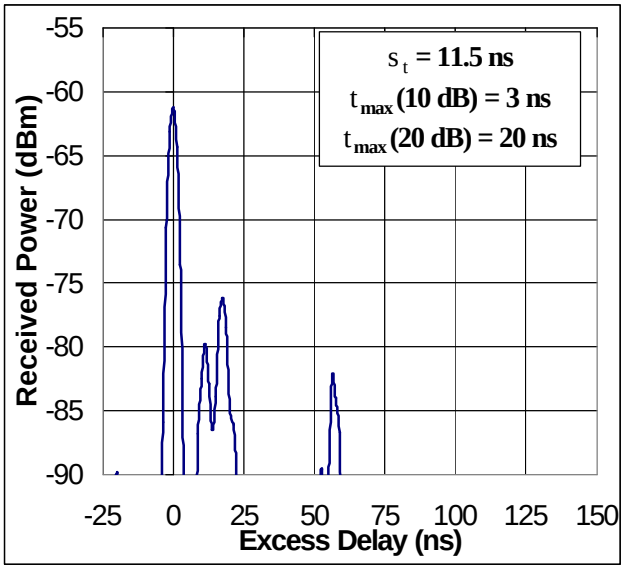

½ meter Track Parallel Local Average PDP

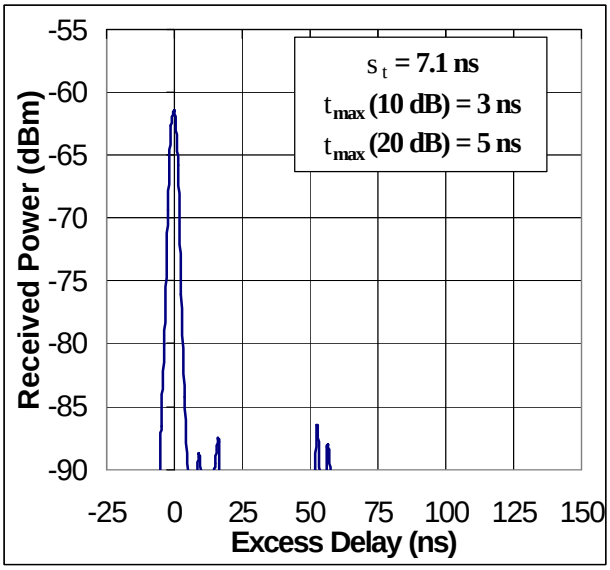

½ meter Track Perpendicular Local Average PDP

Figure B.43: 60 GHz Location 7.2 Power Delay Profiles

B.2.8 60 GHz Location 8 PDPs, 4th Floor Durham Hall, Virginia Tech

Receiver Location 8.1

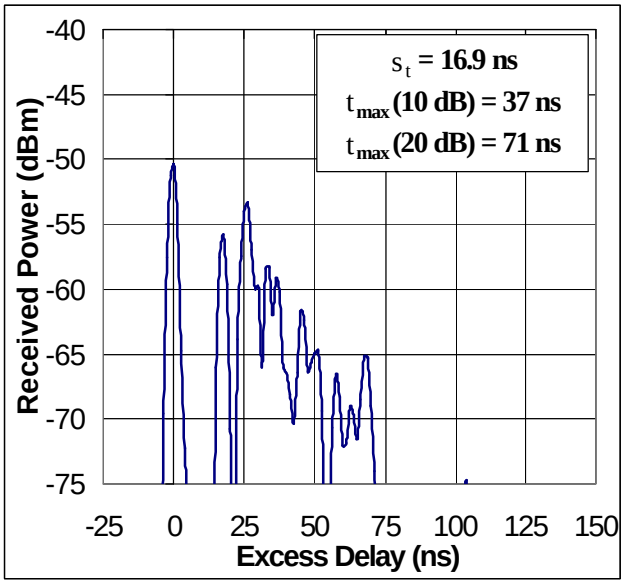

10λ Parallel Local Average PDP

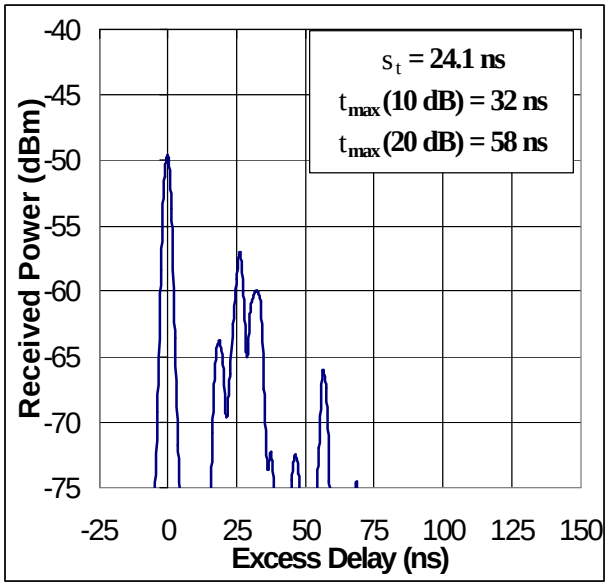

10λ Perpendicular Local Average PDP

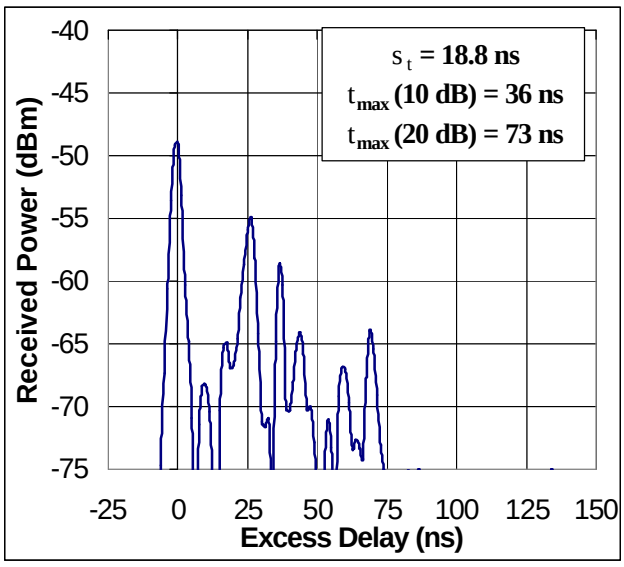

½ meter Track Parallel Local Average PDP

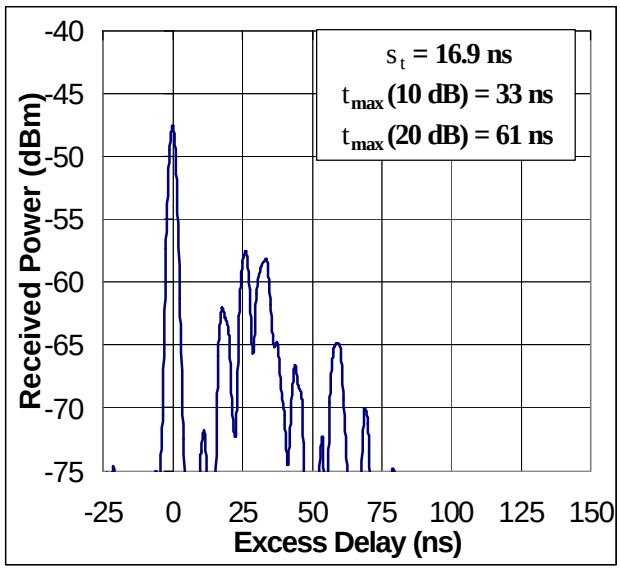

½ meter Track Perpendicular Local Average PDP

Figure B.44: 60 GHz Location 8.1 Power Delay Profiles

B.3 2.5 GHz Transmitter and Receiver Site Photos

B.3.1 2.5 GHz Location 1 Series, 4th Floor Durham Hall, Virginia Tech

Receiver Location 1.1

Receiver Location 1.2

Receiver Location 1.3

Receiver Location 1.4

Transmitter for Location 1 Series

Figure B.45: 2.5 GHz Location 1 Series Site Photos

B.3.2 2.5 GHz Location 2 Series, 4th Floor Durham Hall, Virginia Tech

Receiver Location 2.1

Receiver Location 2.2

Receiver Location 2.3

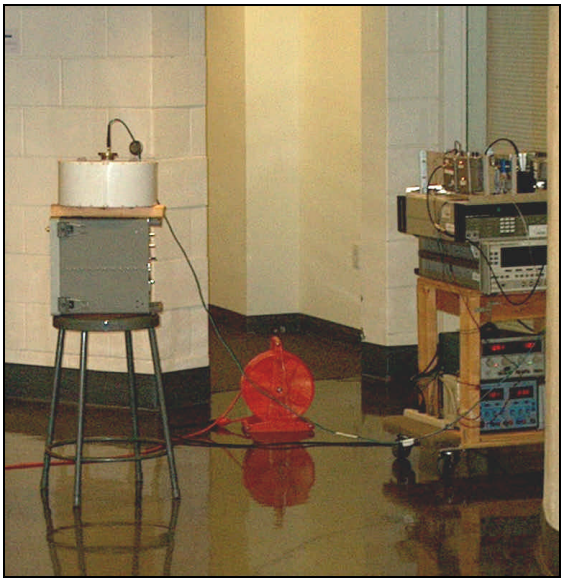

Transmitter for Location 2 Series

Figure B.46: 2.5 GHz Location 2 Series Site Photos

B.3.3 2.5 GHz Location 3 Series, 4th Floor Durham Hall, Virginia Tech

Receive r Location 3.1

Receiver Location 3.2

Transmitter for Location 3 Series

Figure B.47: 2.5 GHz Location 3 Series Site Photos

B.3.4 2.5 GHz Location 4 Series, 4th Floor Durham Hall, Virginia Tech

Receiver Location 4.1

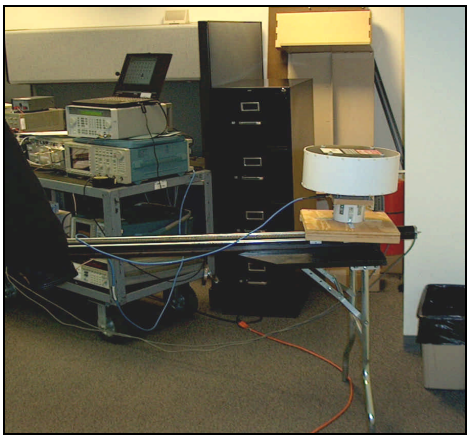

Receiver Location 4.2

Receiver Location 4.3

Receiver Location 4.4

Transmitter for Location 4 Series

Figure B.48: 2.5 GHz Location 4 Series Site Photos

B.3.5 2.5 GHz Location 5 Series, 4th Floor Durham Hall, Virginia Tech

Receiver Location 5.1

Receiver Location 5.2

Receiver Location 5.3

Receiver Location 5.4

Transmitter for Location 5 Series

Figure B.49: 2.5 GHz Location 5 Series Site Photos

B.3.6 2.5 GHz Location 6 & 7 Series, 4th Floor Durham Hall, Virginia Tech

Receiver Location 6.1

Receiver Location 6.2

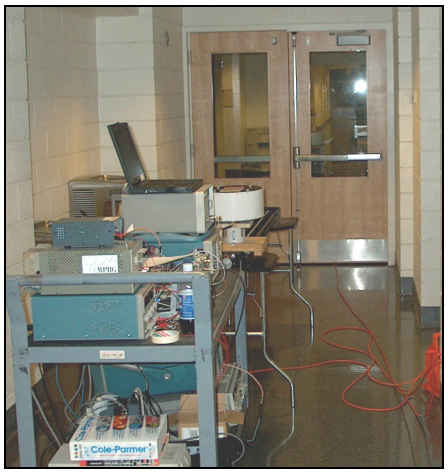

Receiver Location 7.1

Receiver Location 7.4

Transmitter for Location 6 Series

Transmitter for Location 7 Series

Figure B.50: 2.5 GHz Location 6 & 7 Series Site Photos

B.3.7 2.5 GHz Location 8 Series, 4th Floor Durham Hall, Virginia Tech

Receiver Location 8.1

Transmitter for Location 8 Series

Figure B.51: 2.5 GHz Location 8 Series Site Photos

B.4 60 GHz Transmitter and Receiver Site Photos

B.4.1 60 GHz Location 1 Series, 4th Floor Durham Hall, Virginia Tech

Receiver Location 1.1

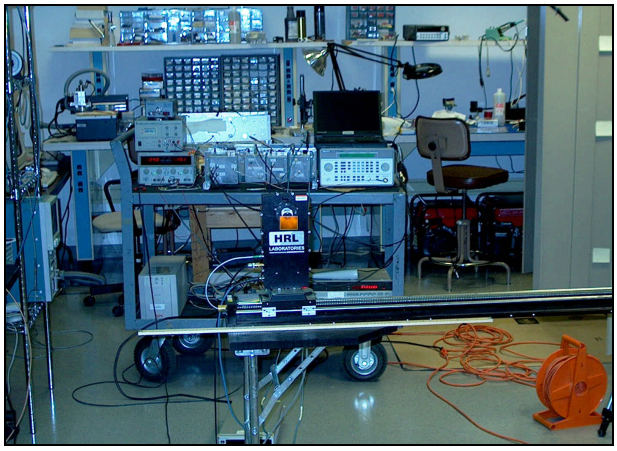

Receiver Location 1.2

Receiver Location 1.3

Receiver Location 1.4

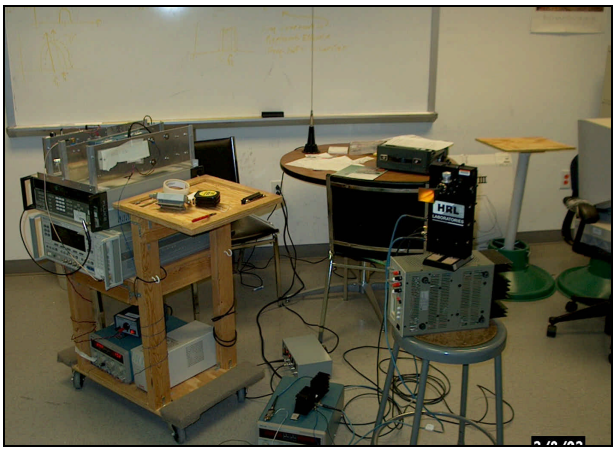

Transmitter for Location 1 Series

Figure B.52: 60 GHz Location 1 Series Site Photos

B.4.2 60 GHz Location 2 Series, 4th Floor Durham Hall, Virginia Tech

Receiver Location 2.1

Receiver Location 2.2

Receiver Location 2.3

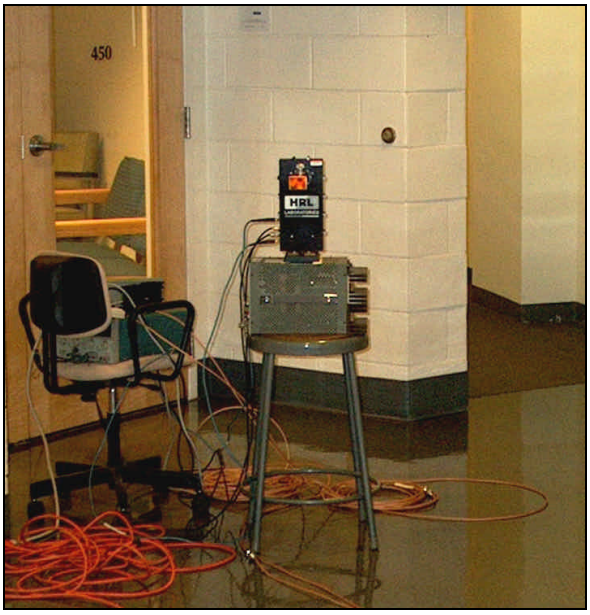

Transmitter for Location 2 Series

Figure B.53: 60 GHz Location 2 Series Site Photos

B.4.3 60 GHz Location 3 Series, 4th Floor Durham Hall, Virginia Tech

Receiver Location 3.1

Receiver Location 3.2

Transmitter for Location 3 Series

Figure B.54: 60 GHz Location 3 Series Site Photos

B.4.4 60 GHz Location 4 Series, 4th Floor Durham Hall, Virginia Tech

Receiver Location 4.1

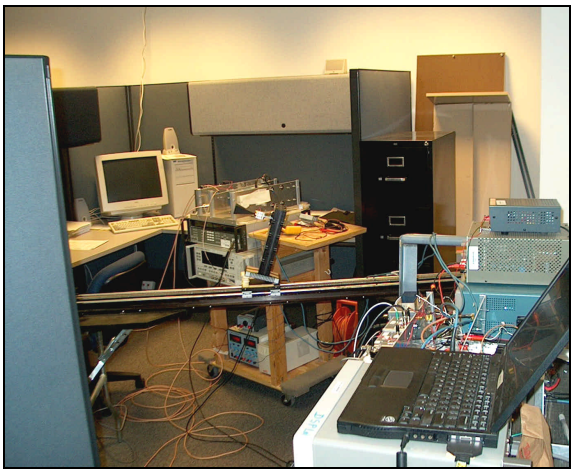

Receiver Location 4.2

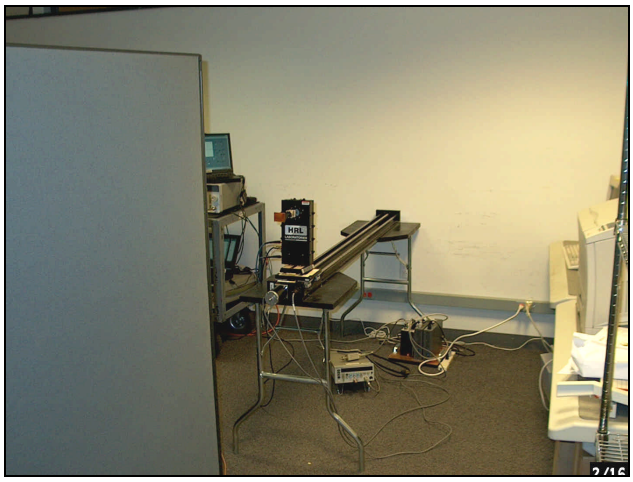

Receiver Location 4.3

Receiver Location 4.4

Transmitter for Location 4 Series

Figure B.55: 60 GHz Location 4 Series Site Photos

B.4.5 60 GHz Location 5 Series, 4th Floor Durham Hall, Virginia Tech

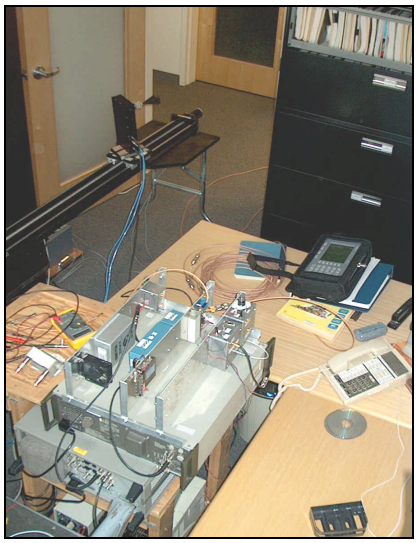

Receiver Location 5.1

Receiver Location 5.2

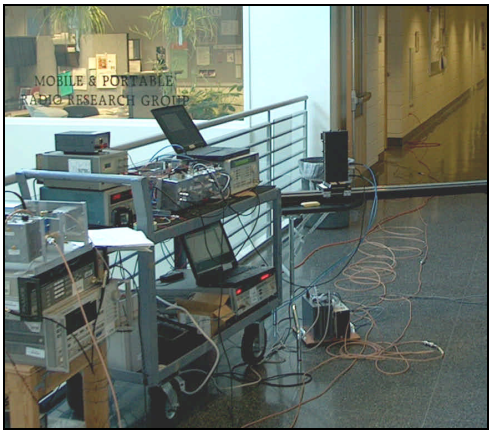

Receiver Location 5.3

Receiver Location 5.4

Transmitter for Location 5 Series

Figure B.56: 60 GHz Location 5 Series Site Photos

B.4.6 60 GHz Location 6 & 7 Series, 4th Floor Durham Hall, Virginia Tech

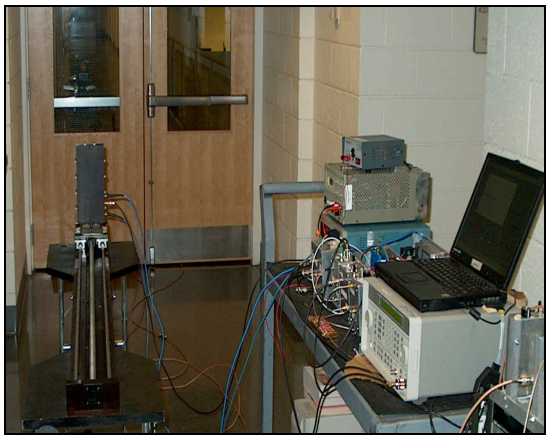

Receiver Location 6.1

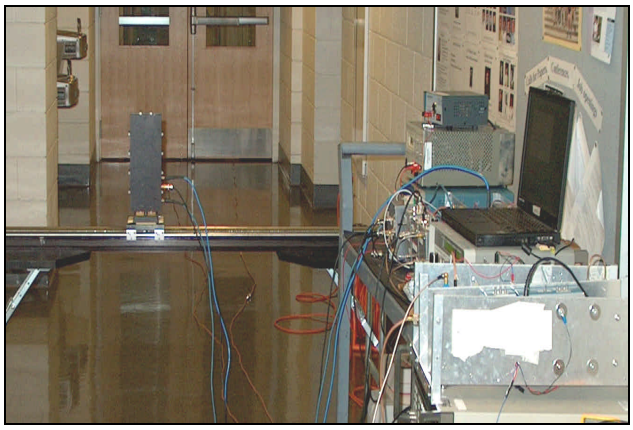

Receiver Location 6.2

Receiver Location 7.1

Receiver Location 7.2

Transmitter for Location 6

Transmitter for Location 7

Figure B.57: 60 GHz Location 6 & 7 Series Site Photos

B.4.7 60 GHz Location 8 Series, 4th Floor Durham Hall, Virginia Tech

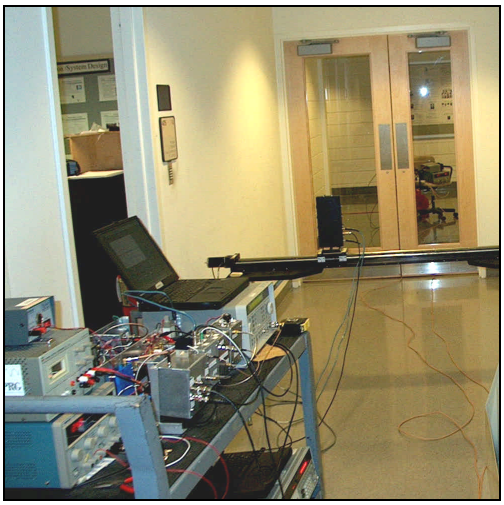

Receiver Location 8.1

Transmitter for Location 8 Series

Figure B.58: 60 GHz Location 8 Series Site Photos

Appendix C

Channel Sounder Users Guide

C.1 Introduction

The Spread Spectrum Sliding Correlator Channel Sounder is used to study the ultrawideband electromagnetic propagation characteristics of a radio channel. Its primary use is to allow researchers to study and quantify the dynamic channel phenomena through the measurement of Power Delay Profiles (PDPs). Recording a number of PDPs at different locations allows researchers to characterize the channel over a local area. Channel models developed as a result of measurements can be used to predict system wide wireless network requirements and performance prior to its deployment.

This manual is divided into two parts, the first describes the setup and operation of the channel sounder, and the second part describes the operation of the LabVIEW Analysis Software. Detailed instructions for using the Matlab Channel Imaging Analysis Suite—which provides a means to visualize, analyze, and compute statistics from sets of PDPs—may be found in [65].

C.2 Channel Sounder Operation

C.2.1 Setup

The block diagram of the transmitter and receiver implementation, shown in Chapters 4 and 5, are repeated here, as Figures C.1 and C.2. Additionally, Figures C.3 and C.4 are

snapshots of the channel sounder, and may be used as an aid to identify channel sounder subsystems.

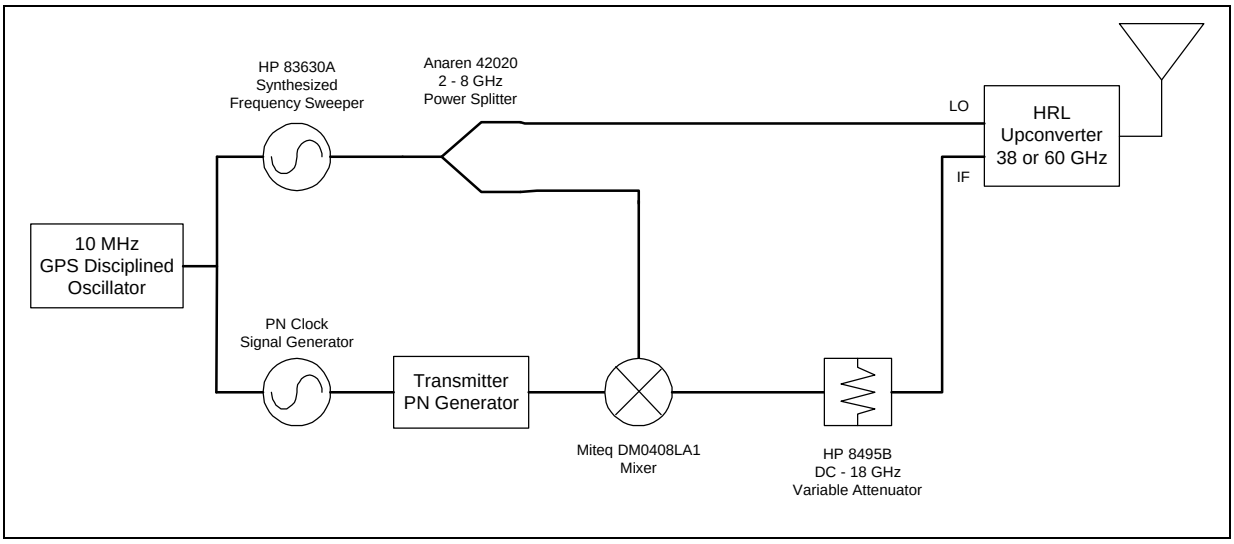

Figure C.1: Channel Sounder Transmitter Block Diagram

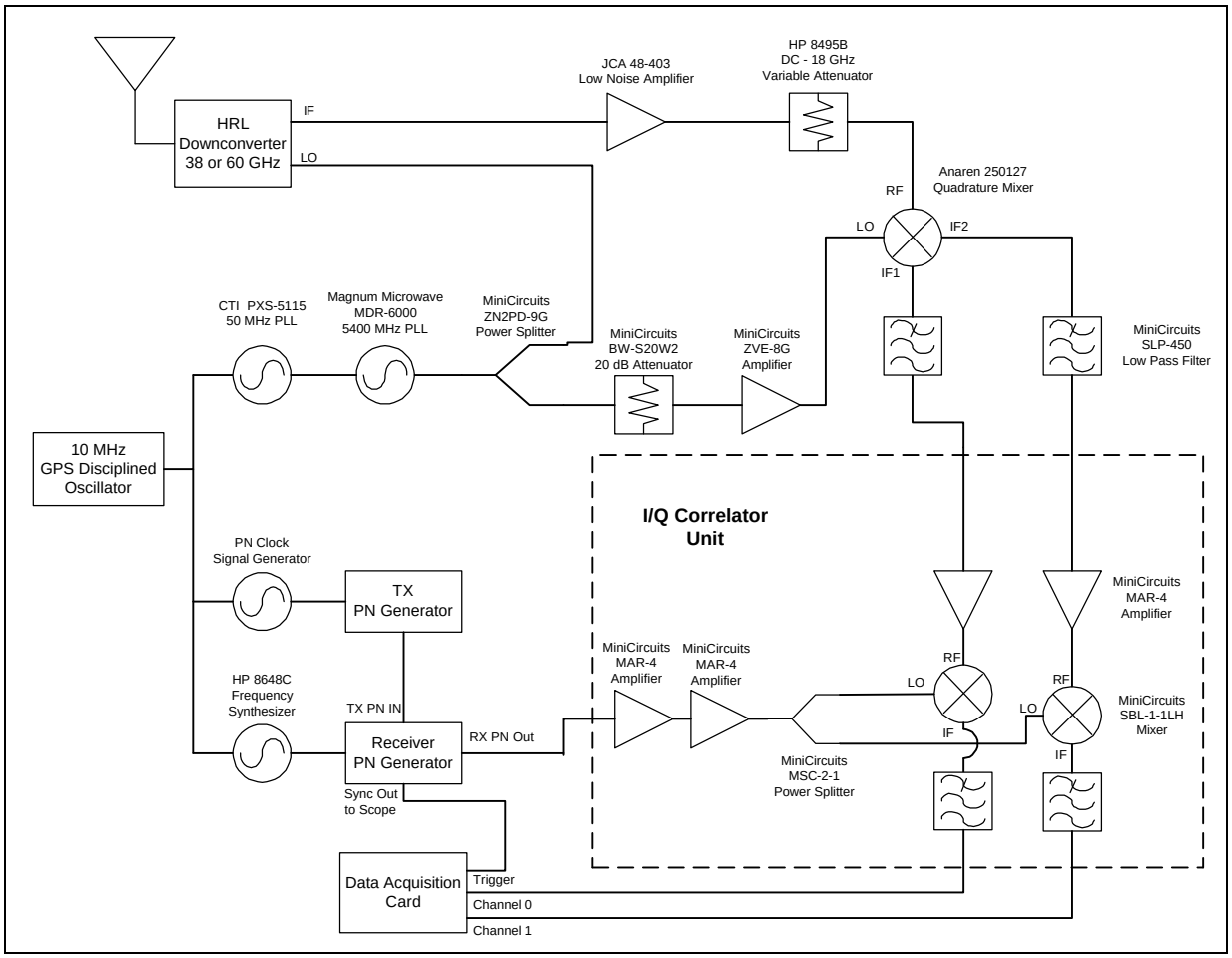

Figure C.2: Channel Sounder Receiver Block Diagram

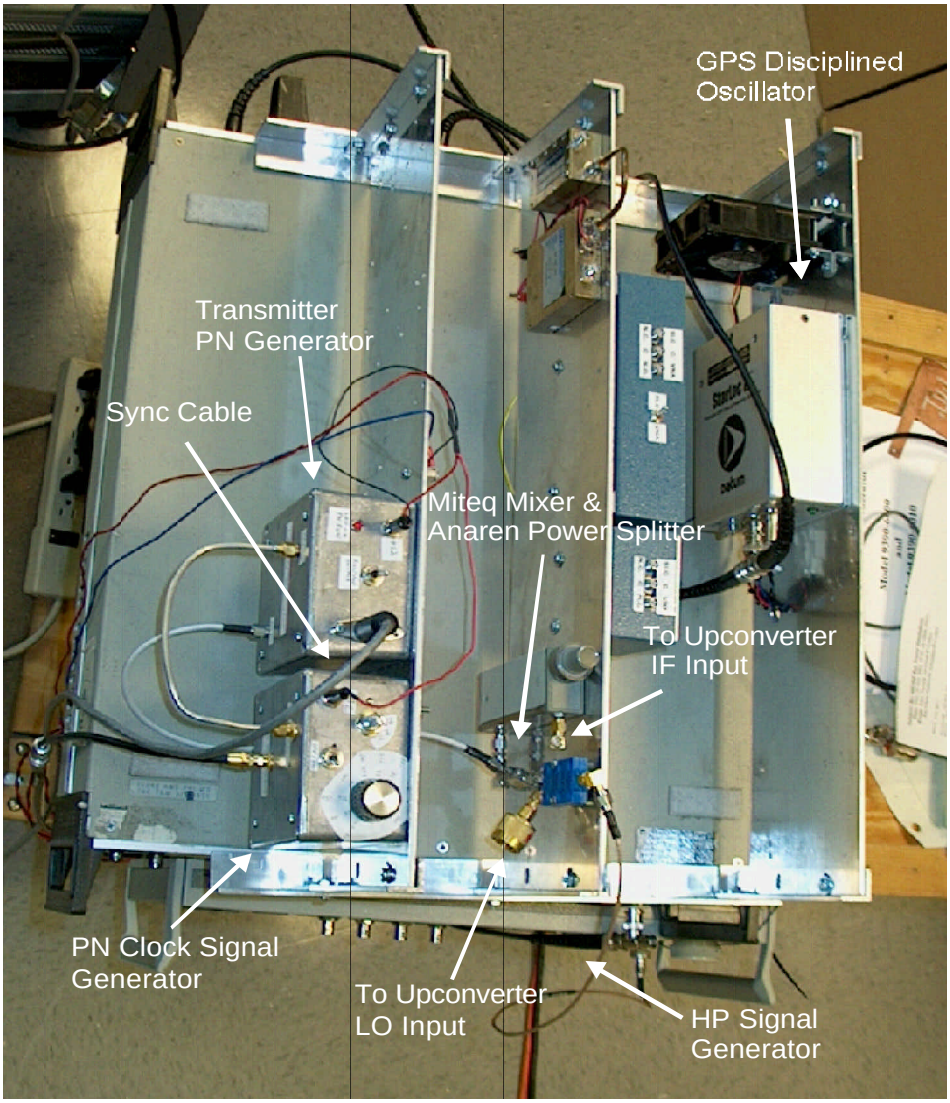

Figure C.3: Channel Sounder Transmitter Baseband and IF Section

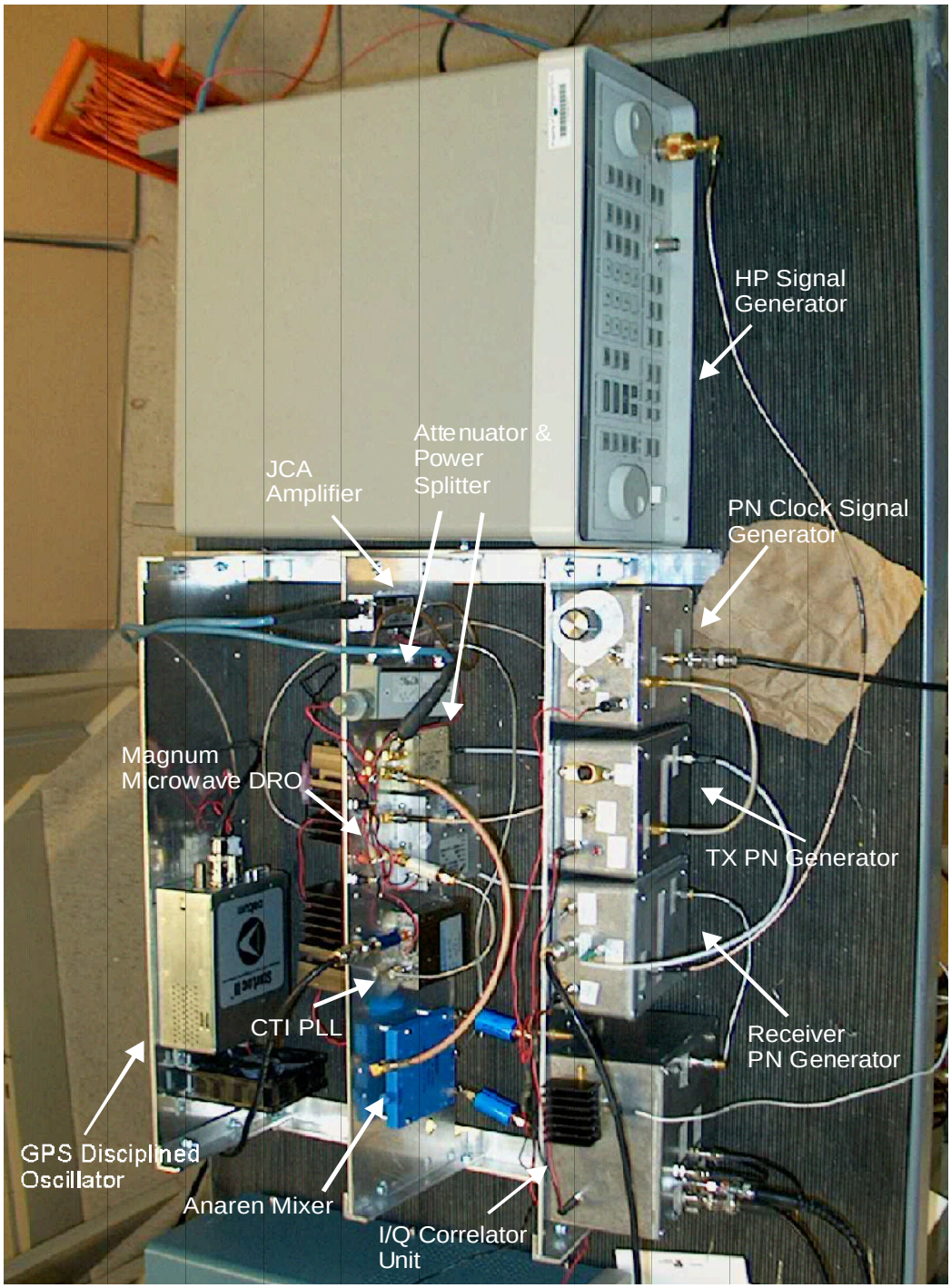

Figure C.4: Channel Sounder Receiver Baseband and IF Section

C.2.1.1 Transmitter Setup

1. The transmitter requires four separate power supplies. The GPS disciplined oscillator requires +24 Volts, the PN Generator and PN Clock Generator require +12 Volts, and the HRL Upconverter requires two +15 power supply connections. For the upconverter, it is particularly important to note that one of the power supplies runs the internal components and the other runs the cooling fan. *The upconverter should never be operated without the cooling fan running, as the power amplifier will overheat and burn out.*

2. The GPS Antenna must be mounted outdoors and in a location that provides an unobstructed view of the sky, in order to maximize the number of satellites that the receiver can track.

3. The GPS Disciplined Oscillator **10 MHz Out** output is connected to the **10 MHz Reference Input** on the HP Frequency Synthesizer as well as the PN Clock Signal Generator. The PN Clock Signal Generator requires a CMOS/TTL voltage level on the input; therefore the 10 MHz signal may need to be amplified prior to connecting it to the PN Clock Signal Generator.

4. The output of the HP Frequency Synthesizer is connected to an Anaren 42020 power splitter. One output from the power splitter provides an LO signal for the Miteq mixer, the other provides an LO signal for the HRL Upconverter. The Frequency synthesizer should be set for a CW frequency of 5400 MHz and a power level of +13 dBm, to ensure sufficient drive level for both the Miteq mixer and the HRL upconverter.

5. The PN Clock Signal Generator output is connected to the **TX PN Clock IN** input on the PN Generator, and the **TX PN OUT** output from the PN Generator is connected to the **IF** port of the Miteq Mixer. The *PN Synchronize cable* is also connected from the Transmitter PN Generator **PN Sync** port to the TX PN Generator **PN Sync** port at the receiver.

6. The **RF** port of the Miteq mixer is then connected—via the HP8495B variable attenuator—to the **IF** Port of the HRL Upconverter.

7. Set the PN Clock Signal Generator for the desired PN clock frequency according to the instructions listed in Section C.2.1.3. Then, flip the **Run/Stop** switch on the PN Generator, which will initialize and begin producing the PN Sequence. When the PN Generator is running (producing a pseudo-noise sequence) the LED on the top panel will turn on.

8. The HP8495B attenuator should be adjusted so that the desired transmitter output power level is achieved. In the event that the transmitter/receiver separation distance is small, the attenuator should be set to a value such that the receiver will not be overloaded.

C.2.1.2 Receiver Setup

1. The receiver requires four separate power supplies. The GPS disciplined oscillator requires +24 Volts, the backplane requires +12 and +15 volts, and the HRL downconverter requires +15 volts.

2. The GPS Antenna must be mounted outdoors and in a location that provides an unobstructed view of the sky, in order to maximize the number of satellites that the receiver can track.

3. The GPS disciplined oscillator **10 MHz Out** output is connected to the **10 MHz Reference Input** on the CTI Microwave 50 MHz PLL, the HP 8648C signal generator, and to the PN Clock Signal Generator. As with the transmitter, the PN Clock Signal Generator requires a CMOS/TTL input level and the 10 MHz reference may need to be amplified. The **RF OUT** output of the CTI PLL is connected to the **REF IN** input of a Magnum Microwave Dielectric Resonator Oscillator (DRO).

4. The DRO **RF OUT** output is connected to a MiniCircuits Power Splitter. One of the power splitter outputs is connected to the **LO** input on the HRL Downconverter, and the other output is connected—via an attenuator and ZVE-8G amplifier, to the **LO** input of the Anaren Quadrature Mixer.

5. The PN Clock Signal Generator output is connected to the **TX PN Clock IN** input of the TX PN Generator; similarly, the HP 8648C signal generator output is connected to the **RX PN Clock IN** input of the Receiver PN Generator.

6. The **TX PN OUT** output from the TX PN Generator is connected to the **TX PN IN** input on the Receiver PN Generator. Internally, the Receiver PN Generator correlates the TX PN sequence and the Receiver PN Sequence, and produces a pulse when the two are maximally aligned. This pulse appears on the **Sync Out to Scope** output, and should be connected to the **Trigger** input on the DAQ Card. Also, the **RX PN Out** output on the Receiver PN Generator should be connected to the **RX PN Input** on the I/Q Correlator Unit.

7. The Receiver PN Clock Signal Generator should be set to a frequency identical to the Transmitter PN Clock Signal Generator. The HP 8648C signal generator should be set at a slightly lower frequency than the PN Clock Signal Generator, in order to achieve the desired slide factor. The output power level of the 8648C should be set to 0 dBm. Then, flip the **Run/Stop** switch on both the TX and Receiver PN Generators to initialize and begin running the PN sequences. The TX PN Generator has an LED that will turn on when the PN sequence is running, however, the Receiver PN Generator does not. The *PN Synchronize cable* may be removed at this point as the TX PN Generator and Transmitter PN Generator codes will be synchronized. Should the system lose power, however, these two PN generators must be re-synchronized.

8. Connect the IF output from the HRL Downconverter to the **RF Input** on the JCA 48-403 Amplifier. The **RF Output** from the amplifier is then connected—via an HP8495B variable attenuator—to the RF input on the Anaren quadrature mixer. If necessary, adjust the HP8495B to prevent overloading the inputs of either the Anaren mixer or the I/Q Correlator unit.

9. The **IF1** (inphase) and **IF2** (quadrature) outputs from the Anaren quadrature mixer are connected to the **I IN** and **Q IN** inputs on the I/Q Correlator unit. The Inphase and Quadrature delay profile outputs from the correlator unit are connected to **Channel 0** and **Channel 1**, respectively, on the DAQ card.

10. The PCMCIA DAQ card should be inserted into the measurements laptop, and the LabVIEW Channel Sounder DAQ program should be opened. The DAQ program should be configured to display the received signal in real-time, causing a delay profile to appear on both the Inphase and Quadrature Waveforms (Figure C.5). Detailed operating instructions for the LabVIEW Channel Sounder DAQ program may be found in [58].

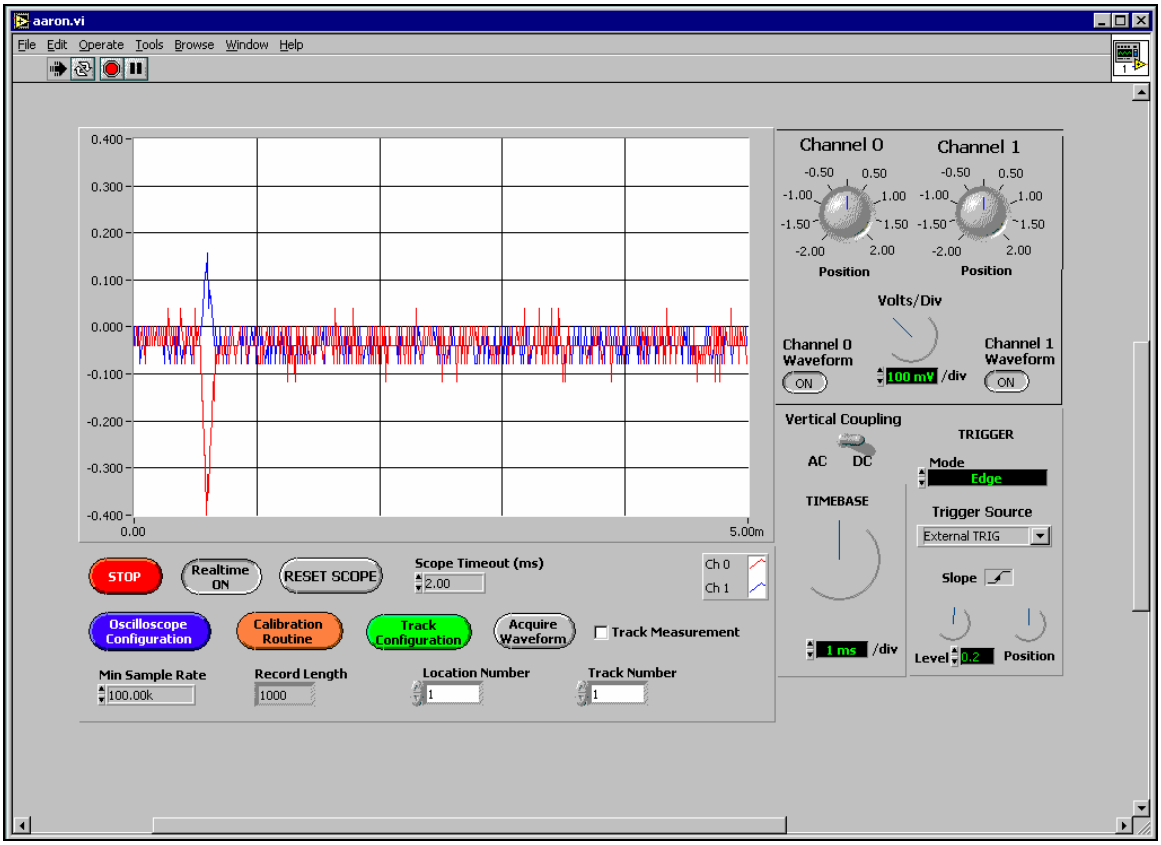

Figure C.5: Channel Sounder DAQ Program

For troubleshooting information, refer to Chapter 6—Measurement System Verification and Calibration.

C.2.1.3 Operating Instructions for the PN Clock Signal Generator

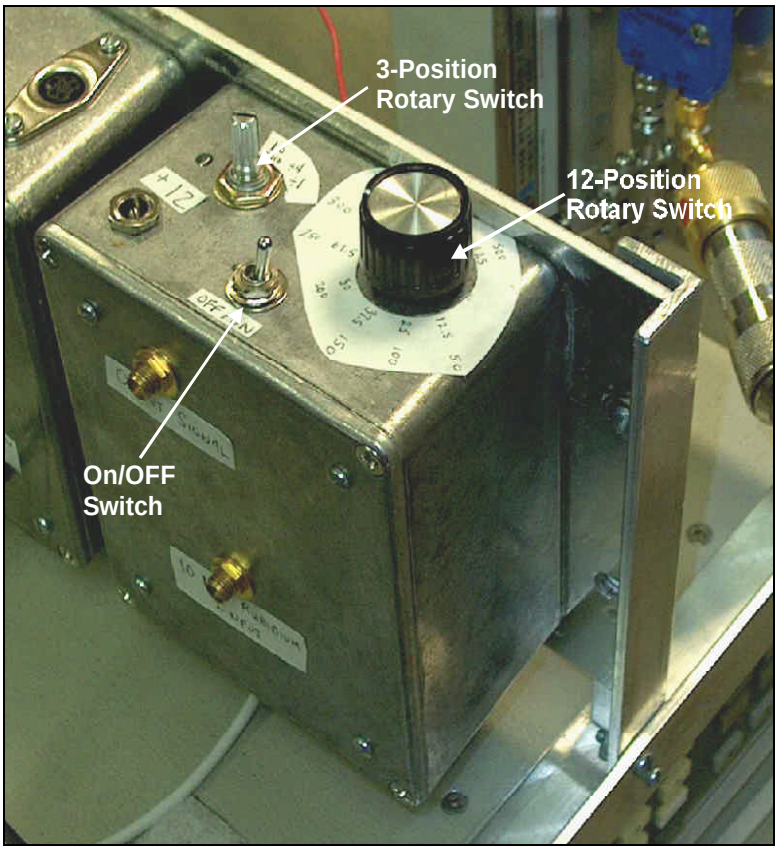

Figure C.6: PN Clock Signal Generator

1. Place the **ON/OFF** toggle switch in the *OFF* position. The **3-position Rotary Switch** is used to select the range of output frequencies. The first position, labeled *10 MHz*, selects the 10 MHz input signal. The second position, labeled *¸4* outputs frequencies in the range of 12.5 to 125 MHz. The third position, labeled *¸1*, outputs frequencies between 150 and 500 MHz. Based on the desired PN Clock frequency, place the rotary switch in the appropriate position.

2. The **12-position Rotary Switch** is used to select the exact frequency of the PN sequence. Each position of the rotary switch has two associated frequency labels. The inner label corresponds to the *¸4* setting of the **3-position Rotary Switch.** The outer label corresponds to the *¸1* setting of the **3-position Rotary Switch.** The **12-position Rotary Switch** is not used when the **3-position Rotary Switch** is placed in the *10 MHz*

position. For example, to set the output frequency at 150 MHz, place the **12-position Rotary Switch** in position 3, corresponding to an inner label reading of *37.5* and an outer label reading of *150*. Since the 150 MHz output is desired, place the **3-position Rotary Switch** in the ¸*1* position.

3. Place the **ON/OFF** toggle switch in the *ON* position. The selected frequency will be output on the **Output Signal** port.

C.2.2 Recording Calibration Measurements

Calibration measurements consist of recording a series of power delay profiles with different receiver attenuator settings at a single transmitter power. The calibration process is described in detail in Chapter 6 of this thesis. From the standpoint of operating the channel sounder, the two calibration methods—*Free Space* and *Cable Connected*—are essentially the same. The only difference is in the setup of the transmitter and receiver. For the Free Space method, the transmitter and receiver are placed a known difference apart in an environment that is free from multipath signals. In the Cable Connected method, the transmitter and receiver antennas are de-mounted and the RF output of the transmitter is connected—through a fixed attenuator—to the RF input of the receiver. Typically, the Free Space method is utilized when the channel sounder is operating at millimeter-wave frequencies and the Cable Connected method is used at lower cellular and PCS frequencies. Conceivably, the Cable Connected method could be used at millimeter wavelength frequencies provided that an appropriate waveguide attenuator is available. It is important to note that the transmitter power level used for calibration should remain constant throughout the measurements campaign, so that a correlation can be drawn between the transmitted and received signal powers.

Because the sliding correlator system may change slightly from one use to another, it is desirable to take calibration measurements as close to the actual time of measurement as possible in order to assure that the changes in the system have been minimal and the calibrated data accurately reflects reality.

After setting up the channel sounder, the GPS disciplined oscillators must be operated for a period of time sufficient to acquire and track as many satellites as possible, allowing the 10 MHz output to fully stabilize. The status of the oscillator can be monitored by connecting the serial port on the oscillator to the serial port on a laptop computer which is running the

StarLocII™ Operation and Management Software. The more satellites that a receiver can track, the less susceptible it will be to transient effects—such as loss of signal from one or more satellites.

When the GPS disciplined oscillators have stabilized, the following procedure should be followed to record calibration measurements (Refer to [58] for more detailed instructions regarding operation of the LabVIEW Channel Sounder DAQ software).

1. Press the **Calibration Routine** button on the front panel of the LabVIEW Channel Sounder DAQ program. This will bring up the *Calibration Configuration* screen (Figure C.7). Information relevant to the particular calibration run should be entered here.

    - **Calibration Directory Name –** the location on the hard drive where the calibration files will be stored.
    - **Effective Transmitter Power** – the power level at the output of the transmitter (at the base of the antenna), and should be measured with a power meter.
    - **Antenna Name –** The type of calibration being performed, either *Cable Connected* or *Free Space*.
    - **Notes/Comments –** Enter any notes or comments regarding the calibration run that may assist in analysis.

    Once the calibration configuration information is entered, press the **Continue** button, which will bring up the *Calibration Routine* screen (Figure C.8).

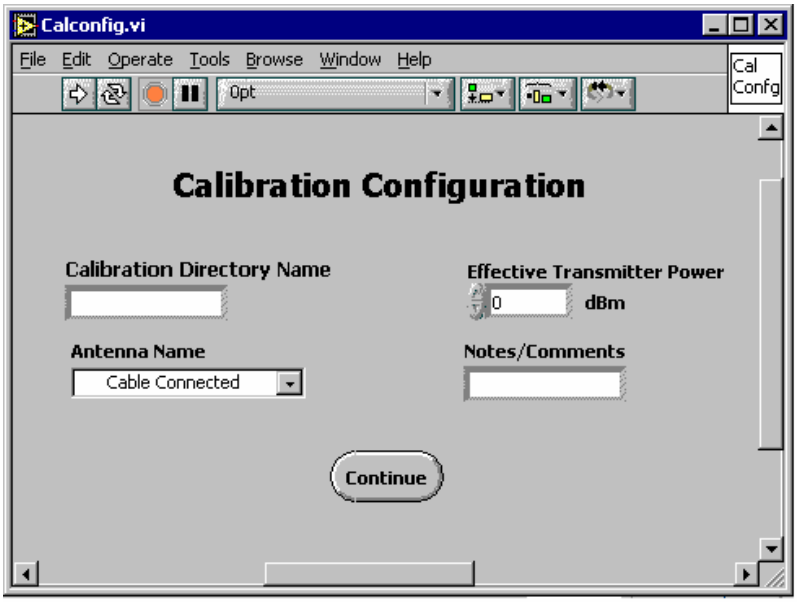

Figure C.7: Calibration Configuration Screen

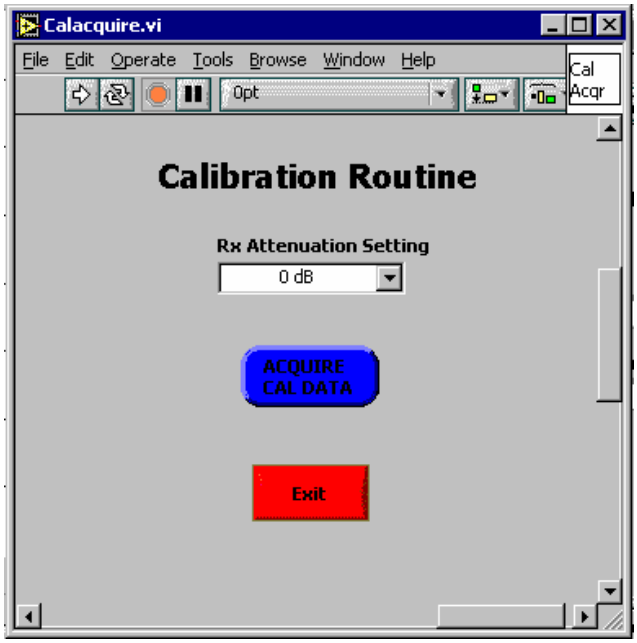

Figure C.8: Calibration Routine Screen

2. Under the *RX Attenuation Setting* listbox, select the number that corresponds to the attenuation setting on the Receiver's HP8495B Attenuator. Then, press the **Acquire CAL Data** button. The laptop will produce a tone when it has finished collecting data.

3. Increase the attenuation setting on the HP8495B Attenuator by 10 dB and repeat step 2. Continue this process until the received signal falls below the noise floor. Pressing the **Exit** button will terminate the calibration routine and save the recorded data to disk.

Calibration data is saved to disk in a series of files that correspond to the three-digit attenuation value, along with a log file *log.txt*. For example, a calibration sequence might contain the following files:

D:\60GHz Measurements\Calibration A\log.txt
D:\60GHz Measurements\Calibration A\010.txt
D:\60GHz Measurements\Calibration A\020.txt
D:\60GHz Measurements\Calibration A\030.txt
D:\60GHz Measurements\Calibration A\040.txt
D:\60GHz Measurements\Calibration A\050.txt

The log file contains all the information entered on the *Calibration Configuration* screen, and should look similar to the following:

```
Type                          = Calibration
Antenna Name                  = Cable Connected
Effective Transmitter Power   = 0 dBm
Minimum Receiver Attenuation  = 0 dB
Attenuation Step              = 10 dB
File Length                   = 1000 samples
Number of Attenuation Steps   = 6
Notes/Comments                = notes
```

Detailed information regarding the structure of the log and data files may be found in [65]. Post processing of the calibration data will be discussed in Section C.3.

C.2.3 Recording Propagation Measurements

Propagation measurements with the channel sounder can be as simple as setting up transmitter and receiver at a single location, or can involve multiple transmitter/receiver locations over an entire building, campus, or city. Prior to beginning measurements, a measurement plan must be drawn up, identifying desired transmitter and receiver placements as well as link budgets. The measurement plan will prevent haphazard measurements or selecting link distances that cause excessive signal attenuation. The receiver may be used with or without the linear positioning track to investigate channel properties over a small local area. If use of the track is desired, operating instructions are can found in [68]. Once the measurement plan is finished, channel measurements may be performed according to the procedure below.

1. Set up and power on the channel sounder according to the procedure in Section C.2.1. Ensure that the Transmitter PN Generator and TX PN Generator are synchronized. The *PN Synchronize cable* can now be disconnected and the Transmitter and Receiver can be moved to the appropriate positions.

2. Press the **Track Configuration** button on the front panel of the Channel Sounder DAQ Program. The *Track Configuration* screen will appear (Figure C.9). Ensure that the parameters entered on this screen are accurate; it is used by both the Channel Imaging Analysis Suite and the LabVIEW Data Postprocessing software to compute power delay profiles and statistical analysis of measured data. Incorrect information will result in erroneous analysis.

- **Carrier Frequency** – Enter the Channel Sounder's carrier frequency.
- **Channel Sounder Bandwidth** – Enter twice the Clock Rate of the PN Generator, equal to the RF Bandwidth of the Channel Sounder.
- **TR Separation Distance** – The distance between transmitter and receiver.
- **Receiver Location** – Indoor or Outdoor Receiver.
- **Transmitter Location** – Indoor or Outdoor Transmitter.
- **Track Orientation** – If using the track, it may be oriented parallel to the line-of-sight signal (i.e. incrementing the track position results in a linear increase in the transmitter-receiver separation distance) or perpendicular to the line-of-sight signal.
- **Effective Transmitter Power** – Enter the power level at the base of the transmitter antenna.
- **Transmitter Antenna Gain** – Enter the gain of the transmitter antenna.
- **Receiver Antenna Name** – Select the type of antenna attached to the receiver (Omnidirectional, Horn, etc.).
- **Calibration File Name** – Enter the directory name where the calibration file is stored, e.g. *cal_a*. Entering the entire directory name is not necessary.
- **Receiver Attenuation Setting** – Enter the attenuation setting of the HP8495B attenuator at the receiver.
- **Channel Sounder Slide Factor** – Enter the slide factor of the channel sounder, as calculated by Equation 2.25.
- **Number of Spatial Steps** – If the track is being used, enter the number of track positions at which power delay profiles will be recorded. If the track is not being used, leave the setting at zero.
- **Notes/Comments** – Enter any comments necessary to describe the particular setup being used or measurement being performed.

In the event that some parameters are unknown at the time of the measurements, enter a "best guess" and then adjust the values later by modifying the measurement log files. When finished, press the **Exit** button, and the configuration window will close.

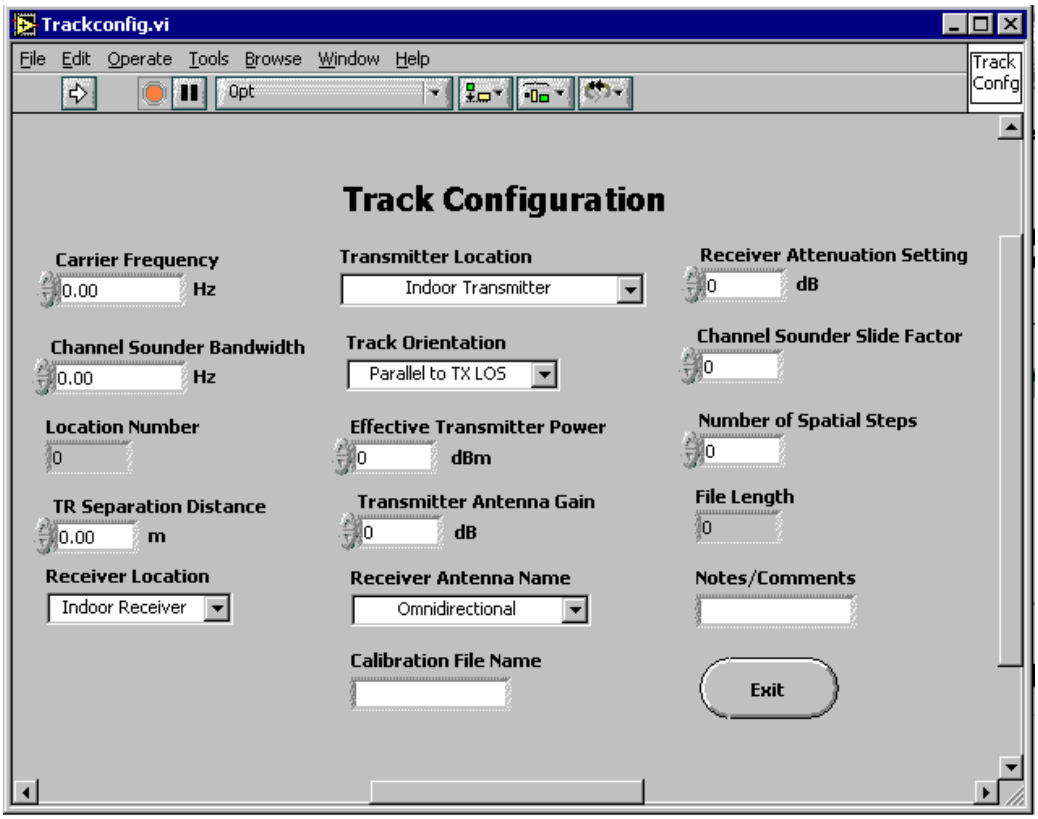

Figure C.9: Track Configuration Screen

3. On the *LabVIEW Channel Sounder DAQ* main screen, select the **Track Measurement** checkbox. The **Location Number** and **Track Number** controls are used to distinguish measurement runs. Location Number refers to a macroscopic receiver location—in an office, in a hallway, and outside a building would correspond to three different receiver locations. Track Number, on the other hand, refers to the microscopic receiver position along the linear positioning track—$\frac{l}{4}$, $\frac{l}{2}$, and $\frac{3l}{4}$ would correspond to three different track positions. If the track is not in use, the track number may be used to identify successive measurement runs at a particular location. PDPs recorded by the DAQ software will adhere to the following directory structure:

   C:\Home_directory\locXXX\trackYYY\Channel 0 PDPZ.txt
   C:\Home_directory\locXXX\trackYYY\Channel 1 PDPZ.txt

   Where *XXX* and *YYY* are the location and track numbers, respectively, entered on the front panel of the DAQ software, and *Z* corresponds to the file number when multiple PDPs are recorded at a given location/track position.

4. Press the **Acquire Waveform** button and the DAQ program will begin recording data to disk. A log file will also be recorded to disk, which will contain all the information entered on the *Calibration Configuration* screen, and should look similar to the following:

```
Date and Time                 = Fri 01 11 05:24:59 2002
Type                          = Track
Carrier Frequency             = 6.0E+10 Hz
Channel Sounder Bandwidth     = 800E+6 Hz
Location Number               = 1
TR Separation Distance        = 10.00 m
Transmitter Location          = 1
Receiver Location             = 1
Track Orientation             = transverse
Effective Transmitter Power   = 0 dBm
Transmitter Antenna Gain      = 3 dB
Receiver Antenna Name         = name
Receiver Attenuation Setting  = 0 dB
Channel Sounder Slide Factor  = 20000
Spatial Step Size             = 0.00125m
Number of Spatial Steps       = 20
File Length                   = 1000 samples
Sampling Period               = 1e-005 s
Calibration Name              = cal_a
Notes/Comments                = notes
PDP's                         = 25
Data Acquisition Time         = 20000 ms
```

5. When the DAQ program is finished recording PDPs, the Location Number and/or Track Number may be incremented and a new set of data recorded.

C.2.4 Reconfiguring the Channel Sounder for a Different Frequency or PN Code Length

C.2.4.1 Reconfiguring for a Different Frequency

The channel sounder was designed in such a way that reconfiguration for operation at a different frequency band would be a relatively simple, painless undertaking. To reconfigure the channel sounder for frequencies above 5.4 GHz, it is highly recommended to take advantage of the modularity of the channel sounder by designing and constructing new upconverters and downconverters, based on the specifications listed in Chapters 4 and 5. Implementing new up/downconverters leaves the IF and Baseband hardware of the channel sounder unchanged, meaning that the transition from one frequency to another is done by simply changing out the RF front end.

If it is desired to operate the channel sounder at a frequency below 5.4 GHz, the following subsystems must be changed out:

At the Transmitter

- Anaren 42020 Power Splitter (For frequencies below 2.5 GHz)
- Miteq DM0408LA1 Mixer

At the Receiver

- Magnum Microwave MDR-6000 DRO
- MiniCircuits ZN2PD-9G Power Splitter (For frequencies below 2.5 GHz)
- MiniCircuits ZVE-8G Amplifier (For frequencies below 2.5 GHz)
- Anaren 250127 Quadrature Mixer
- JCA 48-403 Low Noise Amplifier

Figures C.10 and C.11 are close-up images of the transmitter and receiver that indicates which subsystems must be replaced. It is important to note that any new subsystems must be capable of handling an 800 MHz IF/RF bandwidth, to accommodate the 400 MHz PN code. Additionally, system verification and calibration—detailed in Chapter 6—must be performed again to ensure that the reconfigured channel sounder meets or exceeds the performance specifications of the original channel sounder.

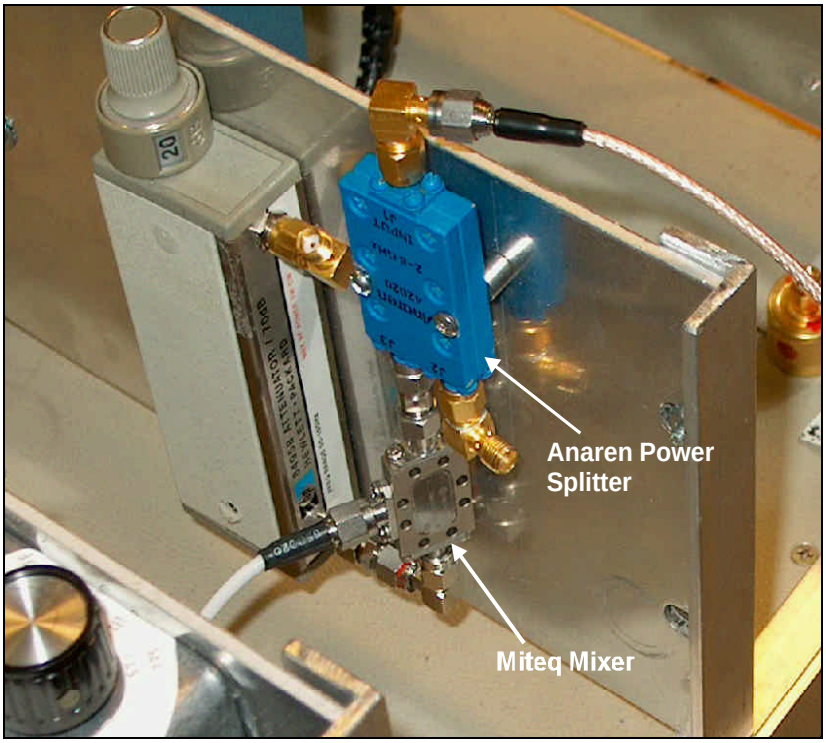

Figure C.10: Transmitter Close Up Image

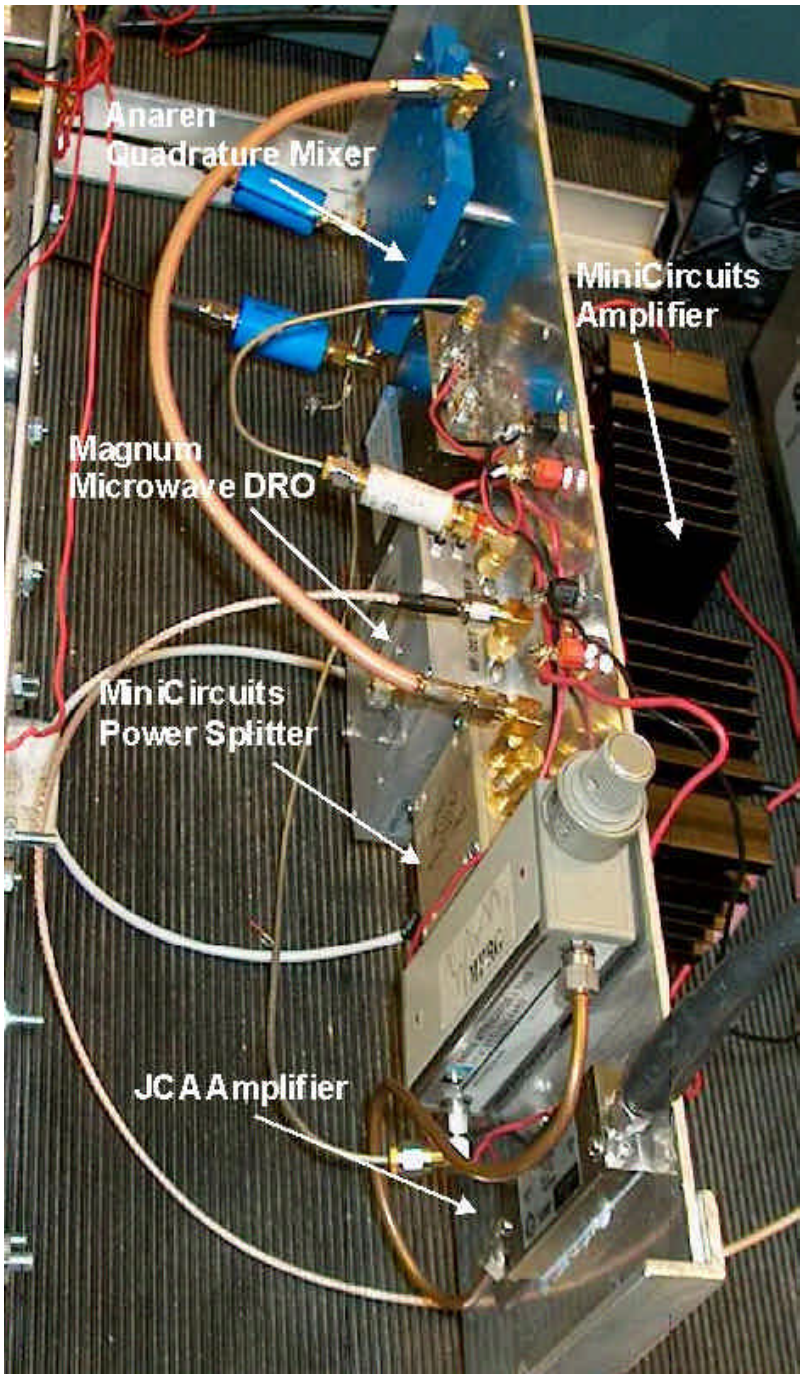

Figure C.11: Receiver Close Up Image

C.2.4.2 Reconfiguring for a Different PN Code Length

The channel sounder is capable of utilizing either an 11-bit PN Generator or an 18-bit PN Generator. For most purposes, the 11-bit PN Generator is adequate, however there may be situations where the use of the 18-bit version is desired. All three PN Generators on the channel

sounder (Transmitter, TX, and Receiver) must be changed out according to the following procedure.

Transmitter and TX PN Generator

1. Disconnect power from the PN Generator, also disconnect the PN Clock input and PN Output.

2. The front panel is held on by four retaining screws (Figure C.12) which must be removed.

Figure C.12: PN Signal Generator Front Panel Detail

3. Remove the front panel from the PN Generator housing. The PN Generator circuit board is attached directly to the front panel using four retaining nuts. Power and Run/Stop wires connect the circuit board to the housing (Figure C.13).

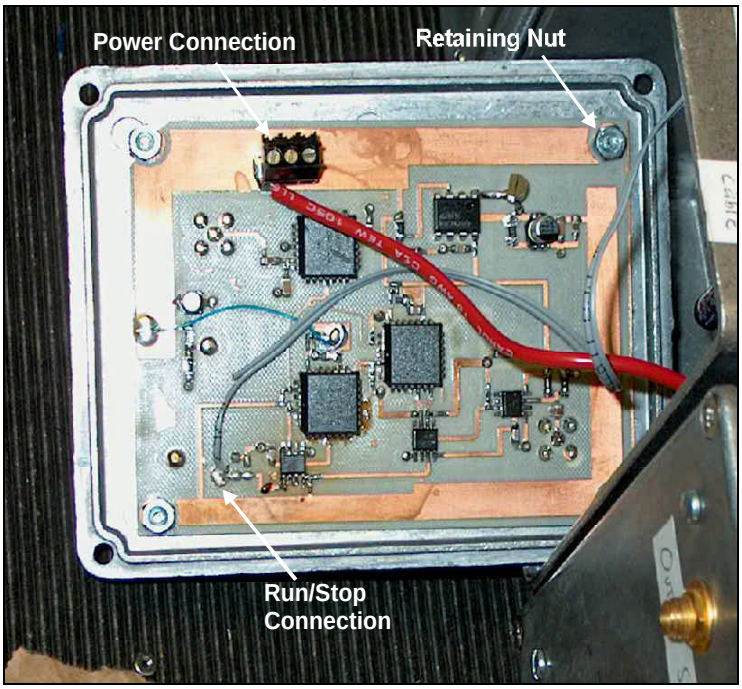

Figure C.13: PN Signal Generator Circuit Board and Connections

4. The power wire is held in place by a set screw, loosen the set screw and remove the power wire from the board. The Run/Stop wire is soldered directly to the circuit board, this wire should be carefully desoldered. Remove the four retaining nuts and separate the circuit board from the front panel.

5. Installation of the 18-bit PN Generator is accomplished by reversing steps 1-4.

Receiver PN Generator

1. Follow steps 1 and 2 for the Transmitter and TX PN Generator.

2. Remove the front panel from the PN Generator housing. The PN Generator circuit board is attached to the front panel, and the Trigger Pulse Generator board is attached as a daughterboard (Figure C.14). The PN Generator Board is connected to the housing with a power wire and Run/Stop wire. The Trigger Pulse Generator board is connect to the housing with the 12 Volt Power, TX PN, and Sync Out wires. The PN Generator board and Trigger Pulse Generator board are connected together through the RX PN wire and 5 Volt power jumper (Figure C.14).

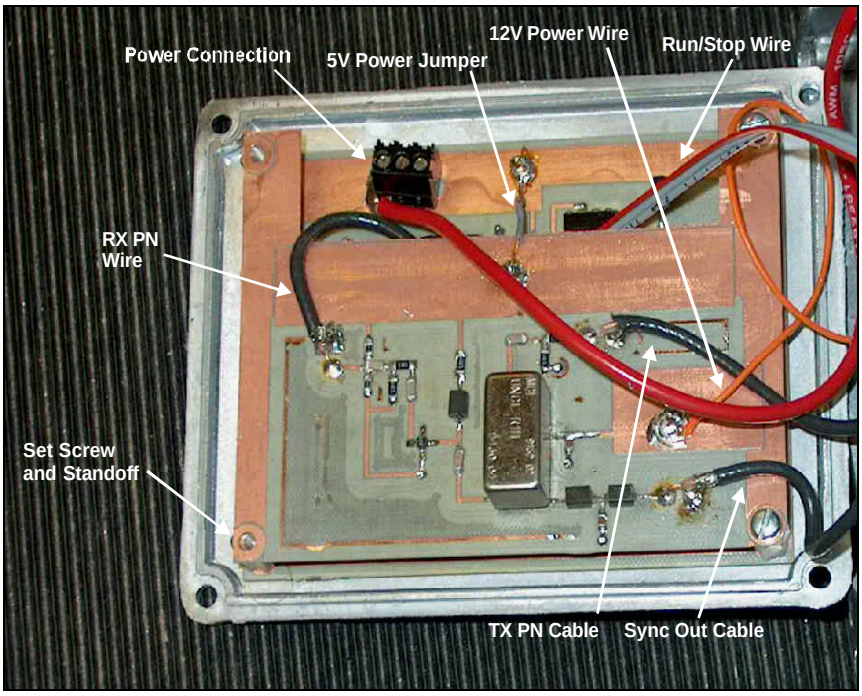

Figure C.14: Receiver PN Generator and Trigger Pulse Generator Boards

3. The power wire is held in place by a set screw; loosen the set screw and remove the power wire from the board. Deslolder the 5V Power Jumper wire from the PN Generator board (Figure C.15).

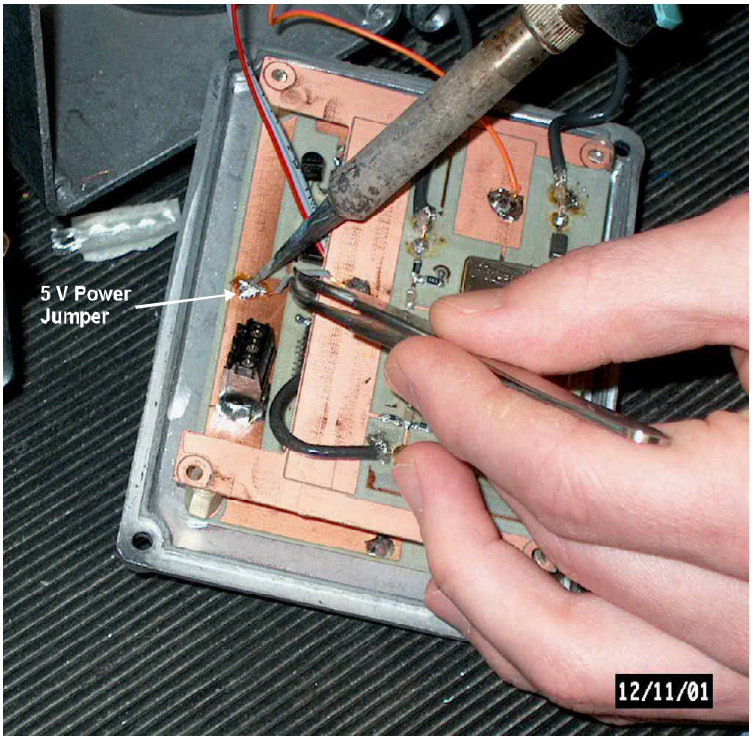

Figure C.15: Desoldering the 5V Power Jumper

4. Remove the four set screws holding the Trigger Pulse Generator board. Carefully lift the board up and move it to the side. Desolder the RX PN and Run/Stop wires from the PN Generator board (Figure C.16). **The Run/Stop wires are soldered to three different pads on the PN Generator Board—take note of which pad each wire is connected to.**

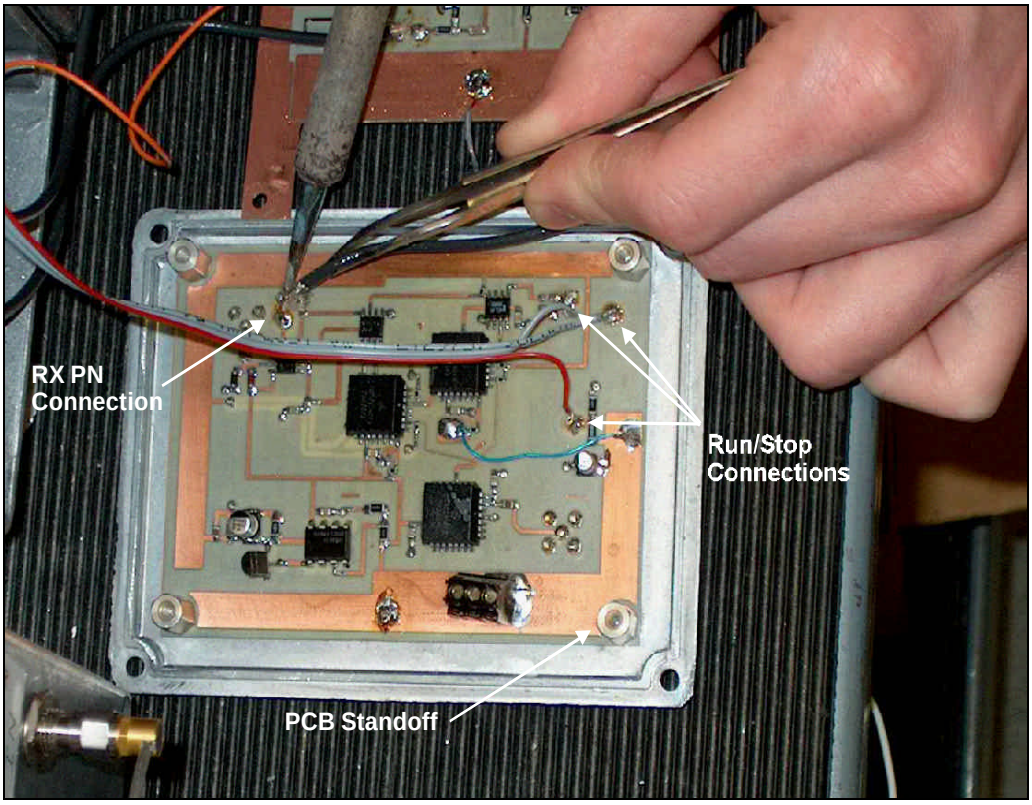

Figure C.16: Desoldering RX PN and Run/Stop Wires

5. The PN Generator board is held in place by four PCB standoffs. Remove the four standoffs and separate the circuit board from the front panel.

6. Installation of the 18-bit PN Generator is accomplished by reversing steps 1-5.

C.3 LabVIEW Data Analysis Software

The LabVIEW Analysis software is a tool for generating and viewing power delay profiles, multipath phase plots, and Doppler spectrum from measured inphase and quadrature delay profiles recorded by the Channel Sounder DAQ program. A screen shot of the ***Analysis Main Screen*** is shown in Figure C.17, along with a brief overview of the different routines that may be run from within this program. Next is a step-by-step guide for using the Analysis software to process and display measured data.

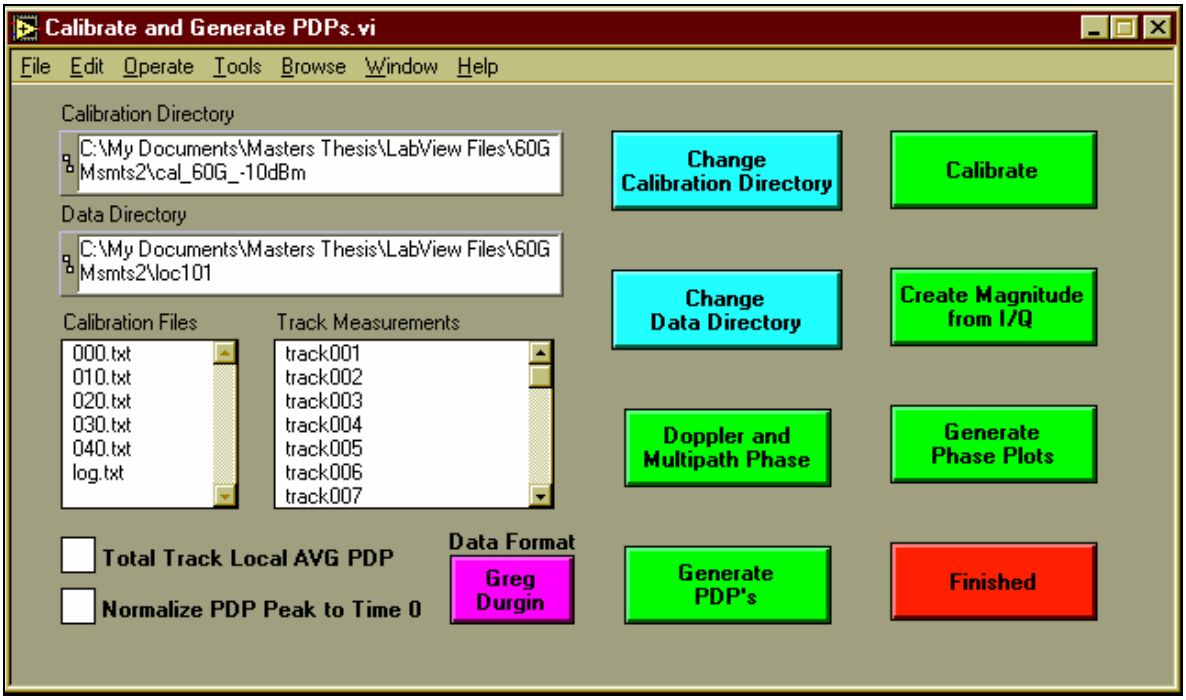

Figure C.17: LabVIEW Analysis Software Main Screen

- **Change Calibration Directory** – Changes to the directory in which calibration files are stored.
- **Change Data Directory** – Changes to the directory in which track measurement files are stored.
- **Doppler and Multipath Phase** – Generates Doppler Spectra and multipath phase angle vs. time graphs.
- **Generate PDP's** – Generates and plots Power Delay Profiles.
- **Create Magnitude from I/Q** – Creates a single waveform representing the magnitude of the channel impulse response from the Inphase and Quadrature delay profiles the DAQ software records to disk.
- **Generate Phase Plots** – Generates multipath phase plots showing the phase angle of the line-of-sight and multipath signals.
- **Total Track Local Average PDP** – Linearly averages all delay profiles in selected track directories into a single aggregate Power Delay Profile.
- **Normalize PDP Peak to Time 0** – Sets the peak of the Power Delay Profile to correspond to 0 on the time axis, so that multipath may be viewed in terms of excess delay.

- **Data Format** – Toggles the way the software processes measurement and calibration data files. Two choices are available *Greg Durgin* and *Aaron Orndorff*. The *Greg Durgin* format is used when delay profiles are recorded using the *MPRG Channel Imaging Software* written by Durgin/Xu/Kukshya. The *Aaron Orndorff* is used when delay profiles are recorded using the *LabVIEW Channel Sounder DAQ* software written by Orndorff.
- **Finished** – Exits the program.

C.3.1 Calibration

Prior to processing measurement data, calibration coefficients must be determined by the software. These coefficients allow the recorded voltage levels to be mapped into power levels, as detailed in Chapter 6.

1. Press the **Change Calibration Directory** button. A selection box will pop up and ask for the directory where calibration measurement files are recorded (Figure C.18). Change to the directory where the calibration files are stored and then press **Select Cur Dir**. The directory path will appear on the ***Analysis Main Screen*** in the box labeled *Calibration Directory.* Additionally, the list of data files in the calibration directory will appear in the listbox labeled *Calibration Files.*

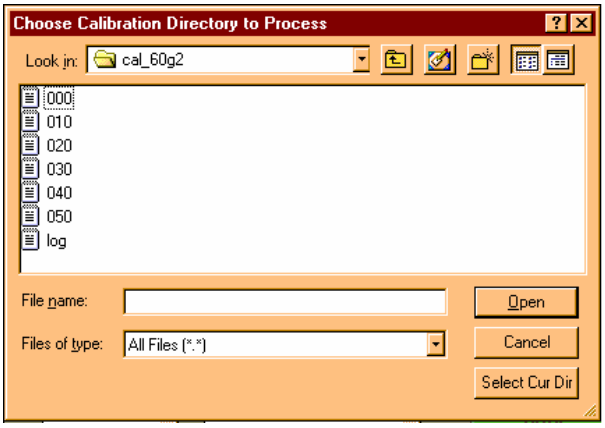

Figure C.18: Select Directory Containing Calibration Files

2. On the Analysis program main screen, press the **Calibrate** button, which will bring up the ***Channel Sounder Calibration Plot*** screen (Figure C.19). On the Calibration screen, the transmitter power (as recorded in the log file) is displayed in the lower left hand corner. The graph plots receiver attenuation settings vs. received voltage (in dBV).

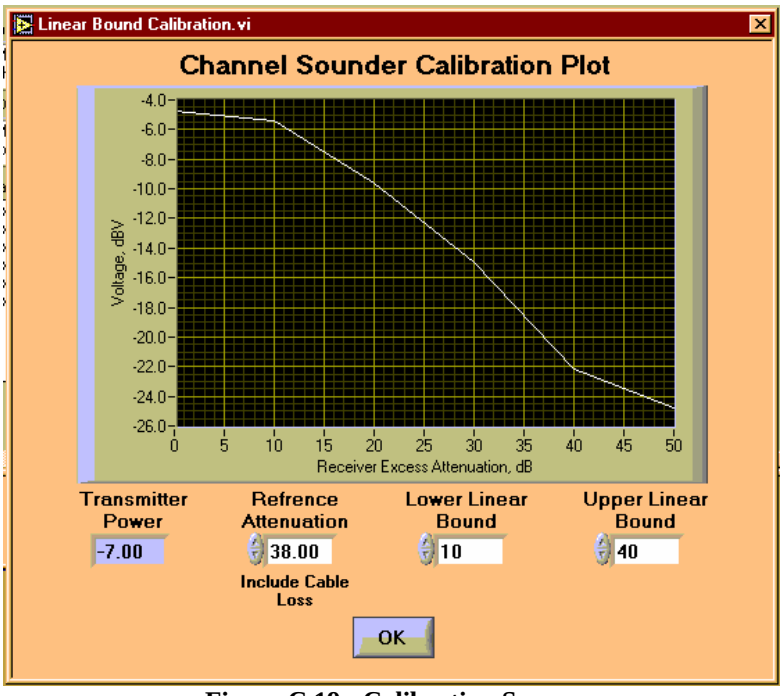

Figure C.19: Calibration Screen

3. Under *Reference Attenuation*, enter the value of attenuation placed between transmitter and receiver. In the case of a Cable Connected calibration, the Reference Attenuation would be the value of the fixed attenuator used, along with any cable loss. For Free-Space Calibration, the Reference Attenuation would be the free-space path loss experienced between transmitter and receiver (including antenna gains).

4. It is important to identify the channel sounder's linear operation region in order to accurately determine the received power of a signal. For the *Lower Linear Bound*, enter the Receiver Excess Attenuation level after which the plot assumes a linear downward slope. For the *Upper Linear Bound*, enter the Receiver Excess Attenuation level at which the slope of the plot begins to level out towards a slope of zero. Press the **OK** button, and the window will close and program control will be returned to the ***Analysis Main Screen***.

**** Note: The calibration plot may not be exactly 100% linear (as in Figure C.19), however, calibration will still work if the plot is approximately linear. In this case, a comparison should be made between the actual received power levels and the received power levels as calculated by the linear regression (Section 6.4.1 and Figure 6.13).**

C.3.2 Power Delay Profiles

Once the calibration coefficients have been determined, power delay profiles may be generated from recorded measurement data using the following procedure.

1. Press the **Change Data Directory** button. A selection box will pop up and ask for the directory where track measurement files are recorded (Figure C.20). Change to the Location directory where the track measurement files are stored and then press **Select Cur Dir**. The directory path will appear on the ***Analysis Main Screen*** in the box labeled *Data Directory.* Additionally, the list of track directories will appear in the listbox labeled *Track Measurements.*

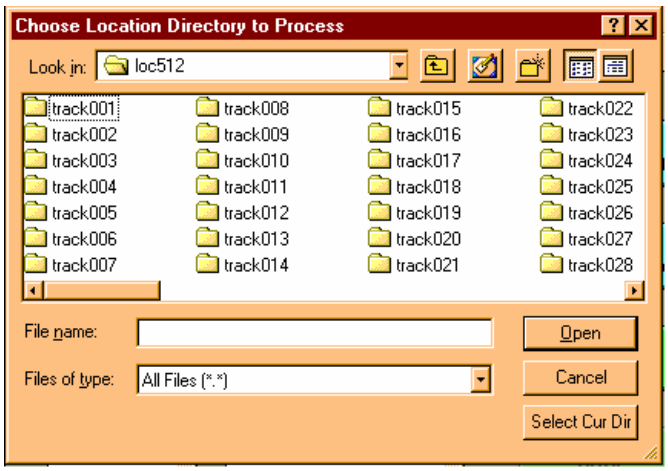

Figure C.20: Select Directory Containing Track Measurements

2. Under the *Track Measurements* listbox, select the track directories to process. Multiple track directories may be selected by holding down the "shift" key. Press the **Create Magnitude from I/Q** button. This operation will read in the inphase and quadrature delay profiles from disk, generate a magnitude delay profile, and save the magnitude delay profile to disk. The files will be numerically named starting with one and counting up to the total number of delay profiles contained in the track directory. For example, some of the files in a measurement might be the following.

D:\60GHz Measurements\loc512\track004\001.txt
D:\60GHz Measurements\loc512\track004\002.txt
D:\60GHz Measurements\loc512\track004\003.txt
D:\60GHz Measurements\loc512\track004\004.txt
D:\60GHz Measurements\loc512\track004\005.txt

3. When the magnitude files have been saved to disk, program control will return to the ***Analysis Main Screen***. At this point, press the **Generate PDP's** button. A progress bar will pop up, indicating that the program is reading in the magnitude delay profiles and generating Power Delay Profiles using the previously defined calibration coefficients. When the progress bar closes, the ***Plot PDP's*** screen will appear (Figure C.21).

Figure C.21: Plot PDPs Screen

4. The upper left-hand corner of the ***Plot PDP's*** screen will show the location and track number of the Local Average Power Delay Profile currently being displayed (the program reads in all measurements in a selected track directory, averages them, and displays the result as a Local Average PDP). The upper right-hand corner will display the peak power level in the PDP.

5. To save a particular PDP to disk, press the blue button labled **Save To Disk**. A file dialog box will pop up asking for a directory and filename. The default filename (*locXXXtrackyy Local Average PDP*) can either be accepted or a new one may be entered.

6. If multiple track directories were selected, the green button will read **Next PDP**, and pressing it will show the next PDP in the sequence of those selected. When the end of

the sequence is reaced, the button will read **Finished** and pressing it will close the screen and return control to the ***Analysis Main Screen***. Pressing the red **Abort** button will also close the screen and return control to the ***Analysis Main Screen***.

C.3.3 Doppler and Multipath Phase

1. Press the **Doppler and Multipath Phase** button. The ***Doppler Array*** screen will appear (Figure C.22).

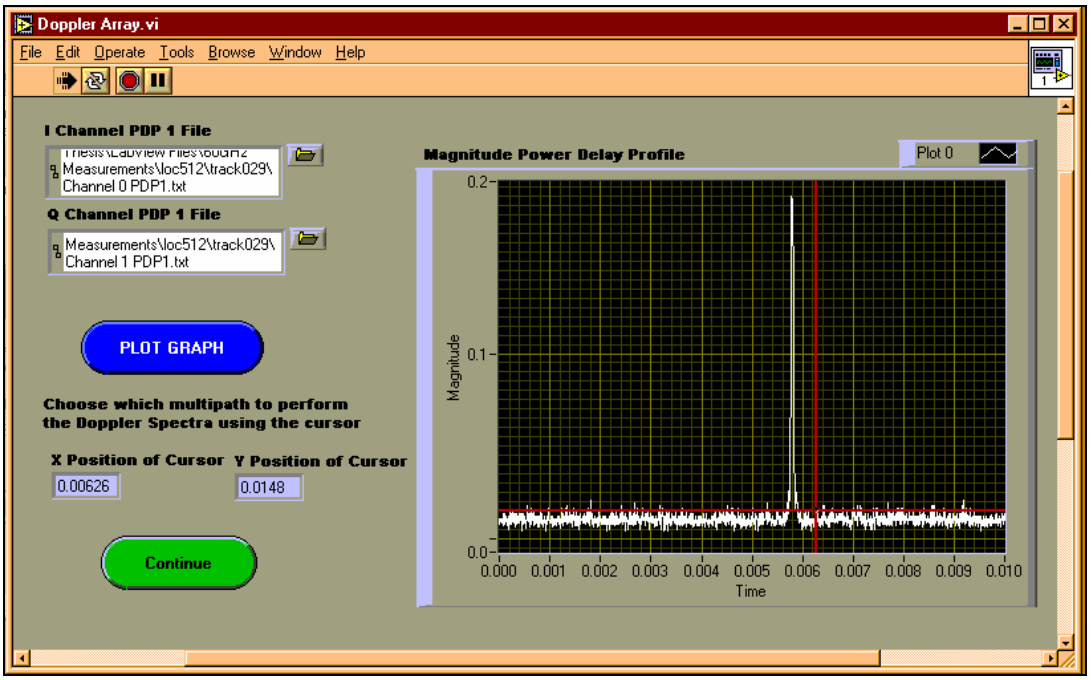

Figure C.22: Doppler Array Screen

2. Click on the folder icon next to the *I Channel PDP 1* box. A file dialog will appear similar to Figure C.23. Change to the desired Location and Track directory, and select the file named *Channel 0 PDP1.txt* and press **Open.** Repeat this process for the *Q Channel PDP 1* box, except select the file named *Channel 1 PDP1.txt*

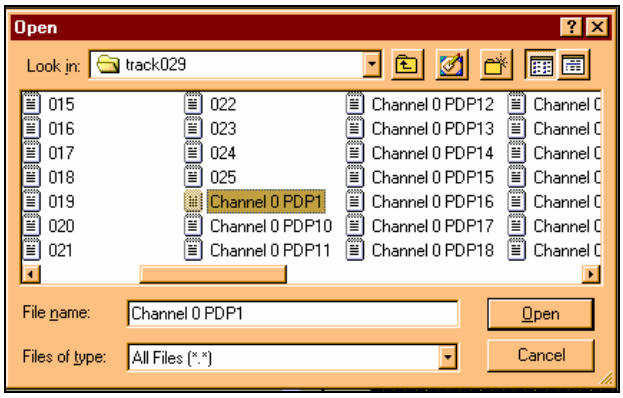

Figure C.23: Doppler Array File Dialog

3. When both files have been selected, press the **Plot Graph** button. The magnitude delay profile—formed by taking the sum of the squares of the selected inphase and quadrature waveforms—will appear in the graph labeled *Magnitude Power Delay Profile.* Using the red cursor, select the peak of the multipath on which to perform Doppler spectra analysis. The value of the excess delay, or x-position of the cursor, is displayed with an indicator, along with the magnitude, or y-position, to allow the user to select a point with the highest magnitude.

4. Once the cursor is placed in the correct position, press the **Continue** button

5. A progress bar will appear on the screen, as the program reads in inphase and quadrature delay profiles in the selected directory and generates the Doppler spectrum.

6. When the program has completed processing, the ***Doppler*** screen will appear (Figure C.24). The switch at the upper left of the screen will select which plot appears in the graph at the right, either the Doppler Spectrum or Phase Change Over Time. The Phase Change Over Time graph is used to view the phase change of the selected multipath component over time. As discussed in Chapter 3, the measurement system will experience a certain amount of phase drift; this graph can be used to observe exactly how much phase drift was experienced. Alternatively, the Phase Change Over Time plot may be used to analyze the phase change of a multipath signal in a dynamic environment.

7. When the switch is in the desired position, press the **Plot Graph** button, and the graph will appear to the right.

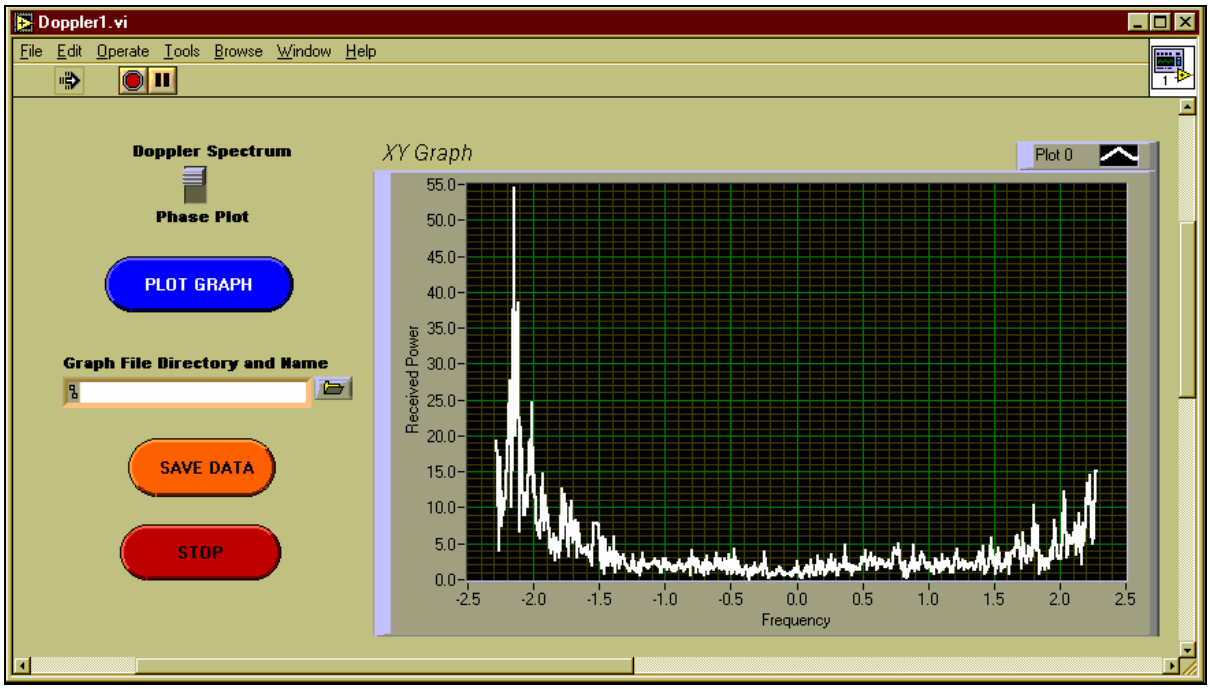

Figure C.24: Doppler and Phase Over Time Screen

8. To save the Doppler Spectrum or Phase Plot waveform to disk, click on the folder icon underneath the *Graph File Directory and Name* box. A file dialog will appear—change to the desired directory where the data is to be saved and enter a filename and press **Save**. Then, press the orange **Save Data** button on the ***Doppler*** screen to record the data to disk.

9. When finished, press the red **Stop** button, and program control will be returned to the ***Analysis Main Screen***.

C.3.4 Delay Profile Phase Plots

1. Press the **Generate Phase Plots** button. The ***Phase*** screen will appear (Figure C.25).

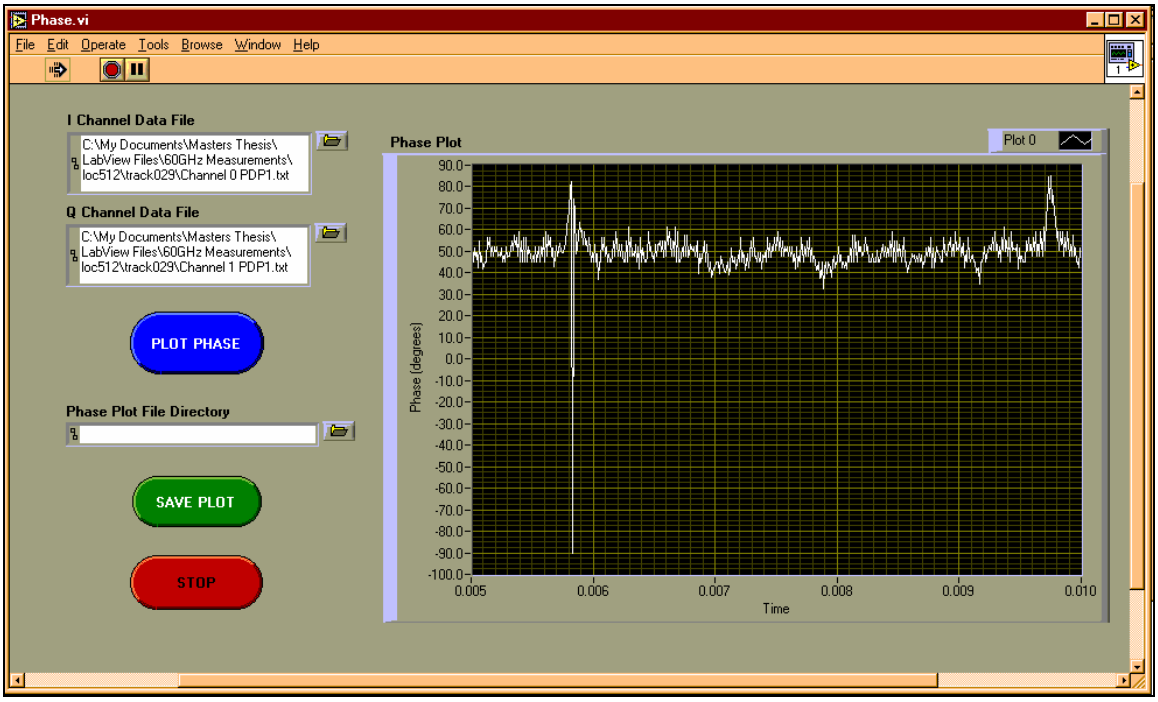

Figure C.25: Phase Screen

2. Click on the folder icon next to the *I Channel Data File* box. A file dialog will appear similar to Figure C.26. Change to the desired Location and Track directory, and select the file named *Channel 0 PDPZ.txt* (where *Z* corresponds to the number of the delay profile to be viewed) and press **Open.** Repeat this process for the *Q Channel Data File* box, except select the file named *Channel 1 PDPZ.txt*

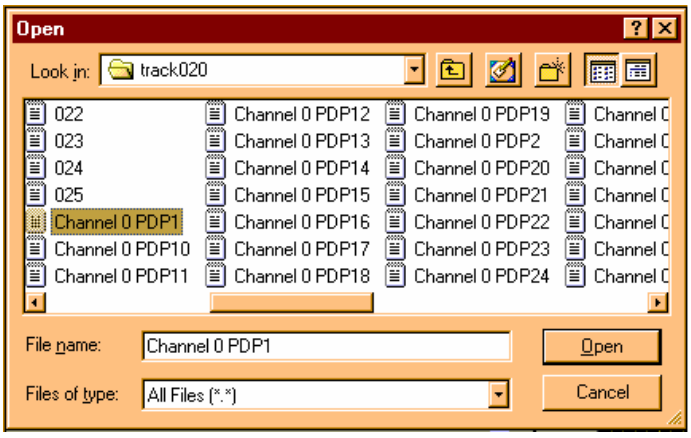

Figure C.26: Phase Screen Dialog Box

3. Press the **Plot Phase** button. On the graph to the right, the phase of the delay profile over time will appear. This graph allows phase change from one multipath signal to another to be analyzed, in addition to allowing signals closely spaced in time to be differentiated based on their respective phase.

4. To save the delay profile phase waveform to disk, click on the folder icon underneath the *Phase Plot File Directory* box. A file dialog will appear—change to the desired directory where the data is to be saved and enter a filename and press **Save**. Then, press the orange **Save Plot** button on the ***Phase*** screen to record the data to disk.

5. When finished, press the red **Stop** button, and program control will be returned to the ***Analysis Main Screen***.

Appendix D

Measurement Data and Source Code File Listing

All data and source code files are stored on *MPRGWEB*, the MPRG Windows 2000 Network File Server, under the user directory named *chanders*.

D.1 Data Files Related to Measurements

D.1.1 2.5 GHz Measurement Data Files

Raw data files for the 2.5 GHz measurements are stored with the following directory format:

\Masters Thesis\2_5 GHz\2_5 GHz Measurements\locXXX\track1\YYY.txt

XXX represents the measurement location. The first digit is the series number, the second digit is a 0 if the data was from a parallel and is a 1 if the data is from a perpendicular track measurement, and the third digit represents the receiver location in the measurement. For example, ***loc102*** means the measurement data comes from the 1-series, with receiver location number 2 (i.e. measurement location 1.2), and the data is from a parallel track measurement.

YYY.txt is the raw measurement data recorded from a particular track position, and is a temporal average of 10 Delay Profiles recorded at that position. The data files are in a Comma Separated Values (CSV) format, where the first column is time in seconds, and the second column is waveform amplitude in Volts. Each track position represents a physical distance the

receiver antenna has traveled along the track, therefore multiply the track position by $\frac{l}{4}$ to obtain the total distance traveled from the end of the track. For example, ***012.txt*** is the Delay Profile recorded from track position number 12, and has traveled $3l$ from the end of the track.

The directory ***\Masters Thesis\2_5 GHz\2_5 GHz Measurements\loc999\cal_a*** contains the calibration files necessary to transform the raw measurement data into meaningful Power Delay Profiles using the LabVIEW software (See Appendix C). A Reference Attenuation of 50 dB was used during the calibration.

Processed measurement data are stored with the following directory format:

\Masters Thesis\2_5 GHz\2_5 GHz PDP\locXXX Local Average PDP.txt

XXX represents the location number as discussed above. These data files are in a Comma Separated Values (CSV) format, where the first column is excess delay in seconds, and the second column is received power in dBm.

D.1.2 60 GHz Measurement Data Files

Raw data files for the 2.5 GHz measurements are stored with the following directory format:

\Masters Thesis\60 GHz\60 GHz Measurements\locAAA\trackBBB\CCC.txt

AAA represents the measurement location. The first digit is the series number, and and the third digit represents the receiver location in the measurement. The second digit is a 0 if the data was from a $10l$ parallel track measurement, a 1 if the data is from a $10l$ perpendicular track measurement, a 2 if the data is from a ½ meter parallel track measurement, and a 3 if the data is from a ½ meter perpendicular track measurement. For example, ***loc102*** means the measurement data comes from the 1-series, with receiver location number 2 (i.e. measurement location 1.2), and the data is from a $10l$ parallel track measurement; ***loc532*** means the measurement data comes from the 5-series, receiver location number 2 (i.e. measurement location 5.2), and the data is from a ½ meter perpendicular track measurement.

BBB represents the track position at which measurement data was recorded. In this directory are ten Delay Profiles that were recorded at that particular track position. As with the 2.5 GHz measurements, each track position represents a physical distance the receiver antenna has traveled along the track. For the 10λ track measurements, multiply the track position by $\frac{\lambda}{4}$ to obtain the total distance traveled from the end of the track. For the ½ meter track measurements, multiply the track position by 10λ to obtain the total distance traveled from the end of the track.

CCC.txt is the raw measurement data recorded at a particular track position. The data files are in a Comma Separated Values (CSV) format, where the first column is time in seconds, and the second column is waveform amplitude in Volts. Ten Delay Profiles were recorded sequentially at each track position, and is represented by the value of ***CCC***. For example, ***008.txt*** is the 8th Delay Profile recorded at a particular track position. These ten delay profiles can be linearly averaged together to form a temporal average Delay Profile for a particular track position.

The directory:
\Masters Thesis\60 GHz\60 GHz Measurements\cal_60G_-10dBm contains the calibration files necessary to transform the raw measurement data into meaningful Power Delay Profiles using the LabVIEW software (See Appendix C). A Reference Attenuation of 35 dB was used during the calibration.

Processed measurement data are stored with the following directory format:
\Masters Thesis\60 GHz\2_5 GHz PDP\locAAA Local Average PDP.txt

AAA represents the location number as discussed above. These data files are in a Comma Separated Values (CSV) format, where the first column is excess delay in seconds, and the second column is received power in dBm.

D.2 LabVIEW Analysis Software Source Code Files

The following is a listing of files required to run the **LabVIEW Analysis Software**, which are located in the ***\Masters Thesis\LabVIEW Files*** directory. The top-level VI is *Calibrate and Generate PDPs.vi*, and may be compiled and run in LabVIEW Version 6i.

Average Track PDP Measurements.vi
Blackman Window.vi
Blackman-Harris Window.vi
Calibrate and Generate PDPs.vi
Close File+.vi
Close Panel.vi
Complex FFT.vi
Create Magnitude.vi
Doppler Array.vi
doppler progress cra.vi
Doppler1.vi
Exact Blackman Window.vi
FFT Power Spectral Density.vi
FFT Power Spectrum.vi
FFT Spectrum (Mag-Phase).vi
Find First Error.vi
Flat Top Window.vi
General Cosine Window.vi
General Error Handler.vi
Generate Calibrated PDP's from Voltage.vi
Get Track Log Data.vi
Hamming Window.vi
Hanning Window.vi
Large Scale Fading.vi
Linear Bound Calibration.vi
Linear Fit Coefficients.vi
ma_Check Block Size.vi
ma_Convert Phase.vi
ma_Convert to dB.vi
ma_Convert to One-Sided Spectrum (complex).vi
ma_Convert to One-Sided Spectrum (real).vi
ma_Force Restart.vi
ma_Linear Averaging Done.vi
ma_One Sided FFT Spectrum.vi
ma_One Sided Power Spectrum.vi
ma_Spectrum Averaging (complex).vi
ma_Spectrum Averaging (real).vi

ma_Spectrum Peak Hold.vi
Mean.vi
Merge Errors.vi
Open File+.vi
Open_Create_Replace File.vi
Phase.vi
Plot PDP's.vi
Power Spectrum.vi
Progress Bar.vi
Read Characters From File.vi
Read File+ (string).vi
Read From Spreadsheet File.vi
Read Lines From File.vi
Real FFT.vi
Scaled Time Domain Window.vi
Scaled Window for 1 Chan.vi
Scaled Window for N Chan.vi
Scaled Window.vi
StringSpacing.vi
Unwrap Phase.vi
Which Button.vi
Write File+ (string).vi
Write To Spreadsheet File.vi

References

[1] K. Siwak and P. Withnington II, "Ultrawideband radios set to play," *Electronic EngineeringTimes*, pp. 92 & 114, February 26, 2001.

[2] W. G. Newhall, T. S. Rappaport, and D. G. Sweeney, "A Spread Spectrum Sliding Correlator System for Propagation Measurements," *RF Design*, pp 40-54, April 1996.

[3] R. C. Dixon, *Spread Spectrum Systems*, 2nd Edition. New York: John Wiley and Sons Inc., 1984.

[4] P. Mannion, "Commercialize 94 GHz, FCC Asked," *Electronic Engineering Times*, pp. 55-56, May 7, 2001.

[5] T. Manabe, K. Sato, H. Masuzawa, K. Taira, T. Ihara, Y. Kasashima, and K. Yamaki, "Polarization Dependence of Multipath Propagation and High-Speed Transmission Characteristics of Indoor Millimeter-Wave Channel at 60 GHz," *IEEE Transactions on Vehicular Technology*, vol. 44 No. 2, May 1995.

[6] C. R. Anderson, "A 500 MHz PN Generator," Undergraduate Honors Thesis, MPRG TR-99-12, Virginia Polytechnic Institute and State University, December 1999.

[7] D. C. Cox, "Delay Doppler characteristics of multipath delay spread and average excess delay for 910 MHz urban mobile radio paths," *IEEE Transactions on Antennas and Propagation*, vol. AP-20, No. 5, pp. 625-635, 1972.

[8] N. Patwari, "Measured and Modeled Time and Angle Dispersion Characteristics of the 1.8 GHz Peer-to-Peer Radio Channel," Masters Thesis, MPRG-TR-99-03, Virginia Polytechnic Institute and State University, http://scholar.lib.vt.edu/theses/index.html, May 1999.

[9] A. J. Viterbi, *CDMA Principles of Spread Spectrum Communication*, Massachusetts: Addison-Wesley, 1995.

[10] W. G. Newhall, "Wideband Propagation Measurement Results, Simulation Models, and Processing Techniques for a Sliding Correlator Measurement System," Masters Thesis, MPRG-TR-97-19, Virginia Polytechnic Institute and State University, November 1997.

[11] D. K. Lindner, *Introduction to Signals and Systems*. New York: McGraw-Hill, 1999.

[12] T. S. Rappaport, *Wireless Communications: Principles and Practice*, 2nd Edition. New Jersey: Prentice-Hall, 2002.

[13] W. G. Newhall, K. Saldanha, and T. S. Rappaport, "Using RF Channel Sounding Measurements to Determine Delay Spread and Path Loss," *RF Design*, vol. 19 No. 1, January 1996.

[14] W. C. Y. Lee, "Overview of Cellular CDMA," *IEEE Transactions on Vehicular Technology*, vol. 40, No. 2, May 1991.

[15] Federal Standard 1037C, "Telecommunications: Glossary of Telecommunication Terms," http://www.its.bldrdoc.gov/fs-1037/, August 7, 1996.

[16] M. Z. Win, F. Ramirez-Mireles, and R. A. Scholtz, "Ultra-Wide Bandwidth (UWB) Signal Propagation for Outdoor Wireless Communications," *IEEE 47th Vehicular Technology Conference*, vol. 1, pp. 251-255, 1997.

[17] J. D. Parsons, D. A. Demery, A. M. D. Turkamani, "Sounding Techniques for Wideband Mobile Radio Channels: A Review," *IEE Proceedings*, vol. 138, no. 5, pp. 437-446, October 1992.

[18] A. Affandi, G. El Zein, J. Citerne, "Investigation on Frequency Dependence of Indoor Radio Propagation Parameters," *IEEE 50th Vehicular Technology Conference*, vol. 4, pp. 1988-1992, 1999.

[19] K. Sohrabi, B. Manriquez, G. J. Pottie, "Near Ground Wideband Channel Measurement in 800-1000 MHz," *IEEE 49th Vehicular Technology Conference*, vol. 1, pp. 571-574, 1999.

[20] S. Y. Tan, M. Y. Tan, and H. S. Tan, "Multipath Delay Measurements and Modeling for Interfloor Wireless Communictions," *IEEE Transactions on Vehicular Technology*, vol. 49, issue 4, pp. 1334-1341, July 2000.

[21] A. G. Siamarou, "Wireless Mobile and Personal Broadband Communications: From Myth to Reality!," *Institution of Electrical Engineers*, http://centres.iee.org/Younger/Premiums/writ2000/writ2000.pdf, 2001.

[22] H. Hashemi, "The Indoor Propagation Channel," *IEEE Proceedings*, vol. 81, issue 7, pp. 943-968, July 1993.

[23] A. M. Saleh and R. A. Valenzuela, "A Statistical Model for the Indoor Multipath Propagation," *IEEE Journal on Selected Areas in Communications*, vol. SAC-5, No. 2, pp. 128-137, February 1987.

[24] V. Erceg, D. G. Michelson, S. S. Ghassemzadeh, L. J. Greenstein, A. J. Rustako Jr., P. B. Guerlain, M. K. Dennison, R. S. Roman, D. J. Barnickel, S. C. Wang, and R. R. Miller, "A Model for the Multipath Delay Profile of Fixed Wireless Channels," *IEEE Journal on Selected Areas in Communications,* vol. 17, No. 3, March 1999.

[25] A. Papoulis, *Probability, Random Variables, and Stochastic Processes,* New York: McGraw-Hill, 1984.

[26] Y. Akaiwa, *Introduction to Digital Mobile Communication*. New York: John Wiley & Sons, Inc., 1997.

[27] W. R. Young and L. Y. Lacy, "Echoes in Transmission at 450 Megacycles from Land-to-Car Radio Units," *Proceedings of the IRE,* vol 38, pp. 255-258, March 1950.

[28] R. Steele, ed., *Mobile Radio Communications*. IEEE Press, 1994.

[29] P. A. Bello, "Characterization of Randomly Time-Variant Linear Channels," *IEEE Transactions on Communication Systems,* vol. CS-11, pp 360-393, December 1963.

[30] J. D. Parsons, *The Mobile Radio Propagation Channel.* New York: John Wiley and Sons, Inc., 1992.

[31] L. W. Couch II, *Digital and Analog Communication Systems.* New Jersey: Prentice Hall, 1997.

[32] J. G. Proakis, *Digital Communications*. New York: McGraw Hill, 1989.

[33] G. L?vens, J. J. Reis, and R. H. R? kken, "Channel Sounding Measurements at 59 GHz in City Streets," *Personal, Indoor and Mobile Radio Communications, 1994,* vol. 2, pp. 496-500.

[34] G. Martin, "Wideband Channel Sounding Dynamic Range using a Sliding Correlator," *IEEE 51st Vehicular Technology Conference,* vol. 3, pp. 2517-2521, 2000.

[35] P. F. Sass, "Propagation Measurements for UHF Spread Spectrum Mobile Communications," *IEEE Transactions on Vehicular Technology,* vol. VT-32, No. 2, pp 168-176, 1983.

[36] M. S. Varela and M. G. Sánchez, "RMS delay and coherence bandwidth measurements in indoor radio channels in the UHF band," *IEEE Transactions on Vehicular Technology,* vol. 50, issue 2, pp. 515-525, 2001.

[37] I. Cuiñas and M. G. Sánchez, "Measuring, Modeling, and Characterizing of Indoor Radio Channel at 5.8 GHz," *IEEE Transactions on Vehicular Technology,* vol. 50, issue 2, pp. 526-535, 2001.

[38] E. A. Lee and D. G. Messerschmitt, *Digital Communication*. Boston, MA: Kluwer, 1998.

[39] M. C. Jeruchim, P. Balaban, and K. S. Shanmugan, *Simulation of Communication Systems*. New York: Plenum, 1992.

[40] A. Brown, and B. Wolt, "Digital L-Band Receiver Architecture with Direct RF Sampling," *Position Location and Navigation Symposium*, pp. 209-216, 1994.

[41] International Telecommunications Union, http://www.itu.int/publications, 2001.

[42] J. Adler, "Jitter in Clock Sources," Application Note, http://www.vectron.com/whatsnew/jitter.htm, Vectron International, 1997.

[43] M. Tschudin, R. Heddergott, P. Truffer, "Validation of a High Resolution Measurement Technique for Estimating the Parameters of Impinging Waves in Indoor Environments," *The 9th IEEE International Symposium on Personal, Indoor and Mobile Radio Communications*, vol. 3, pp 1411-1416, 1998.

[44] S. Haese, C. Moullec, P. Coston, K. Sayegrih, "High Resolution Spread Spectrum Channel Sounder for Wireless Communication Systems," *IEEE International Conference on Personal Wireless Communications*, pp. 170-173, 1999.

[45] S. Guillouard, G. El Zein, J. Citerne, "Wideband Propagation Measurements and Doppler Analysis for the 60 GHz Indoor Channel," *IEEE MTT-S International Microwave Symposium Digest*, vol. 4, pp. 1751-1754, 1999

[46] T. Kobayashi, H. Masui, S. Takahashi, K. Takahashi, and K. Kage, "Delay Profile Measurement System for Microwave Mobile Communications and Delay Characteristics in an Urban Environment," *IEEE Radio and Wireless Conference*, pp. 163-166, 1999.

[47] D. M. Akos, M. Stockmaster, J. B. Y. Tsui, and J. Caschera, "Direct Bandpass Sampling of Multiple Distinct RF Signals," *IEEE Transactions on Communications*, vol. 47, No. 7, pp. 983-988, July 1999.

[48] R. G. Vaughn, N. L. Scott, and D. R. White, "The Theory of Bandpass Sampling," *IEEE Transactions on Signal Processing*, vol. 39, pp. 1973-1984, September 1991.

[49] G. L. Matthaei, L. Young, and E. M. T. Jones, Microwave *Filters, Impedance-Matching Networks, and Coupling Structures.* New York: Artech House, 1964.

[50] G. J. Saulnier, C. M. Puckette IV, R. C. Gaus, Jr., R. J. Dunki-Jacobs, and T. E. Thiel, "A VLSI Demodulator for Digital RF Network Applications: Theory and Results," *IEEE Journal on Selected Areas of Communications*, Vol. 8, No. 8, pp. 1500-1511, October 1990.

[51] D. I. Hoult, "A High Accuracy I-Q Demodulator and Modulator," *RF Design*, Vol. 20, No. 3, pp. 26-38, March 1997.

[52] T. K. Blankenship, "Design and Implementation of a Pilot Signal Scanning Receiver for CDMA Personal Communication Services Systems," Masters Thesis, MPRG-TR-98-02, Virginia Polytechnic Institute and State University, April 1998.

[53] H. Johnson and M. Graham, *High Speed Digital Design: A Handbook of Black Magic.* New Jersey: Prentice Hall, 1993.

[54] C. Beelen-Hendrix and M. Verguld, "Capacitor Sizes," *Trends in Assembly Processes for Miniaturized Consumer Electronics*, Apex CD-ROM, 2001.

[55] Electronic Packaging and Production Online Webcast, "0201 Defects," http://www.e-insite.net/epp/, September 14, 2000.

[56] H. Xu, T. S. Rappaport, J. Schaffner, and H. P. Hsu, "The Sliding Correlator and Network Analyzer Channel Sounding Methods for Wideband Multipath Propagation Measurements at 5.85 GHz," *Advanced Microelectronics-Special Wireless Issue,* pp. 17-28, May 1998.

[57] J. Schaffner, "A Constraint on the Length of the PN-code in the Sliding Correlator Spread Spectrum Channel Sounder," *Hughes Research Laboratories Internal Report.*

[58] A. Orndorff, "Miniaturization of MPRG's Sliding Correlator Channel Sounder," Undergraduate Honors Thesis, to be published in 2002.

[59] G. L. Berger, and H. Safer, "Channel Sounder for the Tactical VHF-Range," *IEEE MILCOM Proceedings*, vol. 3, pp. 1474-1478, November 1997.

[60] H. Xu, *Personal Communications*, May 2000.

[61] D. W. Allan, N. Ashby, C. C. Hodge, "The Science of Timekeeping," Application Note 1289, Hewlett Packard, 1997.

[62] "Starloc II Precision GPS Time and Frequency Reference Installation and Operation Manual", Datum, Inc., 2001.

[63] G. D. Durgin, "Theory of Stochastic Local Area Channel Modeling for Wireless Communications," Ph. D. Dissertation, Virginia Polytechnic Institute and State University, http://scholar.lib.vt.edu/theses/index.html, December 2000.

[64] H. Xu, "Terrestrial Radio Wave Propagation at Millimeter-Wave Frequencies," Ph. D. Dissertation, Virginia Polytechnic Institute and State University, http://scholar.lib.vt.edu/theses/index.html, May 2000.

[65] V. Kukshya, "Wideband Terrestrial Path Loss Measurement Results For Characterization of Pico-cell Radio Links at 38 GHz and 60 GHz Bands of Frequencies," Masters Thesis, Virginia Polytechnic Institute and State University, http://scholar.lib.vt.edu/theses/index.html, June 2001.

[66] J. He, A. Verstak, L. T. Watson, T. S. Rappaport, C. R. Anderson, N. Ramakrishnan, C. A. Shaffer, W. H. Tranter, K. Bae, and J. Jiang, "Global Optimization of Transmitter Placement in Wireless Communication Systems," in proceedings *High Performance Computing Symposium*, A. Tentner (ed.), Soc. for Modeling and Simulation International, San Diego, CA, pp. 328-333, April 2002.

[67] ed. J-P. Linnartz, "Wireless Communication, the Interactive Multimedia CD-ROM," New York: Kluwer Academic, 2001.

[68] C. B. Steger, G. D. Durgin and T. S. Rappaport, "Channel Imaging Analysis Suite User Guide," Technical Report, MPRG, Virginia Tech, August 1999.

[69] G. D. Durgin, V. Kukshya, E. Lau, and T. S. Rappaport, "Measurement-Based Spatial-Temporal Channel modeling for Handheld Multi-media Terminals," Technical Report, MPRG-TR-01-03, Virginia Tech, December 1999.

[70] ON Semiconductor, "High Performance ECL Data," Technical Report, DL140/D rev. 6, January 2001.

[71] T. Nakagawa, T. Tsukahara, "A low phase noise C-band frequency synthesizer using a new fractional-N PLL with programmable fractionality," *IEEE Transactions on Microwave Theory and Techniques*, vol. 44, No. 2, pp. 344-346, Feb. 1996.

[72] R. Davies, N. Bensebti, M. A. Beach, J. P. McGeehan, "Wireless Propagation Measurements in Indoor Multipath Environments at 1.7 GHz and 60 GHz for Small Cell Systems," *IEEE 41st Vehicular Technology Conference*, pp. 589-593, 1991.

[73] M. J. Feuerstein, K. L. Blackard, T. S. Rappaport, S. Y. Seidel, H. H. Xia, "Path Loss, Delay Spread, and Outage Models as Functions of Antenna Height for Microcellular System Design," *IEEE Transactions on Vehicular Technology*, vol. 44, No. 3, pp. 487-497, August 1994.

[74] P. Nobles and F. Halsall, "Indoor Propagation at 17 GHz and 60 GHz – Measurements and Modeling," *IEE National Conference on Antennas and Propagation*, pp. 93 – 96, 1999.

[75] G. Durgin, T. S. Rappaport, and H. Xu, "Measurements and Models for Radio Path Loss and Penetration Loss In and Around Homes and Trees at 5.85 GHz," *IEEE Transactions on Communications*, vol. 46, No. 11, November 1998.

[76] B. Langen, G. Lober, W. Herzig, "Reflection and Transmission Behaviour of Building Materials at 60 GHz," *IEEE 4th International Conference on Personal, Indoor, and Mobile Radio Communications*, vol. 4, pp. 505-509, September 1994.

[77] L. M. Correia and P. O. Françês, "Estimation of Materials Characteristics from Power Measurements at 60 GHz," *IEEE 7th International Conference on Personal, Indoor, and Mobile Radio Communications*, vol. 1, pp. 510-513, October 1994.

[78] K. Sato, T. Manabe, T. Ihara, H. Saito, S. Ito, T. Tanaka, K. Sugai, N. Ohmi, Y. Murakami, M. Shibayama, Y. Konishi, and T. Kimura, "Measurements of Reflection and Transmission Characteristics of Interior Structures of Office Building in the 60-GHz Band," *IEEE Transactions on Antennas and Propagation*, vol. 45, No. 2, pp. 1783-1792, December 1997.

[79] P. Nobles, "A Study Into Indoor Propagation Factors at 17 GHz and 60 GHz," Final Report, http://www.radio.gov.uk/topics/research/topics/propagation/indprop/1propdoc.htm, June 1998.

[80] G. Vannucci and R. S. Roman, "Measurement Results on Indoor Radio Frequency Reuse at 900 MHz and 18 GHz," *IEEE 3rd International Conference on Personal, Indoor, and Mobile Radio Communications*, pp. 308-314, October 1992.

[81] M. Lott and I. Forkel, "A Multi-Wall-and-Floor Model for Indoor Radio Propagation," *IEEE 53rd Vehicular Technology Conference*, vol. 1, pp. 464-468, May 2001.

[82] R. R. Skidmore, T. S. Rappaport, A. L. Abbott, "Interactive coverage region and system design simulation for wireless communication systems in multifloored indoor environments: SMT Plus," *IEEE 5th International Conference on Universal Personal Communications*, vol. 2, pp. 646-650, October 1996.

[83] K. Sato, T. Manabe, J. Polivka, T. Ihara, Y. Kasashima, and K. Yamaki, "Measurement of the Complex Refractive Index of Concrete at 57.5 GHz," *IEEE Transactions on Antennas and Propagation*, vol. 44, No. 1, pp. 35-40, January 1996.

[84] Y. P. Zhang, Y. Hwang, "Measurements of the Characteristics of Indoor Penetration Loss," *IEEE 44th Vehicular Technology Conference*, vol. 3, pp. 1741-1744, June 1994.

[85] D. M. Matic, H. Harada, R. Prasad, "Indoor and outdoor frequency measurements for MM-waves in the range of 60 GHz," *IEEE 48th Vehicular Technology Conference*, vol. 1, pp. 567-571, May 1998.

[86] National Semiconductor, "A/D Converter Definition of Terms," Technical Report, MS101150, January 2000.

[87] J. B. Bullock, T. M. King, H. L. Kennedy, E. D. Berry, and G. Zanfino, "Test Results and Analysis of a Low Cost Core GPS Receiver for Time Transfer Applications," *IEEE International Frequency Control Symposium*, pp. 314-322, May 1997.

[88] M. F. Wacker, "Use Allan Variance to Characterize Oscillator Stability," *Microwaves and RF*, vol. 36, No. 10, pp. 92-103, 190, October 1997.

[89] M. F. Wacker, "Frequency Stability Characterization in the Time Domain," Application Note, http://www.corningfrequency.com/appnotes/fstability.html, Corning Frequency Control, 2002.

[90] G. Y. Delisle, and L. Talbi, "Narrow and Wideband Measurements for Millimeter Waves PCS Channel Characterization," ," *IEEE 4th International Conference on Universal Personal Communications*, pp. 206-210, November 1995.

[91] R. Overduin, and P. M. F. Smulders, "Feasibility of Broadband Inroom Radio Communications at 60 GHz," *IEEE 5th International Symposium on Personal, Indoor and Mobile Radio Communications, 1994*, vol. 1, pp. 119-126, September 1994.

Vita

Christopher R. Anderson was born on July 29, 1976 in North Wilkesboro, North Carolina, and was raised in Boone, North Carolina; graduating from Watauga High School in 1994. Anderson enrolled at Virginia Polytechnic Institute and State University in the Fall of 1994 to pursue a Bachelor of Science in Electrical Engineering. In 1995, he was awarded a Bradley Scholarship from the Bradley Department of Electrical Engineering and in 1999 received the Carlos and Linda Roberts award for an outstanding student in the area of wireless communications. While at Virginia Tech, he participated in the Co-Op program as an Assistant Measurements Engineer for Siecor RD&E in Hickory, North Carolina, and also worked as a summer intern with IRC in Boone, North Carolina. As an undergraduate, Anderson was an active member of the Tau Beta Pi National Engineering Honor Society, Eta Kappa Nu Electrical Engineering Society, IEEE, the Radio Club of America, and served for two years as President of the Virginia Tech Chapter of the National Society of Professional Engineers. He graduated *Magna Cum Laude in Honors* in 1999.

In 2000, Anderson began work towards a Master of Science degree in Electrical Engineering with the Mobile and Portable Radio Research Group at Virginia Tech. Anderson was awarded a Bradley Fellowship from the Bradley Department of Electrical and Computer Engineering in 2000 and a Pratt Presidential Fellowship from the College of Engineering in 2001. His research included designing and fabricating high-speed printed circuit boards, RF test and measurement equipment design and implementation, and wireless propagation studies, and he has co-authored two conference papers. His research activities were supplemented with a summer internship with Allen Telecom's Mikom US division in 2001.

Anderson is an Eagle Scout with Bronze over Silver Palms, and maintains an active interest in Biomedical Engineering as a member of the IEEE Engineering in Medicine and Biology Society.